PREDICTION OF SHEAR STRENGTH AND VERTICAL MOVEMENT DUE TO MOISTURE DIFFUSION THROUGH EXPANSIVE SOILS

A Dissertation

by

XIAOYAN LONG

Submitted to the Office of Graduate Studies of
Texas A&M University
in partial fulfillment of the requirements for the degree of

DOCTOR OF PHILOSOPHY

August 2006

Major Subject: Civil Engineering

PREDICTION OF SHEAR STRENGTH AND VERTICAL MOVEMENT DUE TO MOISTURE DIFFUSION THROUGH EXPANSIVE SOILS

A Dissertation

by

XIAOYAN LONG

Submitted to the Office of Graduate Studies of
Texas A&M University
in partial fulfillment of the requirements for the degree of

DOCTOR OF PHILOSOPHY

Approved by:

Co-Chairs of Committee,	Charles Aubeny
	Robert Lytton
Committee Members,	Jose Roesset
	Alan Palazzolo
Head of Department,	David V. Rosowsky

August 2006

Major Subject: Civil Engineering

ABSTRACT

Prediction of Shear Strength and Vertical Movement due to Moisture Diffusion through Expansive Soils. (August 2006)

Xiaoyan Long, B.S., Changsha Railway University;

M.S., Tongji University

Co-Chairs of Advisory Committee: Dr. Charles Aubeny
Dr. Robert Lytton

This dissertation presents an investigation of engineering behavior of expansive soils. An analytical study was undertaken for the development and modification of a Windows-based two-dimensional finite element computer program FLODEF that performs a sequentially coupled flow-displacement analysis for the prediction of moisture diffusion and the induced volume change in soils supporting various elements of civil infrastructure. The capabilities of the model are illustrated through case studies of shear strength envelope forecast and parametric studies of transient flow-deformation prediction in highway project sites to evaluate the effectiveness of engineering treatment methods to control swell-shrink deformations beneath highway pavements. Numerical simulations have been performed to study the field moisture diffusivity using a conceptual model of moisture diffusion in a fractured soil mass. A rough correlation between field and the laboratory measurements of moisture diffusion coefficients has been presented for different crack depth patterns.

DEDICATION

To my dearest parents, Lingfu Long and Hefeng Ye.

ACKNOWLEDGMENTS

This research was sponsored by the Federal Highway Administration and the Texas Department of Transportation and their support is gratefully acknowledged.

First of all, I would like to express my sincere thanks and gratitude to my advisor, Dr. Charles Aubeny for invaluable guidance, inspiration, encouragement and patience through the past five years.

I would also like to thank Dr. Robert Lytton and Dr. Jose Roessett for providing insight, guidance and suggestions. Also I really respect and appreciate deeply the guidance and help from Dr. Don Murff. I am deeply impressed with their knowledge, ideas, caring and philosophy of life. Their kindness and great support will be remembered deeply through my life.

I also appreciate Dr. Alan Palazzolo for serving on the advisory committee.

I deeply appreciate my dearest parents. They always encouraged me in the difficult times and everything I have achieved today comes from them.

TABLE OF CONTENTS

Page

ABSTRACT……. …….. iii

DEDICATION……. iv

ACKNOWLEDGMENTS…….. v

TABLE OF CONTENTS…… vi

LIST OF FIGURES…… viii

LIST OF TABLES…….. xvii

CHAPTER

I INTRODUCTION..... 1

1.1 General..... 1
1.2 Objectives of Research 5
1.3 Scope of Dissertation 6

II BACKGROUND..... 9

2.1 Soil Suction..... 11
2.2 Soil Properties..... 23
2.3 Stress Variables 28
2.4 Shear Strength Prediction 30
2.5 Unsaturated Moisture Flow Analysis 37
2.6 Prediction of Volume Change Behavior..... 44

III DESCRIPTION OF COMPUTER PROGRAM FLODEF 50

3.1 Overview of Program 51
3.2 Unsaturated Moisture Flow-Soil Deformation Analysis 52
3.3 Program Structure and Input/Output Screens..... 73
3.4 Program Numerical Validation..... 75

TABLE OF CONTENTS (continued)

CHAPTER		Page
IV	APPLICATIONS OF COMPUTER PROGRAM FLODEF: SHEAR STRENGTH FORECAST OF CIVIL INFRASTRUCTURES ON EXPANSIVE SOILS	97
	4.1 Introduction	97
	4.2 Analysis of Earth Retaining Structures	98
	4.3 Analysis of Slopes	121
V	APPLICATIONS OF COMPUTER PROGRAM FLODEF: TRANSIENT FLOW-DEFORMATION ANALYSIS OF HIGHWAY PROJECT SITES	133
	5.1 Fort Worth North Loop IH 820 Study Section A	135
	5.2 Fort Worth North Loop IH 820 Study Section B	146
	5.3 Atlanta US 271	153
	5.4 Austin Loop 1 Uphill of Frontage Road and Main Lane	160
	5.5 Conclusions	166
VI	EFFECT OF DESICCATION CRACKING ON ENGINEERING BEHAVIOR OF EXPANSIVE SOILS	169
	6.1 Criteria of Soil Tensile Strength	170
	6.2 Effect of Vegetation on Soil Desiccation	172
	6.3 Cracking Spacing and Depth	189
	6.4 Effect of Desiccation on Soil Diffusivity	193
	6.5 Needed Research	221
VII	SUMMARY AND CONCLUSIONS	222
	7.1 Conclusions	222
	7.2 Recommendations	223
REFERENCES		225
VITA		238

LIST OF FIGURES

FIGURE		Page
1.1	Pore water in expansive soils (Wheeler and Karube, 1996).....	3
2.1	Pore water pressure in vadose zone (Fredlund and Rahardjo, 1993a)	10
2.2	Total suction calibration test set up (Bulut et al., 2001)	18
2.3	Sketch of a transistor psychrometer probe (Bulut et al., 2001).....	20
2.4	Details of pressure plate apparatus (Oliveria and Fernando, 2006)	22
2.5	Model 1500 PPE device: (a) Sample-retaining rings; (b) Sealed vessel (Hoyos et al., 2006).....	22
2.6	Typical soil-water characteristic curve SWCC (Vanapalli et al., 1996)	24
2.7	Shear strength variation due to matric suction (Tekinsoy et al., 2004).....	31
2.8	Value of f at transistor zone (Lytton, 1995)	32
2.9	Equilibrium suction as a function of climate (Aubeny and Long, 2006).....	40
2.10	The two-dimensional model for simulation of water uptake by vegetation (Ali and Rees, 2006).....	45
2.11	Void ratio and water content constitutive surfaces for unsaturated soils (Fredlund and Rahardjo, 1993b)	47
2.12	Volumetric strain as a function of log (suction) and log (mean principal stress) (Lytton, 1994).....	49
3.1	Schematic dry end test setup (Aubeny and Lytton, 2003)	57
3.2	Typical experimental results for dry end test (Aubeny and Lytton, 2003) ...	58
3.3	Root moisture extraction models for optimal moisture conditions, Q_{smax} as a function of depth Z, where Z_r=depth of the root zone (modified after Gay, 1994).....	62

LIST OF FIGURES (continued)

FIGURE		Page
3.4	Dimensionless sink term coefficient α as a function of the absolute value of matrix suction $\left\|h_m\right\|$ (modified after Gay (1994)).	63
3.5	Schematic sketch of water uptake within tree root zone (Indraratna et al., 2006)	63
3.6	El Paso seasonal surface suction patterns (Long et al. 2006)	64
3.7	Initial conditions for Atlanta US 290	66
3.8	Flowchart of program FLODEF	74
3.9	Input screen 1: site information	76
3.10	Input screen 2: pavement structure dimensions	77
3.11	Input screen 3: subgrade soil properties	78
3.12	Input screen 4: vegetation information	79
3.13	Output plot 1: vertical profile (suction)	80
3.14	Output plot 2: vertical profile (vertical displacement)	81
3.15	Output plot 3: vertical profile (horizontal displacement)	82
3.16	Output plot 4: contour plot (suction)	83
3.17	Output plot 5: contour plot (vertical displacement)	84
3.18	Output plot 6: contour plot (horizontal displacement)	85
3.19	Output plot 7: surface deformation plot	86
3.20	Output plot 8: time history plot (suction)	87
3.21	Output plot 9: time history plot (vertical displacement)	88

LIST OF FIGURES (continued)

FIGURE		Page
3.22	Output plot 10: time history plot (horizontal displacement)	89
3.23	FEM mesh generated in the program	90
3.24	Numerical verification: comparison of flow analysis with 1-D Mitchell's analytical solution	94
3.25	Numerical verification: comparison of flow analysis with 2-D ABAQUS results	95
3.26	Numerical verification: comparison of displacement analysis with 2-D ABAQUS results	96
4.1	Schematic sketch of earth retaining structure	100
4.2	Definition sketch for matric suction prediction (Aubeny and Lytton, 2003)	103
4.3	Matric suction prediction for retaining wall with aspect ratio 4H: 1W and U_0=5	105
4.4	Suction prediction for retaining wall with aspect ratio 4H: 1W and U_0=4	106
4.5	Matric suction prediction for retaining wall with aspect ratio 4H: 1W and U_0=3	107
4.6	Matric suction prediction for retaining wall with aspect ratio 4H: 1W and U_0=2	108
4.7	Matric suction prediction for retaining wall with aspect ratio 4H: 1W and U_0=1	109
4.8	Matric suction prediction for retaining wall with aspect ratio 4H: 1W and U_0=0.5	110
4.9	Matric suction prediction for retaining wall with aspect ratio 8H: 1W and U_0=5	111

LIST OF FIGURES (continued)

FIGURE		Page
4.10	Matric suction prediction for retaining wall with aspect ratio 8H: 1W and U_0=4	112
4.11	Suction prediction for retaining wall with aspect ratio 8H: 1W and U_0=3	113
4.12	Matric suction prediction for retaining wall with aspect ratio 8H: 1W and U_0=2	114
4.13	Matric suction prediction for retaining wall with aspect ratio 8H: 1W and U_0=1	115
4.14	Matric suction prediction for retaining wall with aspect ratio 8H: 1W and U_0=0.5	116
4.15	Mohr circle for the shear strength of unsaturated compacted soils (Lytton, 2001)	118
4.16	Shallow translational landslides in unsaturated soil slope (http://wapi.isu.edu/envgeo/EG4_mass_wasting/EG_module_4.htm)	122
4.17	Definition sketch for shallow slide analysis (Aubeny and Lytton, 2003)	123
4.18	Definition sketch for moisture diffusion analysis (Aubeny and Lytton, 2003)	125
4.19	Engineering treatment scheme for expansive soil embankment (Yang and Zheng, 2006)	129
4.20	Engineering treatment scheme for expansive soil slopes (Yang and Zheng, 2006)	131
5.1	Parametric studies for engineering treatment measures	135
5.2	Schematic sketch of Fort Worth north loop 820 study section A pavement cross section	136
5.3	No moisture control measures (Fort Worth North Loop 820 study section A)	138

LIST OF FIGURES (continued)

FIGURE		Page
5.4	Vertical displacement measures with various depths of vertical moisture barriers, initial dry (Fort Worth North Loop 820 study section A)	139
5.5	Vertical displacement measures with various depths of vertical moisture barriers, initial wet (Fort Worth North Loop 820 study section A)	140
5.6	Vertical displacement measures with different depths of lime stabilization (Fort Worth North Loop 820 study section A, initial dry)	141
5.7	Vertical displacement measures with different depths of lime stabilization (Fort Worth North Loop 820 study section A, initial wet)	142
5.8	Vertical displacement measures of various depths of “inert” material (Fort Worth North Loop 820 study section A, initial dry)	143
5.9	Vertical displacement measures of various depths of “inert” material (Fort Worth North Loop 820 study section A, initial wet)	144
5.10	Vertical displacement measures of median condition (Fort Worth North Loop IH 820 study section A, initial dry)	145
5.11	Vertical displacement measures of median condition (Fort Worth North Loop IH 820 study section A, initial wet)	146
5.12	Fort Worth North Loop 820 study section B pavement cross section sketch	147
5.13	No moisture control measures at Fort Worth North Loop 820 study section B	148
5.14	Vertical displacement measures of various depths of vertical moisture barriers at Fort Worth North Loop 820 study section B	149
5.15	Vertical displacement measures of various depths of lime stabilization at Fort Worth North Loop 820 study section B	150
5.16	Vertical displacement measures of various depths of “inert” material at Fort Worth North Loop 820 study section B	151

LIST OF FIGURES (continued)

FIGURE		Page
5.17	Vertical displacement measures of paving conditions (Fort Worth North Loop 820 study section B, initial wet)	152
5.18	Vertical displacement measures of paving conditions (Fort Worth North Loop 820 study section B, initial dry)	153
5.19	Atlanta US 271 pavement cross section sketch	154
5.20	Vertical displacement measures at Atlanta US 271	155
5.21	Vertical displacement measures of various depths of vertical moisture barriers at Atlanta US 271	156
5.22	Vertical displacement measures of various depths of lime stabilization at Atlanta US 271	157
5.23	Vertical displacement measures of various depths of “inert” material at Atlanta US 271	158
5.24	Vertical displacement measures of various widths of paved shoulder at Atlanta US 271 (initial wet)	159
5.25	Vertical displacement measures of various widths of paved shoulder at Atlanta US 271 (initial dry)	159
5.26	Austin Loop 1 pavement cross section sketch	160
5.27	No moisture control measures at Austin Loop 1 uphill of frontage road	161
5.28	No moisture control measures at Austin Loop 1 uphill of main lane	161
5.29	Vertical displacement measures at uphill outer wheel path of frontage road with various depths of vertical moisture barrier built at frontage road (Austin loop 1, initial dry condition)	162
5.30	Vertical displacement measures at uphill outer wheel path of main lane with various depths of vertical moisture barrier built at frontage road (Austin loop 1, initial dry condition)	163

LIST OF FIGURES (continued)

FIGURE		Page
5.31	Vertical displacement measures at uphill outer wheel path of frontage road with various depths of vertical moisture barrier built at main lane (Austin loop 1, initial dry condition)	163
5.32	Vertical displacement measures at uphill outer wheel path of main lane with various depths of vertical moisture barrier built at main lane (Austin loop 1, initial dry condition)	164
5.33	Vertical displacement measures of paved conditions at uphill outer wheel path of frontage road, Austin Loop 1	165
5.34	Vertical displacement measures of paved conditions at uphill outer wheel path of main lane, Austin Loop 1	166
6.1	Tensile soil strength based on an unconfined torsion test (from Lytton, 2001)	171
6.2	Strength envelopes and the tensile strength (Lee and Ingles, 1968)	172
6.3	Total suction profiles near a row of large eucalypts (Klemzig site, Adelaide, South Australia) (Cameron, 2001)	174
6.4	Total suction profiles near a row of trees of mixed species (Ingle Farm, Adelaide, South Australia) (Cameron, 2001)	175
6.5	Total suction profiles near a row of large eucalypts (Williamstown, Victoria) (Cameron, 2001)	176
6.6	Total suction profiles near a roadside plantation of native trees (Hallett Cove, South Australia) (Cameron, 2001)	177
6.7	Lateral and vertical extent of tree root system (Mitchell, 1979)	181
6.8	Water balance for the Clarens site showing soil water storage for root barrier-to-tree and tree-to-house measurements (Blight, 2006)	186
6.9	Effect of root barrier on soil water content during 2003/2004 year (Blight, 2006)	187

LIST OF FIGURES (continued)

FIGURE		Page
6.10	Contours of soil water content between tree and house during 2004/2005 year (Blight, 2006)	188
6.11	Basic modes of crack surface displacement: (a) tension mode; (b) shear mode; (c) torsion mode (Vallejo, 1989)	191
6.12	Analysis model for the effect of desiccation on diffusivity	193
6.13	Observed seasonal soil movements of an expansive soil in open field in Adelaide, South Australia (Mitchell, 1979)	196
6.14	Measured seasonal suction in open paddock and under well ventilated floor (Mitchell, 1979)	200
6.15	Suction profile with depth illustrating the point where suction becomes constant with depth. (Lytton, 1995)	201
6.16	Suction profile with depth illustrating the inferred presence of a water table (Lytton, 1995)	202
6.17	Suction profile in a tree root zone in summer (Lytton, 1995)	203
6.18	Geometries for different crack depths in the analysis…….	206
6.19	Crack depths (x/dc) vs. field to lab diffusivity ratio	207
6.20	Cumulative probability density function of field to laboratory diffusion coefficient ratio versus the ratio of crack depth d_c to intact soil moisture active zone depth, y_{max} (Aubeny and Long, 2006)	214
6.21	Normalized crack depth versus field to laboratory diffusion coefficient ratio (natural scale)	215
6.22	Normalized crack depth versus field to laboratory diffusion coefficient ratio in logarithmic scale	216
6.23	Reliability versus diffusion coefficient	217

LIST OF FIGURES (continued)

FIGURE Page

6.24 Effect of the mesh size on accuracy: (a) crack depth=1ft; (b) crack depth=2ft; (c) crack depth =4ft; (d) crack depth=8ft; (e) crack depth=16ft 218

LIST OF TABLES

TABLE		Page
1.1	Probable Expansion as Estimated from Classification Test Data (Holtz and Kovacs, 1981)	4
2.1	The Total Suction Levels for Different Cases (Naiser, 1997)	12
2.2	Osmotic Coefficients for Different Solutions (Bulut et al., 2001)	15
2.3	Summary of Suction Measurement Devices (Rahardjo and Leong, 2006)	16
2.4	Empirical Permeability Functions (Leong and Rahardjo, 1997)	29
2.5	Semi-Empirical Equations to Predict Shear Strength in Unsaturated Soils (Garven and Vanapalli, 2006)	35
3.1	Default Equilibrium Suctions in FLODEF	65
3.2	Input Parameters for Mitchell's Default Initial Condition Descriptions	67
3.3	Analysis Similarity of Sequentially Coupled Flow/Displacement Analysis with Sequentially Coupled Thermal Stress/Displacement Analysis	91
4.1	Typical Moisture Active Zone Depths for Surface Suction Change Conditions	101
4.2	Engineering Properties for the Shear Strength Calculation Illustration (Aubeny and Lytton, 2003)	119
6.1	Summary of Suction Data (Cameron, 2001)	179
6.2	Number of Nodes and Elements for the Analyses	212
6.3	Mean, Standard Deviation and Percentiles in Terms of Field to Lab Diffusion Coefficient Ratio	213

CHAPTER I

INTRODUCTION

1.1 General

Expansive soils (or shrink-swell soils) exhibit remarkable volume change with variations in moisture conditions. Moisture can change over time due to environmental factors such as rainfall, evapotranspiration and leakage. Expansive soils experience swell or heave on wetting and shrink on drying. This swell-shrink phenomenon of expansive soils is responsible for the genesis and behavior of vertisols like the linear and normal gilagi (Gay, 1994).

Serious problems can be imposed by expansive soils on civil infrastructure, such as embankments and slopes, retaining walls, landfill covers and liners, pavement structures and foundations. The outer layers of embankments constructed of expansive clays can be subject to dramatic strength loss due to periodic moisture changes, which can begin soon after construction and continue for decades resulting the consequent sloughing and shallow landslides failures (Aubeny and Lytton, 2003). The differential movement induced by uneven moisture distribution will cause the development of pavement roughness and distress in foundations. The moisture and leachate transmission of municipal solid waste (MSW) covers and liners overlying expansive soil subgrades can be increased due to the presence of shrinkage cracks on soil drying or desiccation.

This dissertation follows the style and format of the *Journal of Geotechnical and Geoenvironmental Engineering.*

For the case of foundation walls in basements and crawlspaces, expansive soils will exert horizontal pressure in excess of normal earth pressure loads. If the walls do not have sufficient strength, serious structural damage may occur.

In the United States, expansive soils cover large parts of Texas, Oklahoma and the upper Missouri Valley. Each year, they cause billions of dollars in damage to buildings, roads, pipelines, and other structures, which exceed the total cost induced by floods, hurricanes, tornadoes, and earthquakes (Holtz and Kovacs, 1981).

1.1.1 Description of Expansive Soils

Expansive soils are stable-structured with four phases (soil particle, pore water, pore air and structural membrane) (Fredlund and Rahardjo, 1993a). Typically they contain clay minerals that attract and absorb water such as montmorillonite, kaolinite, illite, vermiculite and chlorite. Montmorillonite is the predominant clay mineral. From the view of soil microstructure, the particles of clay minerals have a distinctive flat shape, large specific surfaces, high cation exchange capacities and more generally, a specific physico-chemical activity and a strong affinity for water (Ferber et al., 2006).

Wheeler and Karube (1996) categorized the pore water into three forms: adsorbed water, bulk water, and meniscus water. The absorbed water is tightly bound to the soil particles and acts as an integral part of the particles. Bulk water occurs in the completely flooded void spaces. The meniscus water occurs at contacts of soil particles, which are not covered by the bulk water, in ring-shaped lenses of water. The bulk water is easily drained out and is immediately replaced by air on drying. Meanwhile, all bulk water can not re-enter in the pores when soil is wetted, which gives an explanation of

the hysteresis occurrence in the water retention curve presented in Chapter II. Figure 1.1 gives a schematic representation of the pore water in expansive soils.

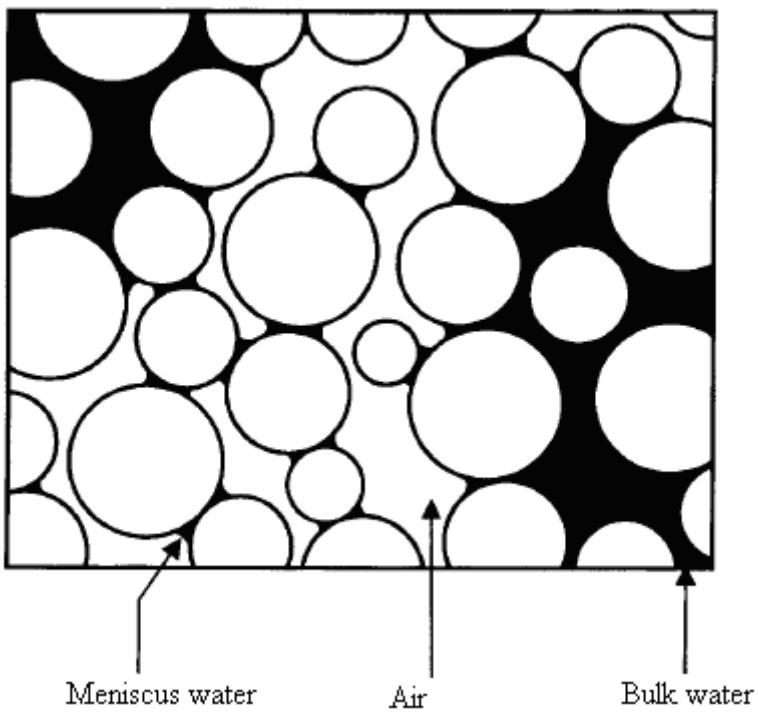

Figure 1.1 Pore water in expansive soils (Wheeler and Karube, 1996)

According to the states of pore air and pore water, expansive soils can be divided into different groups such as expansive soils with discontinuous water and continuous air, expansive soils with continuous water and continuous air and expansive soils with continuous water and discontinuous air. For the expansive soils with discontinuous water and continuous air, the water content is very low and pore water is isolated, which only exists around contact points between soil particles. Therefore pore water pressure can not be transferred while pore air has completely reversed situation. With the increase of degree of saturation (S_r), the continuity of the two phases will change. When isolated

pore water around contact points becomes continuous, both pore water and pore air are continuous and the two fluid phases can endure and transfer corresponding pore water pressure and pore air pressure. When the degree of saturation S_r rises up to around 85%, the pore air exists as isolated air bubbles separated by pore water. Only water phase is continuous and can transfer pressure in voids (Yu and Chen, 1965).

1.1.2 The Identification and Remedy Measures

Expansive soils can be identified with a variety of techniques. The most commonly utilized techniques are: Mineral Identification, Indirect Methods (index properties, potential volume change (PVC), Activity (A_c)). Based on the Atterberg limits index, Holtz and Kovacs (1981) gave some descriptions of degree of expansion for expansive soils in Table 1.1.

Table 1.1. Probable Expansion as Estimated from Classification Test Data (Holtz and Kovacs, 1981)

Degree of Expansion	Probable Expansion (as a percent of the total volume change)	Colloidal Content (percent less than 1μm)	Plasticity Index	Shrinkage Limit
Very High	> 30	> 28	> 35	< 11
High	20 - 30	20 - 31	25 - 41	7 - 12
Medium	10 - 20	13 - 23	15 - 28	10 - 16
Low	< 15	< 15	< 18	> 15

In geotechnical engineering practice, the problems associated with expansive soils can be mitigated with the measures such as vertical or horizontal moisture barriers, soil replacement with inert soils, and soil treatments with lime or cement. The

mechanism of stabilizing expansive soils with lime or cement is to decrease the soil plastic index and the potentials for expansion and contraction.

1.2 Objectives of Research

Serious research attention has been given to the study of expansive soils since the mid 1950's. Considerable progress has been made through the hard work and cooperation among practitioners, investigators and designers. A series of international conferences on topics of expansive soils were commenced to provide the platform for the exchange of research findings since 1965.

Up to date, a relatively sound theoretical framework has been formulated to study the engineering behavior of expansive soils. Field investigations and studies have validated much of this framework. Research and practice have expanded to encompass a great variety of expansive soil problems. New techniques, procedures and devices have been developed and proposed to measure soil suction, estimate the soil properties such as hydraulic permeability and construct the non-linear soil-water characteristic curve. However, there still remain many hindrances in the way for the understanding of expansive soil behavior, for instance, the effect of desiccation cracks on expansive soil behavior.

The objectives of the research proposed herein are to: (1) summarize the existing formulations and approaches for the studies of moisture flow, shear strength and volumetric change behavior through extensive literature review;(2) numerically simulate the moisture flow, strength loss and volume change behavior of unsaturated soils under the cyclic climatic wet and dry cycles for embankments and pavement structures using

finite element techniques. The finite element program FLODEF was written using computer language Fortran 77 and incorporated with a windows-based graphic user interface (GUI). The program is currently in the stage of implementation by practitioners (TXDOT) and is waiting for the feedbacks; (3) present the relationship between laboratory measurements of diffusion coefficient α for intact soils and the field measurements with the presence of different depths of desiccation cracks from the two-dimensional finite element moisture flow analyses.

1.3 Scope of Dissertation

Chapter II presents a thorough literature review of recent study and proposed methods on unsaturated moisture flow, shear strength formulation and volumetric deformation calculation. The concepts of soil suction and related engineering properties as well as their measurements are reviewed. The importance of soil-water characteristic curve SWCC (or the soil-water retention curve, SWRC) in modeling of water flow and stress path for expansive soils is discussed. The empirical relationships between non-linear hydraulic permeability and SWCC proposed by different research investigators have been reviewed here. A simplified analysis for moisture flow proposed by Mitchell (1979) is reviewed. The stress state variables and the existing empirical predictions of unsaturated shear strength using the relationship between water content and soil total suction (SWCC) as a tool along with the saturated shear strength parameters are discussed. Different constitutive models for soil volumetric strain predictions and the related model material parameters are studied. Existing models for the consideration of moisture flux due to surface vegetation is also introduced.

Chapter III describes the computer program FLODEF compiled with Visual Fortran and Visual Basic. The moisture flow model and deformation model are introduced in detail. The sequentially-coupled hydro-mechanical analysis approach and the program flow chart are presented.

Chapter IV addresses the application of FLODEF program to shear strength prediction of expansive soils in embankments, retaining walls and slopes. For earth retaining walls, case studies of shear strength time history for different drain designs and flow boundary conditions at the soil-wall interface are presented. The analytical solution proposed by Aubeny and Lytton (2003) for the analysis of shallow landslides (failure time and strength degradation) is given, followed by the numerical case studies of riprap underpass cut slopes, riprap fill slopes and bare slopes in the parts of western, center and eastern Texas. The diffusion coefficient α varies with the crack propagation for the case of bare slopes, while the change of crack depth with time is calculated based on Lytton's model (2002).

Chapter V presents the application of FLODEF program to the prediction of vertical soil movement (shrinkage and heave) for pavement structures on expansive soils. The parametric case studies at three Texas sites: Atlanta US 271, Fort Worth North loop 820 and Austin loop 1 are given. The effectiveness of remedial measures such as vertical or horizontal moisture barriers, paved medians, and soil replacement with naturally non-plastic or lime-treated soils is discussed.

In chapter VI, a numerical study on the effect of desiccation cracks on field diffusivity is presented. The relationships between field diffusivity and laboratory test

values are given for different crack depths. These studies can largely explain discrepancies between field measurements and laboratory results. Finally, a brief summary of this study and recommendations for future research are given in chapter VII.

CHAPTER II

BACKGROUND

An expansive soil with either discontinuous or continuous pore air phase has negative pore –water pressure relative to pore-air pressure. It should be emphasized that negative pore water pressure can occur even in saturated soils, as shown in Figure 2.1, with the pore –water pressures being negative in the whole vadose zone. Seepage, shear strength and volume change comprise the main categories of expansive soil problems. Shear strength is relevant to the analyses of slope stability, bearing capacity and lateral earth pressure. Volume change is an important aspect of the design of pavements and structural foundations, particularly for light structures.

Suction changes due to moisture flow and seepage control the strength and deformation behavior of unsaturated soils; hence, accurate characteristic of moisture flow is often critical to both stability and deformation problems.

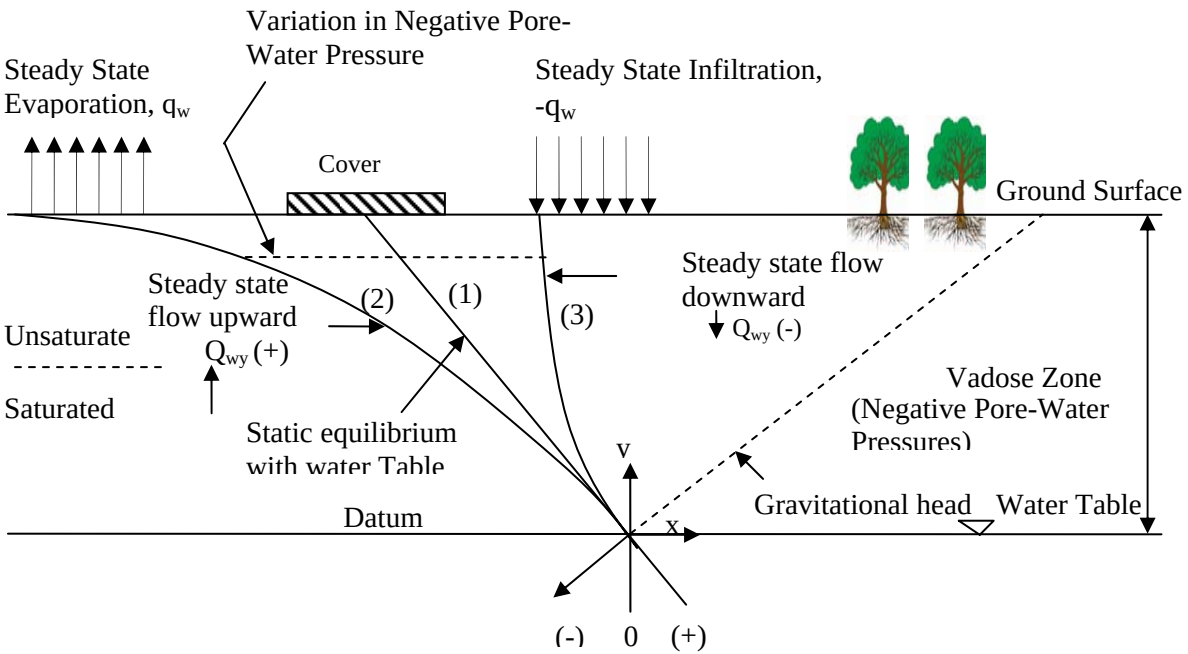

Figure 2.1 Pore water pressure in vadose zone (Fredlund and Rahardjo, 1993a)

2.1 Soil Suction

Soil suction quantifies the energy level in the soil-moisture system. An imbalance of total suction between adjacent soils tends to drive moisture towards regions of higher suction (PTI 3rd Edition, 2005). The rates of moisture flow are determined by total suction, while matric suction controls soil strength and deformation behavior.

2.1.1 Total Suction

Total suction is commonly referred to as the free energy state of soil water, which can be measured in terms of the partial vapor pressure of the soil water (Richards, 1965). Derived from the ideal gas law using the principles of thermodynamics, Fredlund and Rahardjo (1993a) calculate the total suction as:

$$\psi = \frac{RT}{v_{w0} w_v} \ln\left(\frac{\bar{u}_v}{\bar{u}_{v0}}\right) \qquad \text{(Equation 2.1)}$$

where R=universal (molar) gas constant [i.e. 8.31432 J/(mol K)];

T=absolute temperature (K);

v_{w0} = specific volume of water or the inverse of the density of water;

w_v = molecular mass of water vapor (i.e., 18.016kg/kmol) ;

$\bar{u}_v, \bar{u}_{v0}$ =partial pressure of pore-water vapor and saturation pressure of water vapor over a flat surface of pure water at the same temperature. The ratio of $\bar{u}_v / \bar{u}_{v0}$ is defined as relative humidity RH (%).

The typical total suction levels relevant to engineering practice are listed in Table 2.1 for different field cases. Total suction is composed of two components: matric suction (u_a-u_w) and osmotic suction π.

Table 2.1. The Total Suction Levels for Different Cases (Naiser, 1997)

Field Case	Suction Level (pF)
Field capacity	2.5
Wet limit for clays	2.5
Plastic limit	3.5
Wilting point of vegetation	4.5
Tensile Strength of confined water	5.3
Air dry	6.0
Oven dry	7.0

pF=$\log_{10}|h|$. $|h|$ measures the magnitude of suction in centimeters of water.

- p refers to the logarithmic value which is similar to pH and the F refers to free energy.

2.1.2 Matric Suction

Matric suction is associated with the capillary phenomenon arising from the surface tension of water, which is the result of the intermolecular forces acting on molecules in the contractile skin (Fredlund and Rahardjo, 1993a). It is the pressure difference between pore air and pore water, i.e., (u_a-u_w).

2.1.3 Osmotic Suction

Osmotic suction is the equivalent suction derived from the measurement of the partial pressure of the water vapor in equilibrium with a solution identical in composition with the soil water, relative to the partial pressure of water vapor in equilibrium with free pure water (Aitchison, 1965). It is related to the salt content in the soil pore water computed from Van't Hoff's equation (Fredlund and Rahardjo, 1993a):

$$\pi = -vRTm\phi \qquad \text{(Equation 2.2)}$$

where v is the number of ions from one molecule of solute(i.e., v = 2 for NaCl, KCl, NH_4Cl and v = 3 for Na_2SO_4, etc.); R, T are defined as before in equation 2.1; m is molality (moles/1000g of solvent) ; ϕ is osmotic coefficient, which can be computed as follows (Lang, 1967):

$$\phi = -\frac{\rho_w}{vmw}\ln\left(\frac{\bar{u}_v}{\bar{u}_{v0}}\right) \qquad \text{(Equation 2.3)}$$

with w = molecular mass of water;

ρ_w = water density.

Table 2.2 lists the osmotic coefficients at 25°C for several electrolyte solutions which are usually employed in the calibration of filter papers and psychrometers (Bulut et al., 2001). Krahn and Fredlund (1972) found that osmotic suction is relatively constant at various water contents and it is reasonable to assume osmotic suction is a fixed value to be subtracted from the total suction measurements. Miller and Nelson (2006) studied the effect of salt concentration on matric suction SWCCs or matric suction

compressibility and concluded that adding salt did not result in a substantially different soil with respect to its volume change response to changes in matric suction (u_a-u_w).

2.1.3.1 Suction Measurements

Suction measurements are essential due to the important role of suction when dealing with expansive problems. The magnitudes of soil suction can range from 0 kPa to 1 GPa. Currently, there is no technique or single technique can measure the entire suction ranges with decent accuracy. Normally, the suction measurement instruments are available and valid for the measured suction level up to around 10 MPa (Rahardjo and Leong, 2006).

Total suction can be measured with the filter paper (non- contact), transistor or thermocouple or chilled-mirror psychrometers, while matric suction can be measured using filter paper (contact), tensiometers, thermal or electrical conductivity sensors and null-type axistranslation apparatuses (pressure plate or pressure membrane). Table 2.3 gives a brief summary of measurement devices for total suction and matric suction.

Table 2.2. Osmotic Coefficients for Different Solutions (Bulut et al., 2001)

Molality (m)	NaCl	KCl	NH_4Cl	Na_2SO_4	$CaCl_2$	$Na_2S_2O_3$	$MgCl_2$
0.001	0.9880	0.9880	0.9880	0.9608	0.9623	0.9613	0.9627
0.002	0.9840	0.9840	0.9840	0.9466	0.9493	0.9475	0.9501
0.005	0.9760	0.9760	0.9760	0.9212	0.9274	0.9231	0.9292
0.01	0.9680	0.9670	0.9670	0.8965	0.9076	0.8999	0.9106
0.02	0.9590	0.9570	0.9570	0.8672	0.8866	0.8729	0.8916
0.05	0.9440	0.9400	0.9410	0.8229	0.8619	0.8333	0.8708
0.10	0.9330	0.9270	0.9270	0.7869	0.8516	0.8025	0.8648
0.20	0.9240	0.9130	0.9130	0.7494	0.8568	0.7719	0.8760
0.30	0.9210	0.9060	0.9060	0.7262	0.8721	0.7540	0.8963
0.40	0.9200	0.9020	0.9020	0.7088	0.8915	0.7415	0.9206
0.50	0.9210	0.9000	0.9000	0.6945	0.9134	0.7320	0.9475
0.60	0.9230	0.8990	0.8980	0.6824	0.9370	0.7247	0.9765
0.70	0.9260	0.8980	0.8970	0.6720	0.9621	0.7192	1.0073
0.80	0.9290	0.8980	0.8970	0.6629	0.9884	0.7151	1.0398
0.90	0.9320	0.8980	0.8970	0.6550	1.0159	0.7123	1.0738
1.00	0.9360	0.8980	0.8970	0.6481	1.0444	0.7107	1.1092
1.20	0.9440	0.9000	0.8980	n/a	n/a	n/a	n/a
1.40	0.9530	0.9020	0.9000	n/a	n/a	n/a	n/a
1.50	n/a	n/a	n/a	0.6273	1.2004	0.7166	1.3047
1.60	0.9620	0.9050	0.9020	n/a	n/a	n/a	n/a
1.80	0.9730	0.9080	0.9050	n/a	n/a	n/a	n/a
2.00	0.9840	0.9120	0.9080	0.6257	1.3754	0.7410	1.5250
2.50	1.0130	0.9230	0.9170	0.6401	1.5660	0.7793	1.7629

Table 2.3. Summary of Suction Measurement Devices(Rahardjo and Leong, 2006)

Device	Suction component measured	Measurement range (kPa)	Equilibrium time
Jet fill tensiometer	Matric	0-100	Several minutes
Small-tip tensiometer	Matric	0-100	Several minutes
Null-typeaxis translation apparatus	Matric	0-1500	Several hours-days
Miniature tensiometer	Matric	0-1500	Several minutes
Filter paper contact	Matric	0-10000	2-5 days
Filter paper non-contact	Total	1000-10000	2-14 days
Thermal conductivity sensor	Matric	10-1500	Several hours-days
Electrical conductivity sensor	Matric	0-1500	6-48 hours
Psychrometer	Total	100-10000	Several minutes-hours

Osmotic suction can be measured using the pore fluid squeezer technique. The osmotic suction value can be indirectly estimated by measuring the electrical conductivity of the pore-water from the soil. A pore fluid squeezer which consists of a heavy-walled cylinder and piston squeezer can be used to extract the pore-water in the soil. The electrical conductivity of the pore-water, which is often higher than that of pure

water, is measured. By using the calibration curve which relates the electrical conductivity to osmotic pressure, the osmotic suction in a soil sample can be inferred (Fredlund and Rahardjo, 1993b).

2.1.3.2 Filter Paper Method (Contact and Non-Contact)

Filter paper method for total and matric suction measurements was originated in Europe in the 1920's and brought to the United States by Gardner (1937). A filter paper in contact with the soil specimen allows water in the liquid phases and solutes to exchange freely and therefore, matric suction is measured. A filter paper not in contact with the soil specimen only permits water exchange in the vapor phase and therefore measures the total suction (Rahardjo and Leong, 2006). The filter paper comes to equilibrium with the soil after several days (an upper limit of 14 days equilibrium time) in a constant temperature environment. The suction value of the soil and the filter paper is equal then and the water content of the filter paper can be measured. The corresponding suction value can be inferred by using a filter paper wetting calibration curve developed with osmotic salt solutions, which is based on the thermodynamic relationship between osmotic suction and the relative humidity (Bulut et al., 2001). The calibration setup is shown in Figure 2.2.

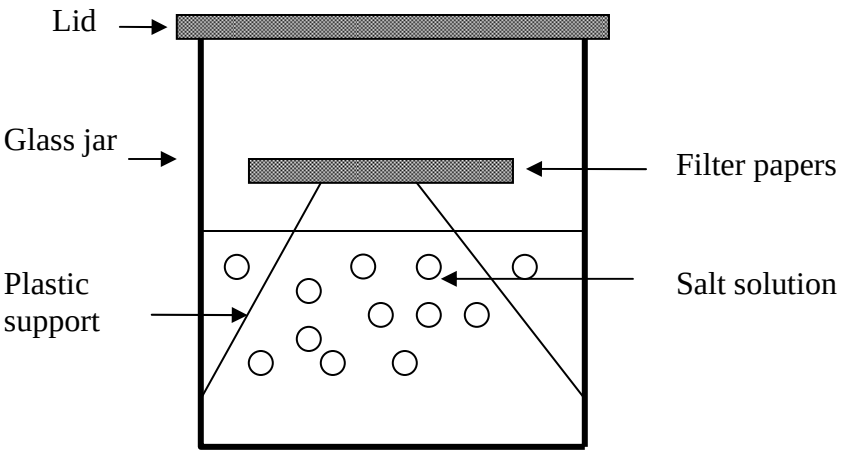

Figure 2.2 Total suction calibration test set up (Bulut et al., 2001)

Whatman No.42 and Schleicher &Schuell (S&S) No. 589-WH are the most commonly used filter papers for suction measurements. The calibration curves for those two filter papers are given in ASTM D 5298-94 (ASTM, 2005b). Bulut et al. (2001) and Leong et al. (2002) have proposed alternative calibration curves.

2.1.3.3 Psychrometers

Thermocouple psychrometers can measure the soil total suction by measuring the relative humidity in the air phase of the soil pores or the region near the soil. The Peltier psychrometer is commonly used in geotechnical practice. It operates on the basis of temperature difference measurements between a non-evaporating surface (dry bulb) and an evaporating surface (wet bulb). The temperature difference is related to the relative humidity. Using Seeback effect and Peltier effect, the thermocouple psychrometer can measure the total suction in a soil sample by using the established calibration curve which relates the microvolt outputs from the thermocouple and a known total suction value. The calibration is performed by suspending the psychrometer which is mounted in

a sealed chamber over a salt solution with known osmotic suction under isothermal conditions (Fredlund and Rahardjo, 1993b). Thermal psychrometers can provide a reliable measurement over the range of pF 3.5 to pF 4.5.

Transistor psychrometers have obtained widespread uses to replace the thermocouple psychrometers for total suction measurement. The transient psychrometer system is composed of three parts: the probes, a thermally insulated bath and a constant temperature room. The probes are enclosed in a thermally insulated bath for the calibration and test purposes. Transient psychrometers can measure the total suction range of pF 3.0 to pF 5.5 with an accuracy of about ± 0.01pF (Bulut et al., 2001). Figure 2.3 gives a schematic depiction of a typical transistor psychrometer probe. The accuracy of transistor psychrometers is very operator-dependent and highly affected by temperature changes in the surrounding environment.

A chilled-mirror psychrometer adopts the chilled mirror dew point technique to measure relative humidity under isothermal conditions in a sealed container (Rahardjo and Leong, 2006). The equalization time to obtain the total suction of soil specimens are normally less than one hour. A chilled-mirror psychrometer can give the measurement of high-range suction greater than 1 MPa.

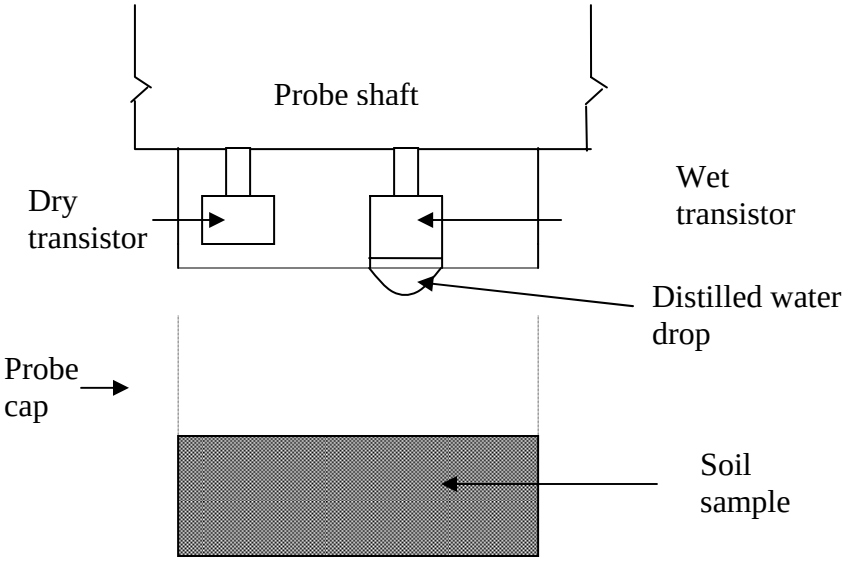

Figure 2.3 Sketch of a transistor psychrometer probe (Bulut et al., 2001)

2.1.3.4 Tensiometers

Tensiometer utilizes a high air entry ceramic cup as an interface between the measuring system and the negative pore-water pressure in the soil. The high air entry, porous ceramic cup is connected to a pressure measuring device through a small bore tube. The tube and the cup are filled with deaired water. Then the cup is inserted into a precored hole and keeps a good contact with the soil. Once equilibrium is established between the soil and the measuring system, the water in the tensiometer has the same negative pressures as the pore-water in the soil (Fredlund and Rahardjo, 1993b), thus matric suction can be measured. Unlike filter paper method and axis-translation apparatus, which can be only used in the laboratory, the tensiometers can be applied both in the laboratory and the field (Fredlund and Rahardjo, 1993b).

2.1.3.5 Axis Translation Apparatus

Hilf (1956) developed the axis-translation technique in which a no-flow condition is maintained during the measurement. Through the use of a high-air entry disk that separates the air phase from the water phase, an air pressure above atmospheric is applied to the soil specimen while the water pressure is kept at a low value that is usually atmospheric. Pressure plate and pressure membrane are typical used to determine the matric suction (u_a-u_w) and the Soil-Water Characteristics Curve (SWCC). The main difference between the pressure plate and pressure membrane apparatus is that the pressure plate uses a ceramic porous disk (normally having the air-entry value of 1 bar, 3 bars, 5 bars or 15 bars) and pressure membrane employs cellulose membranes that can measure higher suction level up to 5 pF (Bulut et al., 2001). The suction equilibrium time is determined by the observation of the variation of the water level in a burette connected to the ceramic disk or cellulose membranes.

Figure 2.4 gives the details of the pressure plate apparatus (Oliveria and Fernando, 2006). Photos of existing MODEL 1500 PPE, which is suitable for measuring matric suction and determining SWCCs for surficial soil conditions with low in-situ over burden pressure, are shown in Figure 2.5. There is no confining pressure applied to the device. Hoyos et al. (2006) proposed a new technique and device for the SWCCs testing for the controlled radial confinement under anisotropic stress state conditions.

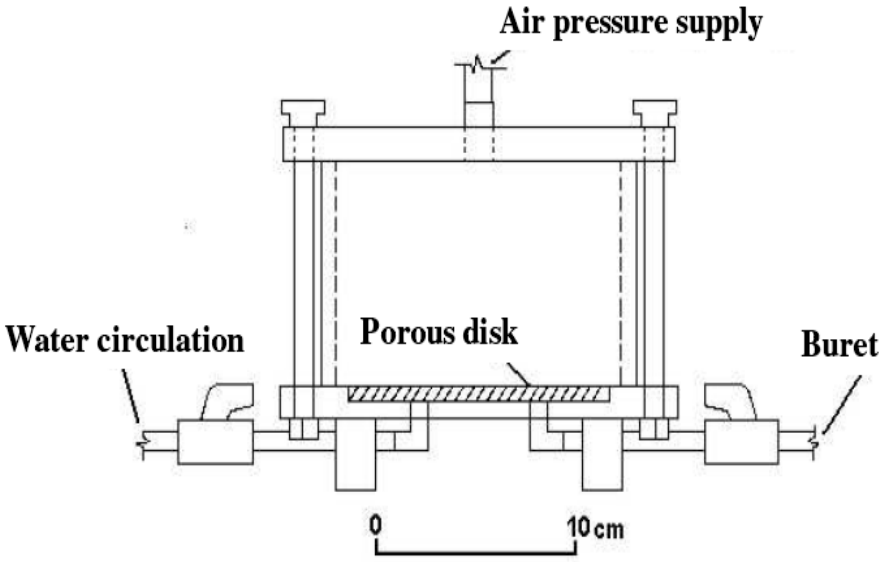

Figure 2.4 Details of pressure plate apparatus (Oliveria and Fernando, 2006)

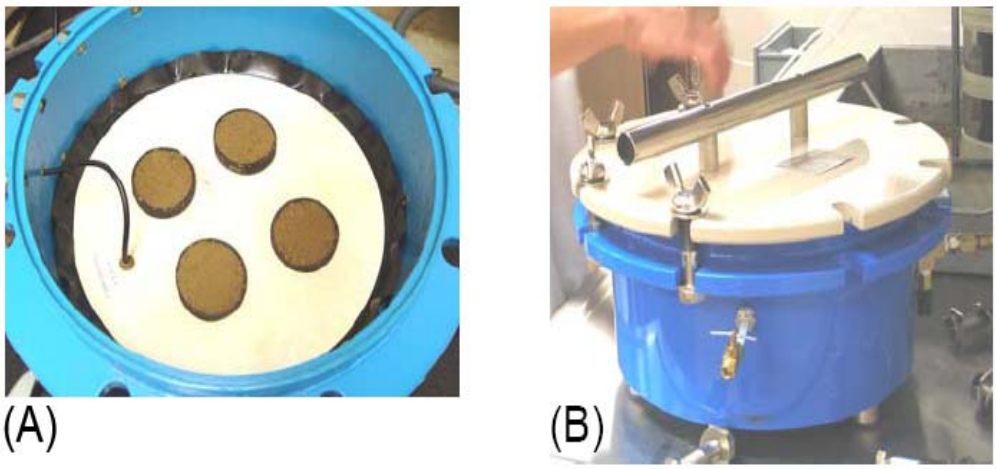

Figure 2.5 Model 1500 PPE device: (a) Sample-retaining rings; (b) Sealed vessel (Hoyos et al., 2006)

2.2 Soil Properties

The non-linear unsaturated soil properties such as Soil-Water Characteristics Curve (SWCC) and permeability function are of paramount importance in analyzing unsaturated moisture flow and forecasting the mechanical behavior (shear strength envelope) of expansive soils. The approaches of empirical equations or laboratory measurements for these properties are summarized below.

2.2.1 Soil Water Characteristic Curve (SWCC)

The soil-water characteristic defines the relationship of soil matric suction (u_a-u_w) and gravimetric water content w, or the volumetric water content θ, or the degree of saturation S_r and is a measure of the water storage capacity of the soil for a given matric suction (u_a-u_w). The air entry value and high residual suction level can be derived from the SWCC. It can also be used as a tool to empirically estimate the permeability function and the shear strength of expansive soils together with the saturated soil properties. In the laboratory, SWCC can be determined from the devices such as the suction plate, the pressure plate and filter paper.

Ng and Pang (2000) found that the soil-water characteristic of the soil specimens is strongly dependent on the confining stress. There is a general and consistent trend for a soil specimen to possess a larger air-entry value when it is subjected to a higher stress.

SWCC is normally plotted on a semi-logarithmic scale for the suction range used in geotechnical practice. A typical soil-water characteristic curve, from which the key features of the curve will be derived and explained, is given in Figure 2.6.

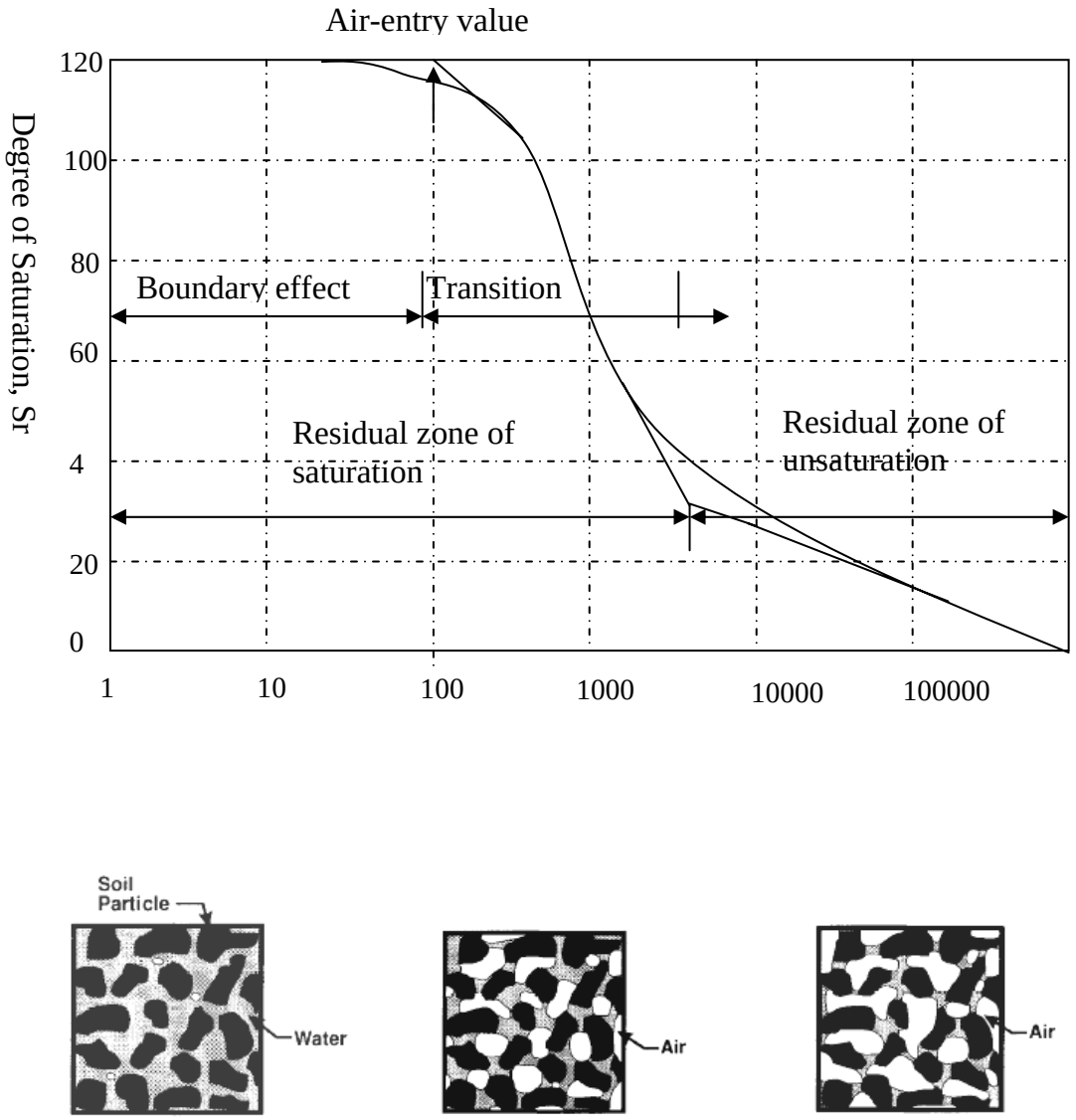

(a) Boundary effect zone (b) Transition zone (c) Residual zone of unsaturation

Figure 2.6 Typical soil-water characteristic curve SWCC (Vanapalli et al., 1996)

In Figure 2.6, the air entry value or bubbling pressure stands for the differential pressure between the air and water that is required to cause desaturation of the largest pores (Vanapalli et al., 1996). It is important to emphasize that the process of desaturation occurs only at suction values greater than the air entry value. At suction values smaller than the air entry value, the soil still remains saturated. The air entry value of the soil can be estimated by extending the constant slope portion of the soil-water characteristics to intersect the suction axis at 100% saturation.

There are three identifiable stages of desaturation: the boundary effect stage, the transition stage and the residual stage of unsaturation. In boundary effect stage, water fills in all the soil pores. The soil is saturated in this region, while in transition zone, the connectivity of the water in the voids or pores continue to reduce with increased values of suction, and eventually large increases in suction lead to relatively small changes in the degree of saturation. And the residual state of saturation can be considered to be the degree of saturation at which the liquid phase becomes discontinuous. The residual state of saturation represents the stage beyond which it becomes increasingly difficult to remove water from a specimen by drainage (Vanapalli et al., 1996).

Hysteresis depending on suction history occurs in the water characteristic curve, due to the fact that there are three forms of pore water in an unsaturated soil as mentioned in chapter I.

2.2.1.1 Soil-Water Characteristic Curve Equations

Since the laboratory determination of SWCCs is normally time-consuming and expertise required, many empirical equations have been proposed to provide a quick and simple prediction using soil parameters such as residual volumetric water content and some fitting numbers.

(a) Gardner's Equation

Gardner (1958) proposed a three parameter soil characteristic curve function shown in Equation 2.4:

$$\theta_w = \theta_r + \frac{\theta_s - \theta_r}{1 + (\frac{u_a - u_w}{a})^b} \qquad \text{(Equation 2.4)}$$

Where θ_w = the volumetric water content;

θ_r =residual volumetric water content;

θ_s =the saturated volumetric water content.

a,b=matric suction value that corresponds to a volumetric water content of $(\frac{\theta_r + \theta_s}{2})$ and the slope factor.

(b) Brooks and Corey's Equation

Brooks and Corey (1966) suggested equation 2.5 for the soil characteristic curve:

$$\theta_w = \theta_r + (\theta_s - \theta_r)(\frac{a}{u_a - u_w})^b \qquad \text{(Equation 2.5)}$$

Where a = the air entry matric suction (u_a-u_w) value;

b = a fitting constant

(c) Lytton's Equation

When the pressure-plate test data are not available, Lytton (1997) presented the following empirical relationship based on a soil-science database with 6000 data points:

$$S = -20.29 + 0.155(LL\%) - 0.117(PI\%) + 0.0684(\%Fines).$$

Where S=slope of the log (matric suction) versus gravimetric water content curve.

LL = the liquid limit; PI = the plasticity index.

% Fines = the percentage of particle sizes passing the No.200 sieve on a dry weight basis.

2.2.2 Coefficient of Permeability

Defined by Darcy's law, the coefficient of permeability is a key parameter for expansive soil problems involving unsaturated moisture flow and seepage analysis. The laboratory measurement of permeability coefficient measurement is usually very time-consuming and difficult to control. The demand for accuracy requirement is to have a good water volume change measurement. In the field, the in-situ soil hydraulic properties are commonly measured using double-ring infiltrometers in conjunction with tensiometers for measuring matric suction values (u_a-u_w). Indrawan et al. (2006) conducted a series of field infiltration tests to study the infiltration characteristics of expansive soil in the field. One-dimensional vertical flow of water can be expected to occur below the inner ring since the infiltrating water through the outer ring acts as a barrier that reduced lateral movements of water from the inner ring.

Since the difficulties and high degree of required expertise involved with the actual measurements, many empirical equations have been developed to express the

coefficient of permeability k_w as a function of water content w and total suction value ψ (Table 2.4), where θ_s stands for saturated water content. In Table 2.4, a and b are fitting constants, and k_s denotes the coefficient of permeability for saturated soils.

2.2.3 Thermal Properties

Duarte et al. (2006) used thermal needles to study the thermal properties of expansive soils and observed that thermal properties (thermal conductivity and specific heat) are not constant for a given soil but varies with gravimetric water content, degree of saturation and temperature. Their results show that the thermal conductivity varies exponentially with gravimetric water content and degree of saturation whereas specific heat alters linearly with gravimetric water content and temperature.

2.3 Stress Variables

Although new evidence supporting the validity of effective stress approach in unsaturated soils has been presented (Khalili et al., 2004), the two independent stress state variable approach proposed by Fredlund and Morgenstern (1977) has been widely accepted for the study of expansive soils. Most commonly, the net normal stress $[\sigma_{ij} - u_a\delta_{ij}]$ and matric suction $\delta_{ij}[u_a - u_w]$ are taken as the stress state variables. Fredlund and Morgenstern (1977) used "null" tests which employed an axis-translation technique (Hilf, 1956) and gave experimental support for the validity of the proposed independent stress state variables. However, other stress variables have been proposed based on their ability to more effectively describe constitutive behavior (Wheeler et al., 2003).

Table 2.4 Empirical Permeability Functions (Leong and Rahardjo, 1997)

Type	Permeability Functions	
$k = f(\theta_w)$	$k_w = a\theta_w^{\ b}$	Gardner (1958)
	$k_w = k_s(\frac{\theta_w}{\theta_s})^{2b+3}$ and b= $\frac{\Delta \log \psi}{\Delta \log \theta_w}$	Campbell (1973), Ahuja (1973, 1974)
	$k_w = k_s(\frac{\theta_w}{\theta_s})^{2b+3}$ and b= $\frac{\Delta \log \psi}{\Delta \log \theta_w}$	Gillham et al. (1976), Zachmann et al.(1981)
	$k_w = k_s \exp[b(\theta_w - \theta_s)]$	Hillel (1982), Davidson et al. (1969), Dane and Klute (1977)
$k = f(\psi)$	$k_w = a + b\psi$	Richards (1931)
	$k_w = a\psi^{-b}$	Wind(1955), Laliberte et al. (1966)
	$k_w = \frac{k_s}{1 + a(\frac{\psi}{\rho_w g})^b}$	Weeks and Richards (1967)
	$k_w = a\exp(b\psi)$	Christensen (1943),
	$k_w = k_s$ for $\psi \le \psi_b$ and $k_w = k_s \exp[b(\psi - \psi_b)]$ for $\psi > \psi_b$	Rijtema (1965), Phillip (1986)

*Gardner's permeability equation can only be applied in the moisture inactive zone

2.4 Shear Strength Prediction

Shear strength prediction is critical in many expansive soil problems, such as slope stability and retaining walls' design. The formulation of shear strength is based on Mohr-Coulomb criterion.

Bishop and Blight (1963) defined the equation of interpreting the shear strength using effective stress approach as given in equation 2.6:

$$\tau_f = c' + (\sigma - u_a)\tan\phi' + \chi(u_{a-}u_w)\tan\phi' \qquad \text{(Equation 2.6)}$$

where c' is the intercept of the extended Mohr-Coulomb failure envelope on the shear stress axis referred to as effective cohesion. Effective cohesion is a function of bulk density, clay content, clay mineralogy, and moisture content (McCormack and Wilding, 1979). And χ is the effective stress parameter, attaining a value of one for saturated soils and zero for pure dry soils.

Fredlund et al. (1978) presented the widely used shear strength formulation using two independent stress variables:

$$\tau_f = c' + (\sigma - u_a)\tan\phi' + (u_a - u_w)\tan\phi^b \qquad \text{(Equation 2.7)}$$

where ϕ^b is the angle indicating the rate of increase of shear strength with respect to the matric suction (u_a-u_w). At the low matric suction level (matric suction less than air-entry value), ϕ^b is equal to ϕ'. ϕ^b decreases to a lower value at high matric suction level (matric suction greater than air-entry value) as indicated in Figure 2.7. However, Gan and Fredlund (1988) conducted multistage direct shear tests and observed that ϕ^b can be

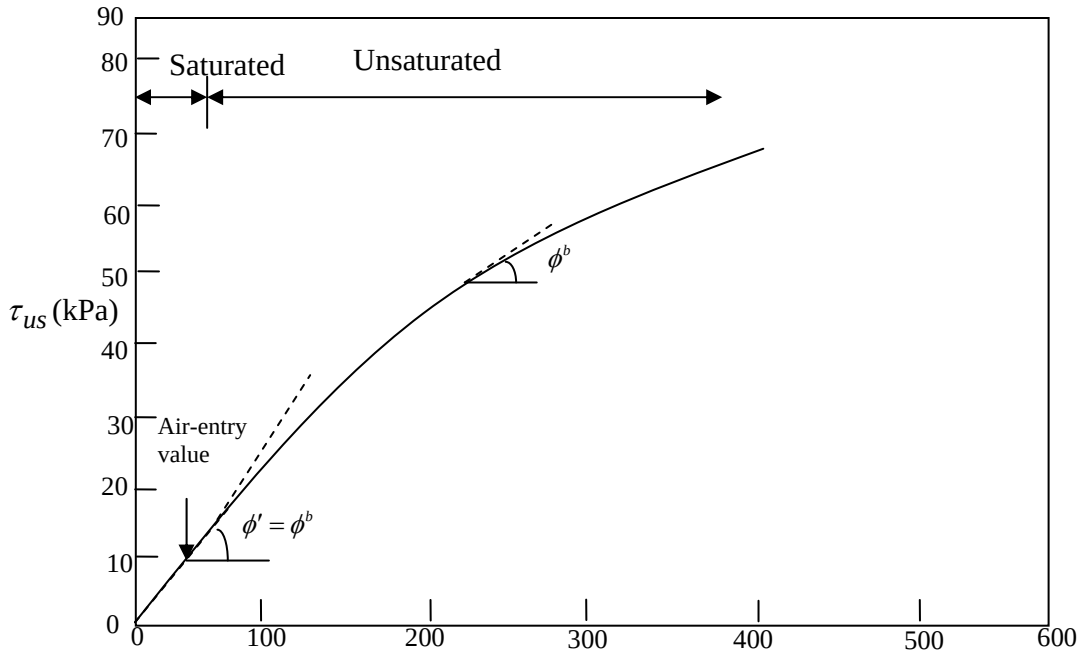

Figure 2.7 Shear strength variation due to matric suction (Tekinsoy et al., 2004)

greater than ϕ' angle. $(u_a - u_w)\tan\phi^b$ is called suction strength, which is the shear strength contribution due to matric suction or capillary force.

Lytton (1995) formulated equation 2.8 for shear strength calculation based on Lamborn's theory (1986):

$$\tau = c' + [(\sigma - u_a) + f\theta(u_a - u_w)]\tan\phi' \qquad \text{(Equation 2.8)}$$

in which, θ is the volumetric water content and f is the unsaturated shear strength function. When the matric suction (u_a-u_w) is lower than air-entry value, the soil is saturated and f equals to $\frac{1}{\theta}$. After the continuous air voids develop or the suction

becomes larger than residual matric suction, f approaches the unity. For the transition zone between the air entry value and a continuous air phase state, f is bounded by a lower limit f_2 and an upper limit f_1 as described by equation 2.9:

$$f_1 = \left(\frac{\theta_a - \theta}{\theta_a - \theta_u}\right) + \frac{1}{\theta}\left(\frac{\theta - \theta_u}{\theta_a - \theta_u}\right)$$

$$f_2 = \frac{1}{\left(\frac{\theta_a - \theta}{\theta_a - \theta_u}\right) + \theta\left(\frac{\theta - \theta_u}{\theta_a - \theta_u}\right)} \qquad \text{(Equation 2.9)}$$

where θ_a is the volumetric water content at air entry point (pF=2.0) and θ_u is the volumetric water content for residual suction (around pF=3.5) (Lamborn, 1986). The upper bound and low bound for transition zone is plotted in Figure 2.8.

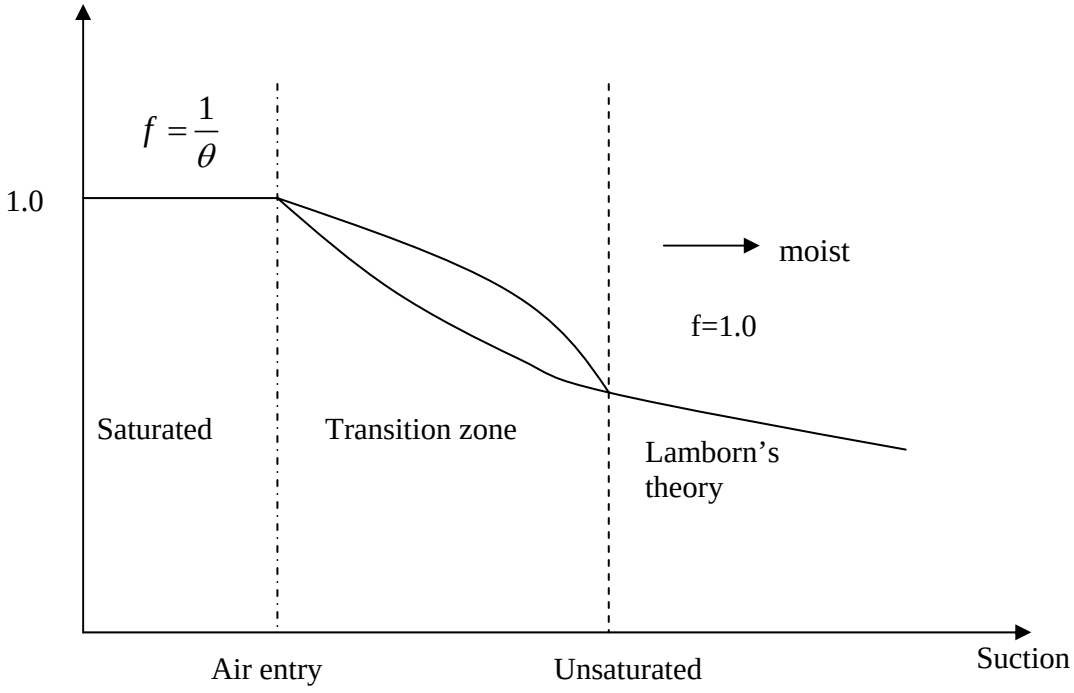

Figure 2.8 Value of f at transistor zone (Lytton, 1995)

2.4.1 Laboratory Measurements

The experimental determination of the shear strength of expansive soil requires elaborate and expensive testing equipment. Also the testing procedures are complex and time-consuming and need expertise to perform the tests.

The modified triaxial apparatus, which allow the control of both pore-air and pore-water pressures using the axis-translation technique (Hilf, 1956), are normally used for the Consolidated Drained (CD) or Constant Water Content (CW) triaxial tests to determine the shear strength of unsaturated soils. The test procedures involve the Saturation stage, Consolidation and Matric Suction Equalization stages, and Shearing stage (Thu et al., 2006). During the Saturation stage, the specimen is saturated by applying a cell pressure σ_3, and a back pressure u_w, until the pore-water pressure parameter B is close to 1 (or greater than 0.97) (Head, 1986). At the stage for matric suction equalization, the water pressure line connected to the top loading cap was disconnected from the water pressure line and reconnected to the air pressure line. Under an isotropic confining pressure, the soil specimen is allowed to consolidate. Normally three to five days are needed for the completion of matric suction equalization stage.

For Constant Water Content (CW) triaxial test, at the shearing stage, the soil specimen is sheared under drained conditions for the pore-air phase and undrained conditions for the pore-water phase. The valve for the air pressure line is opened and controlled at a required pressure while the valve for the water pressure lines is closed during shearing. For the Consolidated Drained (CD) triaxial test, during the shearing stage, the soil specimen is sheared under drained conditions for both the pore-air and

pore-water phases. The valves for the air pressure and water pressure lines are opened and controlled at the required pressures.

Thu et al. (2006) conducted a series of CD and CW tests to study the effects of hysteresis on shear strength envelope. They stated that the non-linearity was observed in the relationship between ϕ^b and matric suction (u_a-u_w) for the tested silt sample. ϕ^b value is the same as ϕ' at suction level lower than air-entry value and high suction level larger than residual matric suction value. However, ϕ^b angles from the CW and CD tests were different at matric suctions between the air-entry value and the residual matric suction value. The difference was due to the lower failure envelope with respect to matric suction from the CW tests as compared to the failure envelope from the CD tests within the test range of matric suction and the difference can be explained given the fact that the hysteretic behavior exists in the Soil-Water Characteristic Curve (SWCC).

2.4.2 Empirical Predictions

Given the difficulty involved in experimental determination of shear strength for expansive soils, several investigators proposed empirical procedures for predicting the suction strength employing SWCC property and the saturated shear strength parameters or using fitting parameters and other mathematical formulations.

Garven and Vanapalli (2006) reviewed the existing empirical prediction equations and provided a summary of nineteen available empirical procedures or techniques as given in Table 2.5 and concluded that to date, there is no single prediction equation which is found suitable for reliably predicting the shear strength of all types of expansive soils.

Table 2.5. Semi-Empirical Equations to Predict Shear Strength in Unsaturated Soils (Garven and Vanapalli, 2006)

Eq 1: Lamborn (1986)

$$\tau_{us} = (u_a - u_w)\theta_w \tan\phi'$$

Eq.2: Abramento & Carvallho (1989)

$$\tau_{us} = a(u_a - u_w)^{\beta}$$

Eq.3: Lu(1992)

$$\tau_{us} = P_S \tan\phi'$$

Eq.4: Vanapalli et al. (1996)

$$\tau_{us} = (u_a - u_w)(\Theta^k)(\tan\phi')$$

Eq 5: Vanapalli et al (1996)

$$\tau_{us} = (u_a - u_w)\left(\frac{\theta_w - \theta_r}{\theta_s - \theta_r}\right)(\tan\phi')$$

Eq.6: Shen (1996)

$$\tau_{us} = \frac{(u_a - u_w)}{1 + d \cdot (u_a - u_w)} \tan\phi'$$

Eq.7: Oberg & Sallfours(1997)

$$\tau_{us} = (u_a - u_w)(S)(\tan\phi')$$

Eq. 8: Xu (1997)

$$\tau_{us} = k^n (u_a - u_w)^{m-n+1}(\tan\phi')$$

Eq.9: Yu (1998)

$$\tau_{us} = \frac{(u_a - u_w)\tan\phi'}{\cot\alpha_1 + \frac{(u_a - u_w)}{\beta_1}}$$

Eq. 10: Bao et al. (1998)

$$\tau_{us} = (u_a - u_w)\left[\frac{\log(u_a - u_w)_r - \log(u_a - u_w)}{\log(u_a - u_w)_r - \log(u_a - u_w)_b}\right]$$

$$(\tan\phi')$$

Eq. 11: Khalili &Khabbaz (1998)

$$\tau_{us} = (u_a - u_w)[(\chi)(\tan\phi')];$$

$$\chi = \left\{\frac{(u_a - u_w)}{(u_a - u_w)_b}\right\}^{-0.55}$$

Eq.12: Rassam and Williams (1999)

$$\tau_{us} = (u_a - u_w)\tan\phi'$$

$$if\ (u_a - u_w) < AEV, \text{else}$$

$$\tau_{us} = (\gamma + \lambda(\sigma_3 - u_a)) \cdot [(u_a - u_w) - AEV]^{\beta 1}$$

$$+ (u_a - u_w)\tan\phi'$$

Eq. 13: Xu and Sun (2001)

$$\tau_{us} = (u_a - u_w)_b^{1-\xi}(u_a - u_w)^{\xi} \tan\phi'; \xi = \frac{2D_S}{3} - 1$$

Eq. 14: Rassam and Cook (2002)

$$\tau_{us} = (u_a - u_w)\tan\phi' + \varphi$$

$$((u_a - u_w) - (u_a - u_w)_b)^{\beta}$$

$$\varphi = \frac{(u_a - u_w)\tan\phi' - \tau_{sr}}{((u_a - u_w)_r - (u_a - u_w)_b)^{\beta}};$$

$$\beta = \frac{\tan\phi'((u_a - u_w)_r - (u_a - u_w)_b)}{(u_a - u_w)_r \tan\phi' - \tau_{sr}}$$

Table 2.5. (Continued)

Eq. 15: Miao et al. (2002) $\tau_{us} = \frac{a(u_a - u_w)}{1 + \frac{(1-a)}{P_{at}}}(u_a - u_w)$ Eq. 16: Schick (2004) $\tau_{us} = \frac{(u_a - u_w)}{a_1 + b_1(u_a - u_w)} \tan\phi^{'};\ a_1 = \tan(\phi^{'} - 90^{\circ})$ Eq. 17: Xu(2004) $\tau_{us} = (u_a - u_w)b^{(1-\varsigma)} \cdot (u_a - u_w)^{\varsigma} \cdot \tan\phi^{'};$ $\varsigma = D_S - 2$	Eq. 18: Tekinsoy et al. (2004) $\tau_{us} = \tan\phi^{'}((u_a - u_w)_b + P_{at}) \cdot \ln[\frac{(u_a - u_w) + P_{at}}{P_{at}}]$ $\tau_{us} = \tan\phi'((u_a - u_w)b + P_{at}) \cdot \ln[\frac{(u_a - u_w) + P_{at}}{P_{at}}]$ Eq. 19: Lee et al. (2005) $\tau_{us} = (u_a - u_w) \cdot (\tan\phi'), if\ (u_a - u_w) < AEV,$ $ELSE$ $\tau_{us} = AEV \cdot (\tan\phi') + [(u_a - u_w) - AEV](\theta^k)$ $[1 + \lambda(\sigma_3 - u_a)](\tan\phi')$

τ_{us} – shear strength contribution due to suction D_s-pore distribution factor

τ_{sr} – contribution of suction shear strength at residual suction

$\phi^{'}$ – effective angle of internal friction

P_{at}- atmospheric pressure (101.3 kPa)
(u_a-u_w)- matric suction
$(u_a-u_w)_b$- air entry value
$(u_a-u_w)_r$ - residual suction
S_r-degree of saturation
S_{rr}- residual degree of saturation
P_s- expansive force
Θ – normalized water content or degree of saturation
θ_w -volumetric water content
θ_s – saturated volumetric water content
θ_r – residual volumetric water content
ς – fractal dimension
AEV- the air entry value an equivalent net normal stress
$k, \gamma, \lambda, \beta, \beta_1, \alpha$ – fitting parameters
a, b_1, d, k-fitting parameters
m,n-parameters relating to the fractal dimension
χ -Bishop's fitting parameter.

2.5 Unsaturated Moisture Flow Analysis

The general non-linear Richard's equation and simplified linear Mitchell's formulation for unsaturated moisture flow analysis are discussed here. The related material parameters such as Equilibrium Suction u_e, depth of moisture active zone, diffusion coefficient α as well as the simulation for modeling water uptake by vegetation are also given.

2.5.1 Richard's Equation

Richards (1931) presents the earliest theoretical work for unsaturated flow analysis. He employed the conservation law of mass and Darcy's law to formulate Richards's equation for transient flow analysis:

$$C(h)\frac{\partial \phi}{\partial t} = \nabla \bullet (k(\theta)\nabla \phi) \qquad \text{(Equation 2.10)}$$

where $\phi = h + z =$ hydraulic head,

h=total suction,

z=elevation head,

c(h)=$\frac{d\theta}{dh}$ =specific moisture capacity,

k(θ)=hydraulic conductivity

θ(h)=volumetric moisture content,

t=time (sec), and ∇ ="del" operator

In this equation, three assumptions are adopted: 1) the soil and moisture are both incompressible; (2) the flow of moisture occurs under isothermal conditions; (3) air within the soil is at the ambient atmospheric pressure.

2.5.2 Mitchell's Simplified Linear Analysis

2.5.2.1 Formulation

Mitchell (1979) proposed a linearized analysis in which the slope of Soil-Water characteristic Curve (suction versus gravimetric water content) S is a constant, by invoking the conservation of mass condition in a manner that parallels the well-known formulation for saturated flow to get the diffusion equation (Equation 2.11):

$$\nabla^2 u + \frac{f(x,y,z,t)}{p} = \frac{1}{\alpha}\frac{\partial u}{\partial t} \qquad \text{(Equation 2.11)}$$

in which u= total suction in a pF scale;

t=time and α =diffusion coefficient=-S $\frac{k_0 h_0}{0.434}\frac{\gamma_w}{\gamma_d}$;

h_0=total suction corresponding to reference state;

γ_d =soil dry unit weight;

f(x,y,z,t)=moisture inflow rate per unit volume;

p=unsaturated permeability, which equals to $\frac{\alpha\gamma_d}{|S|\gamma_w}$

2.5.2.2 Material Parameters

For Mitchell's simplified moisture flow analysis, the paramount material parameters are equilibrium suction u_e, the diffusion coefficient α and depth of moisture active zone as introduced in detail below.

(a) Equilibrium Soil Suction u_e

Equilibrium Soil Suction represents a suction value that develops in a soil deposit at the depth of moisture active zone (the zone of suction variations in response to

environmental factors) as a result of multiple weather cycles at the surface (PTI 3rd Edition, 2005). The constant equilibrium suction is normally expressed as a function of TMI. The constant suction value is also dependent on local site conditions such as cemented soil, high osmotic suction and presence of high water table or rocks, in which case the correlation with TMI is invalid. Recent studies have shown that the equilibrium soil suction at active zone depth at a given TMI heavily depends on the soil type (Perera, 2004), which agrees with the scatter of values and the poor statistical significance of the proposed correlation in the PTI 3rd Edition. Figure 2.9 gives the equilibrium suction as a function of climate (Aubeny and Long, 2006).

Lytton (1997) and PTI 3rd Edition (2005) recommend equilibrium suction values for specific field conditions. When a shallow water table is present and osmotic suction is negligible, the method recommends using a equilibrium suction equal to pF2.0. When large trees are evident at the site, the controlling suction should be equal to pF4.5 throughout the tree root zone. For the scenario that the soil is cemented or known to have high osmotic suction, the equilibrium suction value has to be determined experimentally.

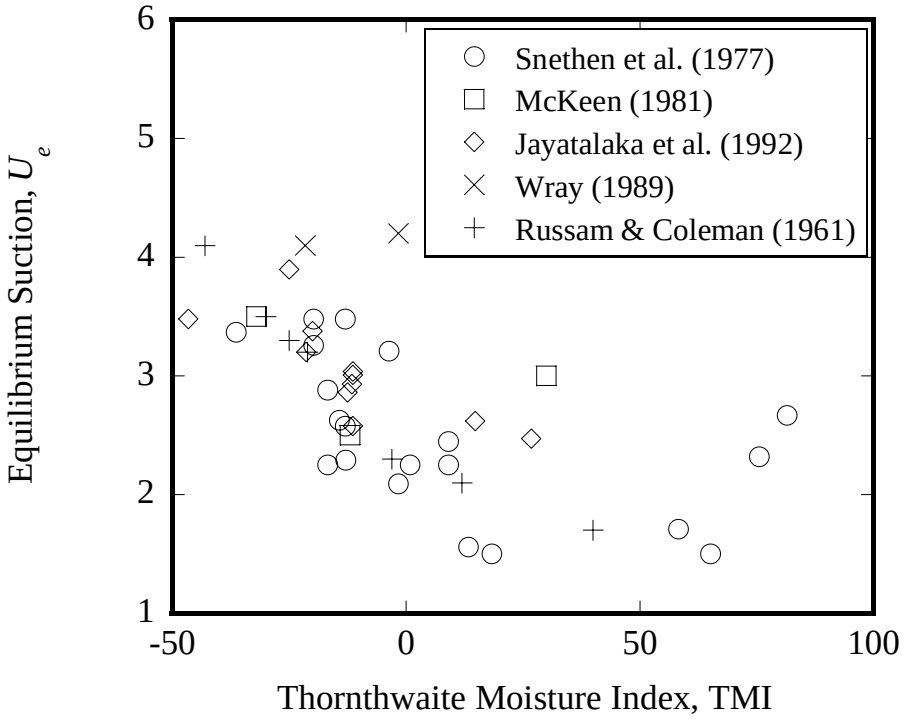

Figure 2.9 Equilibrium suction as a function of climate (Aubeny and Long, 2006)

(b) Depth of Moisture Active Zone Z_m

Moisture active zone depth refers to the depth below the ground surface at which changes in moisture content (soil suction) can be expected due to environmental changes or other causes. It is also the location of the equilibrium soil suction (PTI 3rd Edition, 2005). The soil within moisture active zone can undergo large changes of suction between its established wet and dry limits and subject large and constant shrinkage and swell.

Depth of moisture active zone Z_m depends on the diffusion characteristic of the upper soil region such as the presence of soil broken in to clods and peds, and the

amplitude of moisture variation at the ground surface. Lytton (1997) gives five criterions to indicate the depth of moisture active zone summarized as follows:

(1) The first point at which the total suction does not vary more than $0.08\log_{10}|\text{mm}|$ suction units per meter with depth. The suction level at which it occurs is the equilibrium suction level;

(2) A permanent water table or one that is changing its elevation steadily over a multiple-year period. The location of the water table can be measured in the field or inferred by projecting the total suction in mm downward on a 1:1 slope until it reached the wet limit of suction in clay of 3162mm (pF2.5 or -31kPa);

(3) A distance 0.6m below the deepest recorded root fiber. The moisture active zone is where moisture can move quickly in and out of the soil in the cracks formed principally by vegetation. Roots can fracture the soil approximately 0.6m beyond or deeper than the location of the rot fiber. The soil moisture beyond that point is influenced by changes of suction in the root zone but at the slower rate for intact soil governed by Gardner's relation;

(4) Soils with high matrix suction, like a cemented soil with high level of matrix suction nearly equaling the total suction, can't support vegetation and will not be cracked by it. So the soil is intact and indicates the depth of soil moisture active zone;

(5) Maximum rate of vertical flow criterion, according to which water is permitted to flow vertically upward or downward at a rate no greater than 100mm/yr using the Mitchell hydraulic conductivity relation, can be also applied to mark the lower

limit of moisture active zone. If it happens that two or three criterions can be applied simultaneously, usually the most conservative one should be adopted.

In PTI 3rd Edition, in absence of the computer program VOLFLO 1.5 (2005), the depth of moisture active zone can be assumed to be 9ft below the ground surface. In the computer program FLODEF, the depth of moisture active zone is conservatively set to equal to 20ft in the absence of specific field data.

(c) Moisture Diffusion Coefficient α

The moisture diffusion coefficient α is the function of two soil properties: the coefficient of permeability k_w and slope of Soil-Water Characteristics Curve (SWCC). With the introduction of diffusion coefficient concept, the analysis of moisture diffusion through unsaturated soils can be convenient simplified.

The moisture diffusion coefficient α controls the rate of moisture infiltration during the transient moisture flow process, the depth and distributions of suction variations within the soil mass due to environmental factors. It can be measured in the laboratory with wire-screen thermocouple psychrometers from wetting or drying tests as described by Mitchell (1979) or back-calculated from field suction measurements. Comparisons of field versus laboratory measurements of α show field values can exceed laboratory measurements by up two orders of magnitude. A likely cause of the difference is the existence of root holes and desiccation cracks in the field, which often do not occur in the essentially intact soil specimens tested in the laboratory. Chapter VI gives a relationship between field measurement and laboratory measurement of moisture diffusion coefficient obtained from a series of numerical studies.

2.5.2.3 Simulation of Water Uptake by Vegetation

The prediction of evaporative fluxes from unsaturated soil surfaces is normally required in moisture flow analysis. The surface boundary flux is computed from the difference between the infiltration and exfiltration processes at the surface. Exfiltration was computed from estimates for actual evapotranspiration. Actual evapotranspiration can be estimated from computations of potential evapotranspiration and empirical correlations between actual and potential values for evapotranspiration, while potential evapotranspiration is defined as the moisture loss from a surface completely covered with vegetation when there is an unlimited supply of water available for plant use (Thornthwaite and Mather, 1955).

The water uptake by vegetation is affected by the soil conditions, type of vegetation, and atmospheric conditions. Prasad (1988) suggested a linear variation in root water extraction rate with depth. The model assumed a zero root water extraction rate at the bottom of root zone depth.

Prasad's model is adopted in the computer program FLODEF for moisture flow analysis and will be given a detailed presentation in Chapter III.

Cutler and Richardson (1989) studied the relationship between root spread and the height of trees. They suggested that root spread for a single tree is approximately similar for both depths and radius. Biddle (1998) shows that as the radial distance from the trunk of the tree increases, the water extracted by the roots decreases. In view of the observations by these researchers, Ali and Rees (2006) used several assumptions for their studies of water uptake by tree roots: (1) that root water extraction is the maximum directly beneath the tree; (2) a linear relationship exists between root water extraction and radial distance; (3) and the root water extraction becomes zero at some maximum radius. The two-dimensional model for their simulation is given in Figure 2.10.

2.6 Prediction of Volume Change Behavior

The soil properties recognized as influencing expansive soil volume change behavior include: soil fabric, mineralogy, saturating cation, electrolyte concentration and speciation, clay content, surface area, antecedent soil moisture content. Other factors such as macro- and microclimate, topography, vegetation, frequency of desiccation or rewetting cycles, confining pressures also affect the behavior (Wilding and Tessier, 1988).

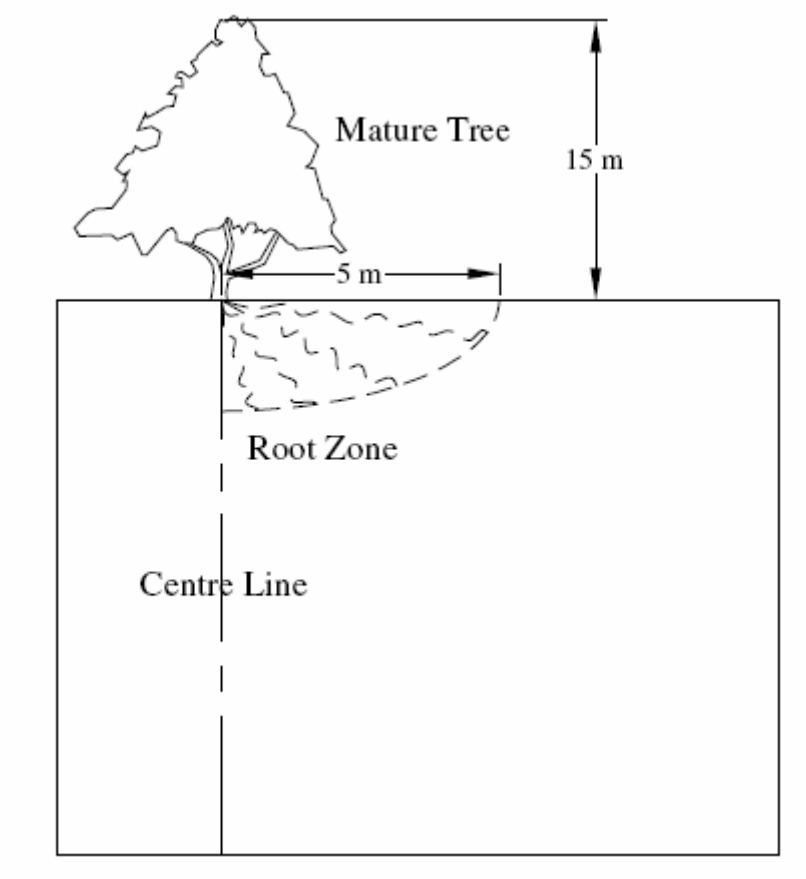

Figure 2.10 The two-dimensional model for simulation of water uptake by vegetation (Ali and Rees, 2006)

2.6.1 Nonlinear Elastic Constitutive Law for Volume Change Prediction

Fredlund and Morgenstern (1977) used elasticity form to present the constitutive law for small strain volume change calculation in equation 2.12:

$$de = a_t d(\sigma_{mean} - u_a) + a_m d(u_a - u_w)$$
$$dw = b_t d(\sigma_{mean} - u_a) + b_m d(u_a - u_w) \quad \text{(Equation 2.12)}$$

where, a_t=coefficient of compressibility with respect to a change in net normal stress, $d(\sigma_{mean} - u_a)$; and a_m=coefficient of compressibility with respect to a change in matric suction, $d(u_a-u_w)$;

b_t= coefficient of water content change with respect to a change in net normal stress and b_m= coefficient of water content change with respect to a change in matric suction

The void ratio and water content constitutive surfaces are given in Figure 2.11.

Lytton (1994) presented a general equation between the volumetric strain, the matric suction and osmotic suction for expansive soil shrink-swell prediction, while. equation 2.13 denotes swelling case and equation 2.14 denotes for shrinkage case:

$$\varepsilon_v = \gamma_h \log_{10}(\frac{h_f}{h_i}) + \gamma_\sigma \log_{10}(\frac{\sigma_f}{\sigma_i}) + \gamma_\pi \log_{10}(\frac{\pi_f}{\pi_i}) \qquad \text{(Equation 2.13)}$$

$$\varepsilon_v = \gamma_h \log_{10}(\frac{h_f}{h_i}) - \gamma_\sigma \log_{10}(\frac{\sigma_f}{\sigma_i}) + \gamma_\pi \log_{10}(\frac{\pi_f}{\pi_i}) \qquad \text{(Equation 2.14)}$$

where h_i, h_f=initial and final matric suction in positive sign;

σ_i =the level of mean principal stress required for the overburden effect

σ_f = the current mean principal stress level for the soil column

π_i, π_f =initial and final osmotic suction;

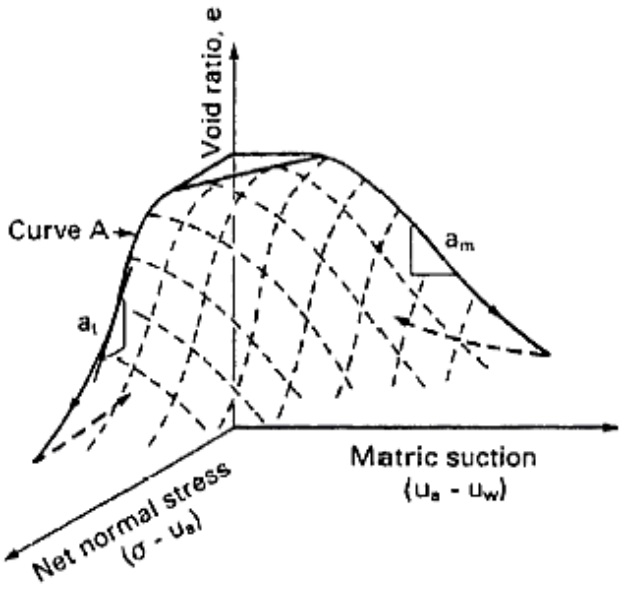

(a) Void ratio constitutive surface

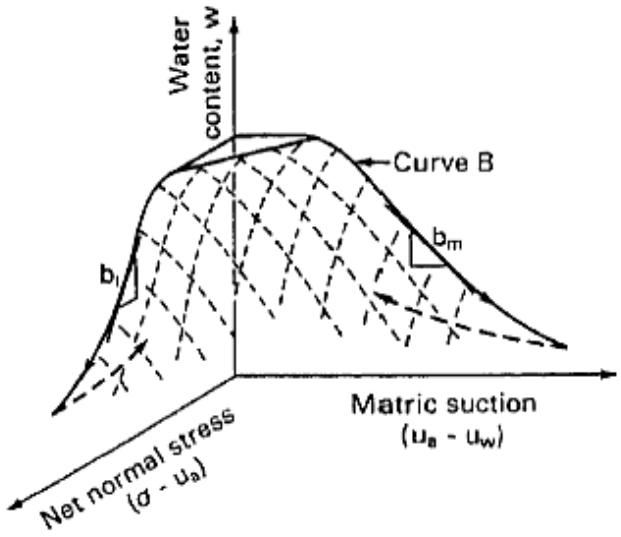

(b) Water content constitutive surface

Figure 2.11 Void ratio and water content constitutive surfaces for unsaturated soils (Fredlund and Rahardjo, 1993b)

γ_h =volume change coefficient due to matric suction changes

γ_σ =volume change coefficient due to overburden change;

γ_π =volume change coefficient due to osmotic suction changes

The relationship between volume strain, suction and mean principal stress is graphically presented in Figure 2.12. Lytton's approach for the volume change calculation is incorporated into the third edition of PTI manual. The computer program FLODEF utilized Lytton's model for the surface movement prediction. The details of the model parameters will be introduced in the later chapters.

2.6.2 Elasto-plastic Constitutive Law for Volume Change Prediction

Plastic strains can occur when the deviatoric stress increases and the matric suction decreases. Also the elastic models can explain poorly the stress path dependence as well as soil collapse behavior (Lloret and Alonso, 1980). For the purpose of a better understanding and explanation of expansive soil behaviors, a variety of elasto-plastic constitutive models are introduced and studied by researchers such as Alonso et al. (1990), (Barcelona Basic Model) and Wheeler et al. (1995), (coupled model). The details for the proposed elasto-plastic constitutive models will not be covered here since lytton's non-linear elastic model is employed for the pavement surface movement analysis. Field experience indicates that for pavement structure, due to periodic wetting and drying cycles, volumetric strain lies in the range of elastic strain. The future improvement for the computer program will be the incorporation of plastic strain and yielding into the program to deal with more severe climate and field conditions.

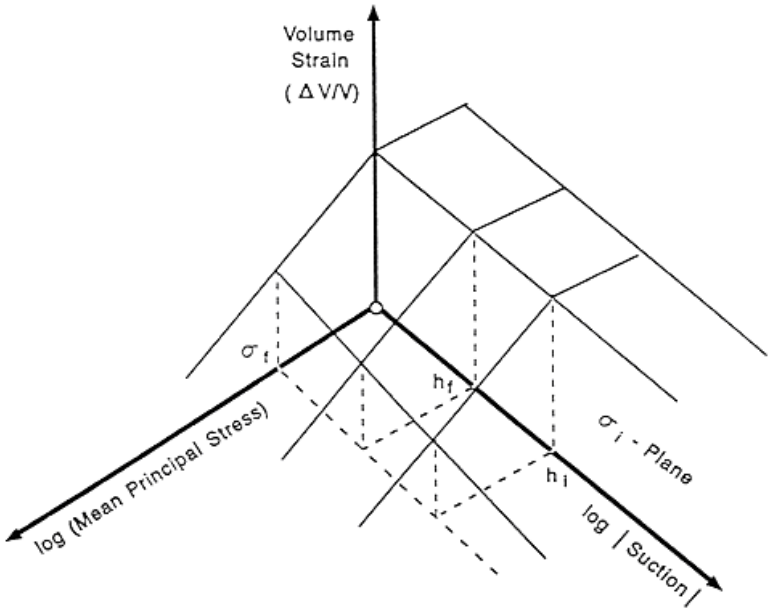

Figure 2.12 Volumetric strain as a function of log (suction) and log (mean principal stress) (Lytton, 1994)

CHAPTER III

DESCRIPTION OF COMPUTER PROGRAM FLODEF

Episodes of wetting and drying of expansive soils and the ensuing soil deformation and movement can incur extensive problems, such as the development of roughness and loss of serviceability of pavement structures (shrinkage cracks at the pavement surface), soil softening and degradation of soil strength. Such episodes can be cyclic in nature, such as the variations in soil moisture associated with seasonal variations in moisture infiltration and evapo-transpiration at the ground surface. Sustained changes in soil moisture can also occur due to a variety of causes, such as the addition or removal of vegetation, construction of features that inhibit evaporation, or ponding of water in low areas. A rational and reliable model for predicting the changes in moisture within soil mass and the induced volumes changes is needed to better understand expansive soil behavior and its significance to engineering applications.

A two-dimensional finite element program FLODEF that performs a sequentially coupled moisture flow-displacement analysis for the prediction of moisture transmission and associated movement will be introduced here in detail. The theoretical formulations of moisture flow and stress-deformation components of the model will be presented, followed by descriptions of program structure and graphic user interface. Examples of numerical verifications of the program for the one-dimensional and two-dimensional transient flow and deformation analysis are also given.

3.1 Overview of Program

The computer program FLODEF was originally developed by Lytton and Gay in 1991 and has had several revisions thereafter. The program is in modular format, i.e., it consists of some subroutines, which can serve the functions of automatic mesh generation and calculating the unsaturated flow and soil displacement.

The primary solution variable in FLODEF is soil suction. Gradients of total suction drive moisture movements within the soil mass, while matric suction is the state variable that, along with net mechanical stress, induces volume changes in the soil. Prediction of suction changes is based on solution of a linear diffusion equation. Prediction of deformations associated with changes in suction in space and time is based on solution of a system of non-linear elastic equations. The fluid flow and mechanical deformation aspects of the program are sequentially coupled. That is, the suction change during a given time interval is computed from a fluid flow calculation that is independent of the mechanical properties of the soil. The mechanical response of the soil due to the suction change is then computed. The elastic stiffness parameters used in the mechanical response calculations are dependent on suction. Therefore, coupling between fluid flow and mechanical response exists in the sense that the mechanical stiffness matrix must be continuously updated to be consistent with the current levels of suction.

In the spatial domain the problem is discretized using a finite element formulation. Solution in the time domain is accomplished using an implicit time-stepping procedure. The structure of the system of equations used in the FLODEF formulation can be represented in matrix form as follows:

$$\begin{bmatrix} [K_f]\Delta t & [0] \\ [0] & [K_m] \end{bmatrix} \begin{bmatrix} [\Delta h_m] \\ [\Delta d_n] \end{bmatrix} = \begin{bmatrix} [\Delta q] \\ [\Delta R] \end{bmatrix} \qquad \text{(Equation 3.1)}$$

where $[K_f]$, $[K_m]$ = flow and mechanical stiffness matrices, respectively

Δt = time step

Δh_m = change in matric suction during time step Δt

Δd_n = nodal displacement during time step Δt

Δq = increment of fluid flow volume during time step Δt

ΔR = equivalent nodal force applied during time step Δt

The equivalent nodal forces ΔR are due to mechanical stresses generated in the soil mass in accordance with the tendency of the soil to shrink or swell with changes in suction. The formulation used in FLODEF parallels that commonly used in thermal stress analysis for structures, where suction h_m may be considered analogous to temperature. The off-diagonal matrices in the global matrix in Equation 3.1 are zero; hence, the formulation is not fully coupled. As noted earlier, the formulation is coupled in the sense that the mechanical stiffness matrix $[K_m]$ is dependent on suction level h_m. Further details on the fluid flow and mechanical response algorithms of the program are described subsequently in this chapter.

3.2 Unsaturated Moisture Flow-Soil Deformation Analysis

Mitchell's simplified approach using the concept of soil diffusivity is used in the program to analyze the process of transient unsaturated moisture flow within the expansive soil domain. Lytton's nonlinear elastic deformation model is utilized for the prediction of induced soil movement.

3.2.1 Simplified Mitchell's Moisture Diffusion Analysis Approach

The permeability of an unsaturated soil is dependent on the total suction level *h* or the degree of saturation. Mitchell employed the suction-permeability relationship proposed by Laliberte et al. (1966):

$$k = k_0 \, (h_0/h)^n \qquad \text{(Equation 3.2)}$$

where k_0=the referenced saturated permeability;

h_0=total suction at a reference state usually corresponding to the air entry suction;

h=current total head value, and *n* is a material parameter that is close to unity for plastic clays.

Mitchell also adopted the assumption that the desorption relationship is linear with the logarithm of suction:

$$c = -\frac{\Delta w}{\Delta \log_{10} |h|} \qquad \text{(Equation 3.3)}$$

Where, c is the slope of soil-water characteristics curve (SWCC), *w* is the gravimetric water content.

By applying Darcy's law and the conservation of mass principle, Mitchell demonstrated that unsteady flow is governed by a linear diffusion equation when suction is expressed on a logarithmic scale (e.g., the pF scale where $u = \log_{10} -h$):

$$\frac{\partial^2 u}{\partial x^2} + \frac{\partial^2 u}{\partial y^2} + \frac{Q(u, x, y, f)}{p} = \frac{1}{\alpha} \frac{\partial u}{\partial t} \qquad \text{(Equation 3.4)}$$

$$\alpha = \frac{\gamma_w}{\gamma_d} \frac{p}{c}, \mathrm{c} = \frac{\partial \mathrm{w}}{\partial \mathrm{u}}, \mathrm{p} = \frac{\mathrm{k}_0 h_0}{0.434} \qquad \text{(Equation 3.5)}$$

where γ_d = dry soil unit weight; γ_w = unit weight of water and Q(u,x,y,f) is a distributed source or sink term of water.

Aubeny and Lytton (2003) observed the fact that existing data by Brooks and Corey (1966) suggest n value can exceed unity for some expansive soil types. They proposed a less restrictive formulation by defining a function ψ such that:

$$d\psi = h^{-n}dh$$
$$\psi = \log_e h \qquad n = 1 \qquad \text{(Equation 3.6)}$$

$$\psi = h^{1-n}/(1-n) \quad n > 1$$

$$\alpha = \frac{-Sk_0 h_0{}^n \gamma_w}{\gamma_d}, S = \frac{\partial u}{\partial w} = -\frac{1}{c}$$

$$\begin{cases} c = -\dfrac{\Delta w}{\Delta \log_e h} = -\dfrac{\Delta w}{\Delta \psi} & \text{n} = 1 \\ c = -\dfrac{\Delta w}{\Delta[(\dfrac{1}{1-n})h^{1-n}]} = -\dfrac{\Delta w}{\Delta \psi} & \text{n} > 1 \end{cases}$$

$$S = \frac{\partial u}{\partial w} = -\frac{1}{c}$$

and accordingly Mitchell's simplified diffusion equation is modified as:

$$\nabla^2 \psi = \frac{1}{\alpha}\frac{\partial \psi}{\partial t} \qquad \text{(Equation 3.7)}$$

Mitchell suggested the total suction at reference state h_0 or air- entry value in Soil-Water Characteristics Curve (SWCC) used a value of 100 cm (pF2). Recent laboratory pressure plate test results presented by Thakur (2005) at Texas A&M University obtained from near 20 soil samples have shown that h_0 level is within the range of 350cm (pF2.5) to 790cm (pF2.9) with the average 500cm (pF2.7).

3.2.1.1 Concept of Moisture Diffusion Coefficient

Paramount material parameter for the flow analysis is the moisture diffusion coefficient (α), which can be input into the program from specialized moisture diffusion and suction tests or be reasonably estimated from data acquired from commonly accepted site investigation methods; i.e., soil borings with index property and classification tests performed for each soil stratum in the profile. For the latter case, FLODEF will estimate the necessary parameters from such data based on empirical correlations.

Equation 3.4 shows that the rate of moisture diffusion is controlled by a single material parameter: the moisture diffusion coefficient α, which is of critical importance because it largely controls the depth and distribution of suction variations within the soil mass due to climatic variations in suction at the ground surface.

For the case of a uniform soil subjected to harmonic seasonal variations in suction ($u(0,t) = \sin(2n\pi t - p\pi)u_0 + u_e$) at the ground surface, the suction profile is given as a function of time and depth by a closed-form equation:

$$u(y,t) = u_e + u_0 \exp(-\sqrt{\frac{m\pi y}{\alpha}}) \cos(2n\pi t - \sqrt{\frac{m\pi y}{\alpha}}) \qquad \text{(Equation 3.8)}$$

where y is the depth measured from the ground surface, m is the frequency of seasonal variations in suction (e.g., cycles/year), u_e is the average suction; and u_0 is the amplitude of the cyclic component of suction.

(a) Laboratory Measurement for Diffusion Coefficient

The moisture diffusion coefficient α can be evaluated with the experimental approach proposed by Mitchell (1979). Two sets of tests (soaking test and evaporation test) are performed on conventional undisturbed soil samples, such as Shelby tube samples. Figure 3.1 shows the sides and one end of the sample sealed in evaporation test (or dry end test). Moisture can flow into or out of the sample through the open end. Small holes drilled into the sides of the sample at several locations provide opening for usually six psychrometers to measure suction. By measuring suction as a function of time and space, for the drying test, the diffusion coefficient α can be back-calculated from the analytical solution where suction u (x,t) is expressed as a function of time and location in the soil sample:

$$u = u_a + \sum_{n=1}^{\infty} \frac{2(u_0 - u_a)\sin z_n}{z_n + \sin z_n \cos z_n} \exp[\frac{z_n{}^2 \alpha t}{L^2}] \cos[\frac{z_n x}{L}]$$

$$\cot z_n = \frac{z_n}{h_e L}$$

$$\left.\frac{\partial u}{\partial x}\right|_{x=L} = h_e(u_a - u_s) \qquad \text{(Equation 3.9)}$$

where, u_a= atmospheric suction;

u_0= initial suction in soil;

α =soil diffusion coefficient;

t=time;

L=sample length;

x=coordinate;

h_e =evaporation coefficient.

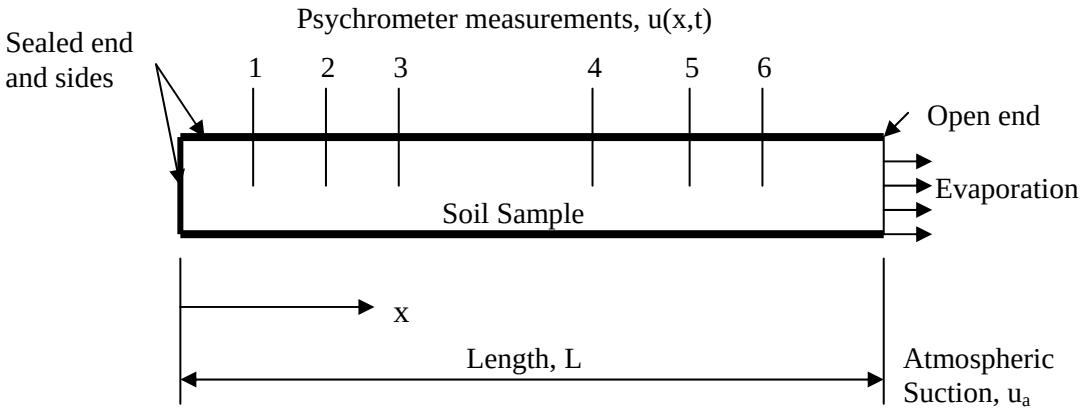

Figure 3.1 Schematic dry end test setup (Aubeny and Lytton, 2003)

In the dry end test, six drilled holes extend to approximately one-half the sample diameter at approximately equally spaced intervals for insertion of the suction measurement probes. A double layer of aluminum foil is utilized to seal all boundaries of the specimen. Locations at which the wires leading to the suction probes penetrated the external plastic wrap and aluminum foil need special attention, as voids may provide possible conduits for moisture loss through the sides of the soil specimen. Silicon sealant and electrical tape seal these locations to minimize the potential for moisture loss. The

test starts with the removal of the foil from one end of the specimen. Electrical tape applied to the foil-soil interface at the open end ensures a proper seal at this boundary. During the test, the foil wrap at the open end need be periodically tightened due to the fact that shrinkage induced in the specimen by drying near the open end of the specimen results in a tendency of the soil to pull away from the external seal (Aubeny and Lytton, 2003).

The test results performed by Tang et al. in Texas A&M University indicated that for intact soils, the n value is usually 2 or 3, while for cracked soils, an n-value of 1 is appropriate. A typical experimental result for dry end test is shown in Figure 3.2 (Aubeny and Lytton, 2003).

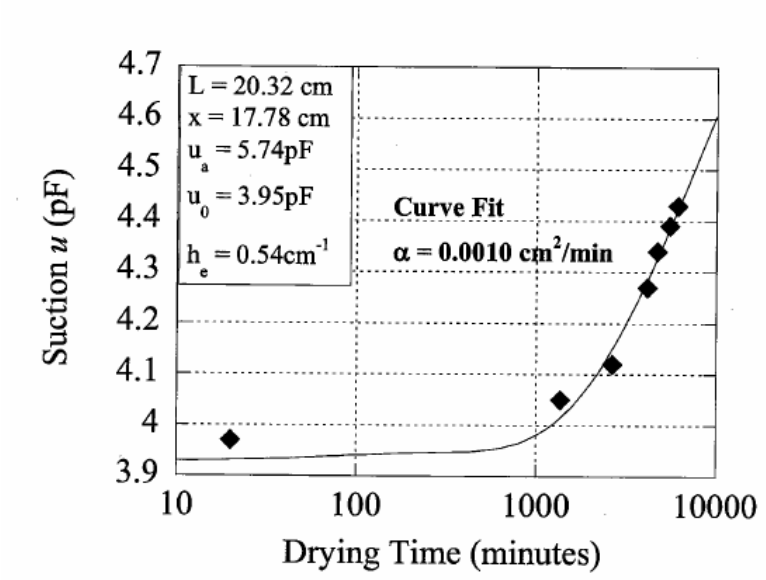

Figure 3.2 Typical experimental results for dry end test (Aubeny and Lytton, 2003)

(b) Estimations of Moisture Diffusion Coefficient in the Field

The moisture diffusion coefficient in the field α_{field} can be estimated from measured profiles of suction in the field by Equation 3.8 which is mentioned previously.

Jayatilaka and Lytton (1997) developed an empirical equation relating the field α_{field} to the slope of Soil-Water Characteristic Curve (SWCC) *S*, which can be obtained from pressure plate laboratory tests or empirically estimated from basic soil properties such as Aterberg limits (liquid limit LL%, plastic index PI%) and percentage of clay content (%#200): S=-20.29+0.1555(LL%)-0.117(PI%)+0.0684(%#200), and suction volumetric change index γ_h:

$$\alpha_{field} = 0.0029 - 0.000162\, S - 0.0122\gamma_h \qquad \text{(Equation 3.10)}$$

Aubeny and Lytton (2003) compared the laboratory measurements of diffusion coefficient α (normally in the range of $10^{-5}cm^2/s \sim 10^{-3}cm^2/s$) with the field α_{field} and observed that field values can exceed laboratory measurements by up two orders of magnitude. Equation 3.10 reflects the effects of such macro-pores and, hence, represents an upper bound estimate of α. It should be noted that beneath the depth of desiccation cracking Equation 3.10 likely over-estimates α and laboratory measurements on intact specimens are likely to be more representative of field conditions.

The importance of diffusion coefficient in determining the moisture flow and soil movement has received increasing recognition among geotechnical practice. The third version PTI manual acknowledges the role of α with other factors such as TMI (Thornswaite Moisture Index) in influencing the edge moisture variation distance, e_m,

which is a distance measured inward from the edge of the slab over which the moisture content of the soil varies due to wetting or drying.

In the program FLODEF, the empirical correlation of diffusion coefficient with soil index has been employed in case of the absence of direct measurement of α. For stabilized soil, the treatment with lime or cement will alter the soil index (LL, PI etc.), i.e., making the soil less plastic, the estimated diffusion coefficient will be increased to a small degree.

3.2.1.2 Flow Boundary Conditions

The FLODEF program has options for imposing either suction or flux boundary conditions to model the effects of climate and vegetation on suction variations within the soil mass. A default no flow boundary conditions exist for the free surface and two sides of the finite element mesh.

a) Vegetation

FLODEF models vegetative flux as either (1) a distributed surface flux in the case of grass where the depth of root penetration is relatively shallow, or (2) a body flux in the case of trees where roots can penetrate to substantial depths. Vegetation is modeled as a flux boundary condition, provided that the suction level at the boundary in question is less than the wilting point of the vegetation. A wilting point of 4.5pF is specified as a default value in the program. If at a given time step during the analysis the suction at the boundary exceeds the wilting point, the program switches from flux to suction control, with a suction of pF4.5 being imposed on the boundary in question.

A sink term Q_s (volume of water per unit volume of soil per unit of time) representing water extraction by a homogeneous isotropic element of a root system is introduced into the continuity equation of moisture of flow. Such a term in conjunction with a function describing the distribution of the root density with depth is then capable of describing the moisture extraction potential of transpiring plants which is subject to moisture availability and the diffusivity of the soil domain.

Feddest et al. (1988) presented a semi-empirical model to describe a sink term Q_s for root systems as follows:

$$Q_s(h_m) = \beta(h_m)\, Q_{smax} \qquad \text{(Equation 3.11)}$$

where Q_{smax} is the maximum possible water extraction by roots and $\beta(h_m)$ is a dimensionless function related to matric suction h_m. Prasad (1988) suggested the format of $Q_{smax}(y) = (2\,T_p / z_r)[1-(z/z_r)]$ to characterize Q_{smax} in terms of the transpiration rate T_p, the depth of root zone y_r, and vertical coordinate y as in Figure 3.3. Transpiration rates T_p typically vary within the range of 1 to 5 mm/day and a default value of T_p = 3mm/day is adopted in the FLODEF program.

The function $\beta(h_m)$ is set to zero when h_m is below h_{m1} (the oxygen deficient or anaerobiosis point) or above h_{m4} (the wilting point). Figure 3.4 shows the assumed form of the moisture uptake function $\beta(h_m)$ in terms of four reference suction levels, h_{m1} through h_{m4}. The assumed values for these suction levels in the FLODEF program are: h_{m1}= -50 cm, h_{m2}= -100 cm, h_{m3}= -650 cm and h_{m4}= -31600 cm.

Indraratna et al. (2006) and Ali and Rees (2006) extend Prasad's methodology to apply to axi-symmetric problem. They assumed that root water extraction reaches

maximum directly beneath the tree trunk and a linear relationship exists between root water extraction and radial distance as shown in Figure 3.5.

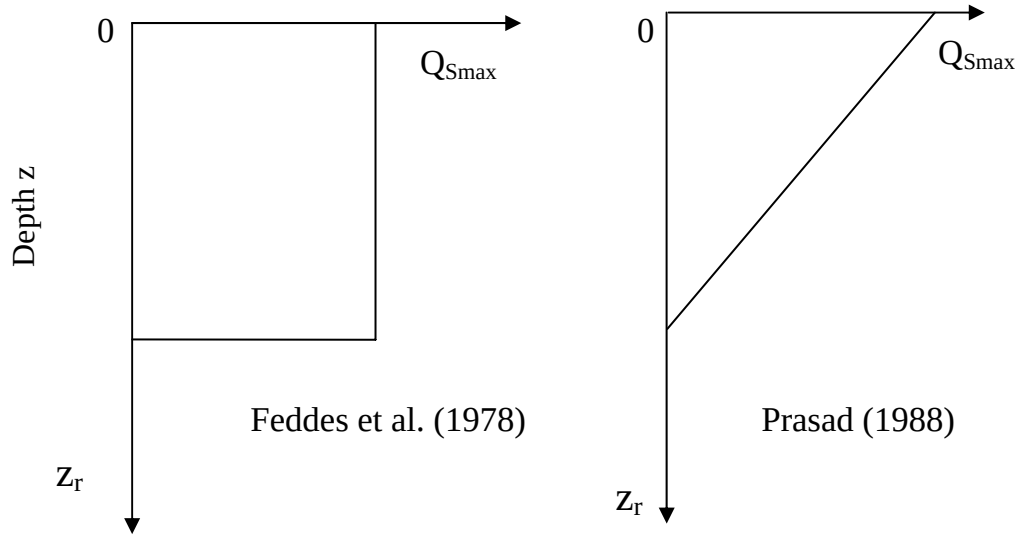

Figure 3.3 Root moisture extraction models for optimal moisture conditions, Q_{smax} as a function of depth Z, where Z_r=depth of the root zone (modified after Gay, 1994))

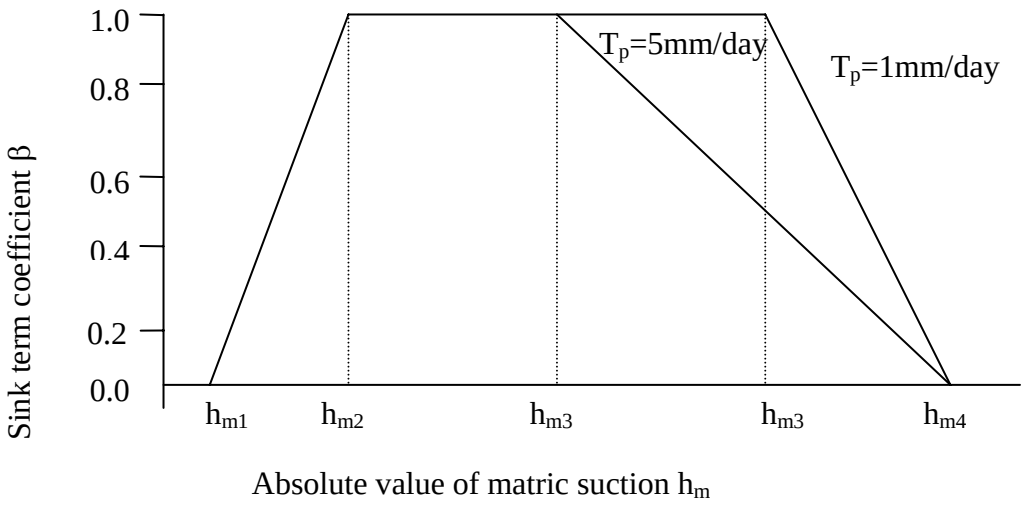

Figure 3.4 Dimensionless sink term coefficient α as a function of the absolute value of matrix suction $|h_m|$ (modified after Gay (1994))

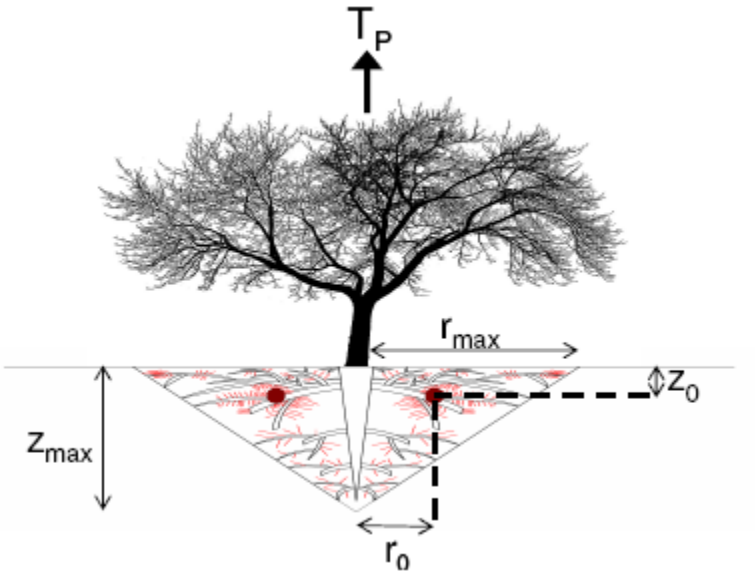

Figure 3.5 Schematic sketch of water uptake within tree root zone (Indraratna et al., 2006)

b) Climate

In areas where a vegetation boundary condition is not imposed, a time-dependent surface suction function is imposed at the ground surface to simulate episodes of wetting and drying associated with seasonal climatic conditions. FLODEF constructs these functions in terms of constant-valued functions and sinusoidal functions: a typical surface suction function (for El Paso, Texas) is depicted in Figure 3.6. FLODEF has a library of surface suction functions for 9 different climatic regions of Texas (El Paso, Snyder, Wichita Falls, Converse, Seguin, Dallas, Ennis, Houston, and Port Arthur).

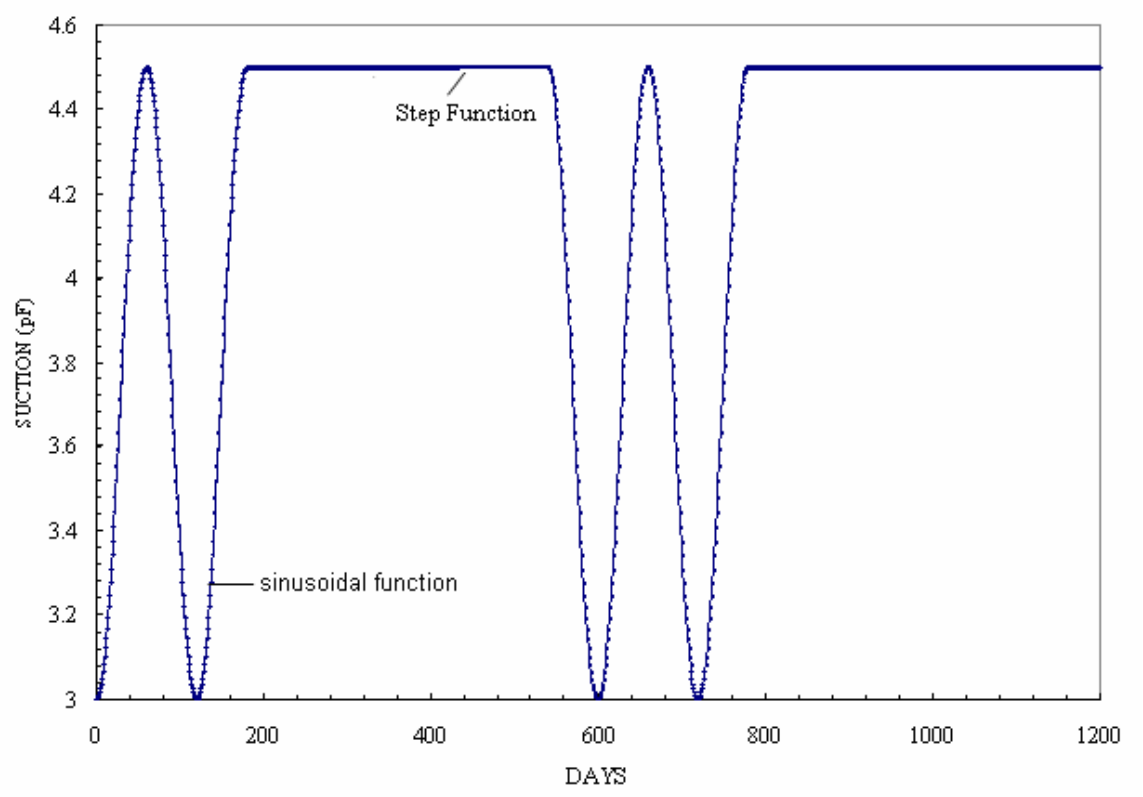

Figure 3.6 El Paso seasonal surface suction patterns (Long et al., 2006)

(c) Equilibrium Suction u_e

Ideally, the magnitude of the equilibrium suction u_e , which is defined as the suction level occurring at a depth in the soil mass that is unaffected by variations in suction at the ground surface, at a given site is inferred from measured profiles of suction. Such profiles could be obtained from filter paper tests for suction performed on undisturbed samples collected from soil borings. Recognizing that such data, while desirable, are not always available, FLODEF can also empirically estimate equilibrium suction from the Thornthwaite moisture index (TMI): $u_e=3.5633\exp^{(-0.0051TMI)}$. If such data are lacking, the program can provide estimates of equilibrium suction for various regions within the state of Texas as in Table 3.1.

Table 3.1. Default Equilibrium Suctions in FLODEF

City	TMI	Equilibrium Suction (pF)
El Paso	-46.8	4.5
Snyder	--	3.9
Wichita Falls	--	3.9
Converse	-21.3	3.85
Seguin	-21.3	3.85
Dallas	-11.3	3.6
Ennis	-11.3	3.8
Houston	14.8	3.1
Port Arthur	26.8	2.9

3.2.1.3 Flow Initial Conditions (Initial Dry/ Initial Wet/ Initial Equilibrium)

Solution of the moisture diffusion equation (Equation 3.4) requires specification of initial conditions of suction. If profiles of existing suction conditions are available for

the site under consideration, they may be input directly into FLODEF as initial conditions. If such data are lacking, profiles of initial suction are estimated using Equation 3.8. FLODEF gives the option of initiating the analysis for wet (winter season), equilibrium (spring or fall season), or dry (summer season) surface suction conditions. A typical initial suction profile used for an analysis of a northeast Texas site (US Highway 290 in Atlanta, Texas) is shown in Figure 3.7.

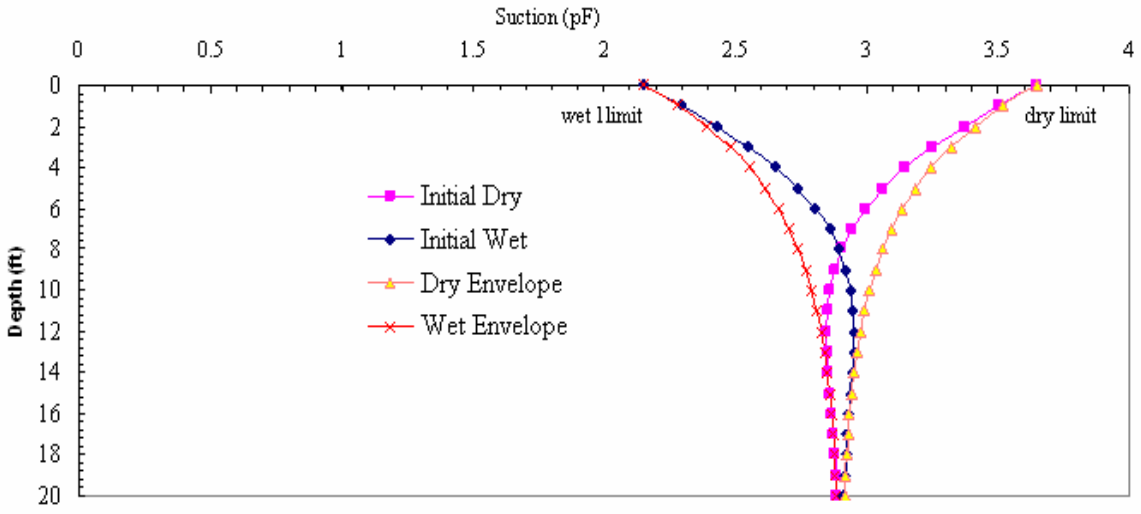

Figure 3.7 Initial condition descriptions for Atlanta US 290

Table 3.2 tabulates the input parameters in the case of initial wet, dry and equilibrium conditions for nine different regions of Texas (El Paso, Snyder, Wichita Falls, Converse, Seguin, Dallas, Ennis, Houston, and Port Arthur) provided in the FLODEF computer program.

Table 3.2. Input Parameters for Mitchell's Default Initial Condition Descriptions

City	TMI	Initial Condition					
		Wet		Equilibrium		Dry	
		Amplitude (pF)	Phase	Amplitude (pF)	Phase	Amplitude (pF)	Phase
El Paso	-46.8	0.75	-1.0	0.75	-0.5	0.75	0.0
Seguin	-21.3	0.65	-1.0	0.65	-0.5	0.65	0.0
Dallas	-11.3	1.00	-1.0	1.00	-0.5	1.00	0.0
Ennis	-11.3	0.70	-1.0	0.70	-0.5	0.70	0.0
Houston	14.8	1.00	-1.0	1.00	-0.5	1.00	0.0
Port Arthur	26.8	0.75	-1.0	0.75	-0.5	0.75	0.0
Snyder	--	0.60	-1.0	0.60	-0.5	0.60	0.0
Wichita Falls	--	0.60	-1.0	0.60	-0.5	0.60	0.0
Converse	-21.3	0.65	-1.0	0.65	-0.5	0.65	0.0

3.2.2 Numerical Solution of Unsaturated Moisture Flow

The numerical solution to Richard's two-dimensional unsaturated moisture flow equation, $r\frac{\partial\theta}{\partial\psi}.\frac{\partial\psi}{\partial t} = r\frac{\partial}{\partial z}(K\frac{\partial\psi}{\partial z}) + K\frac{\partial\psi}{\partial r} + r\frac{\partial}{\partial r}(K\frac{\partial\psi}{\partial r}) + r\frac{\partial K}{\partial z} - rS$, can be obtained via a finite element spatial discretization procedure and a finite difference time-stepping scheme. Zienkiewicz and Taylor (1989) adopted a Galerkin weighted residual approach and yields:

$$\int_{\Omega}\frac{\partial}{\partial r}(rN_r K\frac{\partial \psi}{\partial r})\partial\Omega-\int_{\Omega} rK\frac{\partial \psi}{\partial r}.\frac{\partial N_r}{\partial r}\partial\Omega+\int_{\Omega}\frac{\partial}{\partial z}(rN_r K\frac{\partial \psi}{\partial z})\partial\Omega-\int_{\Omega} rK\frac{\partial \psi}{\partial z}.\frac{\partial N_r}{\partial z}\partial\Omega$$
$$+\int_{\Omega} rN_r\frac{\partial K}{\partial z}\partial\Omega-\int_{\Omega} rN_r\frac{\partial \theta}{\partial \psi}.\frac{\partial \psi}{\partial t}\partial\Omega-\int_{\Omega} rN_r S\partial\Omega=0$$

(Equation 3.12)

here K is the unsaturated hydraulic conductivity, t is the time, r and z are the coordinates, θ is the volumetric moisture content, and ψ is the total suction. $\frac{\partial\theta}{\partial\psi}$ is the slope of soil water characteristic curve (SWCC).

Using Green's formula and introducing boundary terms leads to the final discretization form:

$$K\psi+C\dot{\psi}+j+S=0 \qquad \text{(Equation 3.13)}$$

where $$K=\int_{\Omega} r[K\frac{\partial N_S}{\partial r}.\frac{\partial N_r}{\partial r}+K\frac{\partial N_S}{\partial z}.\frac{\partial N_r}{\partial z}]\partial\Omega \qquad \text{(Equation 3.14)}$$

$$C=\int_{\Omega} r[N_r N_S\frac{\partial\theta}{\partial\psi}]\partial\Omega \qquad \text{(Equation 3.15)}$$

$$J=\int_{\Omega} r[N_r\frac{\partial K}{\partial z}]\partial\Omega-\int_{\Gamma} r[N_r\lambda]\partial\Gamma \qquad \text{(Equation 3.16)}$$

$$S=\int_{\Omega} r[N_r S]\partial\Omega \qquad \text{(Equation 3.17)}$$

Using a backward difference technique yields:

$$K^{n+1}\psi^{n+1}+C^{n+1}[\frac{\psi^{n+1}-\psi^{n}}{\Delta t}]+J^{n+1}+S^{n+1}=0 \qquad \text{(Equation 3.18)}$$

The sink term (vegetation) is dealt with a surface flux q=q(x,t) per surface area for surface grass and a body volumetric flux q=q(x, y, t) per volume. Using Prasad's formula, the element sink term is expressed as:

$$S_z = \frac{2T_p}{z}\beta(1-\frac{z}{z_r}) \qquad \text{(Equation 3.19)}$$

where, z_r is the root zone depth; β is the dimensionless sink term coefficient; z is the vertical coordinate of the integration point in each element within the vegetation influence zone; T_p is the evapotranspiration rate.

3.2.3 Nonlinear Elastic Deformation Model

A highly nonlinear elastic model is applied to compute the incremental deformation value for each node in the expansive soil domain. The Young's Modulus E at each element's integration point is a function of its current mean principal normal stress σ_m, matrix potential h_m, Poisson's ratio υ, and suction volumetric change index γ_h, as seen below:

$$E = \frac{(\sigma_m - \theta h_m)(1+\frac{0.4343}{sw})}{\gamma_h(0.435)}\frac{(1+\nu)(1-2\nu)}{(1-\nu)} \qquad \text{(Equation 3.20)}$$

Given σ_m = current mean principal normal stress at this integration point,

ν = Poisson's Ratio,

γ_h = suction volumetric change index,

S = soil desorptive curve slope (suction versus gravimetric water content w),

w = gravimetric water content (decimal),

h_m = total matrix potential at current incremental time step,

θ = current volumetric water content at this integration point.

Lytton (1994) defines the equation for the volumetric strain calculation which is generalized in each incremental time step:

$$\varepsilon_v = \gamma_h \log \frac{h_f}{h_i} \pm \gamma_\sigma \log \frac{\sigma_f}{\sigma_i} - \gamma_\pi \log_{10} \frac{\pi_f}{\pi_i} \qquad \text{(Equation 3.21)}$$

Here γ_h = suction volumetric compression index as defined previously,

γ_σ = the mean principal stress compression index as defined previously,

h_f = current suction value (pF) at the integration point, negative,

h_i = suction value for previous time step (pF) at the integration point, negative,

σ_f = current mean principal normal stress at the integration point,

σ_i = minimal mechanical stress level for overburden effect, usually expressed as the vertical mechanical stress, caused by 80 cm soil layer depth,

γ_π =the osmotic suction compression index,

π_i, π_f =the initial and final values of osmotic suction.

In Equation (3.21), it is usually assumed that there have not significant osmotic suction changes during the analysis period. Hence, the osmotic suction term is usually omitted. The modified equation becomes: $\varepsilon_v = \gamma_h \log \frac{h_f}{h_i} \pm \gamma_\sigma \log \frac{\sigma_f}{\sigma_i}$. The negative sign denotes soil shrinkage and positive sign denotes soil swelling.

3.2.3.1 Model Material Parameter: γ_h

In computer program FLODEF, suction volumetric change index γ_h is calculated using mineralogical soil classification. Soil has been classified into nine mineralogical soil class based on PI ratio (Soil activity) and LL ratio (LL/%fc), where %fc is the ratio of the percentage clay content (<2 μ m) to the percentage passing No.200 sieve, i.e., the clay fraction. A figure for each mineralogical soil class is provided by Covar and Lytton (2001), which relates LL ratio (LL/%fc) and PI ratio (Soil activity) to the suction compression index for soil consisting of 100% clay, γ_0. Once γ_0 is obtained from the chart, the suction volumetric change index γ_h can be calculated as:

$$\begin{cases} \gamma_{h\,\text{swell}} = \gamma_h e^{\gamma_h} & \gamma_h = \gamma_0 \% fc \\ \gamma_{h\,\text{shrink}} = \gamma_h e^{-\gamma_h} & \gamma_h = \gamma_0 \% fc \end{cases} \qquad \text{(Equation 3.22)}$$

Besides Lytton's approach, the 3rd version of PTI manual (2005) proposes other three methods for estimating suction volumetric change index γ_h: expansion index procedure, consolidation test procedure and overburden pressure swell test procedure. The expansion index, EI, can be determined per ASTM D 4829 (ASTM, 2005a) and the swell suction compression index $\gamma_{h\,\text{swell}}$ is calculated by: $\gamma_{h\,\text{swell}} = \frac{EI}{1700}$. In the consolidation test procedure, $\gamma_{h\,\text{swell}}$ is expressed in terms of the slope of compression rebound curve, C_s, and the void ratio corresponding to the effective stress at the bottom of the curve, e_2, obtained from a typical one-dimensional consolidation test: $\gamma_{h\,\text{swell}} = \frac{0.7C_s}{1+e_2}$. $\gamma_{h_{swell}}$, which is computed from the overburden pressure swell test

procedure, is correlated to the vertical strain ($\frac{\Delta H}{H}$) due to the increased water content and overburden pressure P: $\gamma_{h_{swell}} = \frac{\frac{\Delta H}{H}}{1.7 + \log_{10} P}$. After γ_{hswell} is calculated from the three methods mentioned above, $\gamma_{hshrink}$ is read off from a figure provided in the 3rd edition of PTI manual, which is based on the estimated γ_{hswell}.

3.2.3.2 Model Material Parameter: γ_σ

In FLODEF, the mean principal stress compression index γ_σ is related to γ_h as expressed in equation 3.23:

$$\gamma_\sigma = \frac{\gamma_h}{1 + \frac{0.4343}{sw}} \qquad \text{(Equation 3. 23)}$$

Where S = soil desorptive curve slope as described previously,

w = gravimetric water content (decimal)

3.2.3.3 Current Mechanical Stress σ_m

In the program, the mechanical stress in each incremental time step is updated based on the associated suction value at each node. At each element integration point, the total strains ε are evaluated from the nodal point displacements and then using equation (3.15) to calculate the mechanical stress for this integration point at current time step.

$$\tau_i = C(\varepsilon - \varepsilon_i^{th}), \quad \text{i= x or y} \qquad \text{(Equation 3.24)}$$

where $\varepsilon_x^{th} = \frac{1}{2}\varepsilon_v = \varepsilon_y^{th}$, C is a symmetric matrix of material compliances. For plane strain case used in FLODEF program, the mechanical stress is computed based on equation (3.25):

$$\begin{Bmatrix} \sigma_x \\ \sigma_y \\ \tau_{xy} \end{Bmatrix} = \frac{E}{(1+\nu)(1-2\nu)} \begin{vmatrix} 1-\nu & \nu & 0 \\ \nu & 1-\nu & 0 \\ 0 & 0 & \frac{1-2\nu}{2} \end{vmatrix} \begin{vmatrix} \varepsilon_x \\ \varepsilon_y \\ \gamma_{xy} \end{vmatrix} \qquad \text{(Equation 3.25)}$$

The time step Δt value in FLODEF program is small (30 days for deformation analysis), so explicit method is employed. From the node displacements calculated in previous time step, the total strain ε can be computed. There is no iteration required for the analysis.

In deformation analysis, the boundary conditions are as follows: (1) No horizontal and vertical displacements at the bottom of FEM mesh, like the case of pin support. (2) No horizontal displacements for nodes at the sides, like the case of roller support.

3.3 Program Structure and Input/ Output Screens

FLODEF consists of seventeen subroutines for the purposes of mesh generation, assembly of element stiffness matrix for flow calculation and displacement calculation, flow analysis and deformation computation. The flowchart can be shown as follows in Figure 3.8 In subroutine SOLVER, the program uses an upper triangular Gauss Elimination method to solve the equations for suction/displacement value at each node.

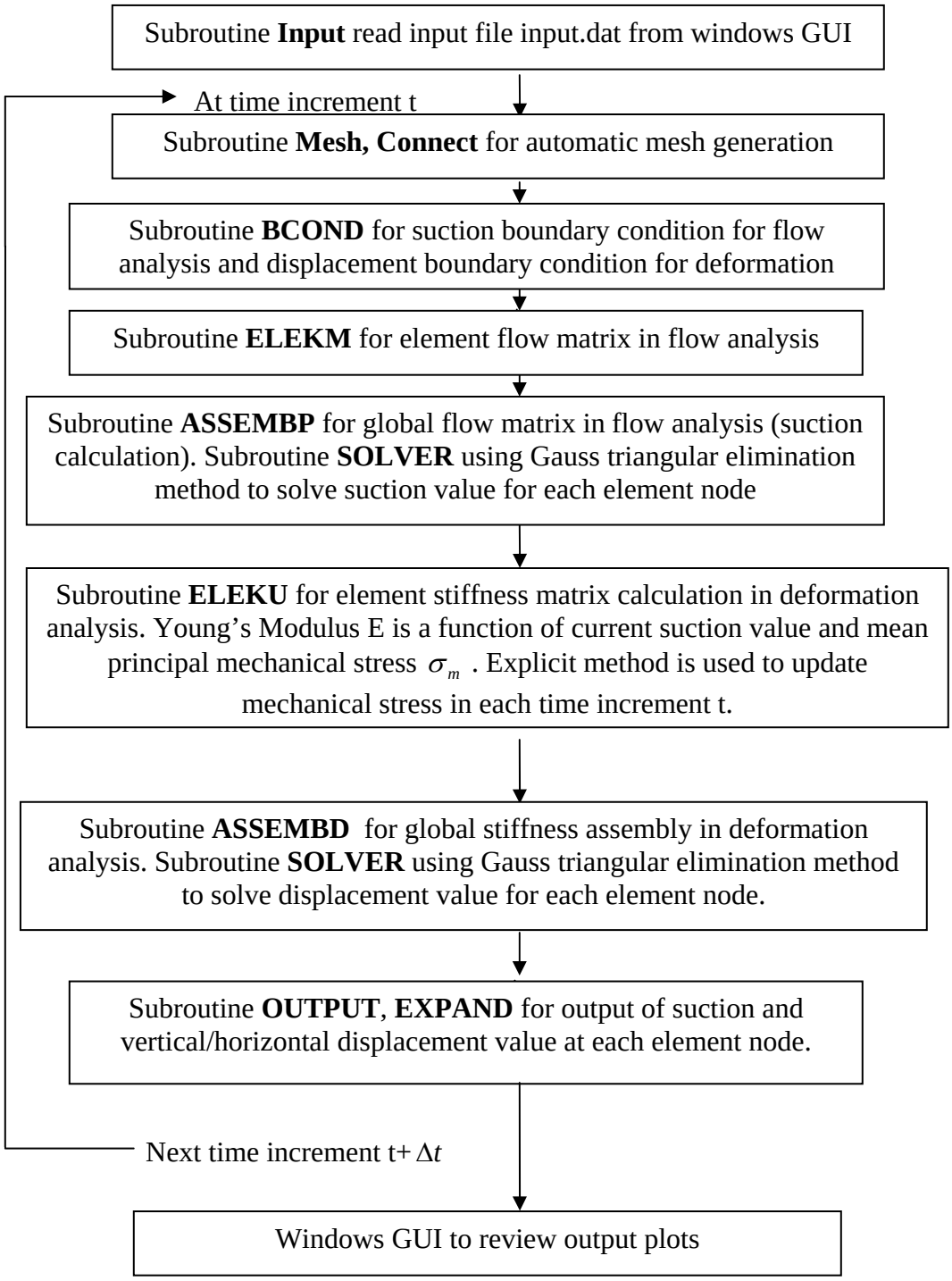

Figure 3.8 Flowchart of program FLODEF

Nine integration points are used for 8- node bilinear element and six integration points are used for 6- node triangular element.

The program windows GUI (graphic user interface) has four input screens for the user to input the site information, soil properties, pavement structure dimensions and surface vegetation locations. The output plots generated by the program are: the vertical profile plots for suction/vertical displacement/horizontal displacement parameter at specific time, time history plot for suction/vertical displacement/horizontal displacement parameter, contour plots for suction/vertical displacement/horizontal displacement parameter at specific time and surface deformation plot. Figures 3.9-3.12 show the typical input screens and Figures 3.13-3.23 give the output plots for results review and automatic generated FEM mesh for analysis.

3.4 Program Numerical Validation

The computer program FLODEF is numerically verified by comparing the analysis results with analytical diffusion equation solution and those of commercial program ABAQUS. The “sequentially coupled thermal-stress” analysis type in ABAQUS is adopted for the comparison. Three example problems are employed. Example one is to verify with one-dimensional Mitchell’s analytical solution. Example two is the verification with ABAQUS using two-dimensional sequentially coupled thermal stress model for the case of no vegetation, while example three is for the comparison of vertical displacement. The ABAQUS input files are listed in Appendix B.

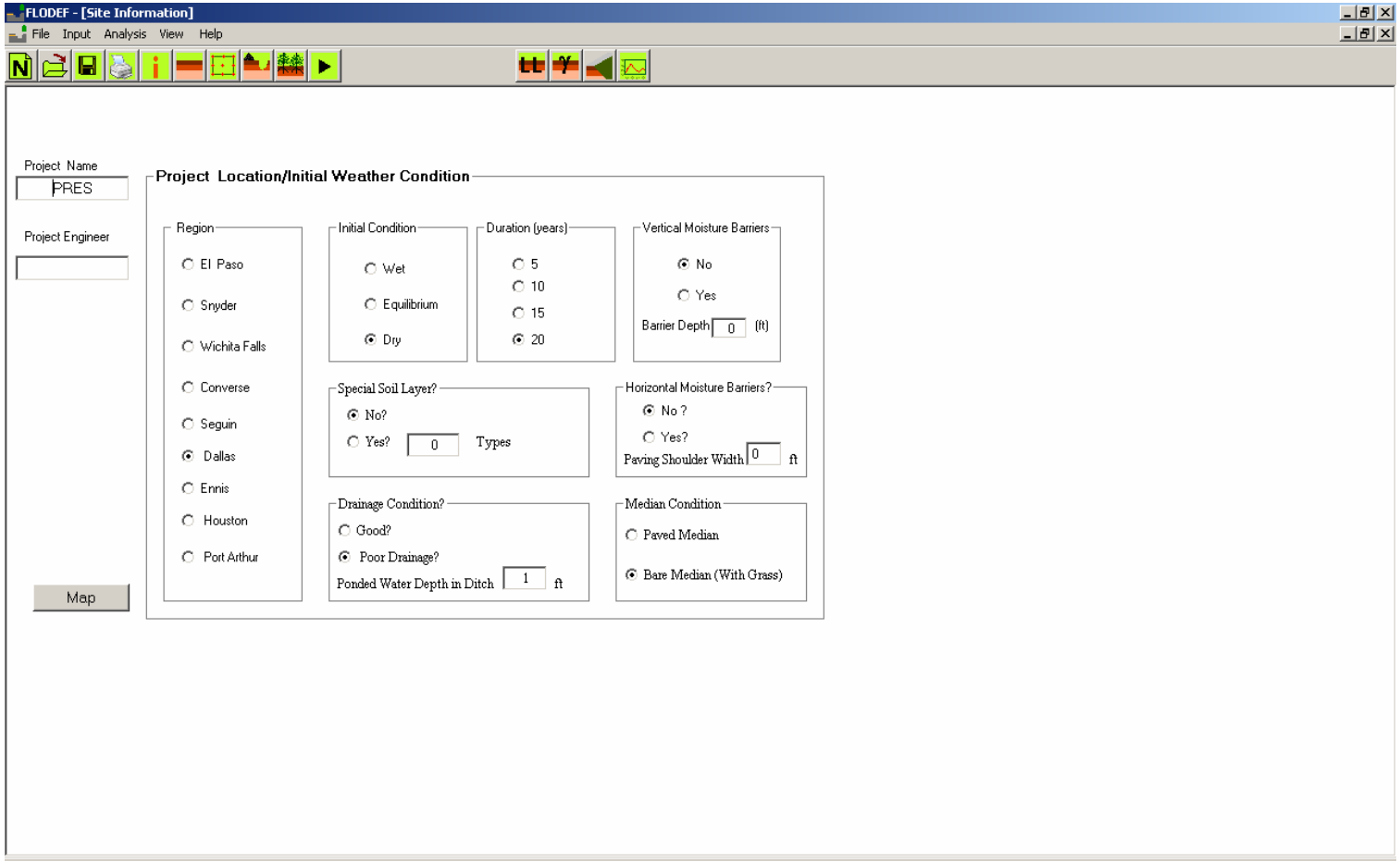

Figure 3.9 Input screen 1: site information

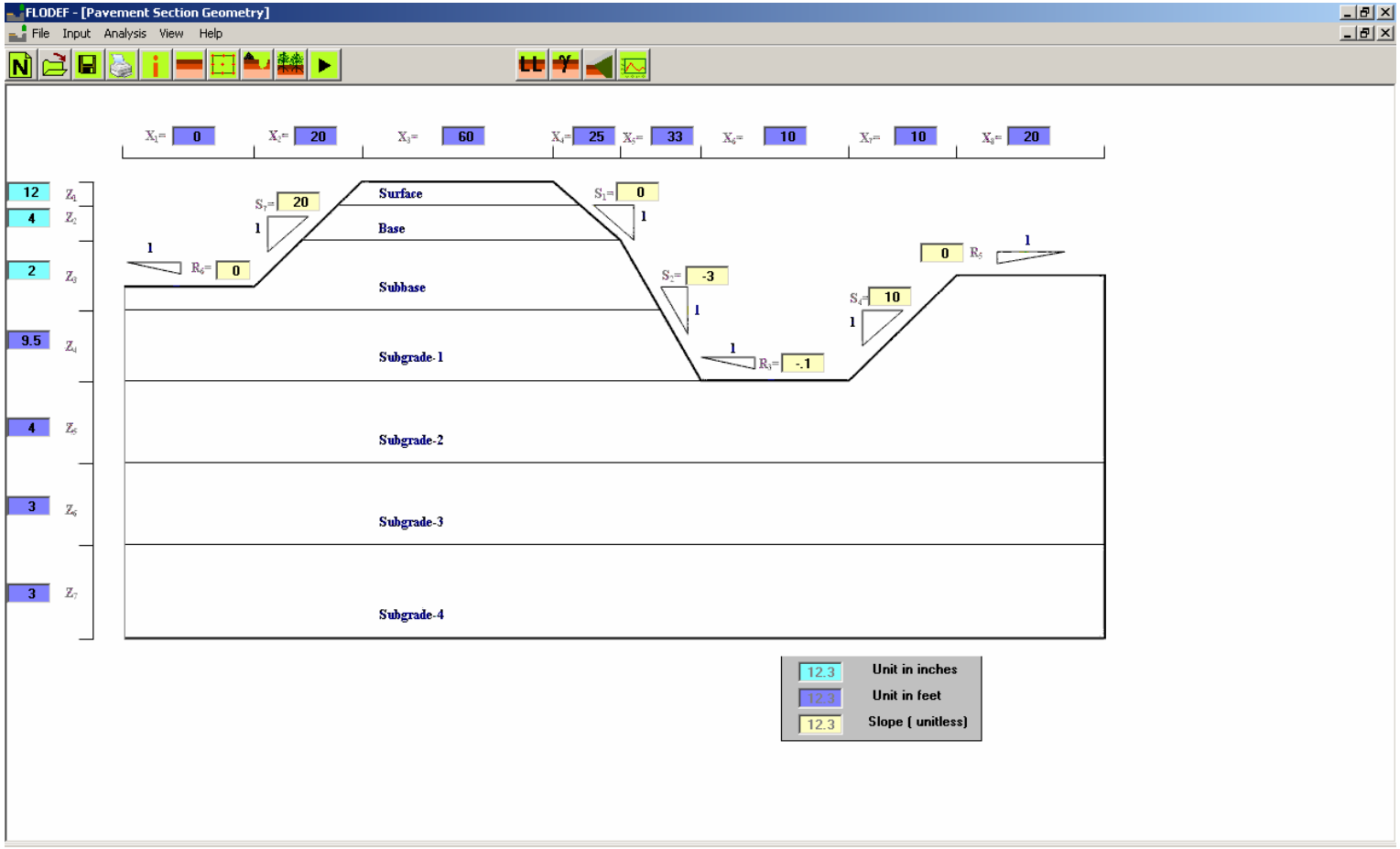

Figure 3.10 Input screen 2: pavement structure dimensions

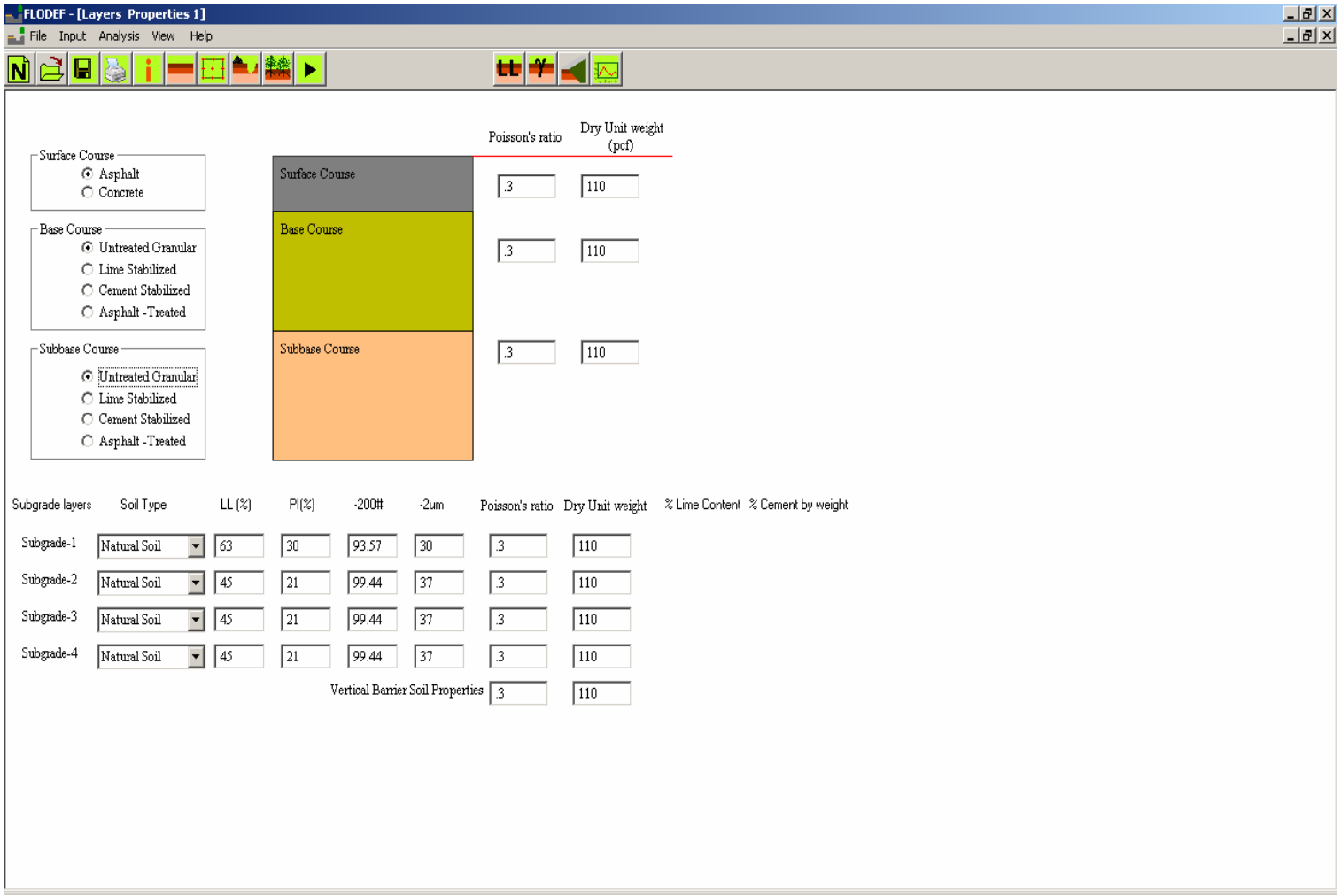

Figure 3.11 Input screen 3: subgrade soil properties

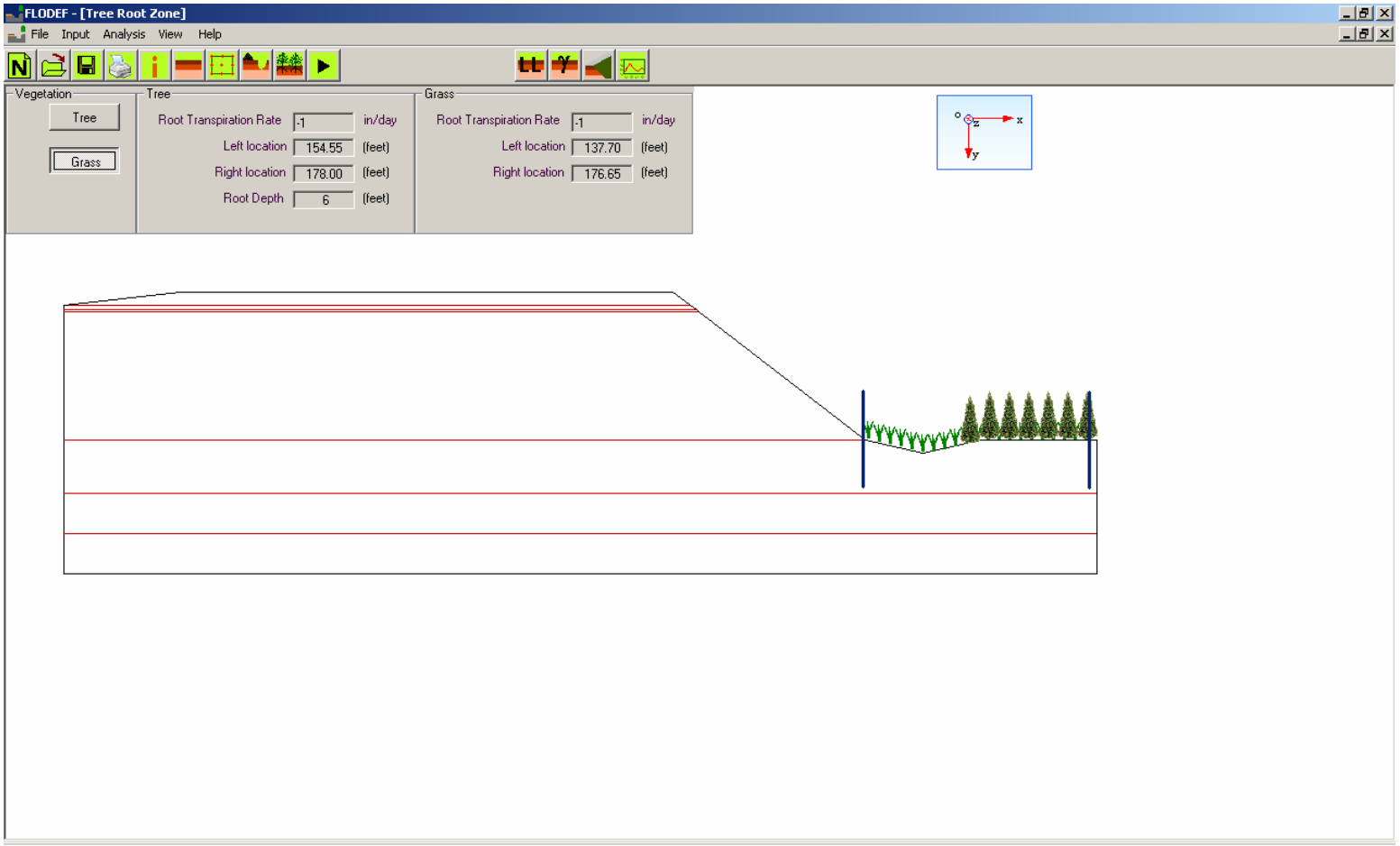

Figure 3.12 Input screen 4: vegetation information

Figure 3.13 Output plot 1: vertical profile (suction)

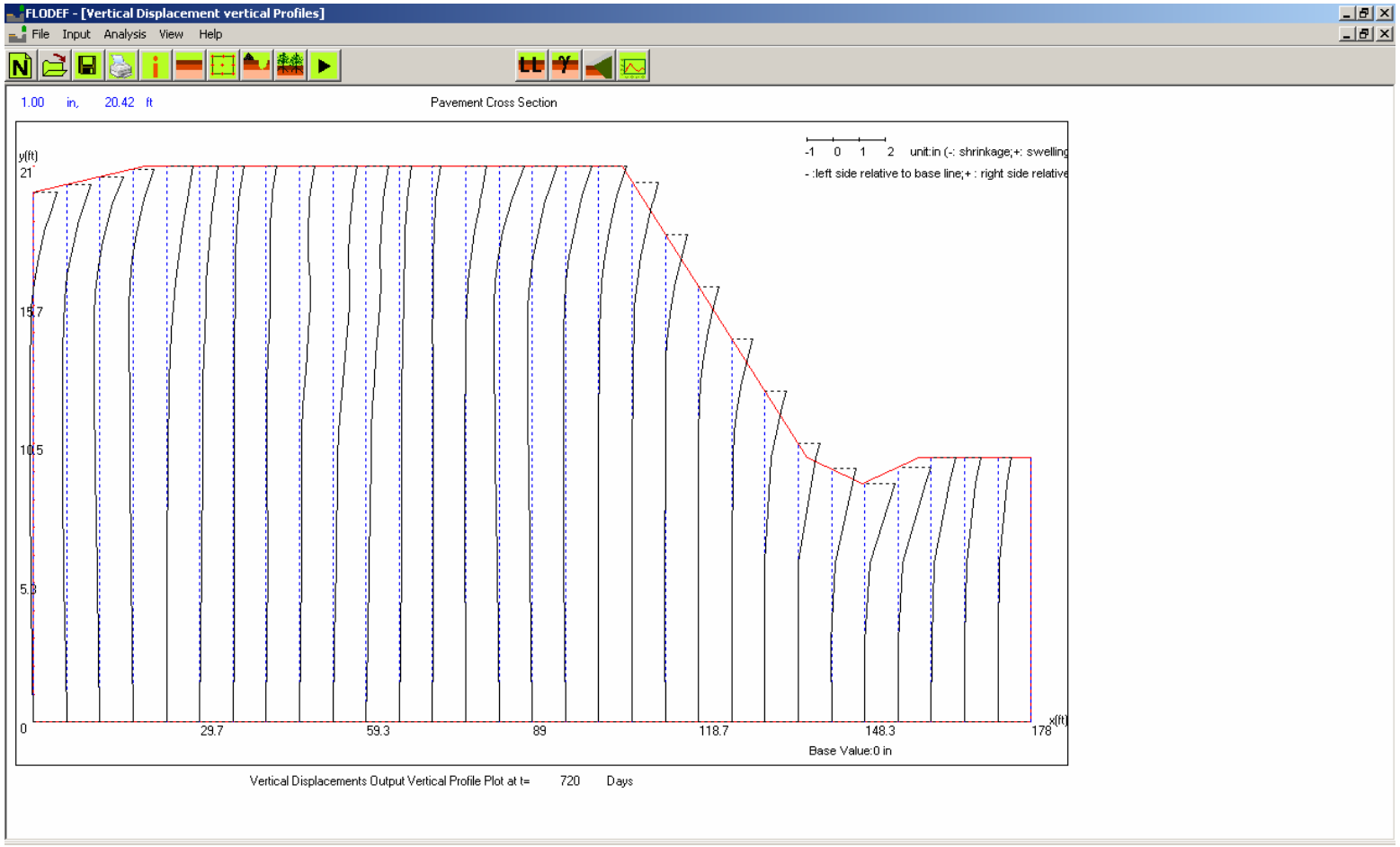

Figure 3.14 Output plot 2: vertical profile (vertical displacement)

Figure 3.15 Output plot 3: vertical profile (horizontal displacement)

Figure 3.16 Output plot 4: contour plot (suction)

Figure 3.17 Output plot 5: contour plot (vertical displacement)

Figure 3.18 Output plot 6: contour plot (horizontal displacement)

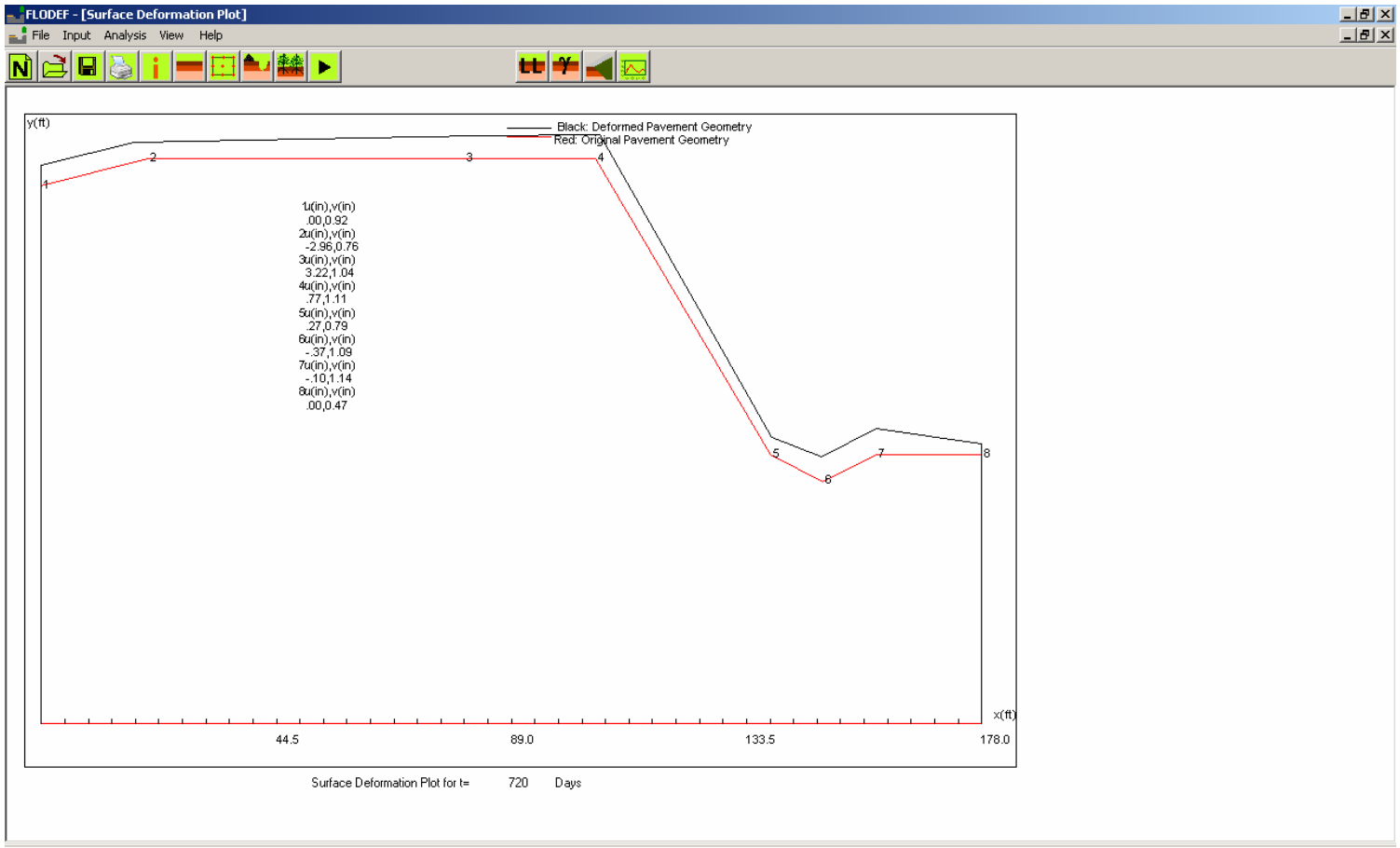

Figure 3.19 Output plot 7: surface deformation plot

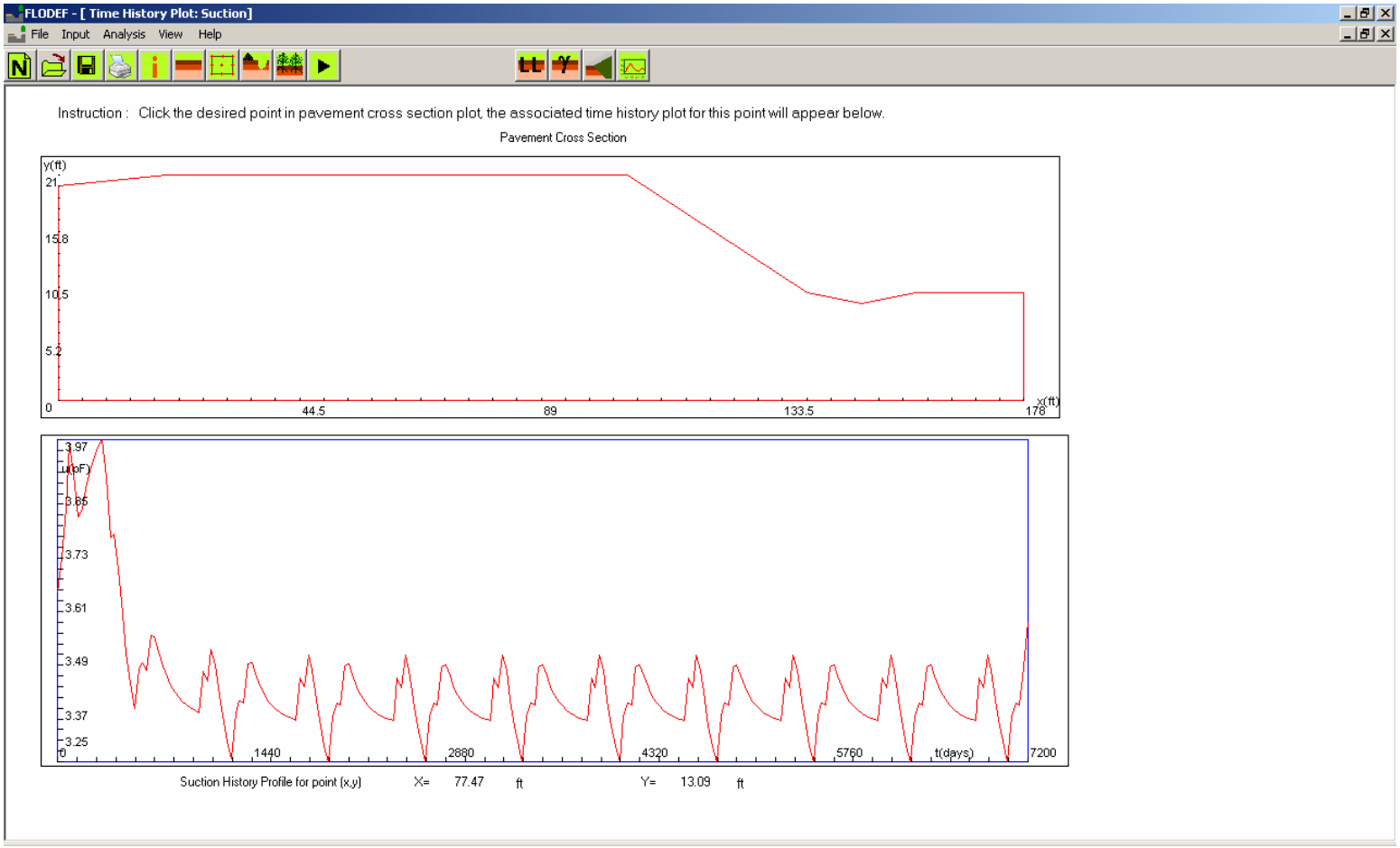

Figure 3.20 Output plot 8: time history plot (suction)

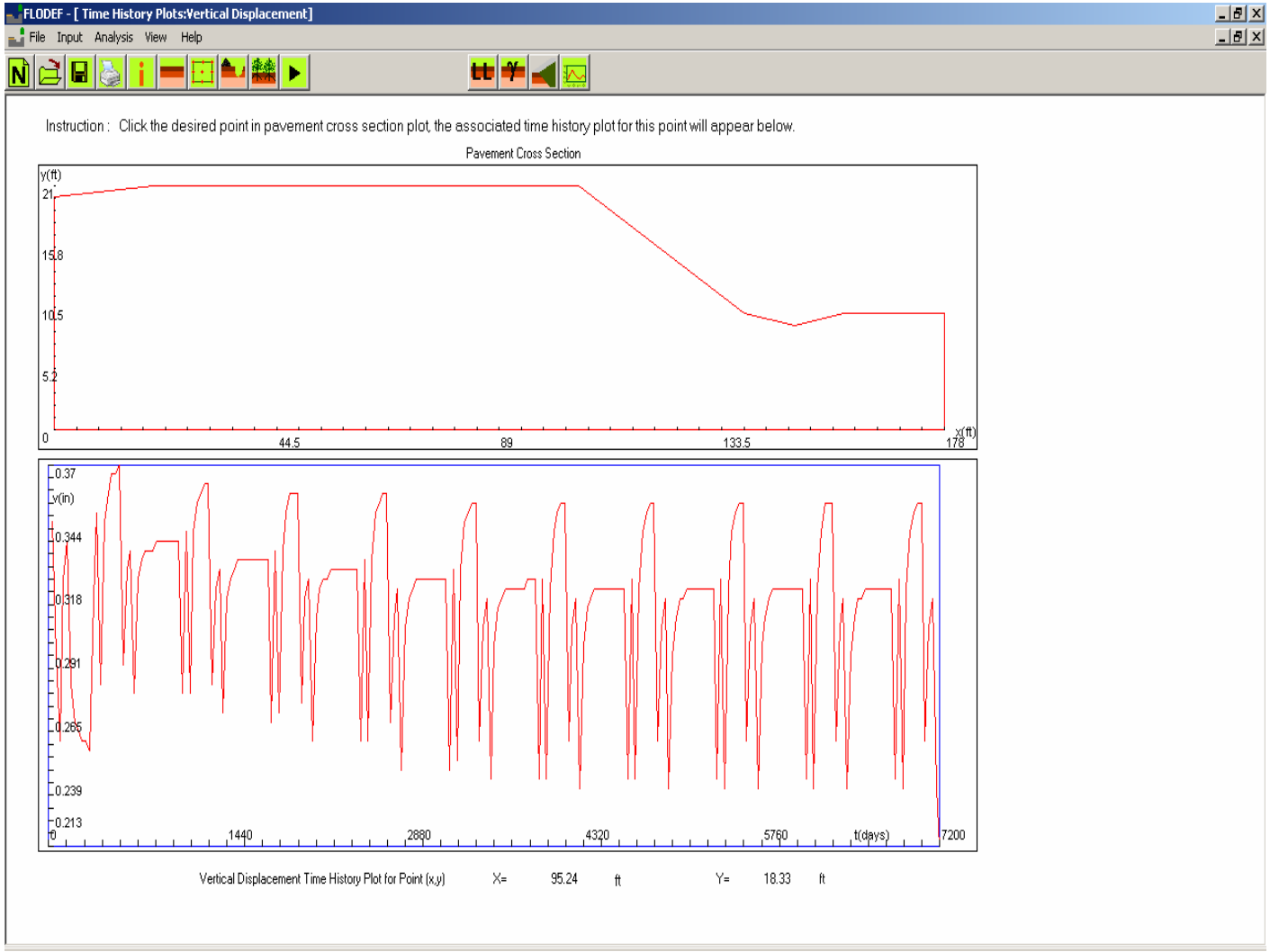

Figure 3.21 Output plot 9: time history plot (vertical displacement)

Figure 3.22 Output plot 10: time history plot (horizontal displacement)

Figure 3.23 FEM mesh generated in the program

3.4.1 Analysis Similarity of Hydro-mechanical Problems with Thermal Stress

Terzaghi (1943) first stated the thermodynamic analogue to process of consolidation.

Table 3.3. Analysis Similarity of Sequentially Coupled Flow/Displacement Analysis with Sequentially Coupled Thermal Stress/Displacement Analysis

Phase	Sequentially coupled flow/displacement analysis		Sequentially coupled thermal stress/displacement analysis	
	Physical Meaning	Symbol	Physical Meaning	Symbol
Mechanical	Stress	$\sigma - u_a$	Stress	σ
	Strain	ε	Strain	ε
	Displacement	u, v, w	Displacement	u, v, w
	Young's Modulus	E	Young's Modulus	E
	Poisson's Ratio	ν	Poisson's Ratio	ν
	Suction Compression index	γ_h	Coefficient of Expansion	α
Flow	Coefficient of Permeability	k	Coefficient of Conductivity	k
	Dry Unit Weight	γ_d	Density	γ
	Diffusion Coefficient	α	Specific Heat Capacity	C_T
Flow/mechanical	Time	t	Time	t

If "γ_w=1" is assumed, the differential equation for the one-dimensional flow of heat through isotropic body becomes identical with the differential equation of Terzaghi's consolidation theory. The relationship between suction compression index γ_h in flow/displacement analysis and coefficient of expansion α for plane strain problems is: $\alpha = \gamma_h(1+\nu)/3.0$.

Table 3.3 describes the analogue of sequentially coupled thermal stress/displacement problem with sequentially coupled flow/displacement analysis in FLODEF program.

3.4.2 Accuracy and Stability

For the transient diffusion flow analysis in FLODEF computer program, the backward Euler method (sometimes also referred to as the modified Crank-Nicholson operator, i.e., time step coefficient $\theta = 1$) is adopted. This method is unconditionally stable for linear problems.

Normally the accuracy of the flow/deformation analysis algorithms increases as the time step decrease in magnitude. However, there is a relationship between the minimum usable time step and the element size as $\Delta t \geq \frac{1}{6}\frac{(\Delta h)^2}{\theta\alpha}$ (ABAQUS User manual 2005), where Δt is the time step, α is the soil diffusion coefficient usually expressed as cm^2/s unit, Δh is a typical element dimension (such as the length of a side of an element). If time step value smaller than this value is used in a mesh of second-order elements, spurious oscillations can appear in the solution, in particular in the vicinity of boundaries with rapid suction changes. These oscillations are nonphysical and may

cause problems if flow (suction)-dependent material properties are present. In FLODEF, second-order element type is adopted (8-node bilinear element and 6-node triangular element types, as shown in Figure 3.23).

3.4.3 Examples of Numerical Verification

3.4.3.1 Flow Analysis Compared with 1-D Mitchell's Analytical Solution

The analysis results by FLODEF are compared with Mitchell's analytical solution using Equation 3. 8: $u(y,t) = u_e + u_0 e^{(-\sqrt{\frac{n\pi}{\alpha}})y} \cos(2\pi nt - \sqrt{\frac{n\pi}{\alpha}}y)$. Figure 3.24 shows the comparison.

3.4.3.2 Flow Analysis Compared with 2-D ABAQUS Calculation

The flow analysis results are also compared with those of ABAQUS calculation as shown in Figure 3.25.

3.4.3.3 Displacement Analysis Compared with 2-D ABAQUS Calculation

The displacement analysis results are also compared with those of ABAQUS calculation as shown in Figure 3.26.

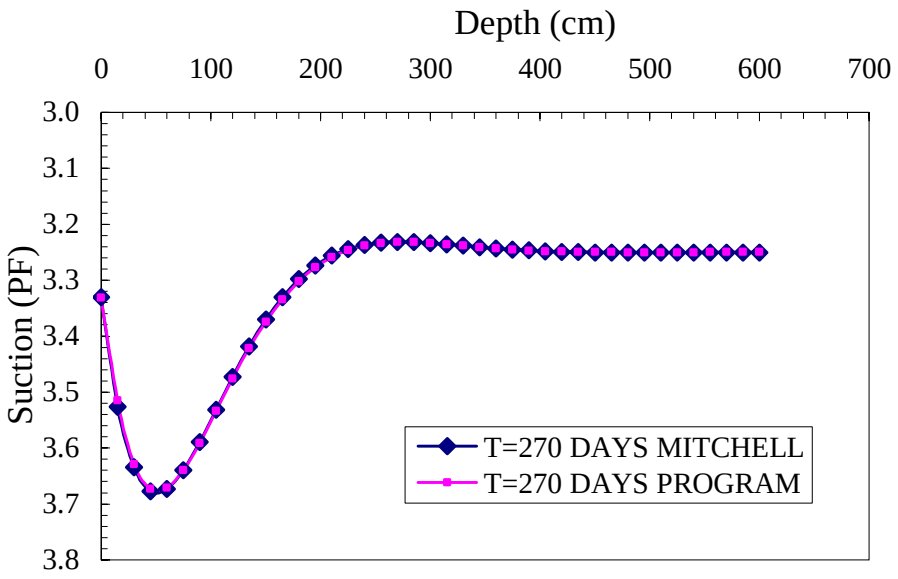

Figure 3.24 Numerical verification: comparison of flow analysis with 1-D Mitchell's analytical solution

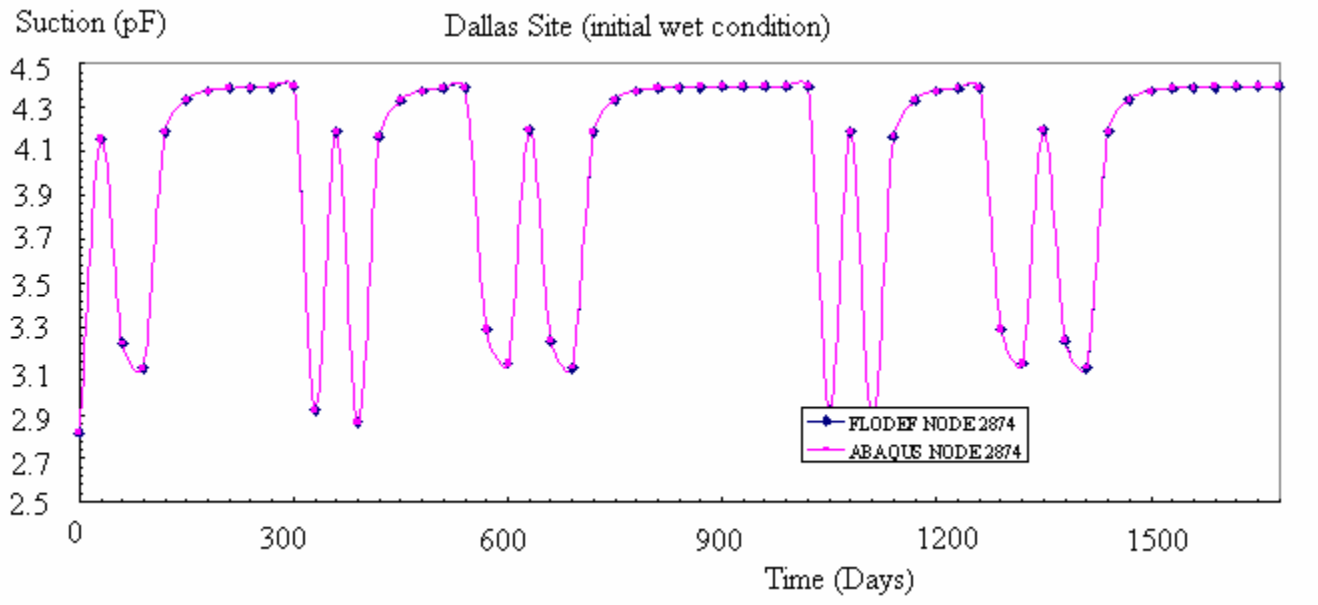

Figure 3.25 Numerical verification: comparison of flow analysis with 2-D ABAQUS results

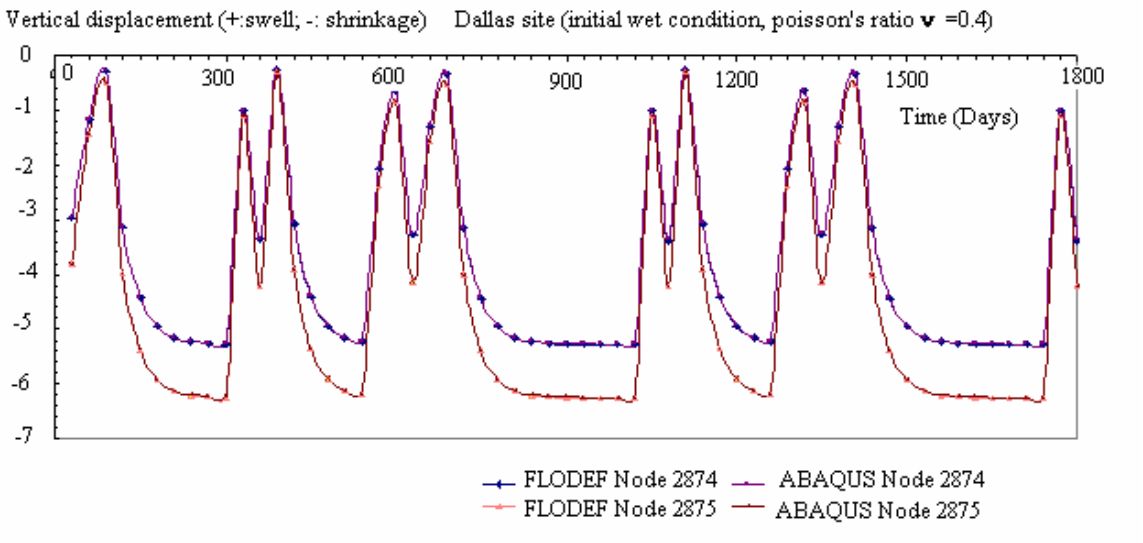

Figure 3.26 Numerical verification: comparison of displacement analysis with 2-D ABAQUS results

CHAPTER IV

APPLICATIONS OF COMPUTER PROGRAM FLODEF: SHEAR STRENGTH FORECAST OF CIVIL INFRASTRUCTURES ON EXPANSIVE SOILS

High plasticity clays are widely employed as an economic construction material for Civil Infrastructures such as highway embankments, retaining walls, pavement subgrades. When placed properly, the earth structures comprised of plastic clays can perform adequately with regard to overall stability and strength. However, softening of the surficial soils often begins soon after construction and continues for decades. Dramatic strength loss may occur, causing a significant maintenance problems associated with sloughing and shallow landslides.

This chapter discusses the use of the FEM computer program FLODEF to address the issue of strength degradation. The rate of strength loss, which is governed by the soil moisture diffusion property (soil diffusivity), is evaluated with the FEM simulations for different geometries of retaining walls, bare slopes and riprap protected slopes. A constant osmotic suction is assumed throughout the analysis period.

4.1 Introduction

The soils in the slopes and earth structures are normally unsaturated. Lytton (1994)'s shear strength equation in terms of stress variables ($(\sigma - u_a)$ and (u_a-u_w) is adopted for the numerical study:

$$\tau_f = c' + [(\sigma - u_a) + f\theta(u_a - u_w)]\tan\phi' \qquad \text{(Equation 4.1)}$$

where τ_f = the shear strength of an unsaturated soil,

c' = the apparent cohesion of saturated soil,

ϕ' = the effective angle of shearing resistance for a saturated soil,

θ = the volumetric water content,

f = the unsaturated shear strength function, which equals to 1 for saturated soils and $\frac{1}{\theta}$ when the water content equals to plastic limit,

$(\sigma - u_a)$ = the net normal stress on the plane of failure at failure,

$(u_a\text{-}u_w)$ = the matric suction of the soil on the plane of failure.

Suction provides a major contribution to unsaturated shear strength. It is primarily the matric suction part (u_a-u_w) that governs the engineering behavior of unsaturated soils for the normal total suction range (pF2.5~pF5.5) encountered in the field conditions. Shear strength loss occurs as surface moisture enters and infiltrates into the soil mass during wet periods, thereby reducing suction and weakening the soils.

4.2 Analysis of Earth Retaining Structures

A typical earth retaining structure comprises of a wall, pavement, drainage layer material adjacent to the wall element, and the compacted earth fill inside as depicted in Figure 4.1. The typical wall height is 20 ft. In this study, the analyses of two different aspect ratios of wall width to wall height (W/H) equaling 4:1 and 8:1 are performed.

4.2.1 Boundary Conditions and Initial Conditions for Flow Analyses

Figure 4.1 shows the boundary conditions and initial conditions for flow analyses. Three regions of Texas are considered in the study with the eastern region being the wettest (equilibrium matric suction pF3.2) and the western being the driest

(equilibrium matric suction pF4). Typical equilibrium matric suction for central Texas is pF3.5. The initial matric suction u_0 in the sub-grade soil is assumed to equal to the equilibrium suction u_e at the bottom of the moisture active zone depth. For compacted earth fill, u_0 is considered to be at the range of pF 3.5 to pF 4 based on past experience.

Moisture can enter the compacted earth fill from sub-grade soil or through the highly permeable drainage zones adjacent to the walls. If the earth fill is covered by a pavement or riprap slope protection, wetting would occur at the soil-pavement or soil-riprap interface due to the fact that evapo-transpiration is restrained by the cover and the moisture can flow inside through the joints and cracking in the surface.

A simple assumption is employed in the analysis that the matric suction at the drainage-earth fill interface equals the suction at the pavement or riprap-earth fill interface, which is pF 2 for wet interface and pF3 for normal interface. The natural sub-grade soils are assumed to have the same moisture diffusion property (moisture diffusion coefficient α) similar to the earth fill materials.

In the FEM analysis, the foundation has been truncated some reasonable horizontal distance from the wall for the no-flow boundary condition (a horizontal distance of one wall height for retaining structures having an aspect ratio of 4:1 and a distance of two times the wall height for aspect ratios of 8:1). An eight-node quadratic element is used and a 3*3 Gauss-Quadrature scheme is adopted for the full integration procedure.

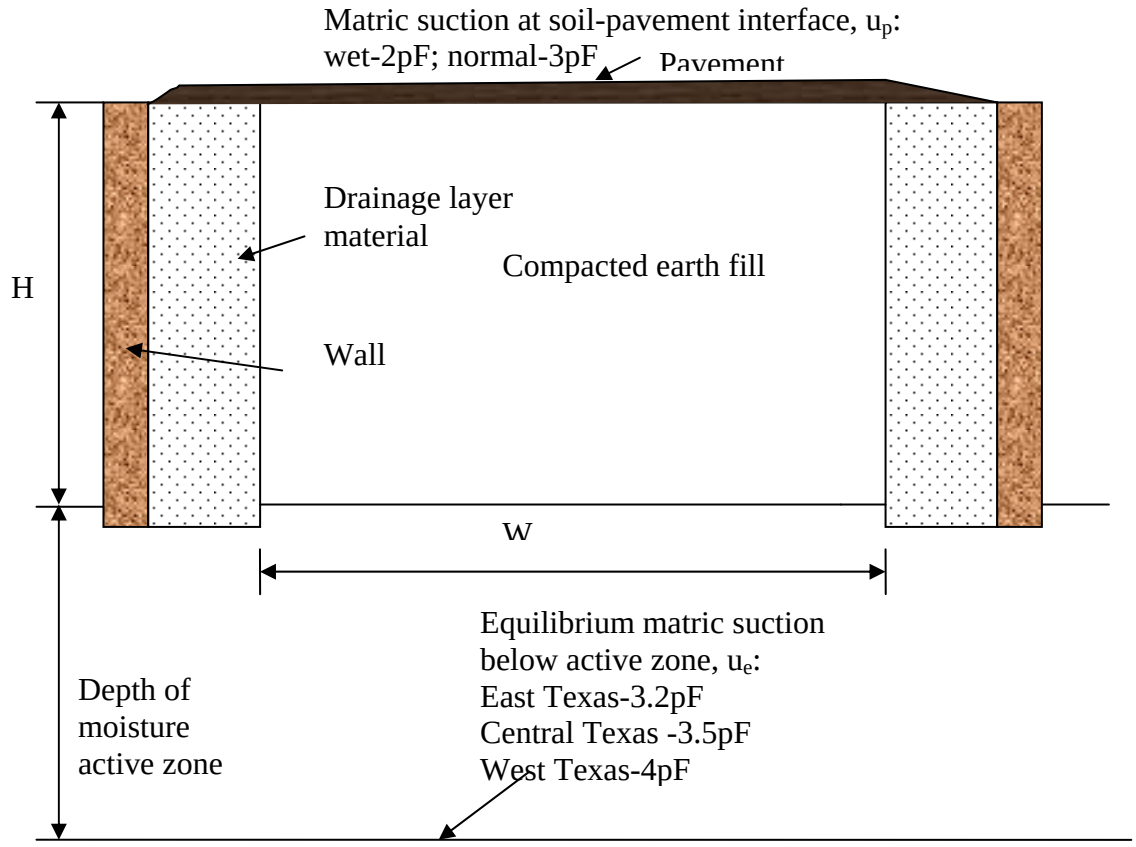

Figure 4.1 Schematic sketch of earth retaining structure

4.2.2 Moisture Active Zone Depth

The moisture active zone depth depends on the intensity of the moisture change imposed at the surface, the duration of that change, the soil fabric or fissures, root zone, diffusivity and expansiveness of the soil. Mckeen and Johnson (1990) used Mitchell's one-dimensional analytical solution for the linear diffusion equation and derived the estimation of the moisture active zone depth z_m as follows:

$$z_m = -\frac{1n(\frac{\Delta u_{\max}}{2u_0})}{\sqrt{\frac{n\pi}{\alpha}}} \qquad \text{(Equation 4.2)}$$

where $\Delta u_{\max}$ is the maximum allowable change in matric suction; u_0 is the amplitude of suction variation from equilibrium suction; n is the frequency of weather pattern (cycles/year) and α is the diffusion coefficient. Table 4.1 shows the typical moisture active zone depths for $\Delta u_{\max} = 0.1$.

Table 4.1. Typical Moisture Active Zone Depths for Surface Suction Change Conditions

Surface suction changes		Active zone z_m (ft) $\alpha=10^{-3}cm^2/sec$)	Active zone z_m (ft) $\alpha=10^{-4}cm^2/sec$)	Active zone z_m (ft) $\alpha=10^{-5}cm^2/sec$)
2 U_0 (PF)	n (cycle/y)			
5	0.5	18.1	5.7	1.8
5	1	12.8	4.0	1.3
4	0.5	17.0	5.4	1.7
4	1	12.0	3.8	1.2
3	0.5	15.7	5.0	1.6
3	1	11.1	3.5	1.1
2	0.5	13.8	4.4	1.4
2	1	9.8	3.1	1.0
1	0.5	10.6	3.4	1.1
1	1	7.5	2.4	0.8

The moisture diffusion coefficient α is normally in the range of 10^{-3} to 10^{-5} cm^2/sec. Surface suction fluctuation u_0 is within the range of pF0.5~pF2.5 (stable climate to extreme conditions and the frequency number n is between 0.5 and 1.5 cycles

per year. For the upper range of diffusion coefficient (10^{-3} cm^2/sec) and typical u_0 and n values, the moisture active zone depth is close to 20ft. In this study, z_m is set to 20ft.

4.2.3 Numerical Estimation of Suction Evolution with Time

The numerical analyses for matric suction prediction are presented in this section. A normalized dimensionless approach is utilized here since the moisture transmission is governed by the linear diffusion equation. The initial matric suction in the compacted earth fill is characterized by a parameter (U_0) as expressed in equation 4.3 (Aubeny and Lytton, 2003):

$$U_0 = \frac{u_0 - u_p}{u_e - u_p} \qquad \text{(Equation 4.3)}$$

where u_0 is the initial matric suction in the compacted earth fill and u_p is the matric suction at the soil-pavement interface . The numerical study of (U_0) values equaling 5, 4,3,2,1, and 0.5 is conducted. Also a normalized dimensionless term U is adopted for the prediction of matric suction u(x,y,t) as described in equation 4.4:

$$U = \frac{u - u_p}{u_e - u_p} \qquad \text{(Equation 4.4)}$$

The normalized time factor T is defined as follows:

$$T = \frac{\alpha t}{H^2} \qquad \text{(Equation 4.5)}$$

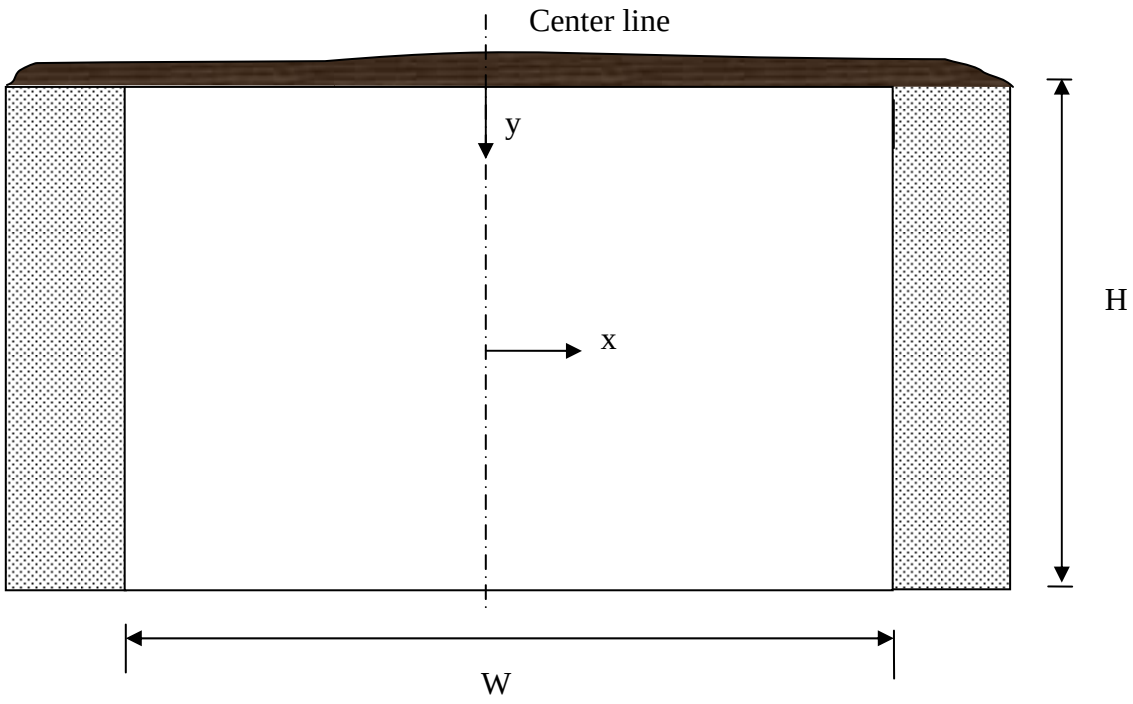

Figure 4.2 Definition sketch for matric suction prediction (Aubeny and Lytton, 2003)

where H=the height of the retaining wall structure,

α = the moisture diffusion coefficient of the clay;

t =real time; u_p and u_e are described as in Figure 4.1.

As depicted in Figure 4.2, the x-coordinate is measured from the centerline of the earth-retaining structure and the y-coordinate is measured from the bottom of the pavement. Since the structure is assumed to be symmetric, predicted suctions in the left half of the structure will be a mirror image of those in the right half. Horizontal and vertical dimensions are normalized by the height of the wall H, i.e., x/H and y/H. The suction profiles along horizontal cross-section at four locations (at the bottom, quarter, half and three-quarter elevations of the wall) are presented.

Consistent units should be employed in the analysis. For example, if foot and years are selected as the units of the height of the wall and real time, the moisture diffusion coefficient α should be expressed in ft^2/year.

The matric suction prediction for different values of normalized initial matric suction U_0 equaling 5, 4,3,2,1 and 0.5 with two aspect ratios 4H: 1W or 8H: 1W are given in Figures 4.3-4.14.

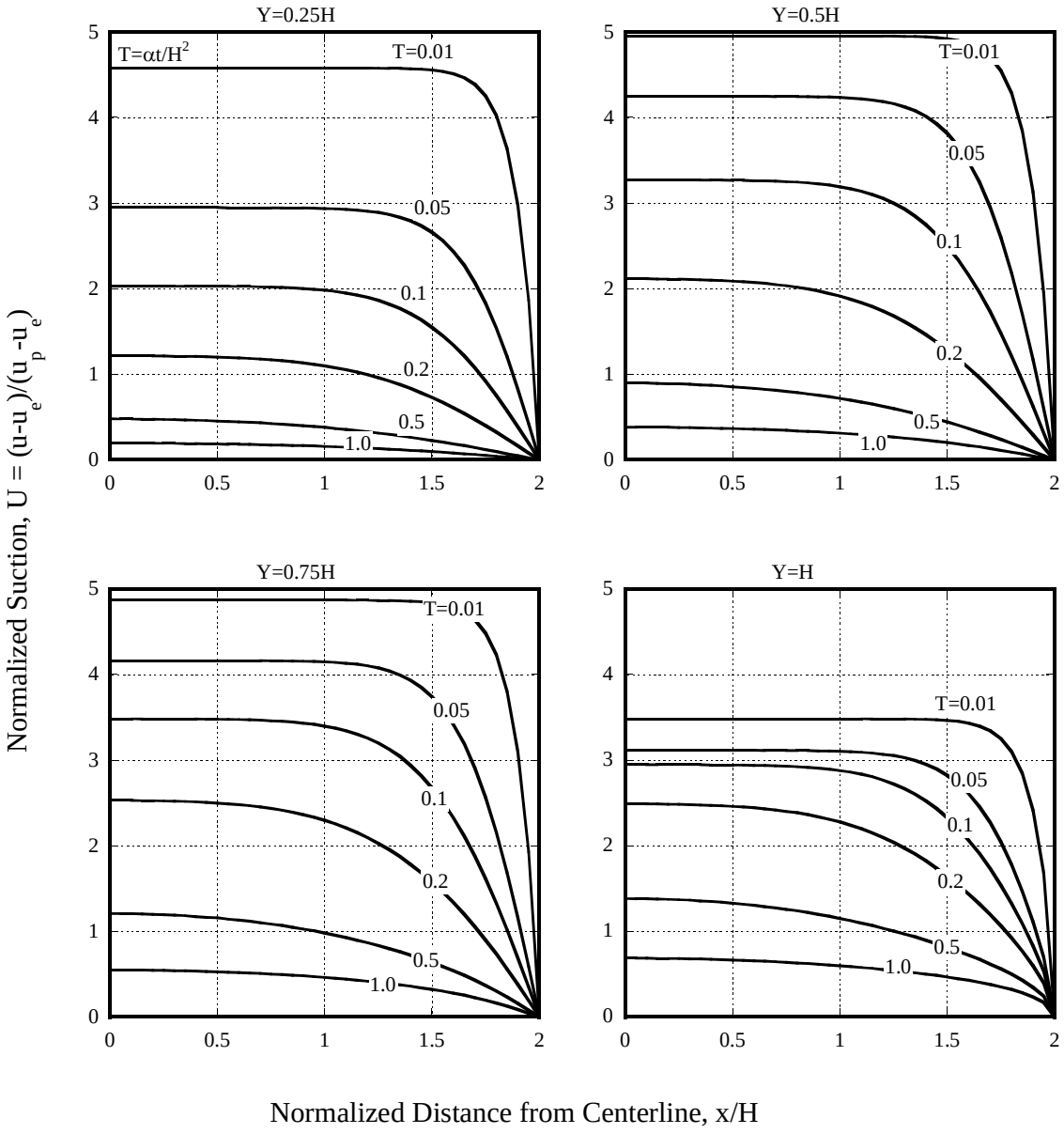

Figure 4.3 Matric suction prediction for retaining wall with aspect ratio 4H: 1W and U_0=5

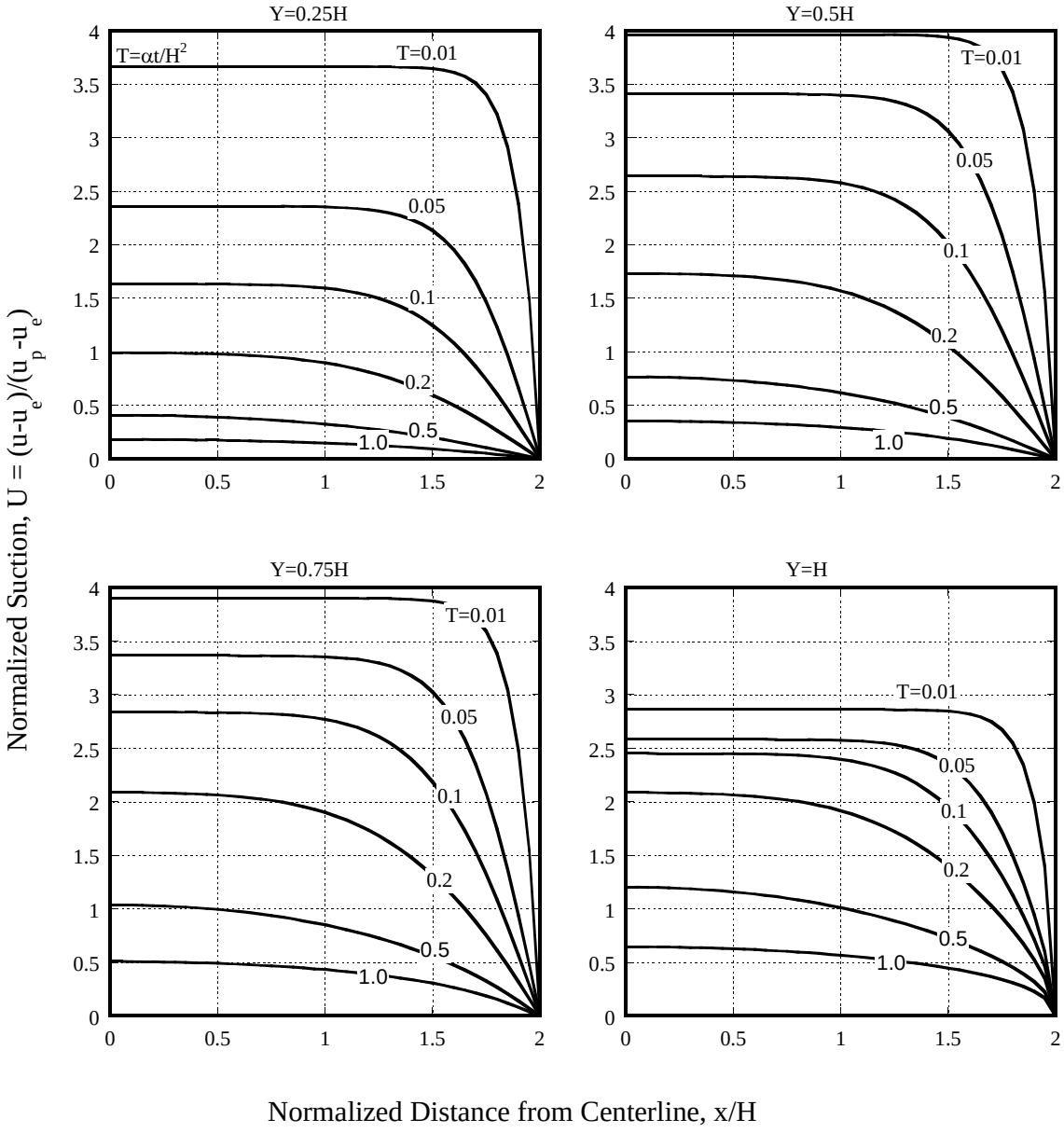

Figure 4.4 Suction prediction for retaining wall with aspect ratio 4H: 1W and U_0=4

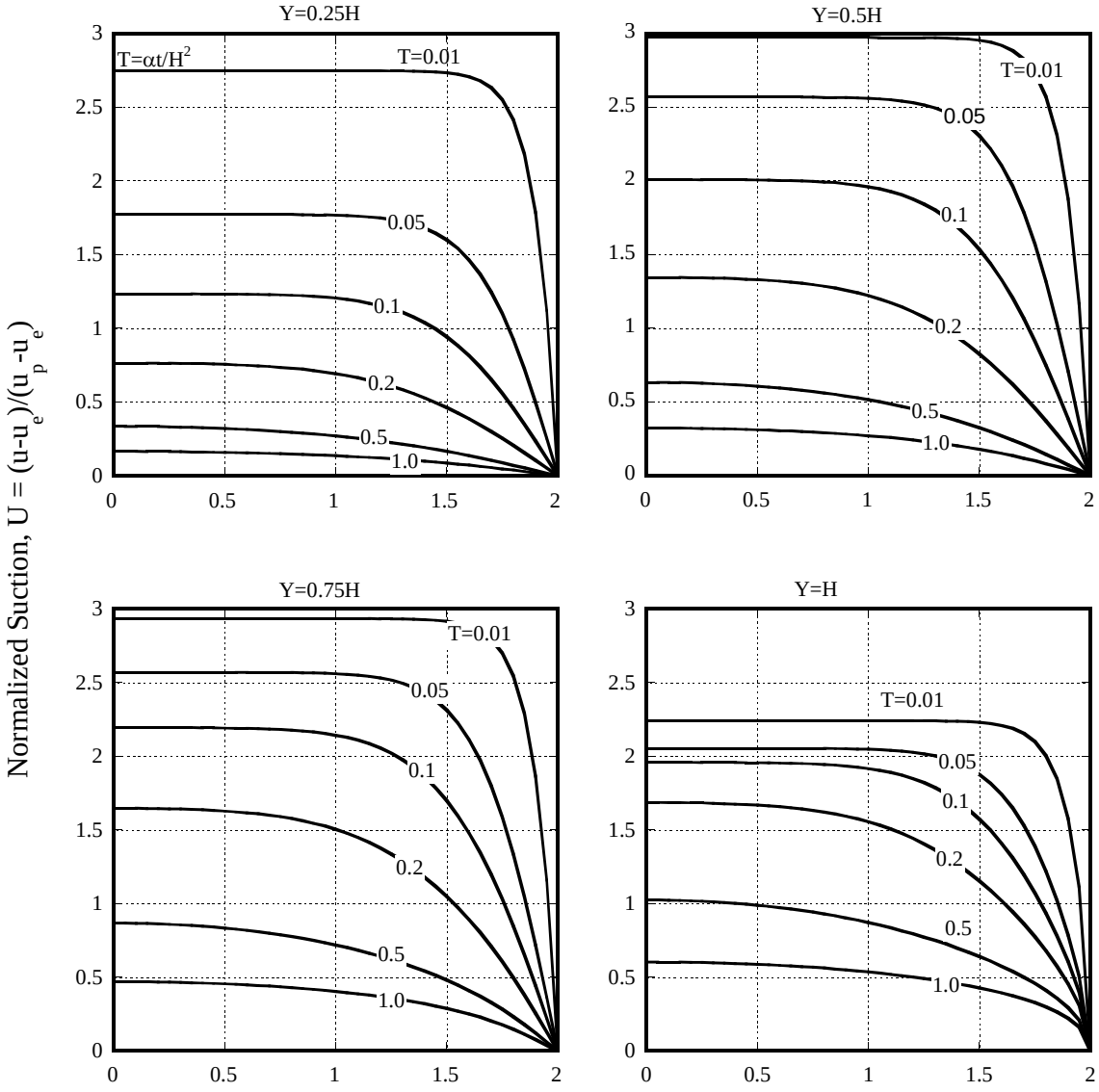

Figure 4.5 Matric suction prediction for retaining wall with aspect ratio 4H: 1W and U_0=3

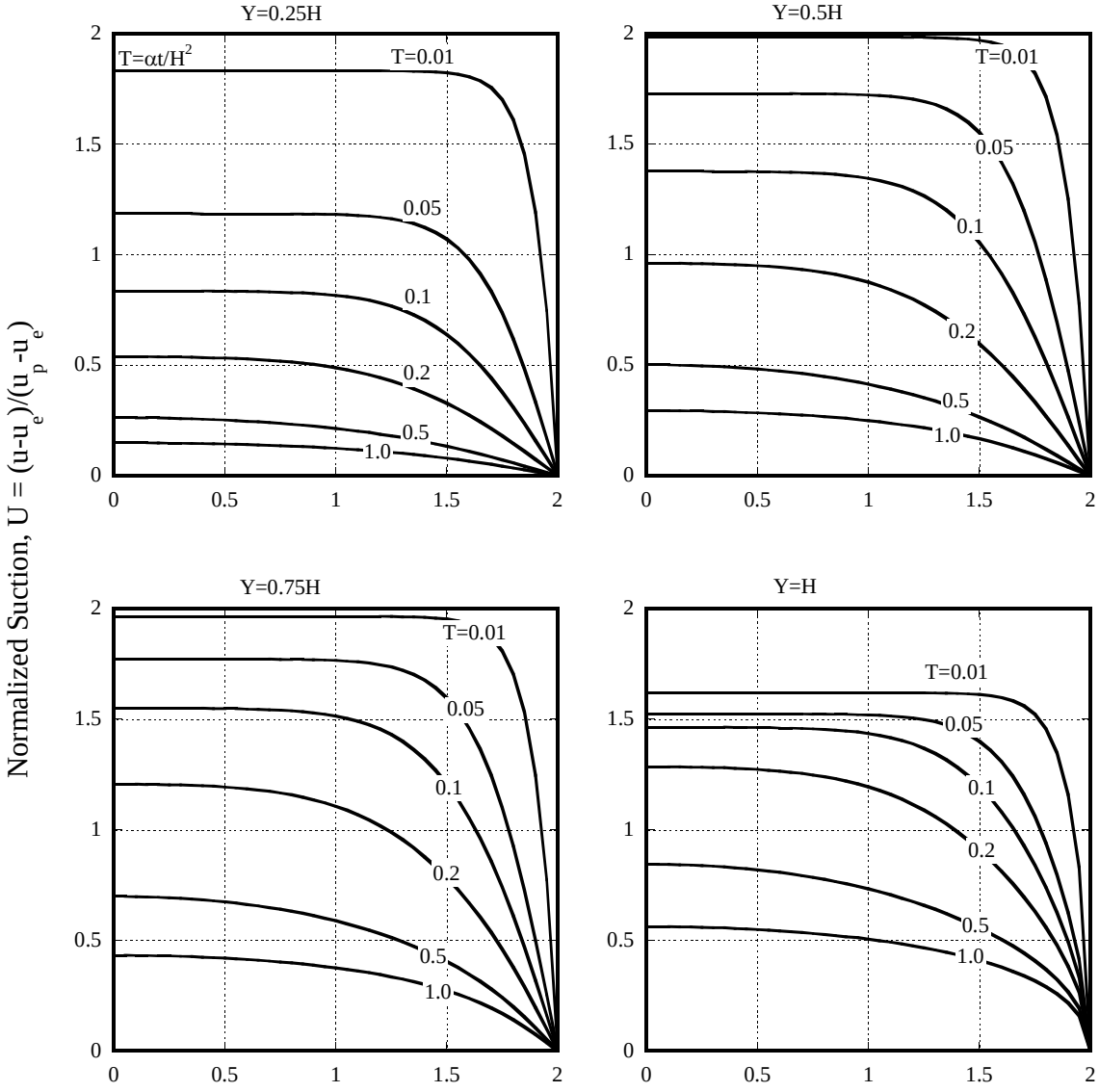

Figure 4.6 Matric suction prediction for retaining wall with aspect ratio 4H: 1W and U_0=2

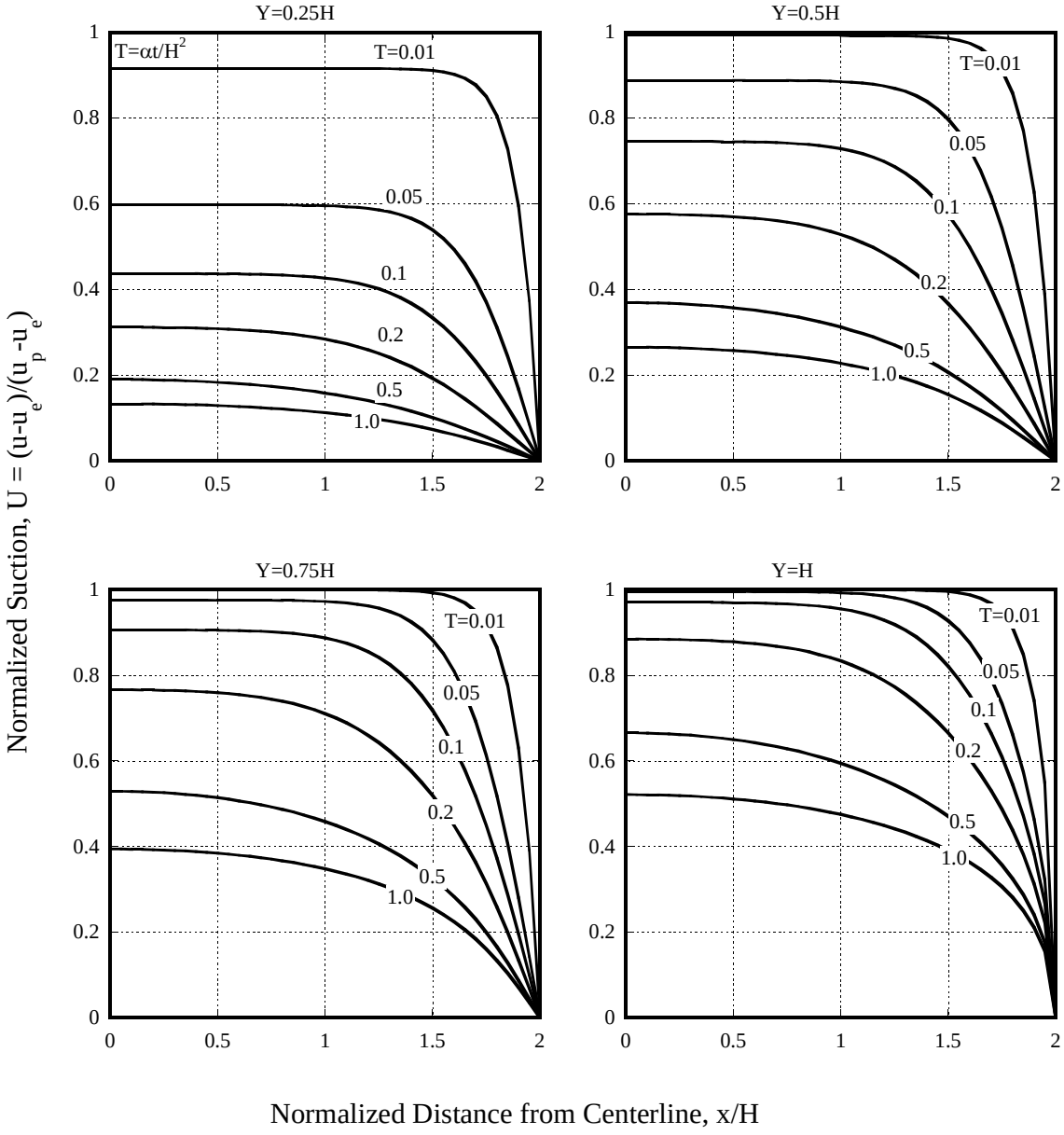

Figure 4.7 Matric suction prediction for retaining wall with aspect ratio 4H: 1W and U_0=1

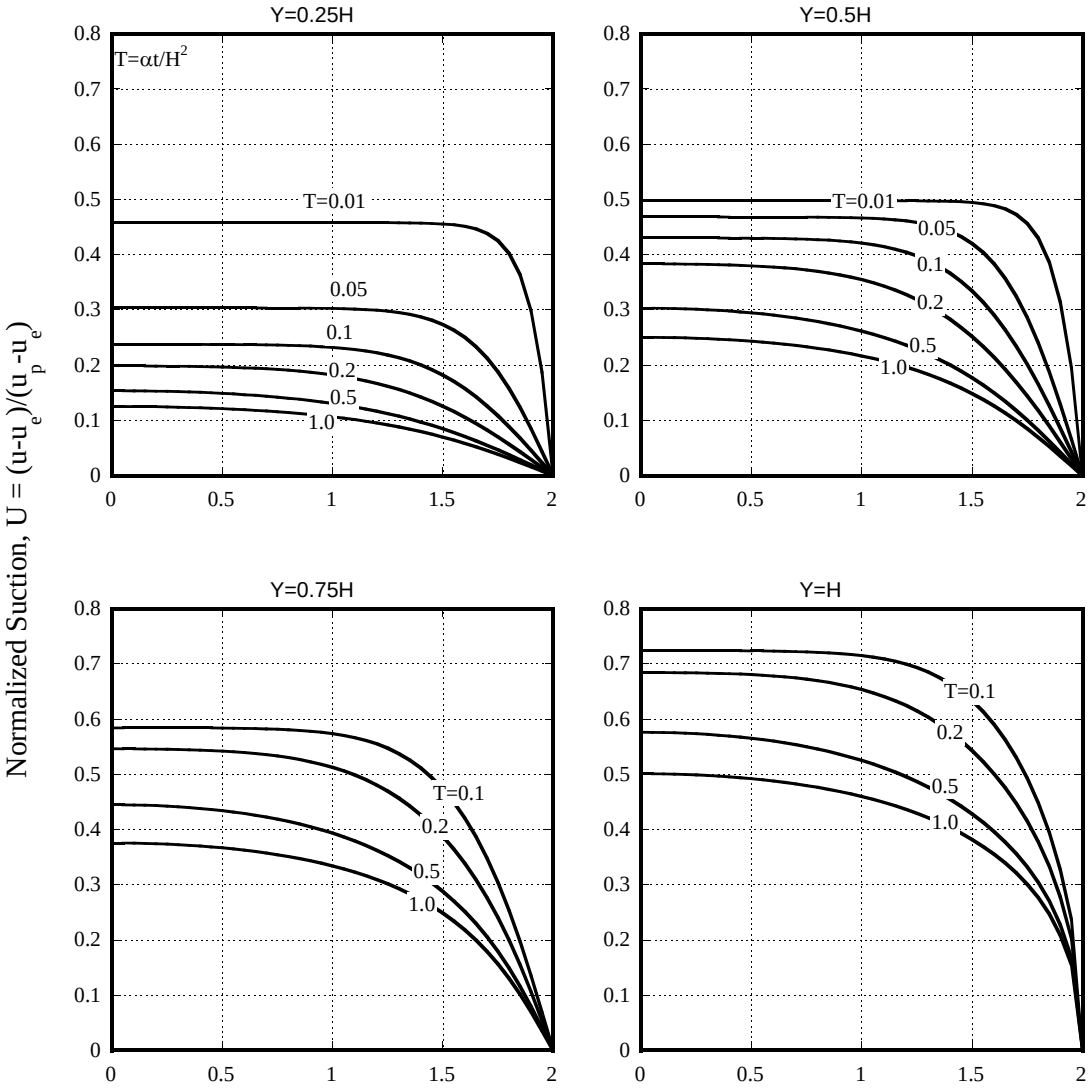

Figure 4.8 Matric suction prediction for retaining wall with aspect ratio 4H: 1W and U_0=0.5

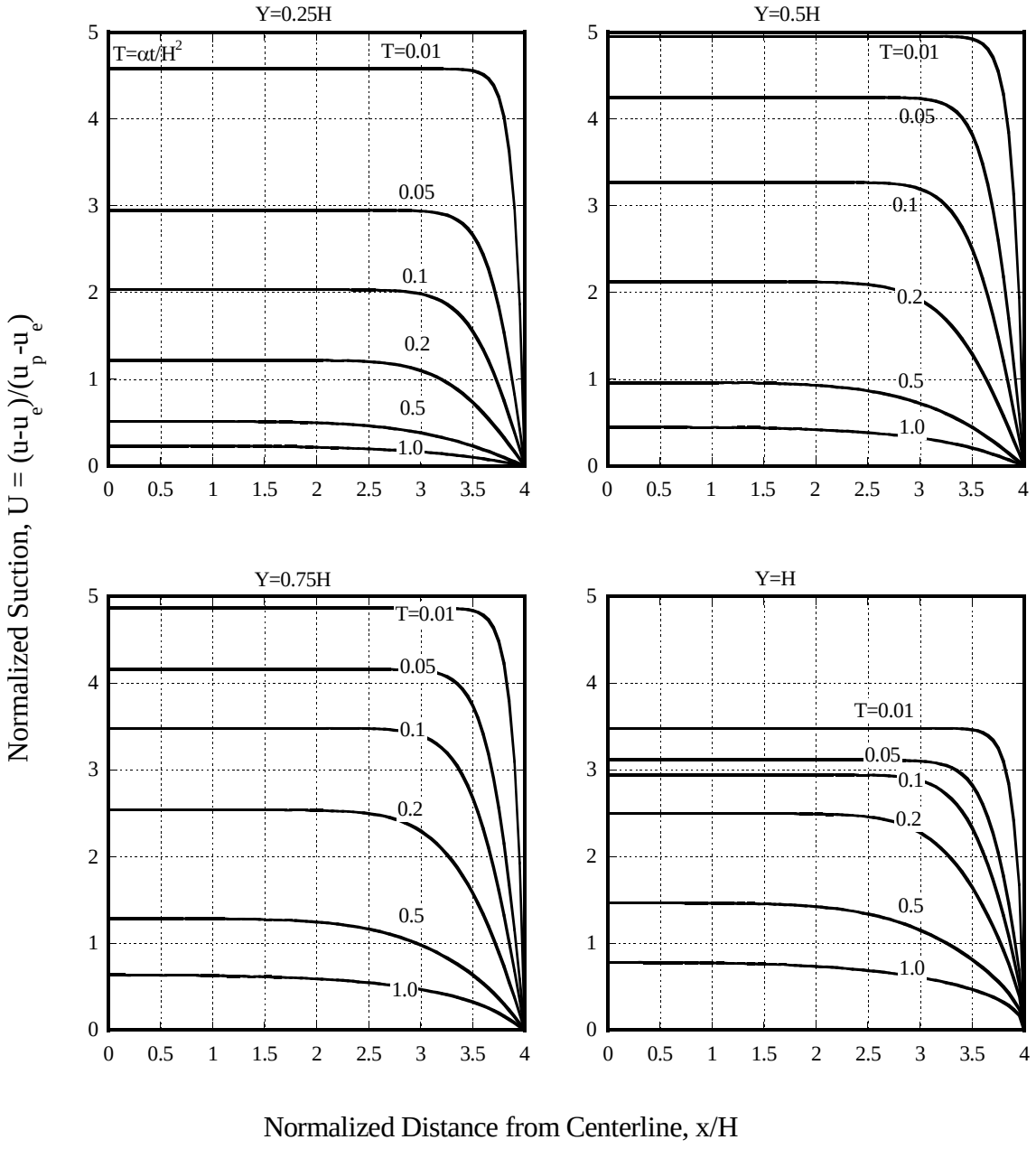

Figure 4.9 Matric suction prediction for retaining wall with aspect ratio 8H: 1W and U_0=5

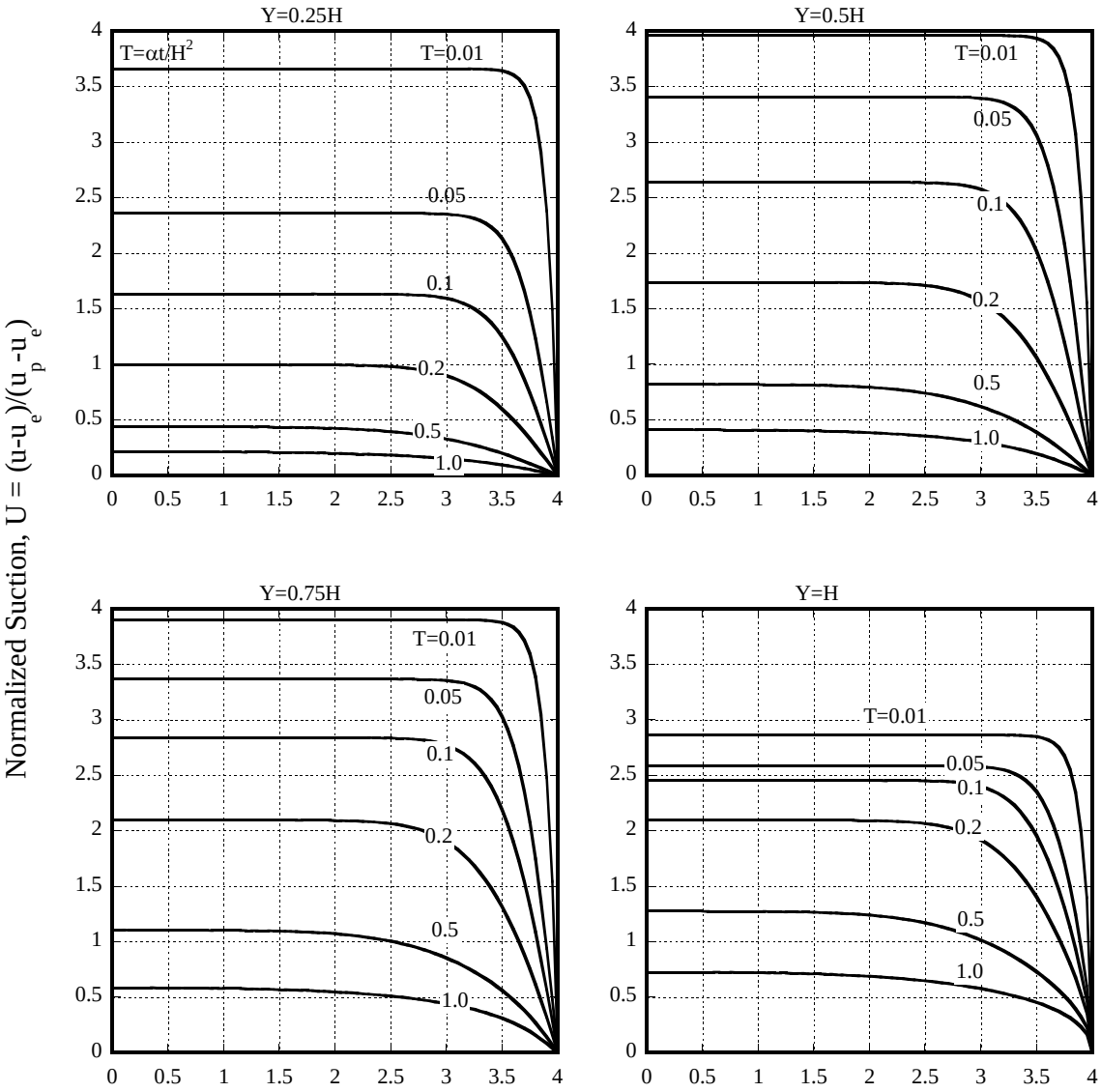

Figure 4.10 Matric suction prediction for retaining wall with aspect ratio 8H: 1W and U_0=4

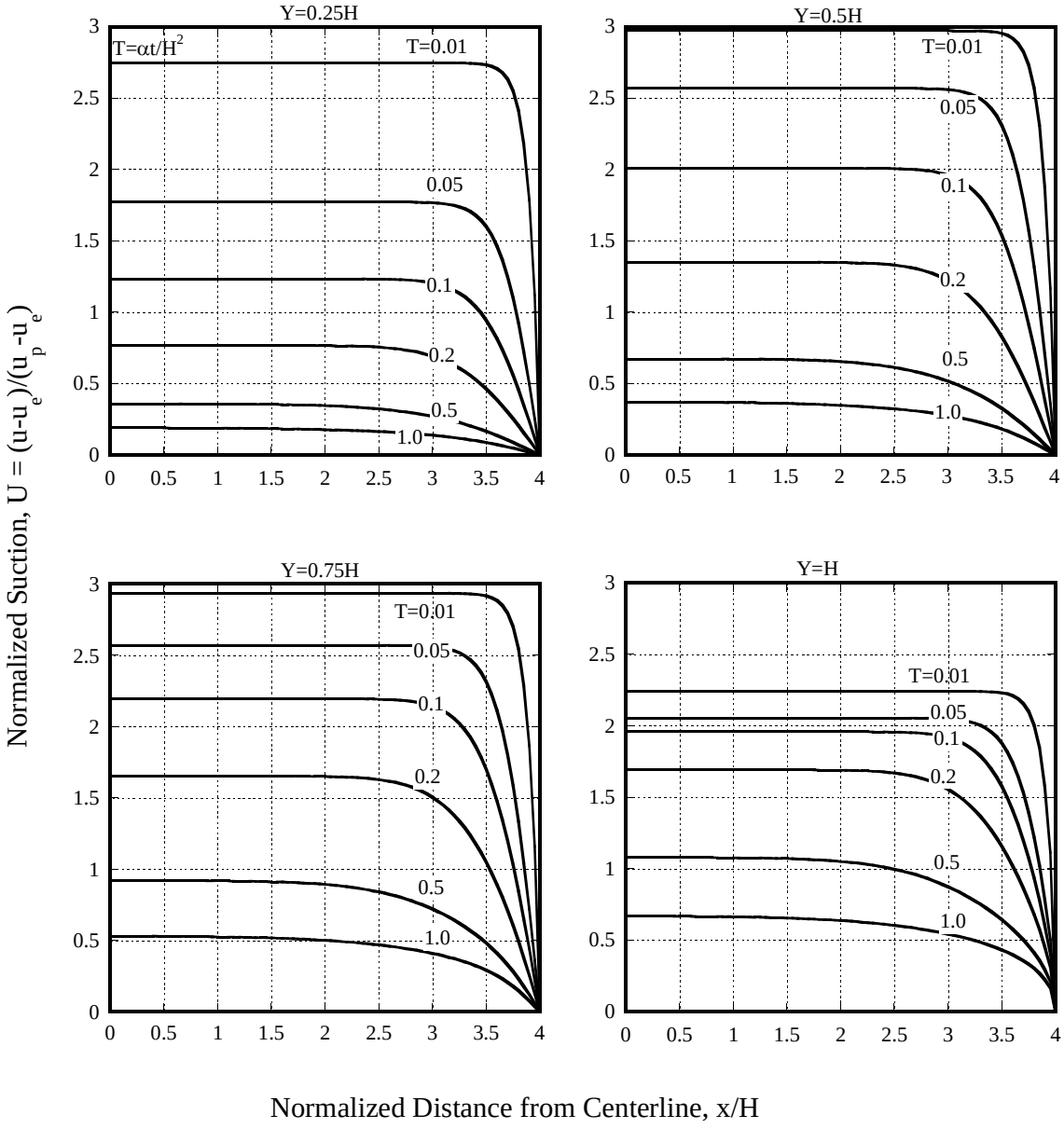

Figure 4.11 Suction prediction for retaining wall with aspect ratio 8H: 1W and U_0=3

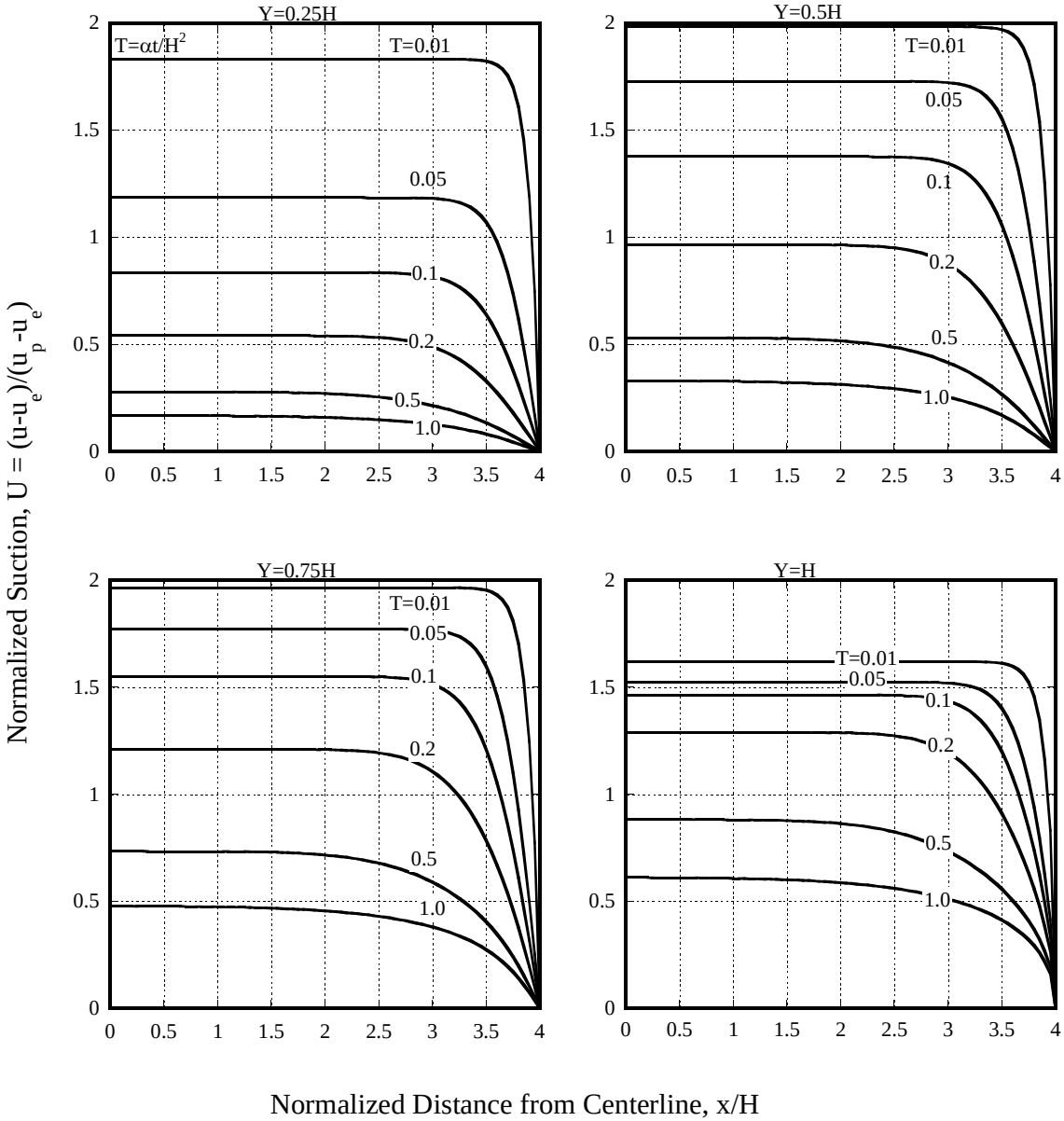

Figure 4.12 Matric suction prediction for retaining wall with aspect ratio 8H: 1W and U_0=2

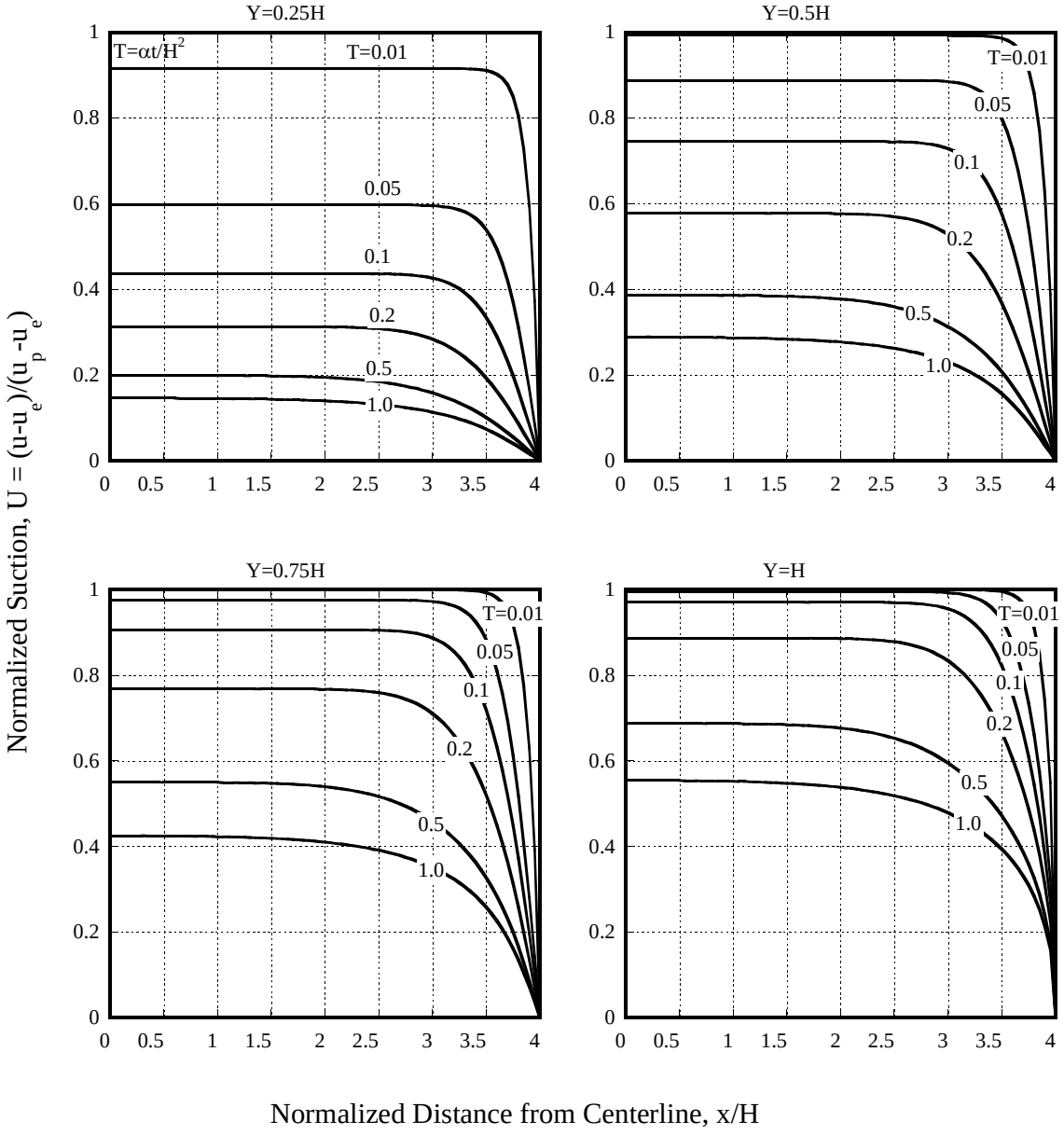

Figure 4.13 Matric suction prediction for retaining wall with aspect ratio 8H: 1W and U_0=1

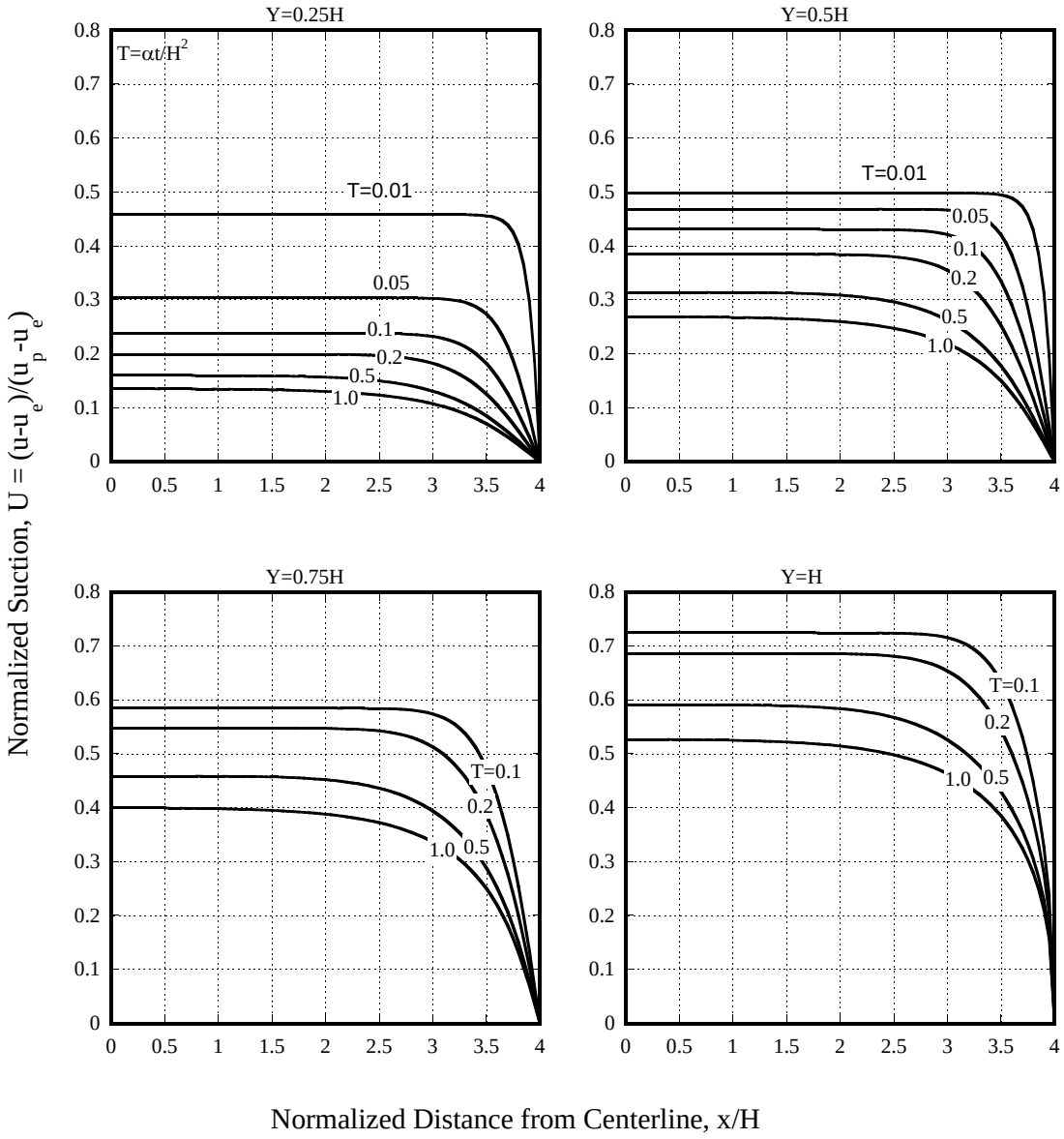

Figure 4.14 Matric suction prediction for retaining wall with aspect ratio 8H: 1W and U_0=0.5

4.2.4 Shear Strength Envelope Prediction

4.2.4.1 Formulation

The shear strength in unsaturated compacted soil can be calculated as follows (Figure 4.15):

$$\sin\phi' = \frac{c_{uc}}{c_{uc} - \theta f h_m}$$
$$c_{uc}\sin\phi' - \theta f h_m \sin\phi' = c_{uc} \qquad \text{(Equation 4.6)}$$
$$c_{uc} = -h_m f\theta\left(\frac{\sin\phi'}{1-\sin\phi'}\right)$$

where ϕ'=mechanical stress internal friction angle, h_m= matric suction, f= the unsaturated shear strength function, which equals to 1 for saturated soils and $\frac{1}{\theta}$ when the water content equals to plastic limit as previously described.

The effective friction angle ϕ' can be directly measured in the laboratory, using a consolidation-drained (CD) shear test or a consolidation-undrained (CU) shear test with pore pressure measurements. Also, the effective friction angle can often be satisfactorily estimated from equation 4.6 (Holtz and Kovacs, 1981):

$$\sin\phi' = 0.8 - 0.22\log_{10}(PI) \qquad \text{(Equation 4.7)}$$

where PI is the plastic index.

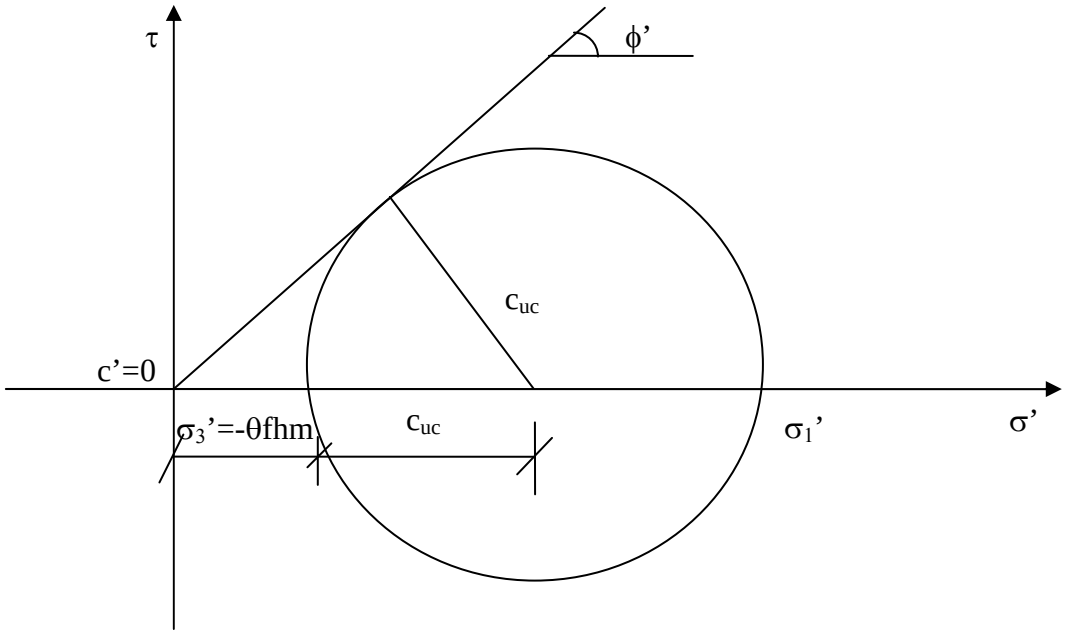

Figure 4.15 Mohr circle for the shear strength of unsaturated compacted soils (Lytton, 2001)

Considering the generated load-induced pore pressures as full saturation is approached during wetting of a soil, Aubeny and Lytton (2003) proposed Equation. 4.7 for prediction of unsaturated compacted soil shear strength:

$$c_{uc} = -h_m f\theta\left(\frac{\sin\phi'}{1-(1-a_f)\sin\phi'}\right) \qquad \text{(Equation 4.8)}$$

where a_f is the Henkel pore pressure coefficient at failure. A typical value of Henkel's coefficient a_f for a compacted soil wetted to saturation is 1.4, which corresponding to a Skempton A-parameter at failure A_f=1 typical of a normally consolidated soil in triaxial compression. Research has shown that wetting a soil tends to erase the memory of

previous mechanical stress and compacted overconsolidated natural clays act essentially as a normally consolidated clay when wetted (Stark and Duncan, 1991; Kayyal and Wright, 1991). Equation 4.7 is a lower bound (undrained) estimate of the unconfined shear strength for unsaturated compacted soil.

The numerical prediction for matric suction h_m evolution with time (Figures. 4.3-4.14) can be utilized for the forecast of shear strength envelope as shown in an example problem in the following part.

4.2.4.2 Example Problem

In Table 4.2, the engineering properties of a compacted earth fill for an earth-retaining structure 20ft high with 80ft wide (4H:1W) are given.

Table 4.2. Engineering Properties for the Shear Strength Calculation Illustration (Aubeny and Lytton, 2003)

Engineering Parameter	Value
ϕ'	30
α (cm^2/sec)	3×10^{-5}
γ_d (lb/ft^3)	93
w (%)	26.2
G_s	2.71
Plastic limit	26

For a point located 30 ft from the centerline at the mid-depth of this retaining structure, the shear strength of compacted earth fill after 20 years can be computed. The retaining wall is built in West Texas, i.e., the equilibrium suction value u_e is 4pF. The matric suction in the earth fill at the time of placement is u_0=4pF. Wet conditions prevail beneath the pavement, i.e., the matric suction at the pavement-earth fill interface u_p equals to 2pF.

Figure 4.6 is employed for the matric suction prediction. The dimensionless coordinates for this point is: x/H=30ft/20ft=1.5, y/H=0.5H/H=0.5.The dimensionless time factor T for 20 years is calculated as: T=$\frac{\alpha t}{H^2} = 0.05$. Dimensionless initial suction is equal to:$U_0 = \frac{u_0 - u_p}{u_e - u_p} = 1$. Entering Figure 4.6 these values, the dimensionless suction can be observed as 0.80, which can be converted to real suction in Equation 4.9:

$$u = U(u_e - u_p) + u_p \qquad \text{(Equation 4.9)}$$

The real suction value at 20 years is 3.6pF, i.e., -8138.5psf. After the hydrostatic pressure correction for the case in which the water in the soil voids is continuous, the corrected matric suction is -7518.5psf. The void ratio e can be computed from Equation 4.10:

$$e = (\frac{G_S \gamma_w}{\gamma_d}) - 1 = 0.818 \qquad \text{(Equation 4.10)}$$

The degree of saturation S is calculated as: $S=\frac{wG_s}{e}=87\%$. Volumetric moisture $\theta = w(\frac{\gamma_d}{\gamma_w})$ =39%. By interpolation, the unsaturated shear strength function f is taken as 2.07. Based on Equation 4.6, the unsaturated soil shear strength for this point at 20 years is computed as 6067 psf and the lower limit of shear strength is 2529 psf from equation 4.7.

4.3 Analysis of Slopes

Slope failures of engineered embankments or cuts due to the weakened self-retain ability of the earth can cause severe problems and damages to highways, homes and water–retaining earth structures. The slope failures or mass movements can be triggered by atmospheric process (weather events, such as rainfall, freezing and thawing of soil water), geological process, and human modification of the landscape or some interaction of all the above.

The saturation and desaturation process is a critical issue for the assessment of potential landslides in unsaturated soil slopes. Steep slopes with an inclination greater than the effective friction angle of soil can maintain the overall stability due to the effect of soil suction, which can augment the shear strength and shear resistance. As the moisture infiltrates into the soil mass, the stabilizing effect of suction will be decreased and the attenuation of shear strength can lead to the occurrences of shallow slides (Figure 4.16) even in slopes that were flatter than the estimated normally consolidated friction angle of the soils (Kayyal and Wright, 1991).

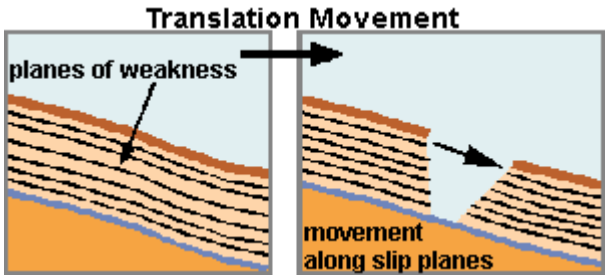

Figure 4.16 Shallow translational landslides in unsaturated soil slope (Watkins and Hughes, 2006. Available: http://wapi.isu.edu/envgeo/EG4_mass_wasting/EG_module_4.htm)

Aubeny and Lytton (2003) studied the 34 documented shallow translational landslides in Texas high plasticity clays (Paris clay and Beaumont clay) from the Kayyal -Wright study and observed the vertical depths of slides ranged from 0.7 to 3 m, mostly around 1.2~1.8 m as shown in Table 4.2. Thielen and Springman (2006) used TDR (time domain reflectometry) method to study the response of moisture condition change to rainfall. They found that in summer, a response to rainfall infiltration could be observed in the upper soil layer (depth close to 0.6 m) and during the winter, the suction change and saturation appear at greater depth (>1.20m) and up to 1.50m.

Suction is a key parameter for the assessment of shallow slides in unsaturated clay slopes and the failure mechanism involves the moisture infiltration into the slope surface and the resultant decreases of suction and shear strength during wetting process.

4.3.1 Methodology for Stability Analyses of Unsaturated Soil Slopes

The stability analysis can be preceded within the framework of a classical infinite slope analysis (Figure 4.17) given the fact that the shallow slides have small vertical dimensions relative to the lateral extent (Aubeny and Lytton, 2003). The unsaturated

flow analysis and structural stability analysis are the essential two parts to investigate the pore pressure distribution and the degree and time rate of strength degradation which resulting in the driving forces in the slopes exceeding the resisting stresses and the occurrence of slope failures.

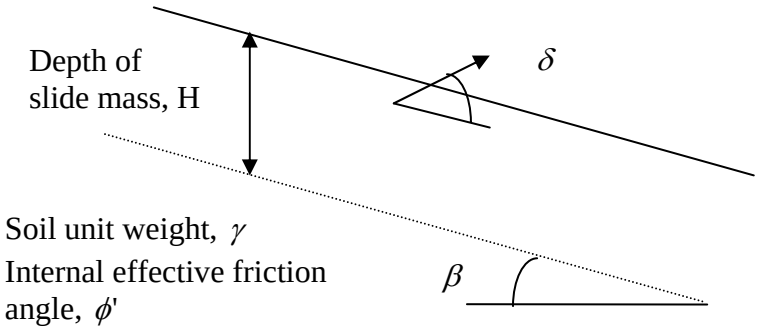

Figure 4.17 Definition sketch for shallow slide analysis (Aubeny and Lytton, 2003)

4.3.1.1 Flow Analysis

The unsaturated flow analysis is governed by the gradient of total suction or matric suction if uniform constant osmotic suction condition is prevalent. The moisture diffusion process depends on the moisture diffusion characteristics of the soil (diffusivity), local drainage condition, climate, vegetation and surface desiccation cracking. The boundaries of soil suction exposed to prolonged wetting are assigned a matric suction u_b=2pF or total suction 2.5pF at the field capacity.

In engineering practice, two types of slopes are prevalent: soil mass in bare slope with or without vegetation cover in which surface desiccation cracks exist and an intact soil mass covered by concrete protective slabs referred to as “riprap”.

Figure 4.18 gives the definition sketch for moisture diffusion analysis regarding intact slopes and bare slopes. For the bare slope analysis, the assumption of crack spacing equaling crack depth is based on the study of crack pattern in the field by Knight (1971) and Konrad and Ayad (1997) as described in detail in Chapter VI. Removal of slabs and pavements often shows that moisture eventually penetrates through joints in the slab such that the soil directly beneath the slab becomes extremely wet. Also the presence of the slab tends to inhibit drying during dry climatic periods and prevents the onset of desiccation cracks; therefore, the soil directly beneath the slab is typically in a permanently moist condition. A normalized dimensionless approach is adopted for the matric suction prediction same as the retaining wall analysis. A net normalized suction U is brought and defined as:

$$U = \frac{u_0 - u}{u_0 - u_b} \qquad \text{(Equation 4.11)}$$

where u_0 is the initial suction of soil mass after construction of the slope and u_b is the matric suction (2pF) at the slope surface boundary. The dimensionless time factor T is related to real time t at any distance of interest from the free slope surface z by:

$$T = \frac{\alpha t}{z^2} \qquad \text{(Equation 4.12)}$$

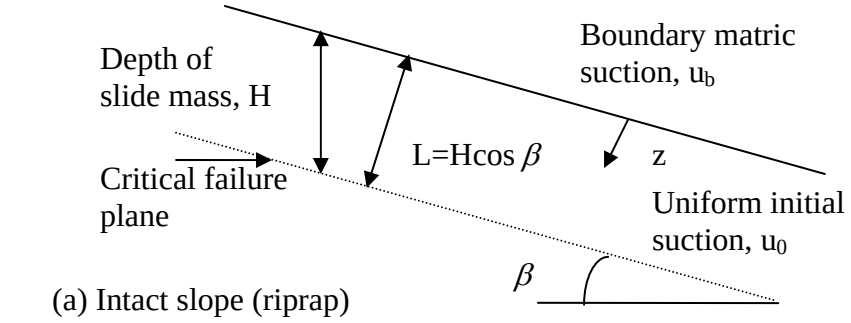

(a) Intact slope (riprap)

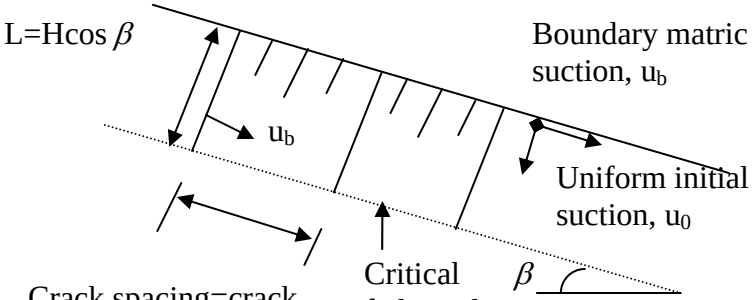

(b) Cracked surface (bare slope)

Figure 4.18 Definition sketch for moisture diffusion analysis (Aubeny and Lytton, 2003)

Desiccation cracks subdivide the soil mass into a series of square columns with the column heights equaling the crack space. Surface cracks can provide conduits for moisture infiltration and the deepest cracks will be the least affected by drying periods and the most likely to remain permanently wet. In the moisture diffusion analysis, as a first approximation, only the primary deepest cracks are considered.

Both analytical solutions can be found for the flow analyses for intact slopes and bare slopes for heat flow problems. For the case of intact surface, the analytical solution

can be expressed in terms of the complementary error function (erfc) (Lawton and Klingenberg, 1996):

$$U = \frac{u - u_0}{u_b - u_0} = erfc(\frac{1}{2\sqrt{T}}) \qquad \text{(Equation 4.13)}$$

and in case of bare slopes , the analytical solution for this boundary value problem is:

$$U = \frac{u - u_b}{u_0 - u_b} = \sum_{m=1}^{\infty}\sum_{n=1}^{\infty} A_{mn}\phi_{mn} \exp\left\{-\pi^2(m^2 + n^2)T\right\};$$
$$A_{mn} = \frac{4}{\pi^2 mn}[\cos(m\pi) - 1][\cos(n\pi) - 1] \qquad \text{(Equation 4.14)}$$
$$\phi_{mn} = \sin(m\pi x / L)\sin(n\pi y / L)$$

where L is the perpendicular depth from the free slope surface to the critical failure depth. Summaries of analytical solution and numerical simulations give the dimensionless time factor T_f=0.3 for the moisture migration from the wet boundary $u_{b=}$ (2pF) to the center of the soil mass, i.e., x=L/2 and y=L/2 and the time factor T is well above 10 for the suction at critical depth on the order of 1.5mto decline to the field capacity, in the case of intact slopes.

The back calculated time factors from Kayyal – Wright study are T_f=0.42-1.2 for Paris clays and T_f=1.2-3.7 for Beaumont clays. The plausible explanations may be the overestimation of the moisture diffusion coefficient for the back-calculation of time factor T, time period for crack initiation and propagation, crude estimation of cracking pattern and field capacity soil boundary condition assumption (Aubeny and Lytton, 2003). Also it should be bear in mind that the analysis is executed under the two-dimensional scenario while the actual landslides occur three-dimensionally. Duarte et al. (2006) concluded that three-dimensional effects are important and an increase of the

safety factor above 30% from the 2D to the 3D analyses can be observed in some case studies.

4.3.1.2 Slope Stability Analysis

Aubeny and Lytton (2003) considered the shear-induced pore pressure during the process of gradual moistening and softening of the soil mass and derived the expression for the pore-water pressure at the base of potential slide mass of critical depth H:

$$u_w = u_{w0} + \gamma H \cos^2 \beta + \sqrt{\frac{2}{3}} a \gamma H \sin \beta \cos \beta \qquad \text{(Equation 4.15)}$$

where u_w=pore-water pressure at a vertical depth H below slope surface; u_{w0}=pore-water pressure on surface of slope; γ = total unit weight of the soil; β = slope angle measured from horizontal; H=vertical depth; and a=Henkel shear-induced pore pressure coefficient.

The factor of safety (FS) against sliding under the assumption of a neutral case of no moisture entering or exiting the slope is:

$$FS = (\frac{\gamma_b}{\gamma}) \frac{\tan \varphi'}{\tan \beta} - \frac{u_{w0} \tan \varphi'}{\gamma H \sin \beta \cos \beta} - \sqrt{\frac{2}{3}} a_f \tan \varphi' \qquad \text{(Equation 4.16)}$$

where γ_b =buoyant unit weight of the soil; γ =total unit weight of the soil; u_{w0}=pore-water pressure on the surface of the slope; and a_f=Henkel coefficient at the failure state.

If moisture flow across the slope face occurs, Equation 4.15 can be modified as follows:

$$FS = (\frac{\gamma_b}{\gamma}) \frac{\tan \varphi'}{\tan \beta} - \frac{u_{w0} \tan \varphi'}{\gamma H \sin \beta \cos \beta} - \sqrt{\frac{2}{3}} a_f \tan \varphi' - (\frac{\gamma_w}{\gamma}) \frac{\sin \delta}{\cos \beta} \tan \varphi' \qquad \text{(Equation 4.17)}$$

where $\tan\delta$ =ratio of the hydraulic gradient of water flow normal to the slope to that parallel to the slope, with a positive δ denoting moisture exiting the slope (evaporation) and vice versa.

Equation 4.16 implies that the most critical condition experienced by an unsaturated clay slope is a period of evaporation following a prolonged infiltration period, when the suction reduction is at the maximum and the hydraulic gradient is unfavorably for the overall slope stability.

4.3.2 Engineering Treatment Techniques for Expansive Soil Slopes

There are many technical measures to treat expansive soil slopes in engineering practice, which can be classified as two types: rigid support method and flexible support method. The rigid support method is a treatment measure consisting of masonry structure (self-weight retaining wall, anti-slide piles) in conjunction with other necessary protective measures. The rigid support method is used widely in slope stabilization works. Since the slope soil body supported by the method is not permitted to deform, the swelling pressure inside the expansive soil mass can not be released. When it cumulates to a high level, the retaining wall structures can be snipped or pushed away and destroyed. The flexible support method uses treatment measures such as chemical improving, reinforcement with geogrid, in conjunction with other necessary protective schemes. The flexible support method can permit expansive soil deformation to some degree and the flexible support body can absorb the stress relief due to construction.

Yang and Zheng (2006) utilized flexible support schemes for the successful engineering treatment of expansive soils subgrade in Guangxi Nanning-Youyi Guan

expressway. They adopt the scheme of reinforcing side slope with geogrid to increase the overall stability for embankments and use root pile, blind drain and geogrid for the treatment of underpass cut slope as shown in Figures 4.19 and 4.20.

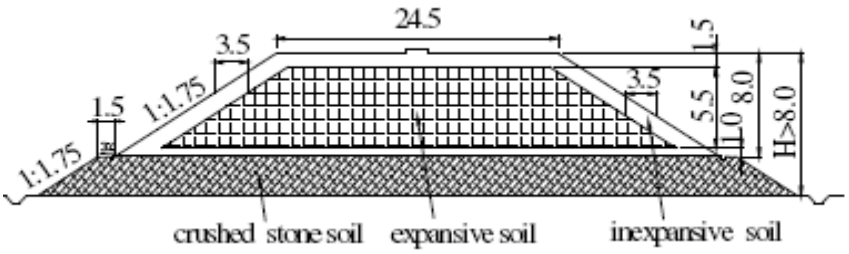

(a)

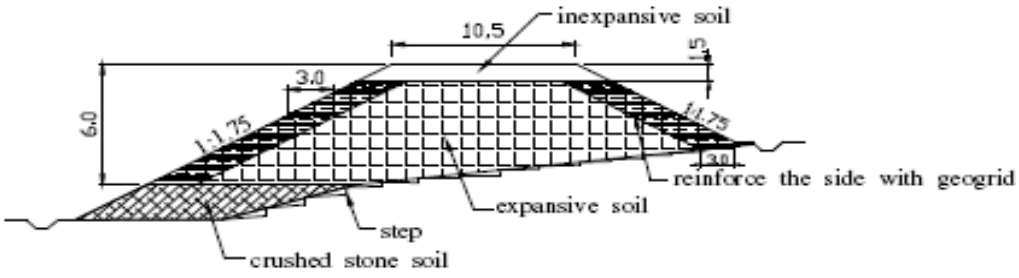

(b)

Figure 4.19 Engineering treatment scheme for expansive soil embankment (Yang and Zheng, 2006)

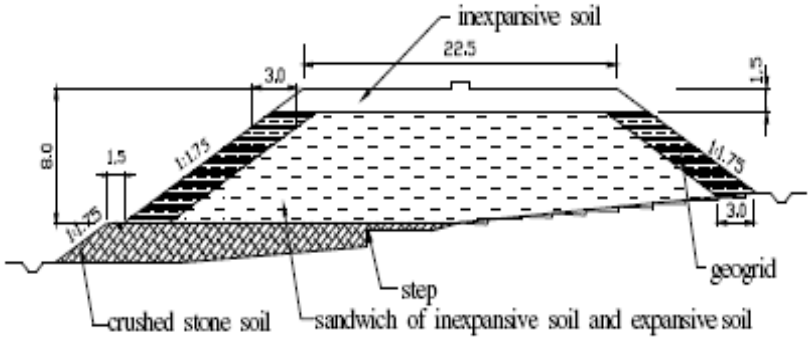

(c)

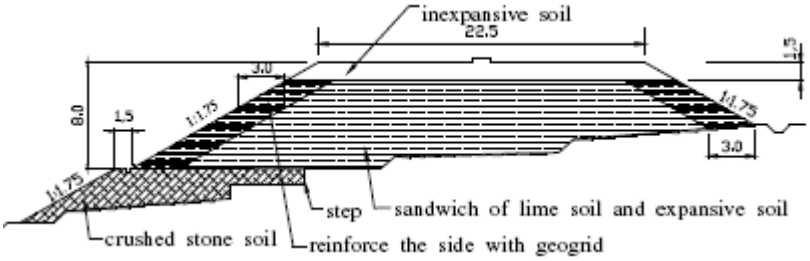

(d)

Figure 4.19 (Continued)

(a)

Figure 4.20 Engineering treatment scheme for expansive soil slopes (Yang and Zheng, 2006)

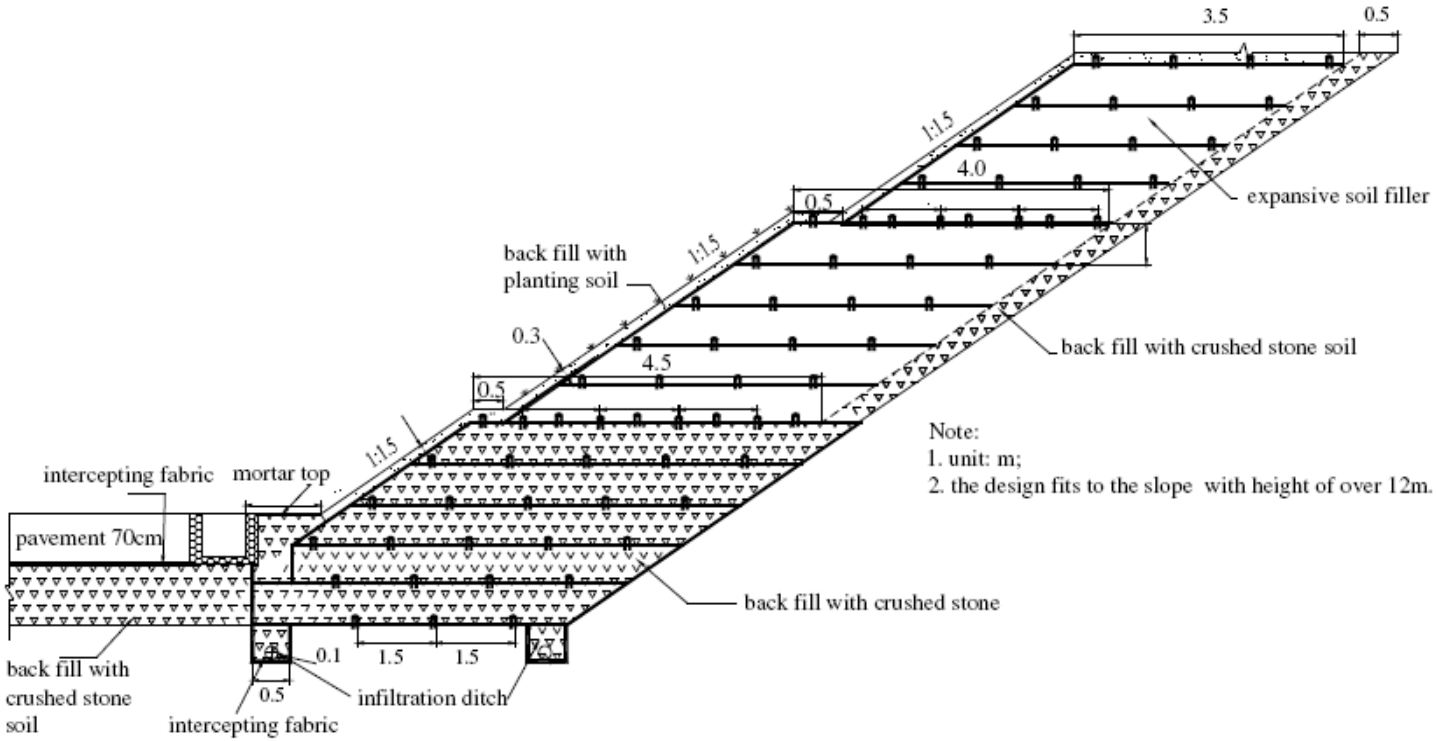

(b)

Figure 4.20 (Continued)

CHAPTER V

APPLICATIONS OF COMPUTER PROGRAM FLODEF: TRANSIENT FLOW-DEFORMATION ANALYSIS OF HIGHWAY PROJECT SITES

The engineering problems associated with expansive soils are widespread. The differential vertical surface movement in response to the subgrade moisture condition changes can cause the development of roughness (surface unevenness) and longitudinal cracks for pavement structures overlying expansive soil layers.

Prolonged and numerous efforts have been made by practitioners and researchers to mitigate the volume change problems of expansive soils using various engineering treatment methods. Based on the treatment mechanism, these measures can be categorized into two groups (Jayatilaka and Lytton, 1997): (1) alteration of expansive material by mechanical, chemical or physical means; and (2) control of subgrade moisture conditions.

Mechanical alteration includes ripping, scarifying, and then compacting the soil with moisture and/or density control. In the physical alteration method, expansive soil is excavated and replaced with granular or non-swelling material. Normally the application depth of ripping or scarifying is limited to approximately 45 cm to 60 cm, while sub excavation is confined to a maximum depth of 180 cm to 240cm. The chemical alteration refers to the addition of chemical compounds such as lime or cement to alter the characteristics of clay minerals.

The control of the subgrade moisture conditions can be achieved by isolating subgrade soil from moisture variation. The uses of physical barriers made with waterproofing membranes (vertical moisture barrier, horizontal barrier) and paving median have been utilized extensively in engineering practice to alleviate the problems. The use of a vertical moisture barrier installed in the shoulder of a pavement has been proved to be effective in stabilizing the moisture conditions beneath the highway (Picornell, 1985; Bredenkamp et al., 1998). The installation of a vertical barrier normally involves the excavation of trench, placing of an impervious fabric membrane, backfilling the trench with sand or gravel and mounting of a cement stabilized base cap over the backfill material.

In this chapter, FLODEF computer program is utilized in the evaluations of the design measurements such as vertical moisture barriers, horizontal moisture barriers (paved shoulder), soil replacement or improvement with lime stabilization and paving the median in reducing surface soil vertical displacement as shown in Figure 5.1. The reference pavement sites are located in Fort Worth Loop 820 Study Section A and B, Atlanta US 271, and Austin Loop 1. In the program, the moisture barrier is simulated by assigning a finite but very low diffusion coefficient α (around $10^{-8}cm^2/s$) to the barrier material. The thickness of moisture barrier is assumed to be 10cm. The major effect of lime treating or replacement of natural expansive soils with inert soils is to reduce the suction volumetric change index γ_h, which is the primary mechanism for reducing the magnitude of shrinkage and swelling movements. For the case of inert soils, the correlation of Atterberg limits, percent fines and percent clay to γ_h are based on actual

data. For lime-treated soil, an assumption is made that the change in soil properties due to the addition of lime can be fully characterized in terms of the effect of lime on Atterberg limits. It neglects the fact that lime treating can induce other changes in soil besides its change on PI, i.e., the effects of phenomena such as cementation are neglected.

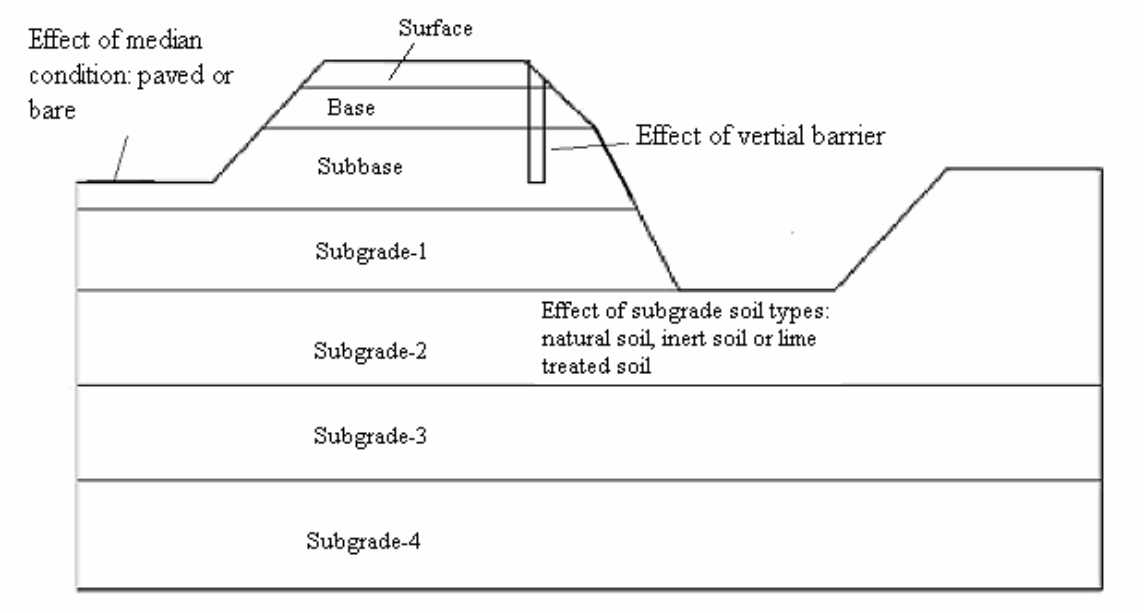

Figure 5.1 Parametric studies for engineering treatment measures

5.1 Fort Worth North Loop IH 820 Study Section A

In order to broaden the existing pavement structure, an additional embankment is proposed to add to the original highway at the site of Fort Worth North Loop IH 820 study section A. The proposed pavement structure will be composed of 12 inches of continuously reinforced concrete pavement (CRCP) and 4 inches asphaltic concrete pavement (ACP).The two-dimensional pavement cross section is sketched in Figure 5.2.

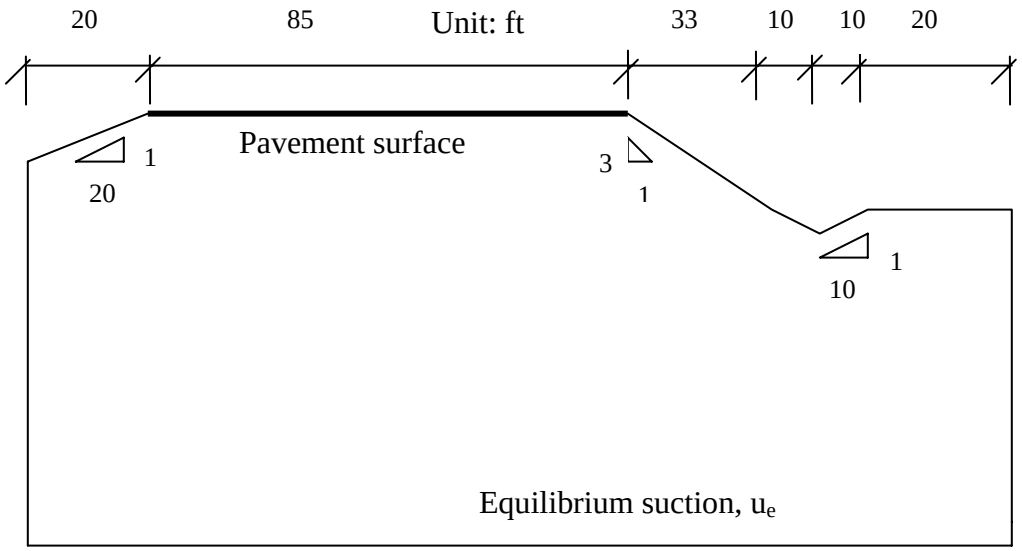

Figure 5.2 Schematic sketch of Fort Worth north loop 820 study section A pavement cross section

5.1.1 No Moisture Control Measures

The results of the FEM analysis indicate that, for a 20-year period, the vertical displacement at the outer wheel path at pavement surface will be around 0.7 inch swelling for initial dry condition and 1.2 inch shrinkage for initial wet condition as shown in Figure 5.3. The maximum total surface movement is close to 1.9 inches.

5.1.2 Effects of Various Depths of Vertical Moisture Barriers

In the parameter studies, the FEM analyses have been executed to study the effect of vertical moisture barrier on volume change control. Two different depths of vertical moisture barrier, i.e., 4 ft and 8 ft, have been employed for the companions. The vertical barrier is internally built with a 2 ft width outside the pavement surface course edge. The analyses results are plotted in Figures 5.4 and 5.5.

It can be seen from Figures 5.4 and Figure 5.5 that the installation of a vertical moisture barrier can reduce the shrinkage and swelling value from 1.9 inches of no moisture control to around 1.4 inches for the 4 ft vertical moisture barrier case. The vertical displacement difference for the 4 ft and 8 ft vertical moisture barrier is not significant in this analysis.

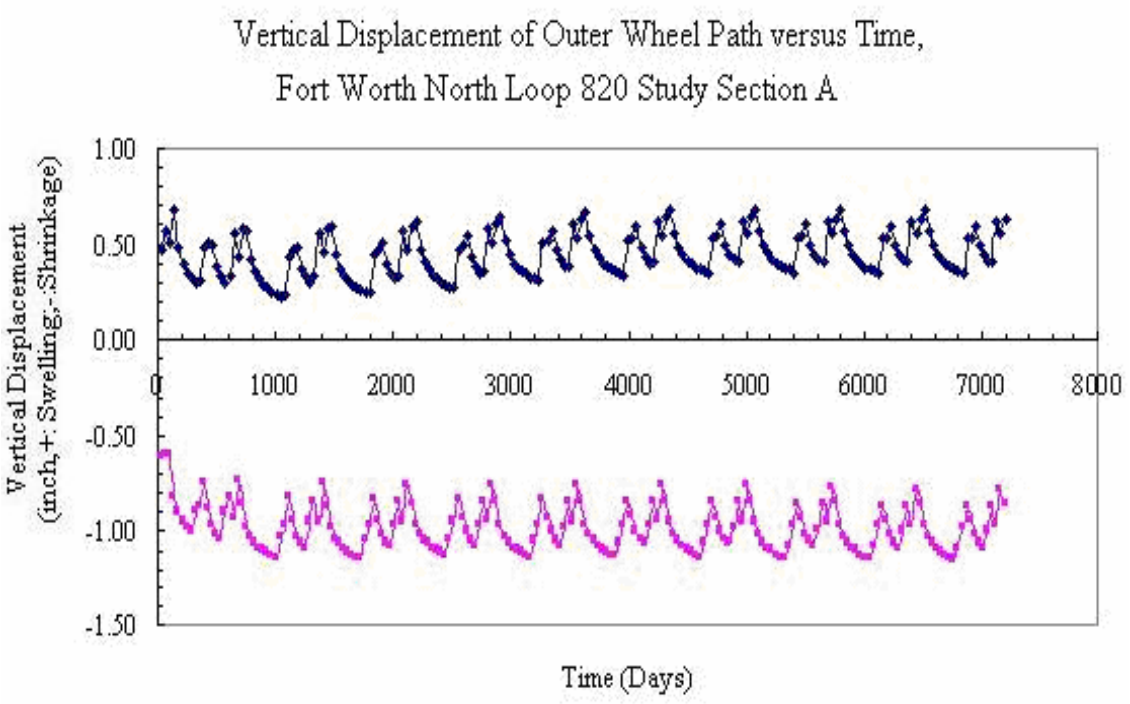

Figure 5.3 No moisture control measures (Fort Worth North Loop 820 study section A)

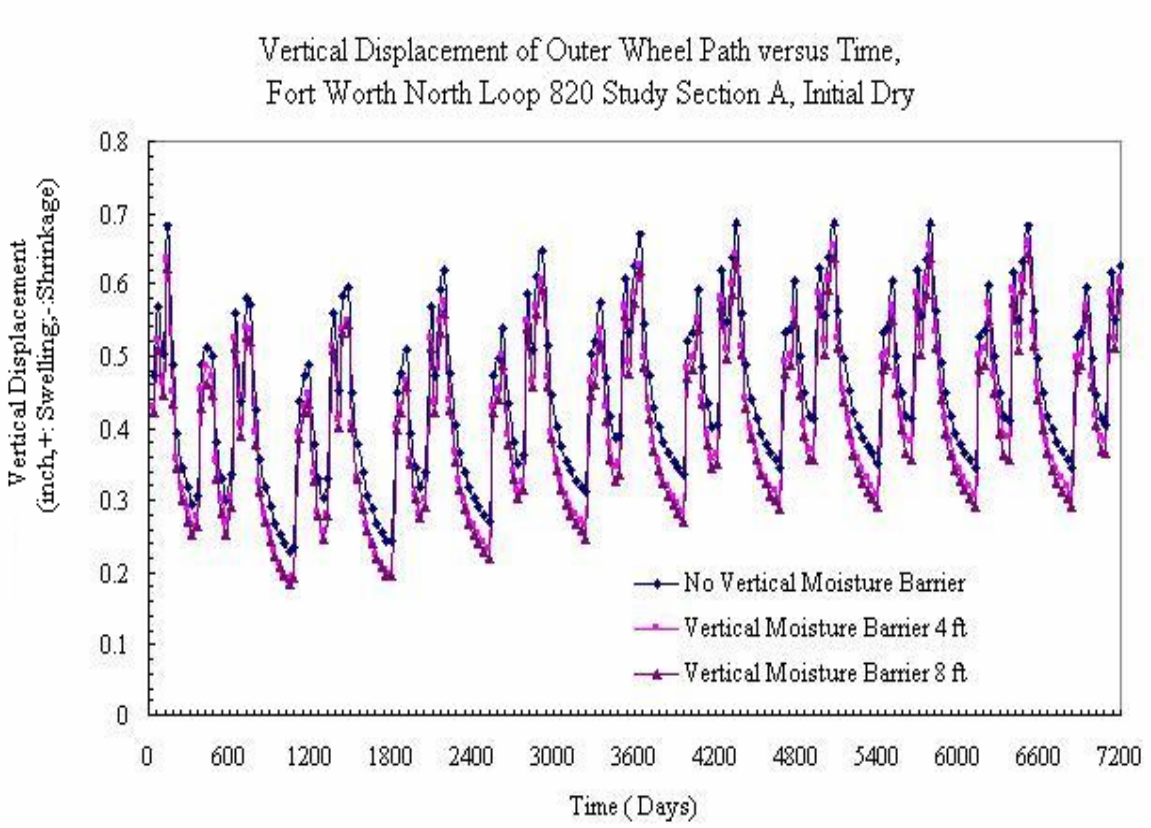

Figure 5.4 Vertical displacement measures with various depths of vertical moisture barriers, initial dry (Fort Worth North Loop 820 study section A)

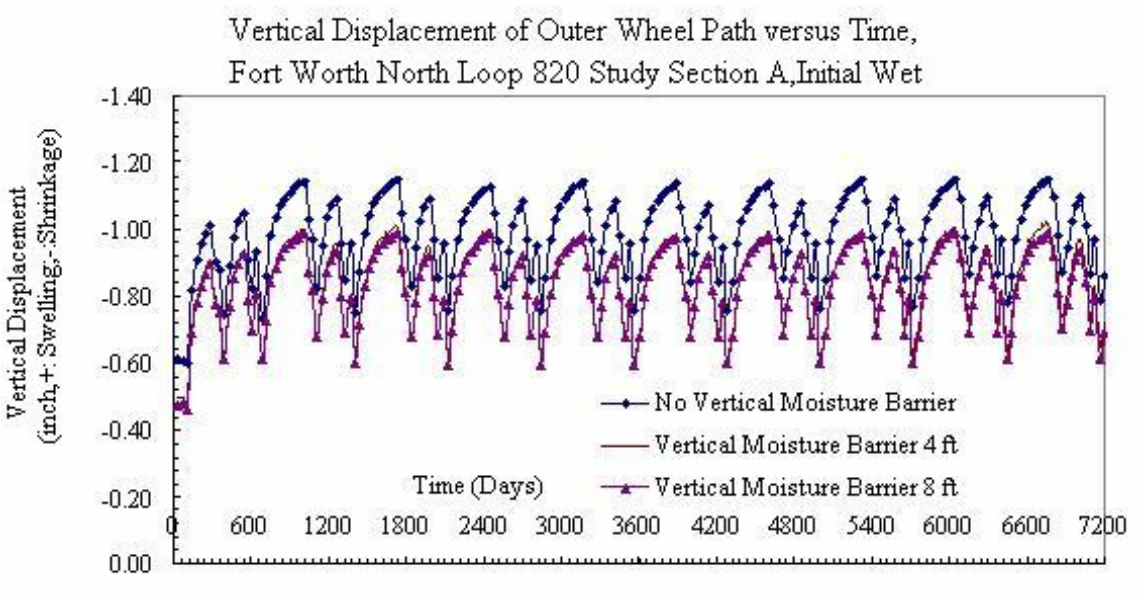

Figure 5.5 Vertical displacement measures with various depths of vertical moisture barriers, initial wet (Fort Worth North Loop 820 study section A)

5.1.3 Effects of Various Depths of Lime Stabilization

The effect of various depths of lime stabilization on controlling pavement surface deformation has also been studied in this analysis. The researchers proposed 18 inch depth lime stabilization, as usually used in engineering practice, for the comparison (Figures 5.6 and 5.7).

From Figure 5.6 and Figure 5.7, it can be seen that with the 18 inch lime stabilization, the total soil movement has been decreased by 25% and limited to 1.4 inches at 20 years' analysis period.

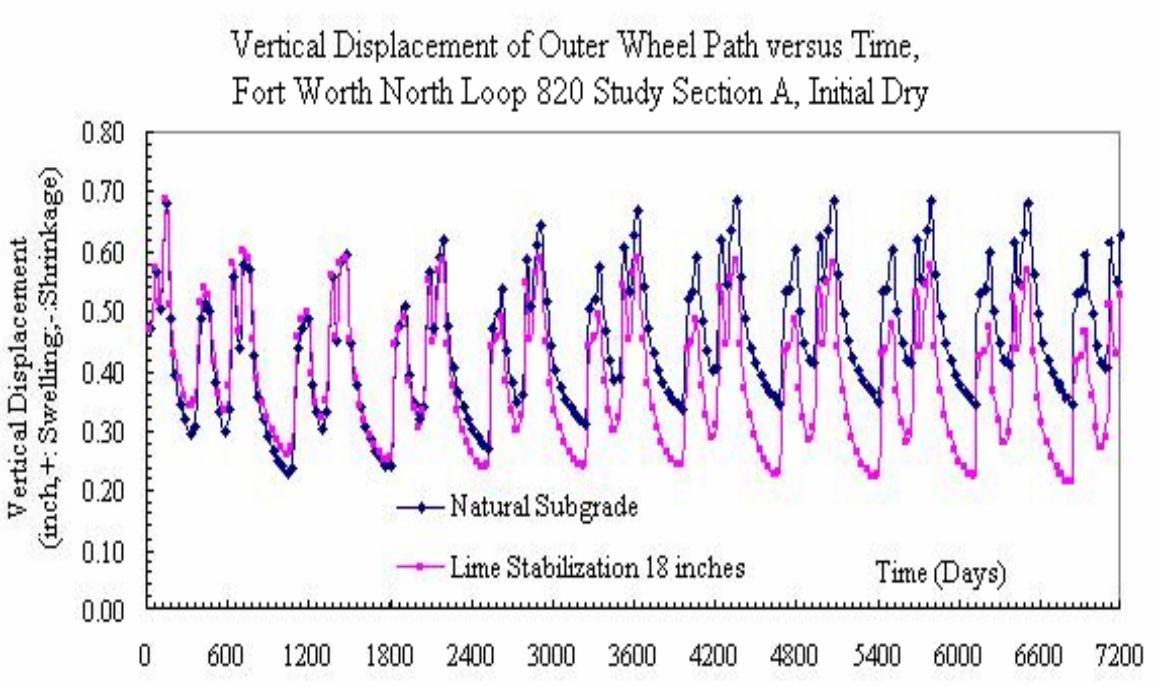

Figure 5.6 Vertical displacement measures with different depths of lime stabilization (Fort Worth North Loop 820 study section A, initial dry)

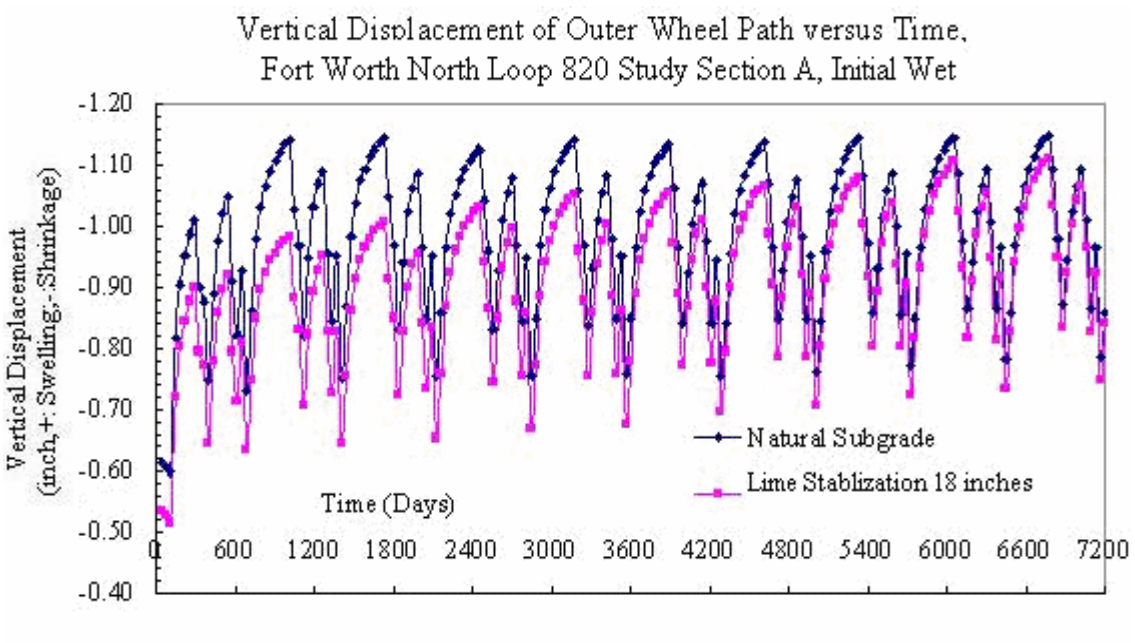

Figure 5.7 Vertical displacement measures with different depths of lime stabilization (Fort Worth North Loop 820 study section A, initial wet)

5.1.4 Effects of Various Depths of "Inert" Material

Two different depths of "inert" material, 2 ft and 6 ft, are adopted for this parametric study. The results are shown in Figures 5.8 and 5.9. It can be inferred from the analyses results that the replacement of natural subgrade with inert soil can reduce the vertical soil movement to a considerable degree. The total vertical movement using inert soil treatment is controlled below 1.2 inches. In the analyses, the plasticity index (PI) of inert soil is chosen as 25.

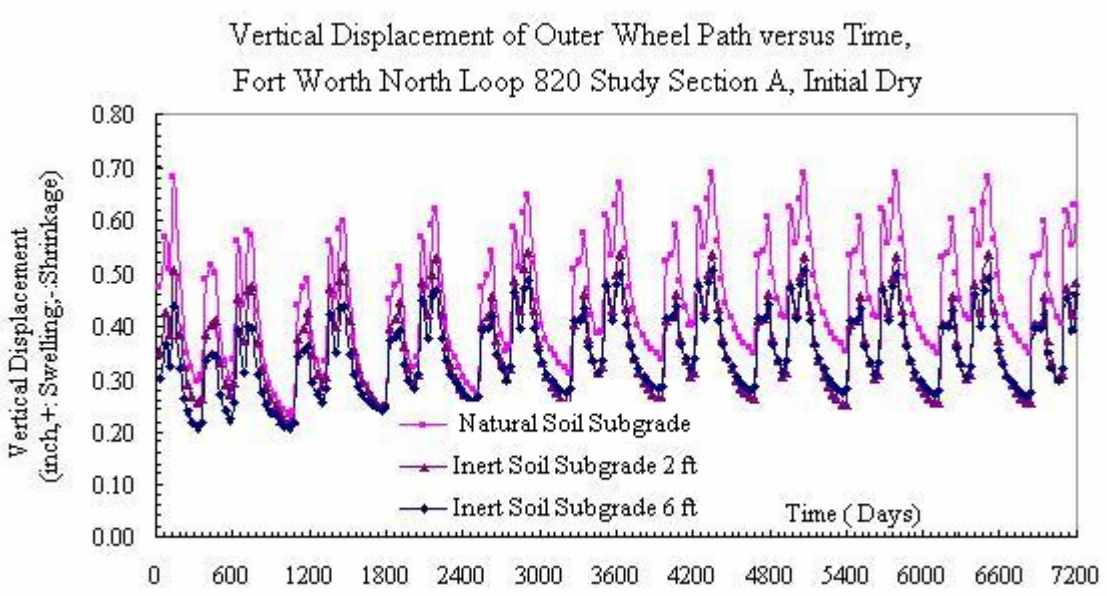

Figure 5.8 Vertical displacement measures of various depths of "inert" material (Fort Worth North Loop 820 study section A, initial dry)

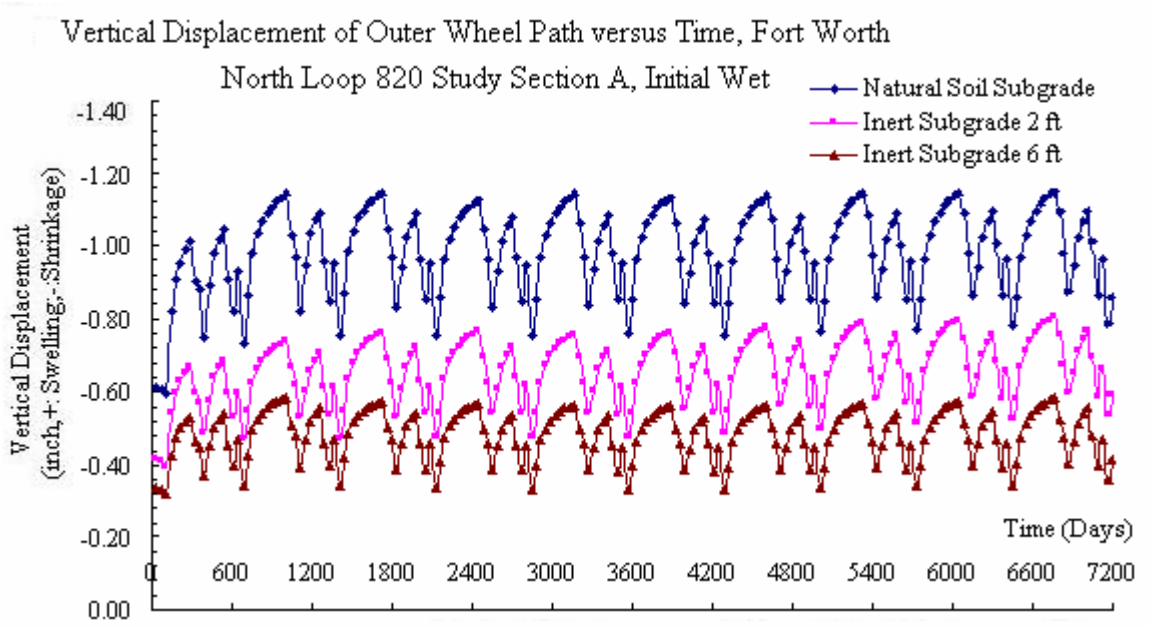

Figure 5.9 Vertical displacement measures of various depths of "inert" material (Fort Worth North Loop 820 study section A, initial wet)

5.1.5 Effects of the Paved Median

In engineering practice, paving the median is also an effective method to reduce surface vertical movement. The effects of paving the median on the outer wheel path vertical displacement measures at two different initial conditions (initial dry and initial wet) are demonstrated in Figures 5.10 and 5.11.

From Figures 5.10 and Figure 5.11, it can be seen that the effect of the paved median condition for the initial dry condition on soil swelling is not obvious, while the measure of paving median can have a significant effect on controlling soil shrinkage movement at the initial wet condition.

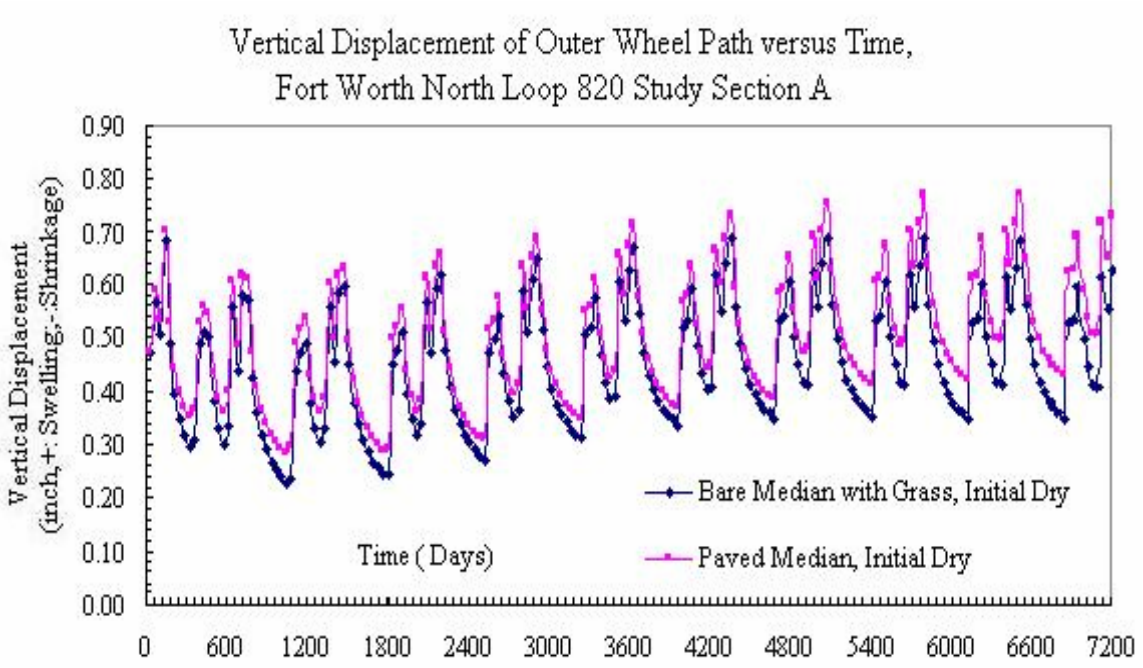

Figure 5.10 Vertical displacement measures of median condition (Fort Worth North Loop IH 820 study section A, initial dry)

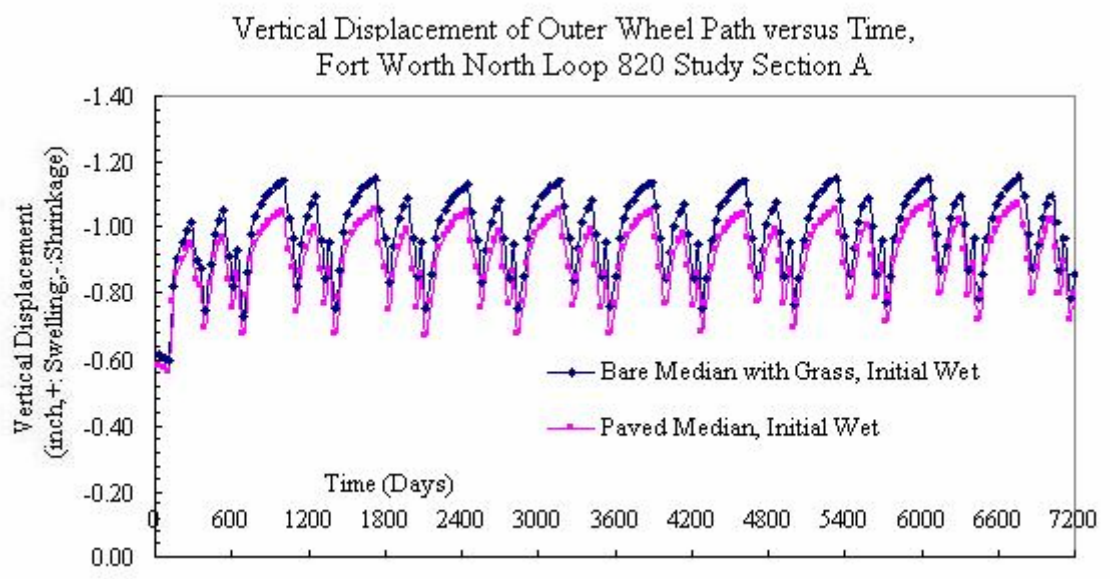

Figure 5.11 Vertical displacement measures of median condition (Fort Worth North Loop IH 820 study section A, initial wet))

5.2 Fort Worth North Loop IH 820 Study Section B

Figure 5.12 shows the two-dimensional cross session of the site in Fort Worth Loop IH 820 study section B. The proposed pavement structure will be composed of 12 inches of continuously reinforced concrete pavement and 4 inches asphaltic concrete pavement.

5.2.1 No Moisture Control Measures

The FEM analyses results for no moisture control measures at two different initial conditions (initial dry and initial wet) are plotted in Figure 5.13.

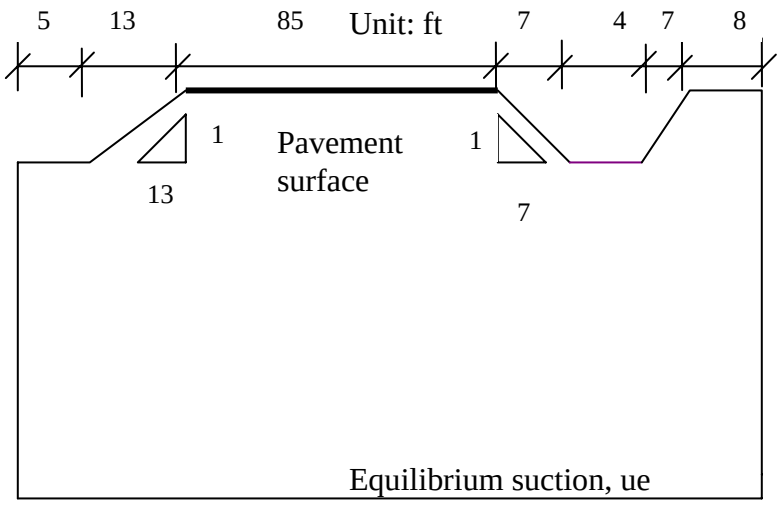

Figure 5.12 Fort Worth North Loop 820 study section B pavement cross section sketch

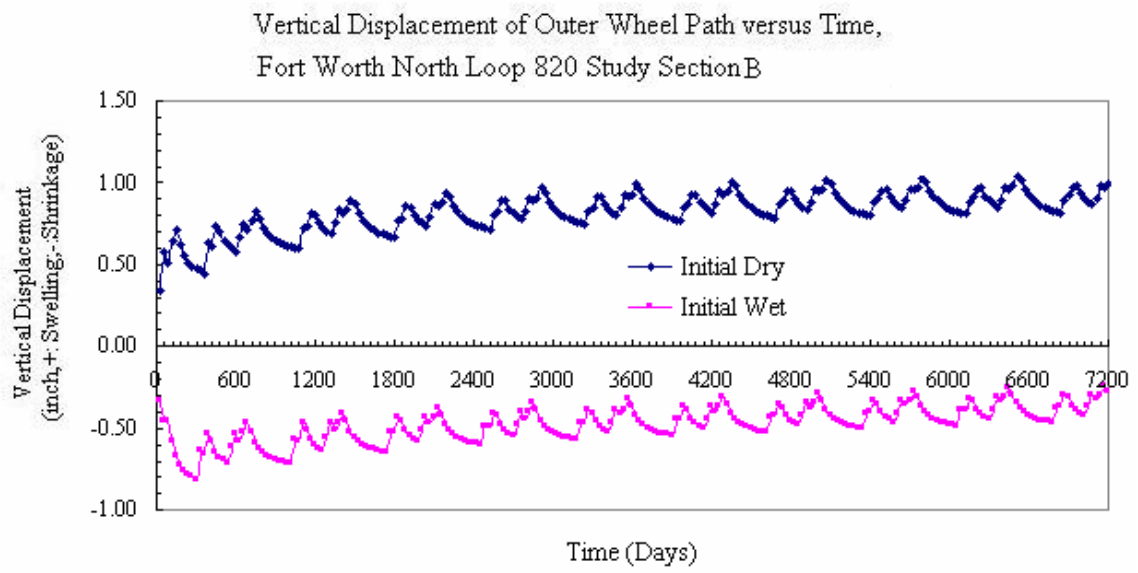

Figure 5.13 No moisture control measures at Fort Worth North Loop 820 study section B

From Figure 5.13, it can be inferred that the total vertical soil movement at the "no moisture control" condition at Fort Worth North Loop 820 study section B is around 2 inches.

5.2.2 Effect of Various Depths of Vertical Moisture Barriers

The parameter studies of various depths of vertical moisture barriers (4 ft and 8 ft) on the effect of vertical surface displacement controls are shown in Figure 5.14.

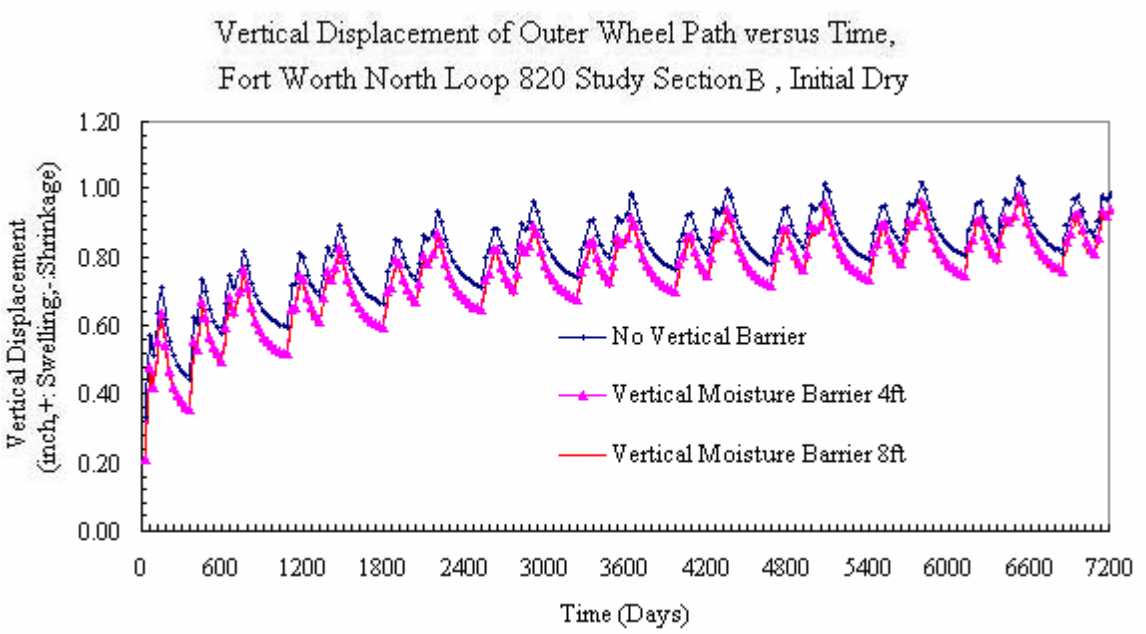

Figure 5.14 Vertical displacement measures of various depths of vertical moisture barriers at Fort Worth North Loop 820 study section B

5.2.3 Effect of Various Depths of Lime Stabilization

A depth of 18 inches of lime stabilization has been employed for the companion in this site. The corresponding vertical displacements at the outer wheel path for a 20-year period have been shown in Figure 5.15.

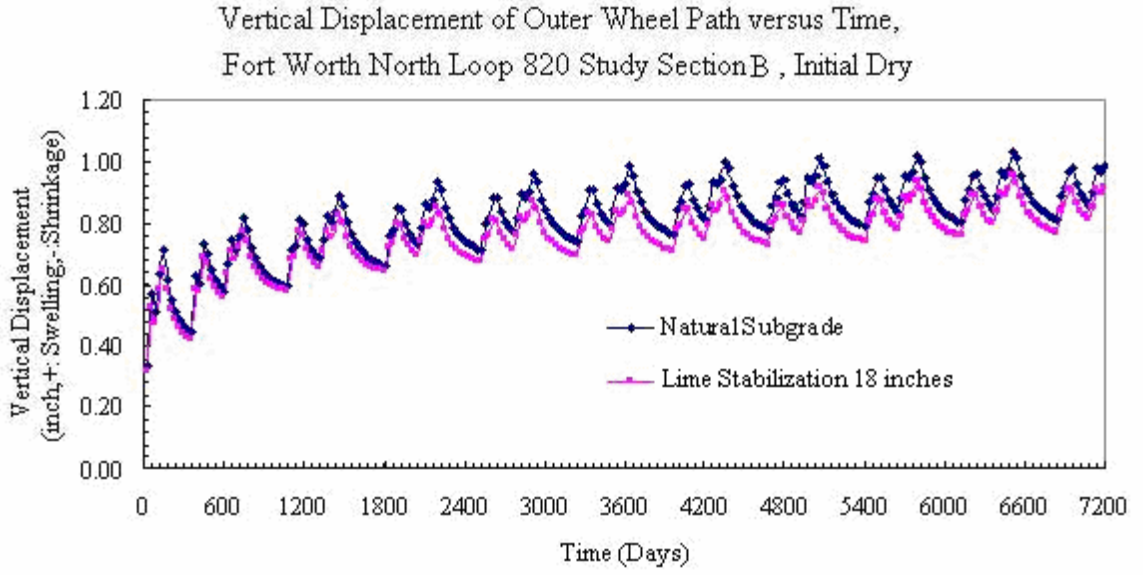

Figure 5.15 Vertical displacement measures of various depths of lime stabilization at Fort Worth North Loop 820 study section B

5.2.4 Effect of Various Depths of "Inert" Soil

Figure 5.16 shows the effect of various depths of "inert" material (2 ft and 6 ft) on controlling the vertical displacement values of the outer wheel path**.**

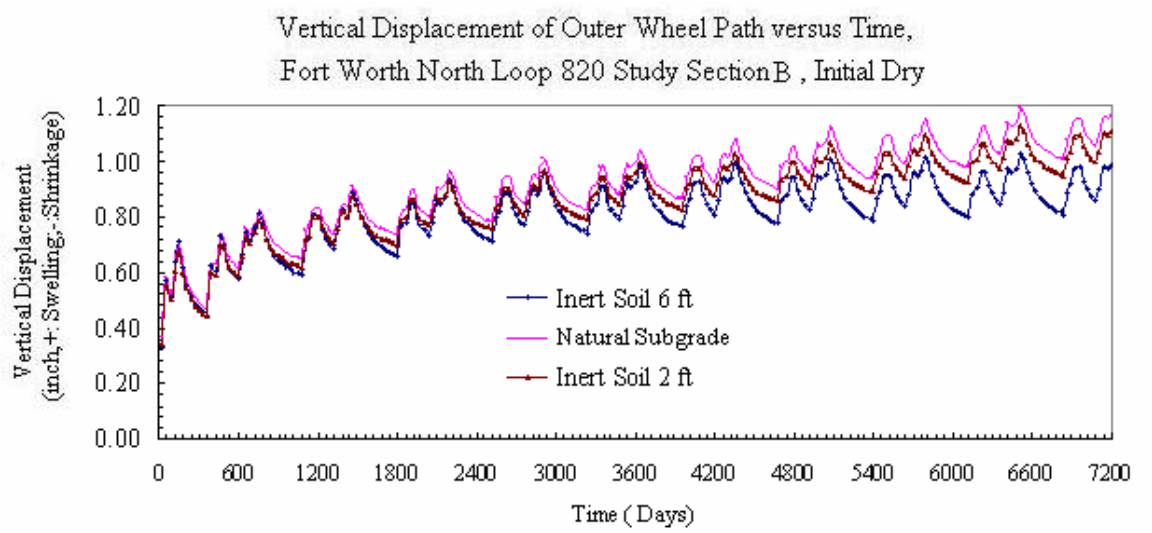

Figure 5.16 Vertical displacement measures of various depths of "inert" material at Fort Worth North Loop 820 study section B

5.2.5 Effect of the Paved Median

The effect of paved median condition on vertical displacement control at two initial conditions (initial dry and initial wet) has been studied and the results are shown in Figures 5.17 and 5.18. It can also be concluded that the effect of the paved median condition on controlling soil shrinkage movement is more significant than controlling soil swelling movement.

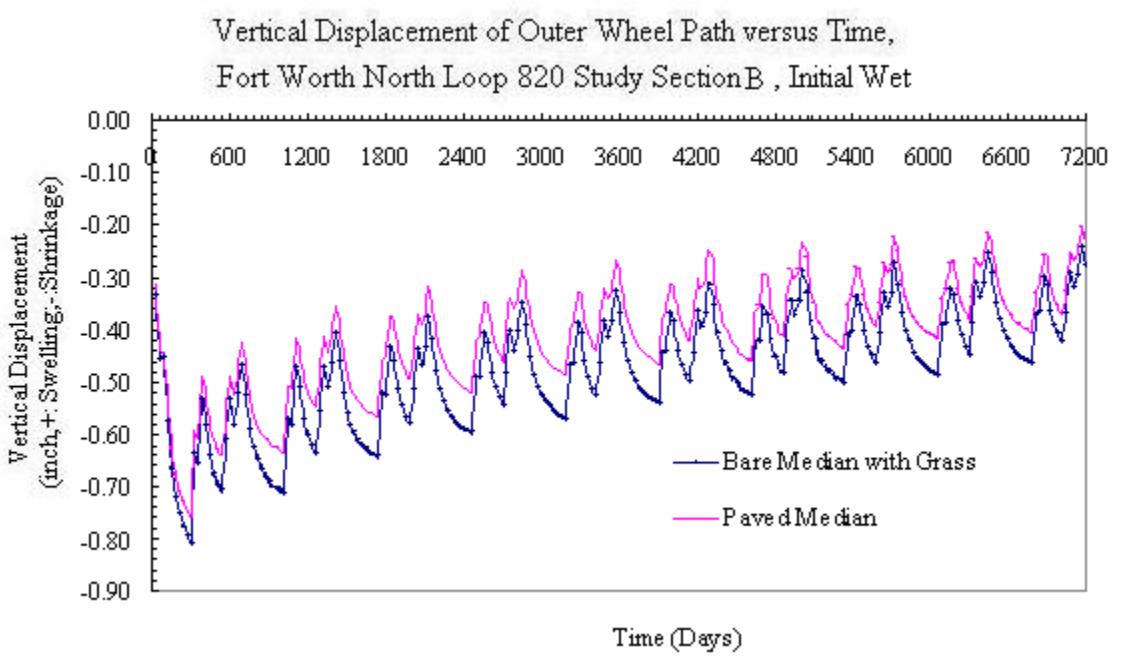

Figure 5.17 Vertical displacement measures of paving conditions (Fort Worth North Loop 820 study section B, initial wet)

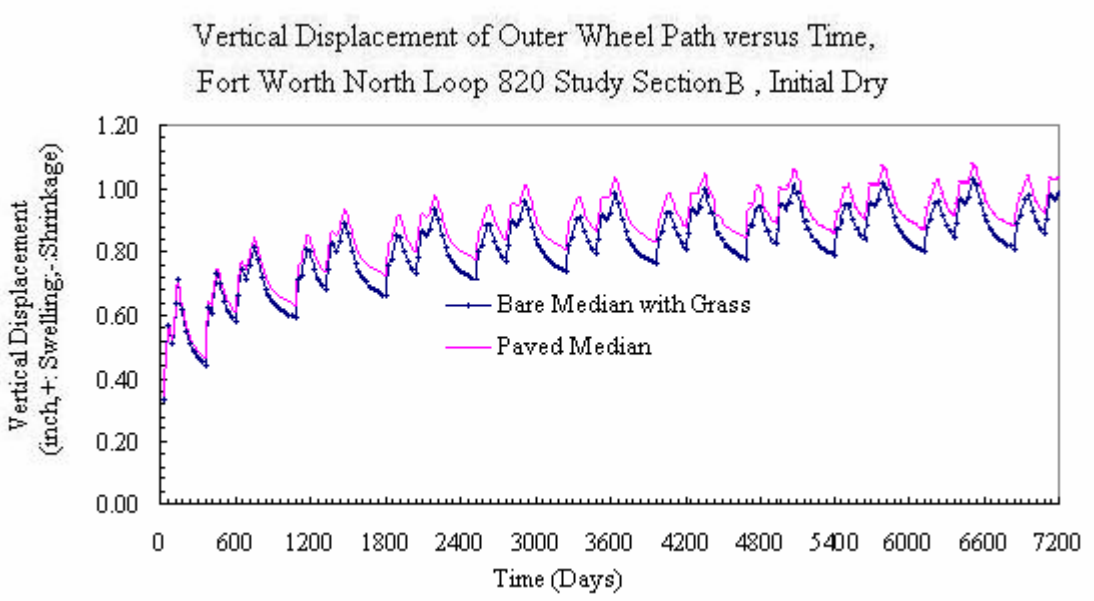

Figure 5.18 Vertical displacement measures of paving conditions (Fort Worth North Loop 820 study section B, initial dry)

5.3 Atlanta US 271

In the Atlanta US 271 site, surface vegetation such as trees is existent at the site located in region AB (from the ditch line through the median). In the FEM analysis, the depth of tree root zone is assumed to be 14 ft based on the borehole data and Shelby-tube sample. The cross section used in the analysis is shown in Figure 5.19. Red line in the bottom stands for the equilibrium suction, u_e.

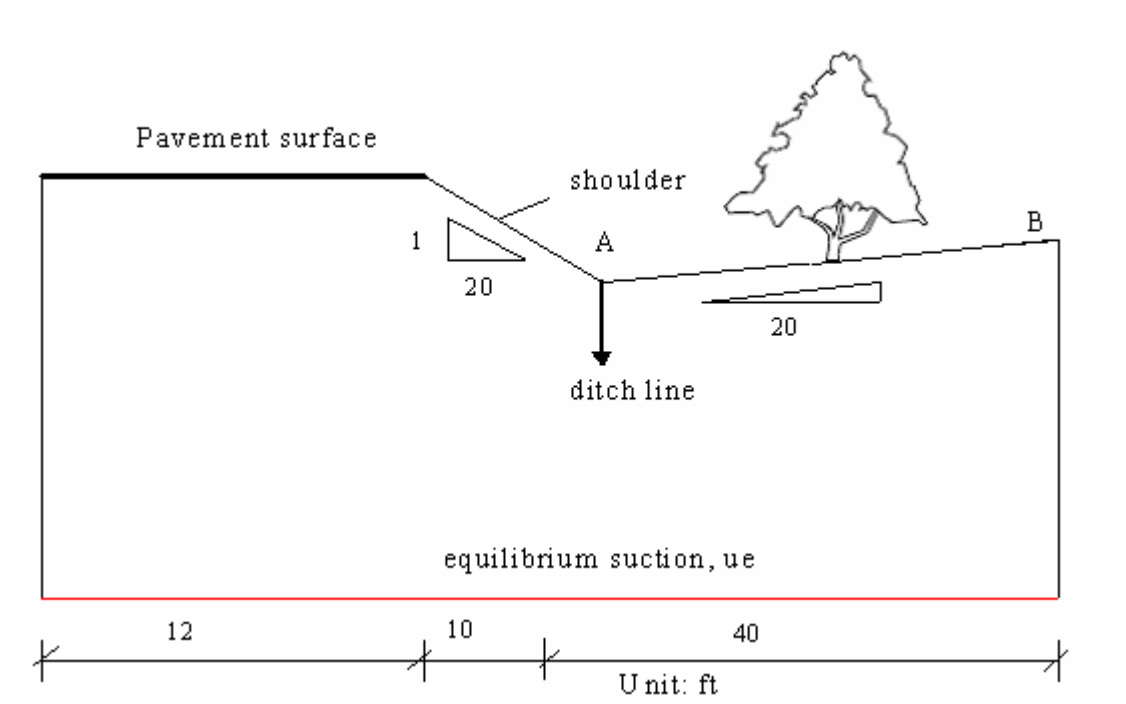

Figure 5.19 Atlanta US 271 pavement cross section sketch

5.3.1 No Moisture Control Measures

The computation results for “no moisture control measures” in this site at two different initial conditions (initial dry and initial wet) are given in Figure 5.20. The total soil vertical movement (accumulation of soil shrinkage and swelling) at this site is around 1 inch.

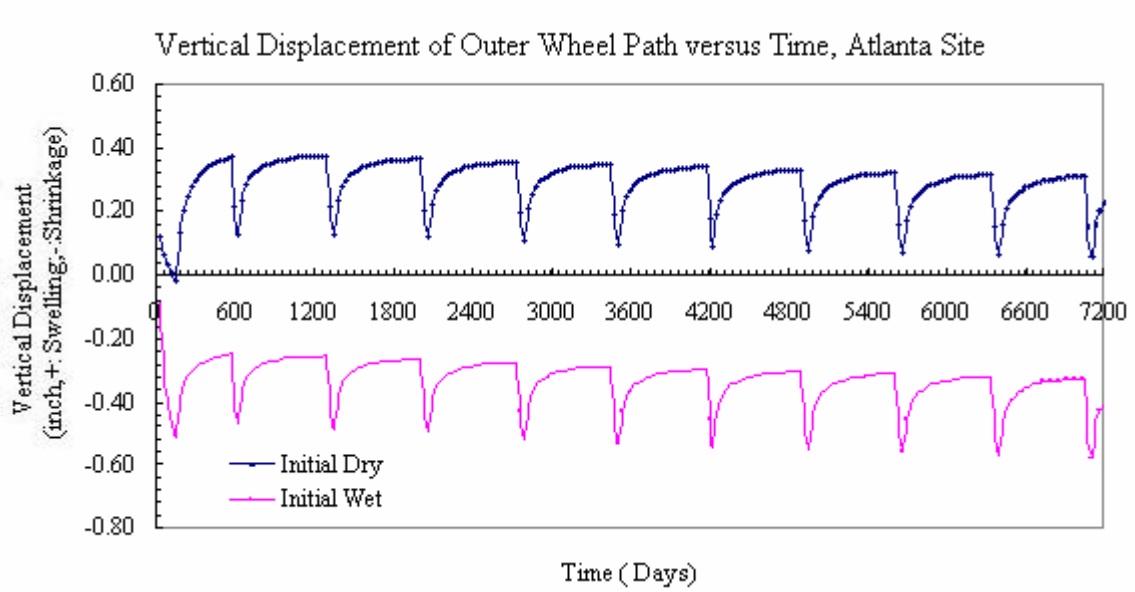

Figure 5.20 Vertical displacement measures at Atlanta US 271

5.3.2 Effect of Various Depths of Vertical Moisture Barriers

Same as in Fort Worth Loop 820 study sections A and B, the effects of two different depths of various moisture barriers (4 ft and 8 ft) are analyzed and compared in Figure 5.21. Same observation can be made that the installation of a vertical moisture barrier can effectively reduce the soil vertical movement by decreasing the degree and extent of moisture condition changes.

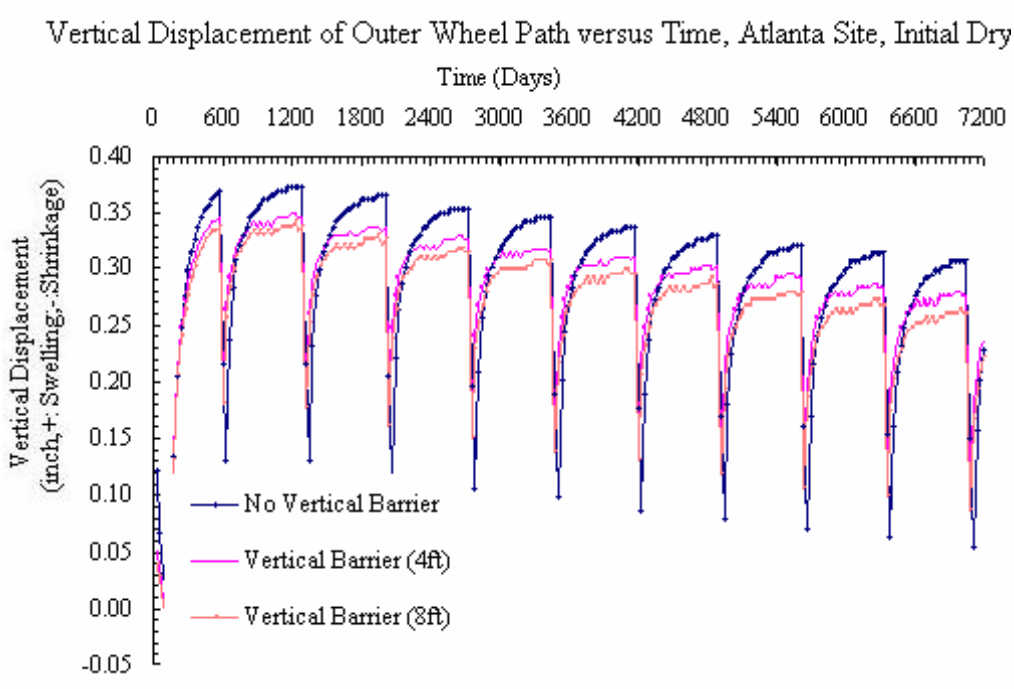

Figure 5.21 Vertical displacement measures of various depths of vertical moisture barriers at Atlanta US 271

5.3.3 Effect of Various Depths of Lime Stabilization

Figure 5.22 shows the effect of two different depths of lime stabilization (8 inch and 18 inch) on the reduction of the surface vertical movement at the outer wheel path in the Atlanta US 271 site.

5.3.4 Effect of Various Depths of "Inert" Material

Figure 5.23 gives the vertical movement measures for different depths of "inert" material (2 ft, 4 ft, and 6 ft) for the subgrade materials.

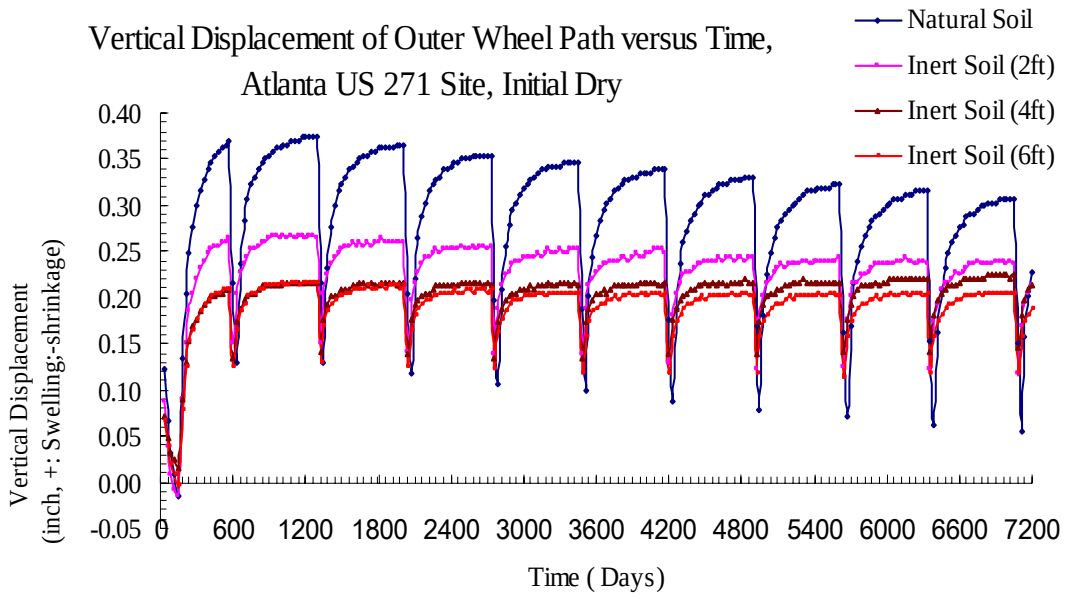

Figure 5.22 Vertical displacement measures of various depths of lime stabilization at Atlanta US 271

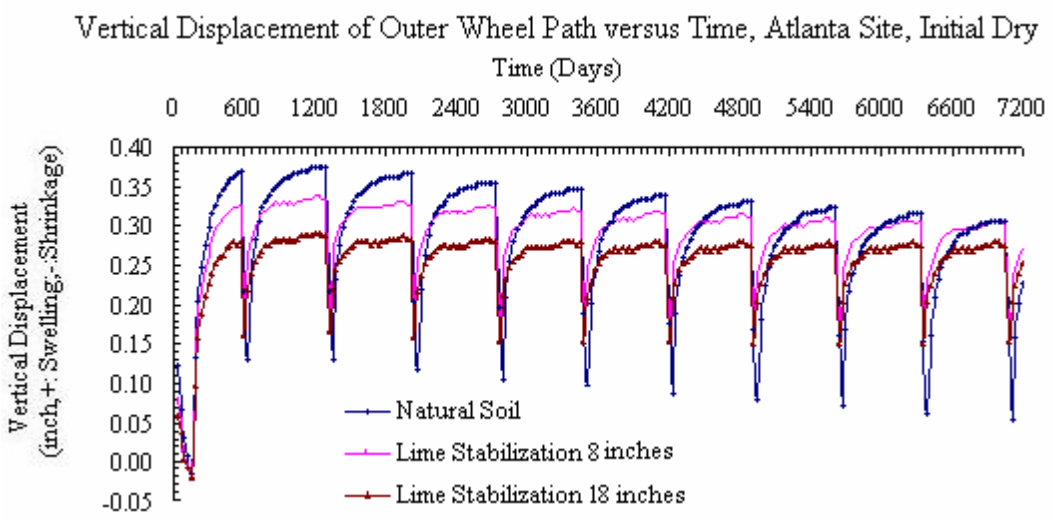

Figure 5.23 Vertical displacement measures of various depths of "inert" material at Atlanta US 271

5.3.5 Effect of Paved Widths of Shoulder

Two types of paved shoulder widths (i.e., 4 ft and 8 ft) have been used for this parameter study. The effects of the paved widths of shoulder (horizontal moisture barrier) at the initial wet condition and the initial dry condition are shown in Figures 5.24 and 5.25. It can be seen that the employment of paved shoulders can effectively reduce the total soil vertical movement and decrease the fluctuation of displacement values associated with the cyclic weather conditions.

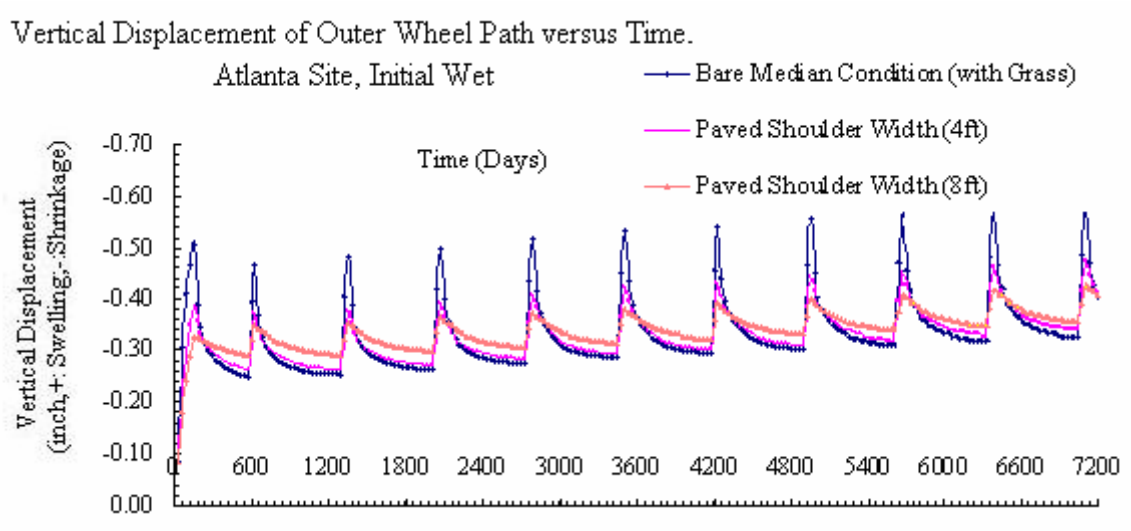

Figure 5.24 Vertical displacement measures of various widths of paved shoulder at Atlanta US 271 (initial wet)

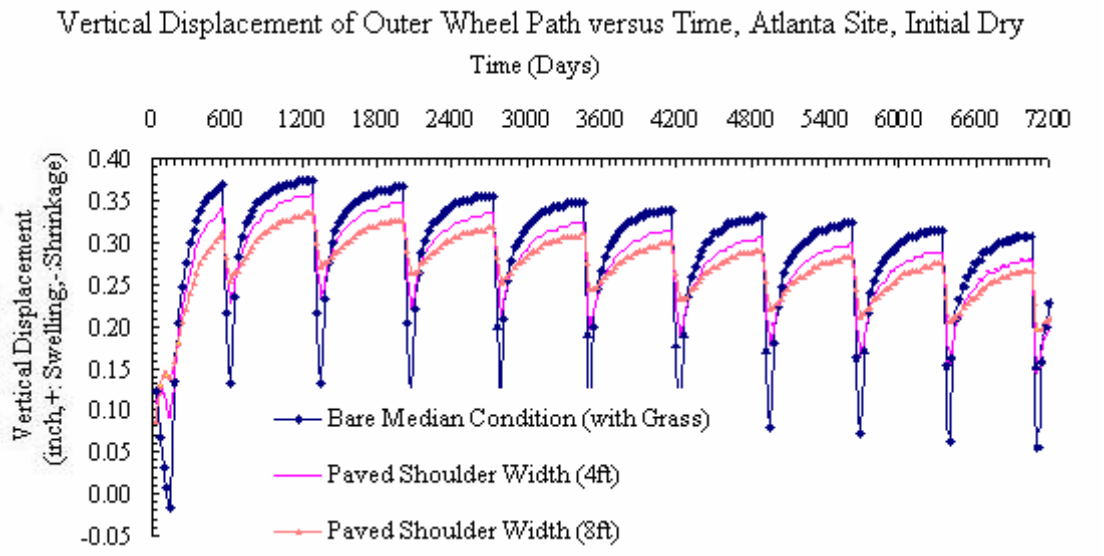

Figure 5.25 Vertical displacement measures of various widths of paved shoulder at Atlanta US 271 (initial dry)

5.4 Austin Loop 1 Uphill of Frontage Road and Main Lane

Figure 5.26 illustrates the analyzed two-dimensional pavement cross section for the analysis of vertical displacement measures at uphill of the frontage road and the main lane. A long sliding intact limestone layer exists around 10 ft beneath the main lane pavement surface in the field.

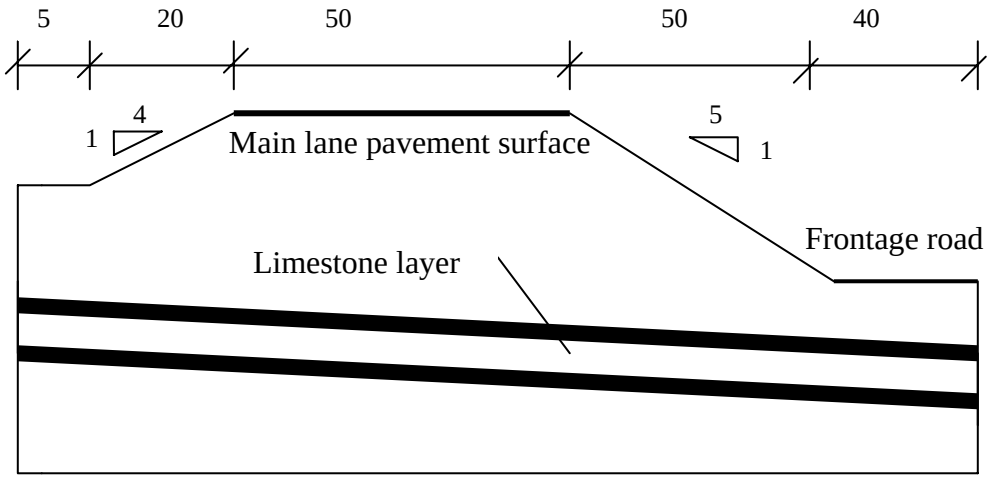

Figure 5.26 Austin Loop 1 pavement cross section sketch

5.4.1 No Moisture Control Measures

The computation results of “no moisture control measures” for Austin Loop 1 at the uphill outer wheel path of the frontage road and at the uphill outer wheel path of the main lane are shown in Figures 5.27 and 5.28. The total vertical soil movement for no moisture control at the outer wheel path of uphill of the frontage road is around 1.4 inches and the vertical soil movement value at the outer wheel path of uphill of the main lane for no moisture control is around 1.6 inches.

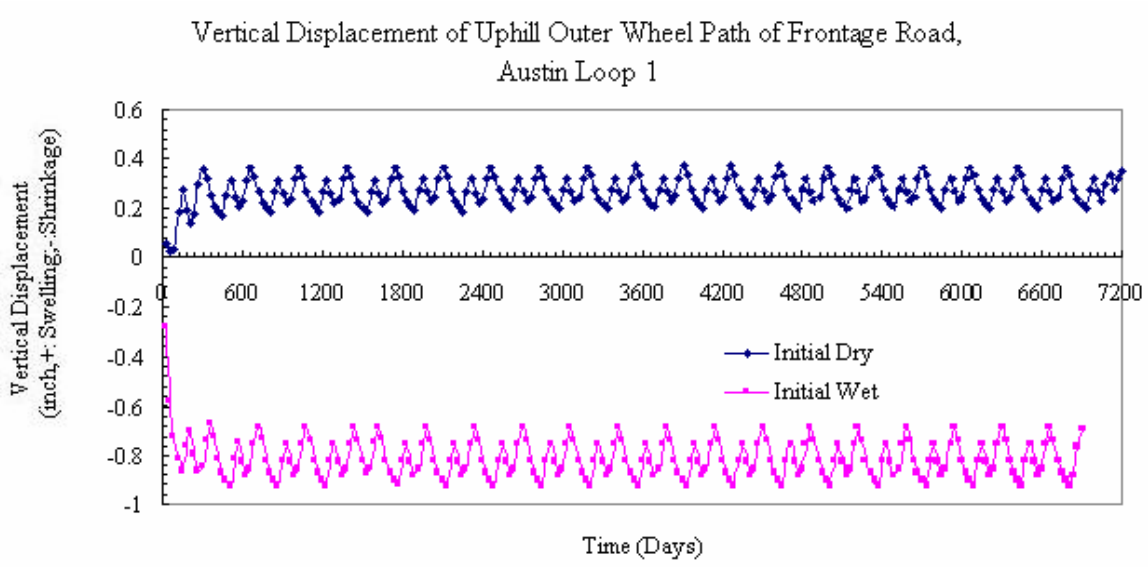

Figure 5.27 No moisture control measures at Austin Loop 1 uphill of frontage road

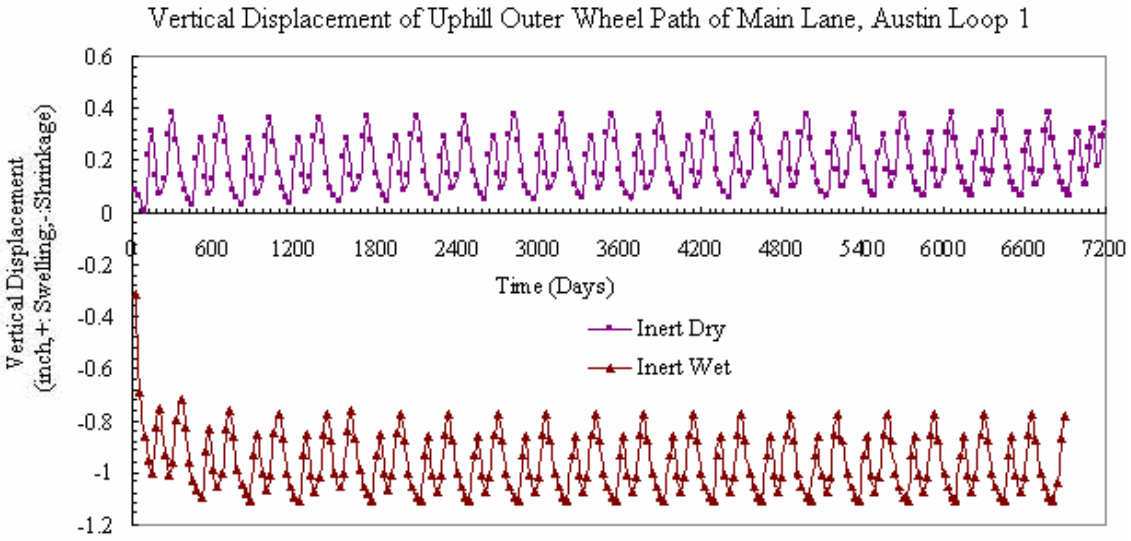

Figure 5.28 No moisture control measures at Austin Loop 1 uphill of main lane

5.4.2 Effects of Various Depths of Vertical Moisture Barriers

Figures 5.29-5.32 demonstrate the effect of two different depths of vertical moisture barriers, i.e., 4 ft and 8 ft, on the control of vertical movement at the uphill outer wheel path of the frontage road and the outer wheel path of the main lane at the Austin Loop 1 site. In the case study at this site, the installation of a vertical moisture barrier has no effect on reducing the vertical soil movement.

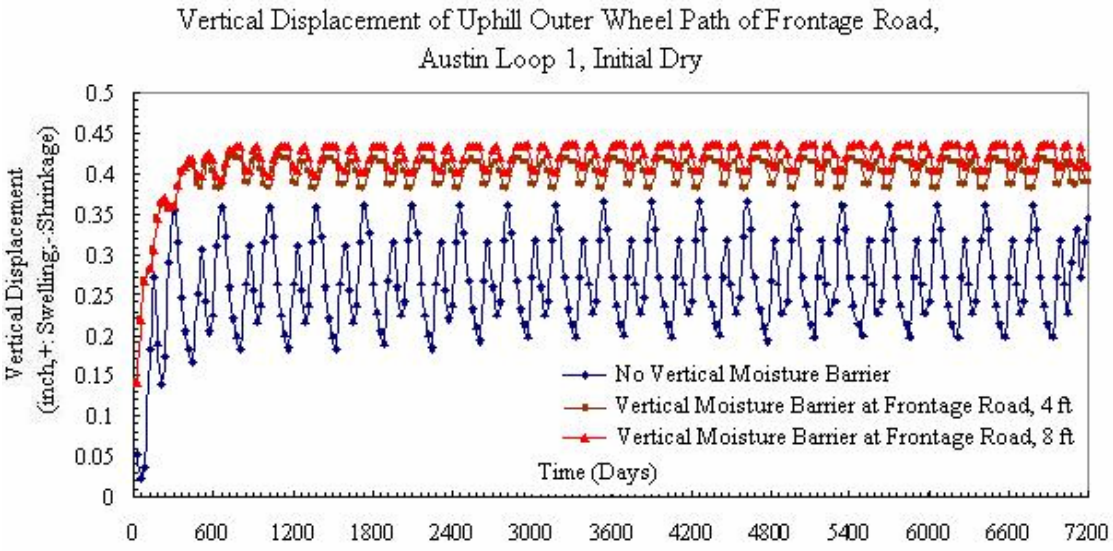

Figure 5.29 Vertical displacement measures at uphill outer wheel path of frontage road with various depths of vertical moisture barrier built at frontage road (Austin Loop 1, initial dry condition)

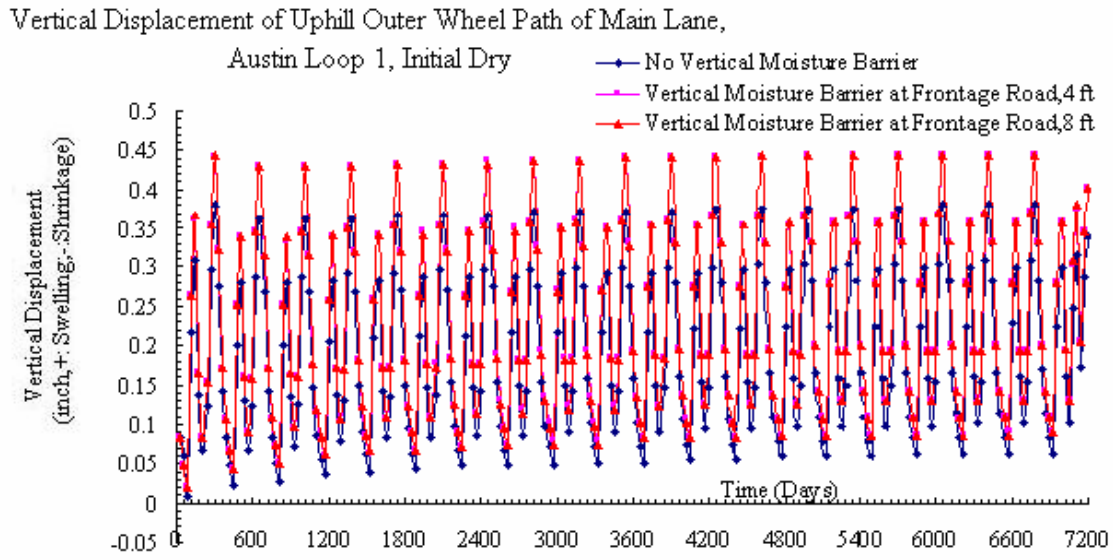

Figure 5.30 Vertical displacement measures at uphill outer wheel path of main lane with various depths of vertical moisture barrier built at frontage road (Austin Loop 1, initial dry condition)

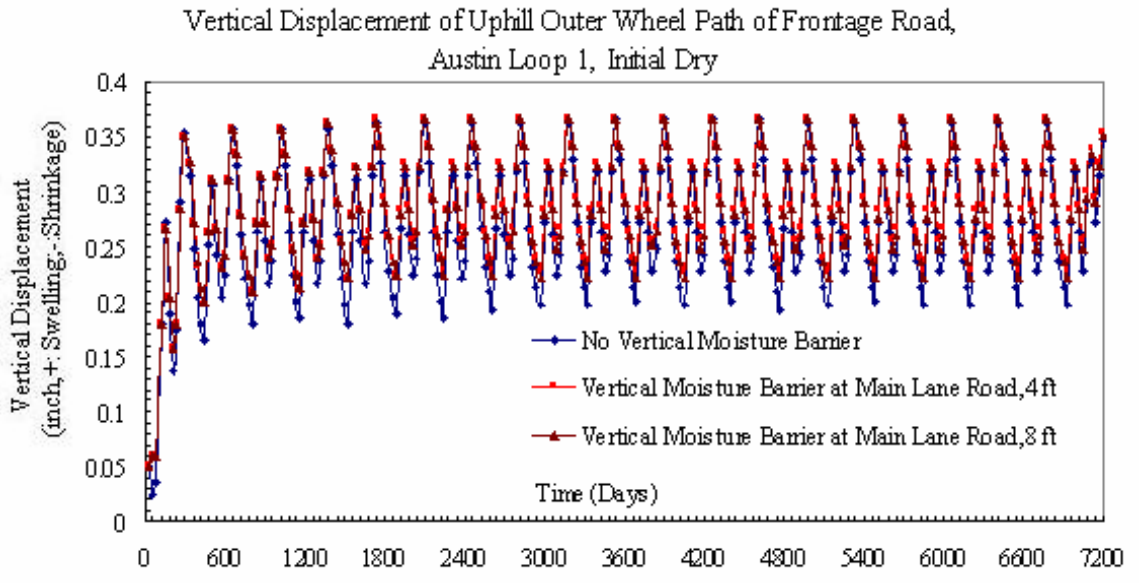

Figure 5.31 Vertical displacement measures at uphill outer wheel path of frontage road with various depths of vertical moisture barrier built at main lane (Austin Loop 1, initial dry condition)

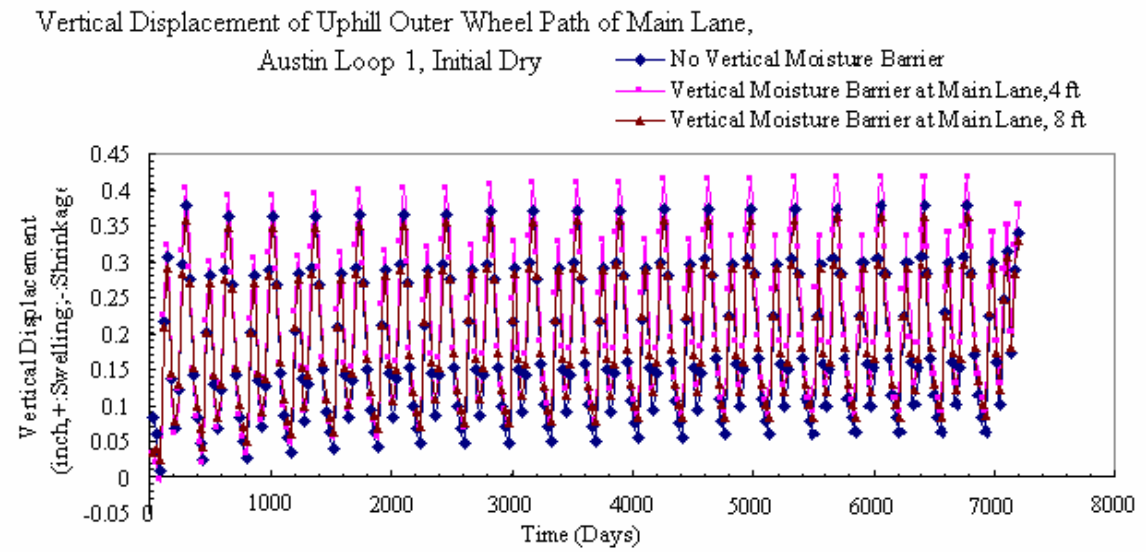

Figure 5.32 Vertical displacement measures at uphill outer wheel path of main lane with various depths of vertical moisture barrier built at main lane (Austin Loop 1, initial dry condition)

5.4.3 Effects of the Paved Median

The effects of the paved median condition on vertical movement at the uphill outer wheel path of the frontage road and the main lane are illustrated in Figure 5.33 and Figure 5.34.

From Figures 5.33 and Figure 5.34, it can be concluded that the paved median condition has significant effect on reducing the vertical displacement measures at the uphill outer wheel path of the main lane. But the paved median condition has slight effect on the vertical displacement measures at the uphill outer wheel path of the frontage road.

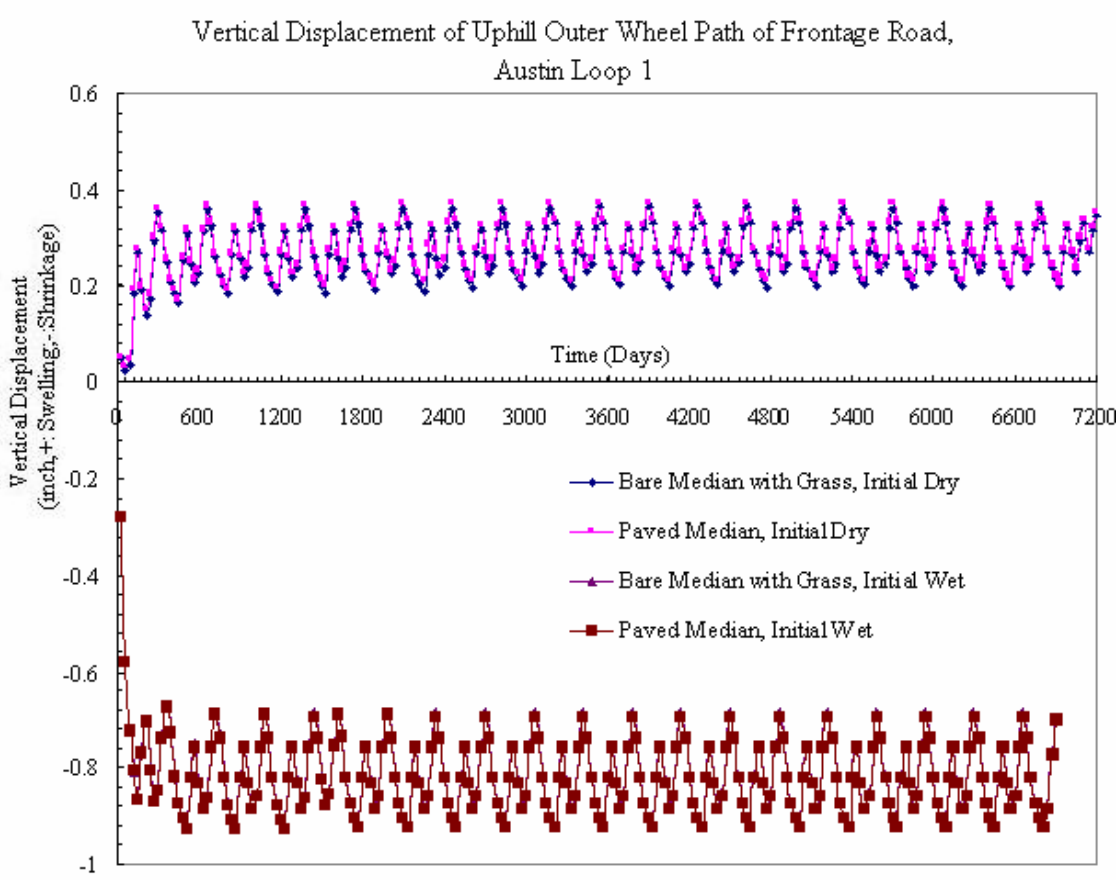

Figure 5.33 Vertical displacement measures of paved conditions at uphill outer wheel path of frontage road, Austin Loop 1

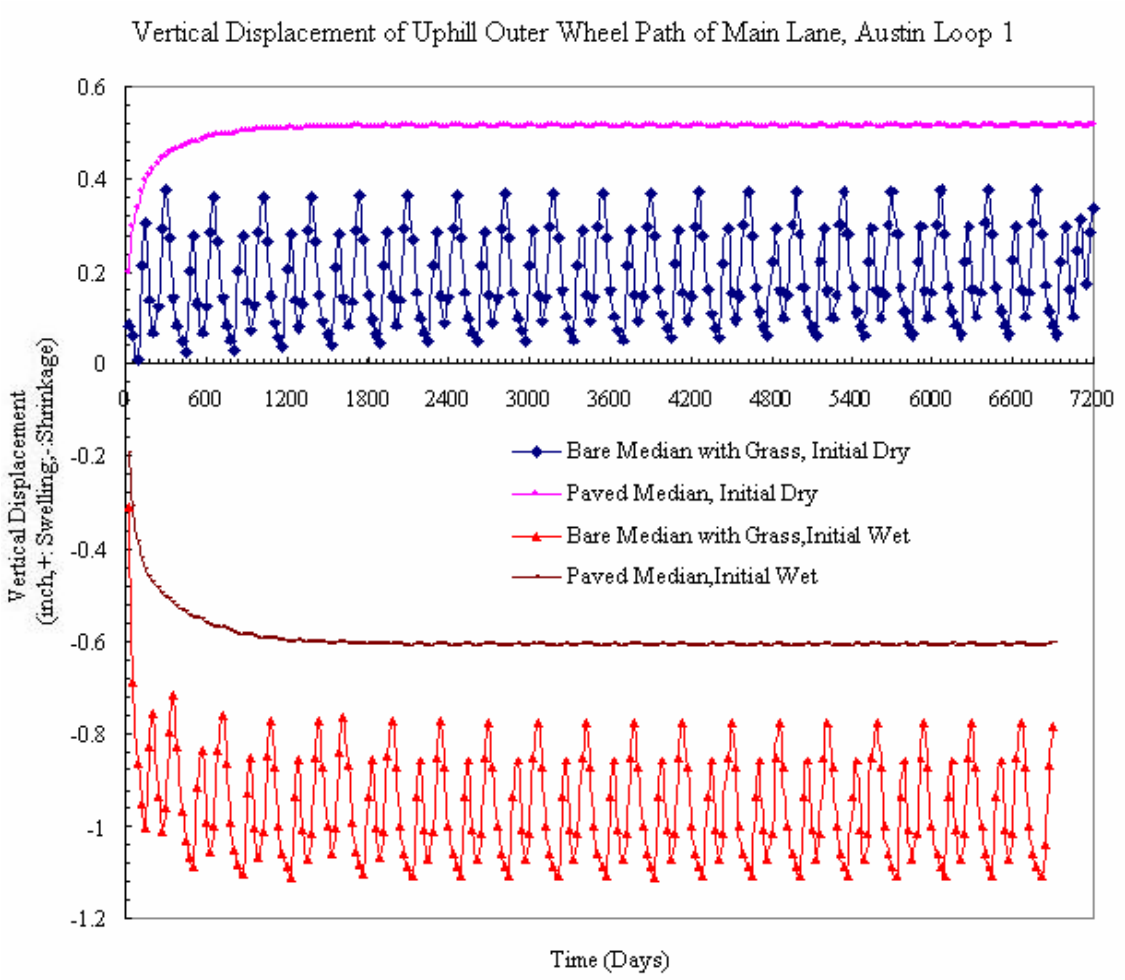

Figure 5.34 Vertical displacement measures of paved conditions at uphill outer wheel path of main lane, Austin Loop 1

5.5 Conclusions

From the analyses results of the parameter studies at these four companion sites, several conclusions can be made as follows:

- The analysis program can simulate a 20-year performance period in around one hour on a desktop computer of 1 GHZ CPU and is capable of analyzing both

asphalt and concrete pavements on expansive soils. The flow boundary conditions that may be used include drainage (ponded water of different depth in the roadside ditches), grasses and trees.

- A vertical moisture barrier is normally an effective method to reduce total vertical movement at the pavement surface. However, for the Austin site, due to the existence of an intact limestone layer, the effect of a vertical moisture barrier is not obvious; and it may even increase the vertical total movement at the outer wheel path.
- Paving the median can significantly reduce the pavement surface shrinkage compared with the bare median case; however, it does not have much effect on reducing the swelling value. The reason for this is that the grass usually existing in the case of bare median dries out the underlying soil layers and thus causes a large soil shrinkage movement. With the median paved, the path of moisture evaporation via grass is cut off, so the soil shrinkage value is decreased.
- Paving the shoulder, i.e., use of horizontal moisture barrier, is effective in decreasing the pavement surface displacements and reducing the fluctuation of vertical displacement change associated with cyclic climatic conditions.
- Lime stabilization and “inert” material are both effective in reducing the pavement vertical movement. In the parametric study, lime stabilization thicknesses of 8 inches and 18 inches are employed.

  Also it is observed that the value of time step Δt is a very important factor in the FEM analysis. In order to avoid the problem of numerical non-accuracy due to

the high nonlinearity in the displacement analysis, a small time step value should be employed as a compromise with computational speed.

CHAPTER VI

EFFECT OF DESICCATION CRACKING ON ENGINEERING BEHAVIOR OF EXPANSIVE SOILS

Desiccation cracking and surface subsidence arise from the lowering of ground water table and the drying of clays soils due to evaporation from the soil surface and transpiration by vegetation, i.e., trees, grasses or bushes, if present. This cracking can be assumed to occur when the stress at the tip of a crack becomes more tensile than the tensile strength of the soil. Field evidence has shown that shrinkage cracks are generally vertical (or sub vertical) and horizontal, and they can extend to the full depth of a soil deposit around 15m (Graham and Shields, 1985).

Four shrinkage phases can be distinguished during the soil drying and cracking processes, i.e., structural shrinkage, normal shrinkage, residual shrinkage and zero shrinkage (Haines, 1923; Keen, 1931; Stirk, 1954; Bronswijk, 1991). Structural shrinkage is defined as the process, when the soil is dry, large water-filled pores may be emptied without an accompanying volume change. The volume decrease of soil aggregates is equal to water loss during normal shrinkage. In the process of residual shrinkage, despite a volume reduction of soil aggregates, water loss exceeds the volume decrease. Air enters the pores of the soil aggregates. During the phase of zero shrinkage, the soil particles have reached their densest configuration. The water loss equals the increase of the air volume in the soil aggregates. The volumes of soil aggregate have stabilized and do not change any further.

Desiccation cracks have significant effects on the engineering behavior of expansive soils, such as the soil's diffusivity, hydraulic conductivity, its mechanical strength, lateral earth pressure, deformation and the surface energies of the water and soil particle surfaces. The presence of shrinkage cracks can reduce the stability, serviceability and hydraulic performance of earthworks and foundation structures. Due to the significance of the consequences, an understanding of swelling and shrinkage behavior of clay soils and the mechanics of desiccation cracking in drying soils is essential for the development of a rational analytical framework to analyze engineering problems associated with expansive soils.

6.1 Criteria of Soil Tensile Strength

Desiccation crack propagation starts when the horizontal soil stress equals the tensile soil strength. For expansive soils, the tensile strength is strongly dependent on soil mineralogy and the current moisture stress state (suction level). Based on Mohr-Columb failure criteria and the analysis of components of unsaturated soil shear strength, Lytton derived an expression for the unsaturated soil tensile soil strength as follows:

$$\sigma_t = -\theta f (u_a - u_w)\frac{\sin\phi'}{1-\sin\phi'} + c'\frac{\cos\phi'}{1-\sin\phi'} \qquad \text{(Equation 6.1)}$$

where σ_t is current tensile soil strength, $(u_a\text{-}u_w)$ is the current matric suction level, θ is the volumetric water content, c' is the effective cohesion due to cementation, ϕ' is the effective angle of internal friction and f is the ratio of $\tan\phi_b$ and $\tan\phi'$ as described in

the previous chapter, where ϕ_b describes how the strength increases with matrix suction (u_a-u_w). Figure 6.1 gives a graphical illustration of the tensile strength.

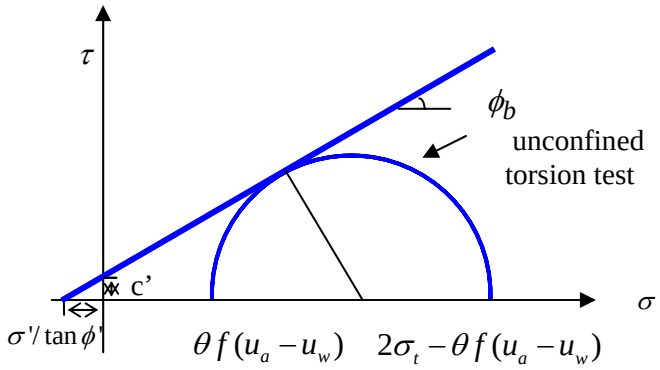

Figure 6.1 Tensile soil strength based on an unconfined torsion test (from Lytton, 2001)

The modification of shear failure criteria when the stresses are tensile is shown in Figure 6.2 (Lee and Ingles, 1968). Bagge (1985) and Morris (1992) suggest that the soil tensile strength can be estimated as $\sigma_t = 0.5[c' + (u_a - u_w)\tan\phi^b]\cot\phi'$, which is empirical and can be derived from or consistent with Equation.6.1 above. Soils such as slurries and mine tailings drying from very wet conditions normally have low effective cohesion c' around 2-5kPa, which is negligible for the purpose of conservative analysis.

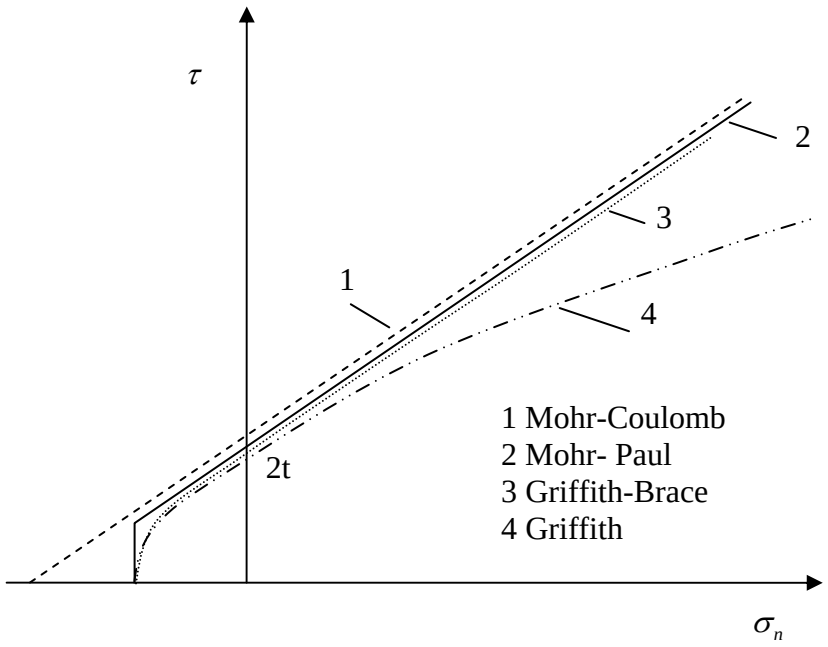

Figure 6.2 Strength envelopes and the tensile strength (Lee and Ingles, 1968)

6.2 Effect of Vegetation on Soil Desiccation

The effect of vegetation on clay soil desiccation has been a concern for the study of the mechanics of cracking. During the drying process, in response to the suction gradients set up, water moves to the evaporating surface and the soil becomes drier and drier. When the water content of soil surface drops to a value in equilibrium with the atmosphere, the drying rate begins to decrease and equilibrium is attained. For the vegetation to take up water, the suction in the vegetation must be higher than the soil suction around. As the soil gets drier, the suction in the vegetation must also increase in order to continue to extract moisture. However, the suction in the vegetation is limited by the osmotic pressure of the leaf cells, i.e., the wilting point, where the soil water is

held so tightly that the tree root cannot extract it. When the total suction reaches the pressure, the vegetation wilts and evaportranspiration rate is markedly reduced (Gardner, 1961).

6.2.1 Wilting Point

The wilting point is dependent on the species of vegetation. Russell (1977) stated that a soil suction of 4.2 pF throughout the root zone leads to wilting of crop plants. Rode (1969) concluded the soil total suction at plant wilting is usually between pF 3.9 and pF 4.7, with suctions of some plants being as high as pF 5.1. Aitchison (1956) gives limits as pF 3.7 to pF 5.3, with a mean as pF 4.2. Mitchell (1979) and Gardner (1961) observed from their research that, for most cases, the wilting point is around pF 4.5.

Cameron (2001) measured suction profiles for four sites as given in Figures 6.3 - 6.6. The suction profiles provide a snapshot of relative differences in soil moisture condition about a site at the time of taking the soil samples. The trees near the sites were usually native Australian species, often eucalypts. Linearity of the extreme suction profiles was assumed.

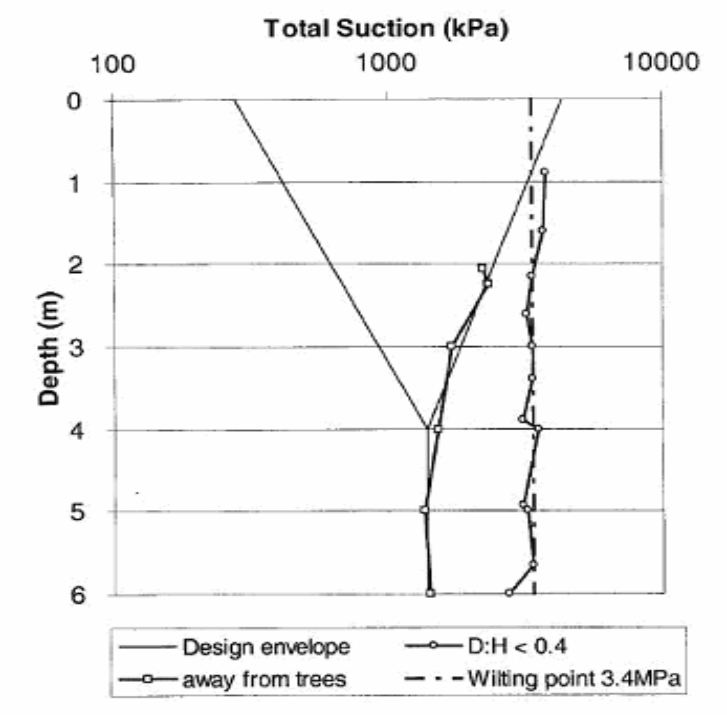

Figure 6.3 Total suction profiles near a row of large eucalypts (Klemzig site, Adelaide, South Australia) (Cameron, 2001)

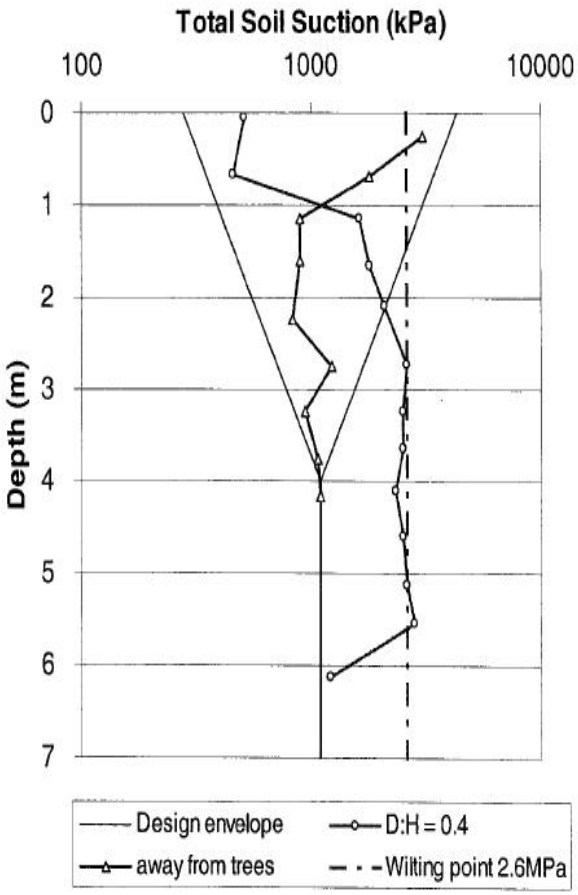

Figure 6.4 Total suction profiles near a row of trees of mixed species (Ingle Farm, Adelaide, South Australia) (Cameron, 2001)

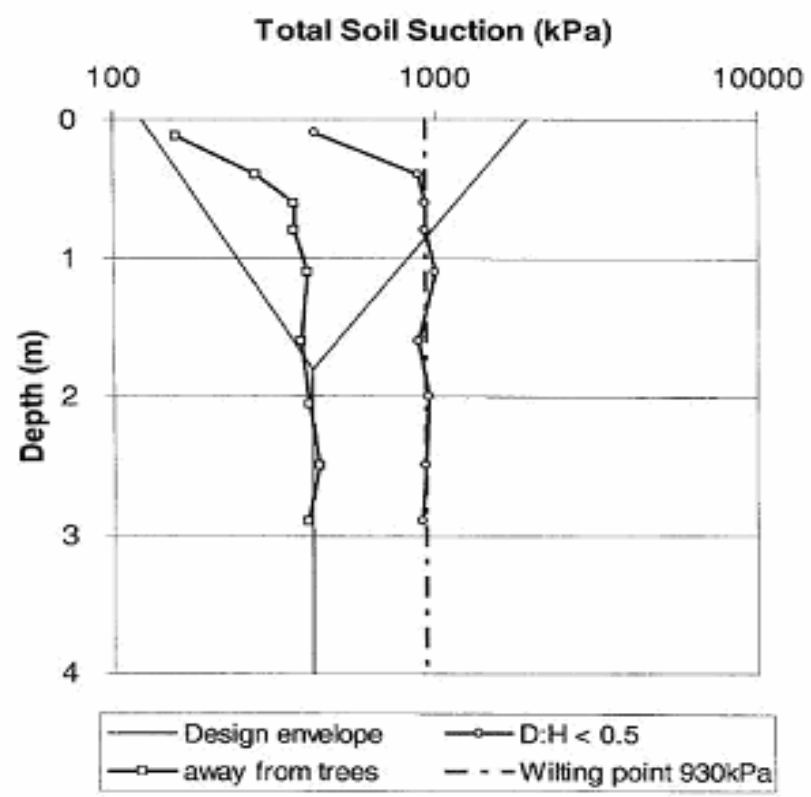

Figure 6.5 Total suction profiles near a row of large eucalypts (Williamstown, Victoria) (Cameron, 2001)

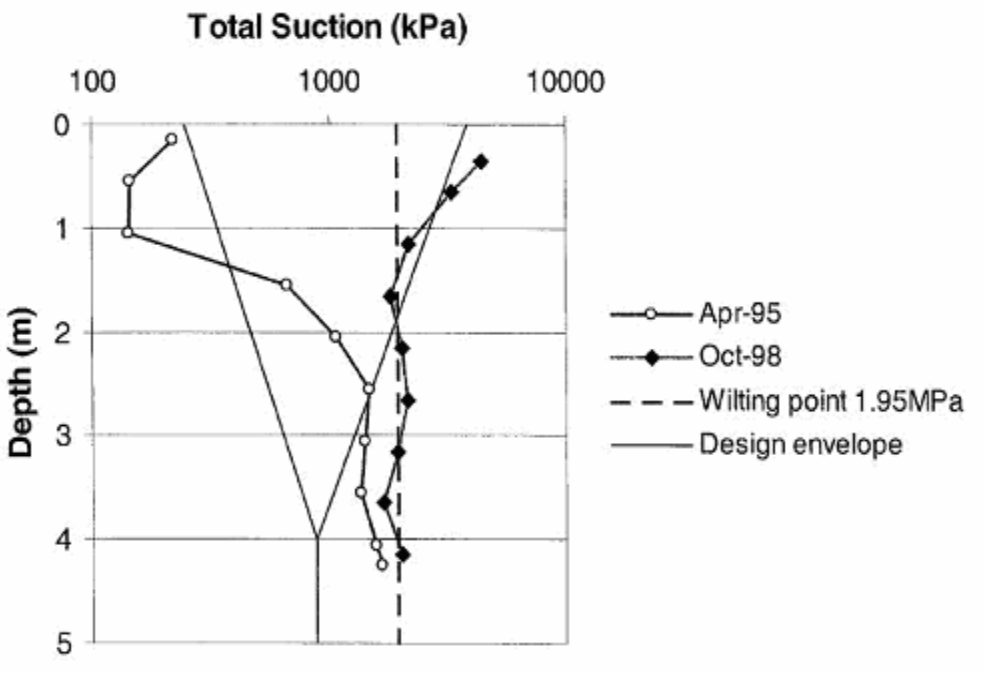

Figure 6.6 Total suction profiles near a roadside plantation of native trees (Hallett Cove, South Australia) (Cameron, 2001)

In Figure 6.3, the suction profiles relate to a row of trees consisting mainly of eucalypts. The profile close to the tree was wetter in the top one meter than the suction profile at the location away from trees. Cameron (2001) suspected that presumably attempts had been made by the homeowners to water the ground in the vicinity of the trees. In the figure, the ratio, D: H, refers to the ratio of the minimum horizontal distance, D, between the base of the tree and the location in question for soil profile measurements, to the height of the tree, H. The suction profile at D:H of 0.4 lay outside the design dry envelope below a depth of 2m. At a depth of 6.1m, the suction approximated the equilibrium suction which is judged to be 1.1MPa (4.04 pF).

In Table 6.1, wilting point is expressed in terms of total suction, u_{wp}, which forms a dry side boundary to the potential soil suction range in a soil profile, at depth within the soil. U_{eq} is the equilibrium suction beneath the moisture active zone depth. The wilting point suction ranged between 1.95 and 3.4 MPa (4.29 pFand 4.53 pF), similar to the range suggested by McKeen (1992), who reported that the wilting points for a variety of spices reached values of total suction of 1.55-3.1 MPa (or 4.29~4.49pF). Richards et al. (1983) also report a wilting point near 3.5MPa (4.54 pF), which is close to the upper limit by Cameron (2001).

Table 6.1. Summary of Suction Data (Cameron, 2001)

Site	Trees (H)	D: H	u_{eq} (pF)	u_{wp}(pF)	u_{tree} *
Broadview, SA	Gum (9 m)	<0.5	3.99	4.34	0.35
Greenacres, SA*	e. Torquata (8.3m)	0.4-0.7	4.06	4.29	0.23
Greenacres, SA*	2 smaller gums	0.6	4.06	4.29	0.23
Ingle Farm, SA	Row of eucalypts (8m)	1.5	4.04	4.29	0.25
Ingle Farm, SA	Row of eucalypts (10m)	0.4	4.04	4.42	0.37
Klemzig, SA	Row of mature eucalypts	<0.5	4.14	4.53	0.39
Hallett Cove, SA	Native plantation	0.1	3.94	4.29	0.35
The Levels, SA	Native plantation	<0.5	3.99	4.49	0.35
Williamstown, Vic.	Row of gums	<0.5	3.62	3.97	0.35

- Data from Jaksa (1998). Available: http://training.ce.washington.edu/WSDOT/Modules/04_design_parameters/shink-swell_soils.htm.
- $\Delta u_{tree} = u_{wp} - u_{eq}$

6.2.2 Drying Effects Caused by Trees

The drying effects of tree roots in clay soils vary with the species and soil salinity. The root system of a tree can be grouped as either tap or lateral as shown in Figure 6.7 (Mitchell, 1979). The vertical tap roots grow vertically downwards along earthworm holes or soil fissures to considerable depths (root zone depth), to convey water and trace elements from the soil at depth, and to anchor the tree. Normally, it is

considered that tap roots are confined to the vicinity of the tree trunk itself, and are thought to have only an insignificant effect on the tree surroundings. The laterals grow horizontally and parallel to the soil surface and form a mat over a certain limited depth where microbiological processes are most active and nutrients are more abundant. These lateral root systems extend a considerable distance from the trunk and extract moisture from surrounding soils. Biddle (1983) conducted a series of studies of soil moisture deficits around specimens of certain tree species in open grassland in the UK and he found that the extent of drying, both horizontal and vertically, appeared to be species dependent. Poplars caused soil drying to a radius of over 1.5 times the tree height and caused the deepest drying close to the trees, probably to a depth in excess of 4m.

Trees increase the dry side of the suction profile at depth and the drying effect extends to the range of root zone depth. Cameron (2001) stated that a group of trees would potentially generate approximately 50% more movement than the same site without trees. Cooling and Golder (1942) observed that the effects of a larger poplar and ash in the United States extended to at lest 2m, while they also found trees causing drying to a depth of 3m. Perpich et. al. (1965) found the depth of desiccation from trees in the United States to be from 2 to 4m, and over a horizontal distance of up to that equal to the height of the tree.

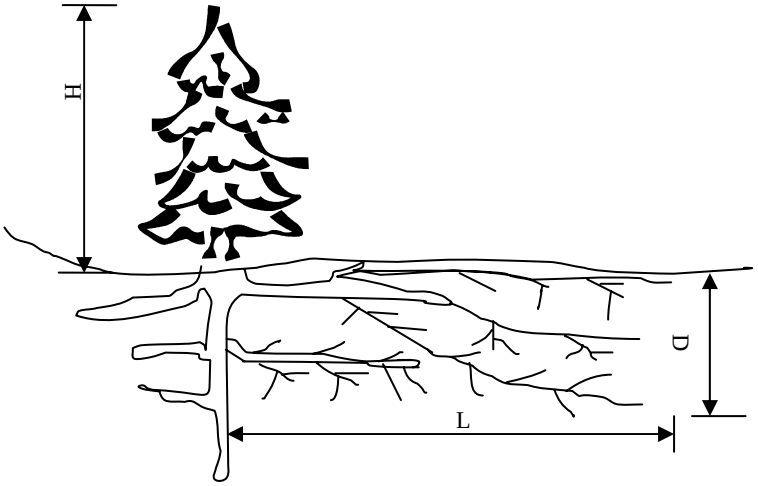

Figure 6.7 Lateral and vertical extent of tree root system (Mitchell, 1979)

6.2.2.1 Root Zone Depth

Root zone depth is an important material parameter for the consideration of drying effects caused by trees (Agriculture and natural resources, 2005. Available: http://ucce.ucdavis.edu/files/filelibrary/2019/2945.pdf). The pores in soil structures (soil particles) serve as a conduit to move the water and air into root zone. Soil compaction and pore plugging can change the distributions of pores from macro to micro pores, and thus decrease water holding capacity, infiltration rate and root zone depth.

Root zone has been reported to reach a depth of 20 ft. A recorded root fiber of 4.3m was reported by Lytton (1995) near a large oak tree in Texas during a hot, dry summer. Normally, roots can fracture the soil approximately 0.6m beyond or deeper than the location of the root fiber.

Rooting depth located in shallow soils or those with root zone limiting conditions can be much less. The root zone limiting conditions can be caused by soil texture and

structure, such as fine textured soils with poor internal drainage characteristics and /or poor structure or soils with dense, compact, or cemented sub-soils and layered or stratified soils where abrupt, significant changes in soil texture may disrupt water movement in the vicinity of the interface. Other factors like rock and water table whether static or fluctuating can limit the depth of root zone. Roots may grow back into the deeper depths when water recedes, however, they will die back when water table rises. (Agriculture and natural resources, 2005. Available: http://ucce.ucdavis.edu/ files/filelibrary/2019/2945.pdf). Besides the soil structure, the irrigation system and the amount of rainfall can also have an influence on root zone depth. The use of moisture measuring devices can help define the root zone over the season by monitoring the soil water disappearance at soil depths in and below the suspected root zone (Agriculture and natural resources, 2005. Available: http://ucce.ucdavis.edu/ file/filelibrary/2019/ 2945. pdf).

6.2.2.2 Root Barrier

The use of a root barrier as a remedy to protect existing foundations from the effects of desiccation is always subject to disputation. Inserting rot barriers close to trees can be dangerous. If the foundation was constructed after the existence of trees, a barrier that cuts off the root system beneath the foundation can cause soil heave as if the tree were entirely removed from the site since the suction profile would be altered from the dry side to wetter side. The British Building Research Establishment (1985) gave the following statement regarding the effect of root barriers: “Little is known about the effectiveness of root barriers in preventing root activity beneath house foundations. They

are usually fairly expensive to install. As with underpinning, there is uncertainly about how extensive a root barrier should be, both laterally and in depth. If the trees are older than the building, a barrier that cuts off the root system beneath a house will cause swelling and heave as if the tree were entirely removed. Inserting root barriers close to trees can be dangerous. If sufficient of the root system is severed, the tree may lose lateral stability and fall. Even if rapid instability is not caused, the tree may slowly die and become unstable at a later date."

Nunn et al. (1992) observed the effect of a root barrier on protecting an extensive single storey office building from the effects of desiccation occurring in an adjacent garden, although the observation was only made for five months after the installation of tree root barrier. Blight (2006) performed a detailed field study on the effect of root barrier on soil water content and effect of tree without root barrier. The experimental site is at Clarens, which is situated in the Free State Province of South Africa. The trees involved are a willow (*Salix tortuosa*) presently 8.5m high and growing 7.5m from the west wall of the house, and an American ash (*Fraxinus americana*) presently 9m high, growing 6.5m from the south wall. Desiccation by roots from the Fraxinus has clearly caused the south wall to subside and crack.

The construction of root barrier is relatively simple. A trench 500mm deep was excavated and severed all the roots it crossed. The trench was lined with corrugated glass-fiber reinforced acetate sheeting with the corrugations running vertically. Each 450mm long sheet overlapped by two corrugations to form a barrier that extended

around 50mm below surface. Then the trench was backfilled with the soil excavated from it. The backfill was well compacted in layers placed at 100mm depth intervals.

The first soil moisture content measurements were taken at the end of October 2003 (spring) after the installation of root barrier during July 2003 (winter). The water balance diagram and the water content profiles measured by sampling with a 50mm diameter hand auger are given in Figures 6.8 and 6.9. Each sample hole was backfilled with the soil that came out of it and the hole was sealed with the soil placed back in 50 mm layers. Each layer was rammed and the surface was left slightly proud.

After December 2003, in Figure 6.9, the A-line, representing the total water stored in the soil between the barrier and the house, lies consistently above the B-line, representing the total water stored in the soil under the tree. Blight (2006) observed that the soil water content adjacent to the house became relatively stable once the root barrier was in place. Hence the south wall has been stabilized. Blight (2006) also provided the water content contours (Figure 6.10) for the study of effect of tree without root barrier, which clearly show the persistent desiccation of the soil around the tree. The main influence of the willow tree (*Salix tortuosa*)'s root system extended to a radius of about 4m from the tree, whereas the tree's leaf canopy had a radius of 3.7m. The water stored

in the soil over distance T (tree to 4m from tree) and H (4m from tree to wall of the house) have also been shown in Figure 6.8 (water balance diagram), which clearly states that the soil within the radius of main influence of the tree was consistently drier than the soil beyond the radius.

6.2.3 Soil Desiccation by Grass and Bushes

The desiccating effects of grass and bushes have been ignored by most researchers in the past due to the concentration of the study of larger desiccation caused by trees. Russam and Dagg (1965) studied the effects of various surface treatments for road shoulders on soil moisture under roads in Kenya. They found that shoulders planted with a local grass (*Pennisetum clandestinum*) desiccated the soil to a depth of 3m. De Bruijn (1965) found that desiccation in open fields under indigenous grasses in South Africa penetrated to a depth of 6m, which is comparable with the depth of desiccation under trees. Parry (1992) investigated water content profiles on London clay in an open grassed field and was surprised by the evidence of desiccation down to a depth of 4m. It is not too much to emphasize that grass and bushes can cause clay soils drying and several desiccation problems (Blight, 2005).

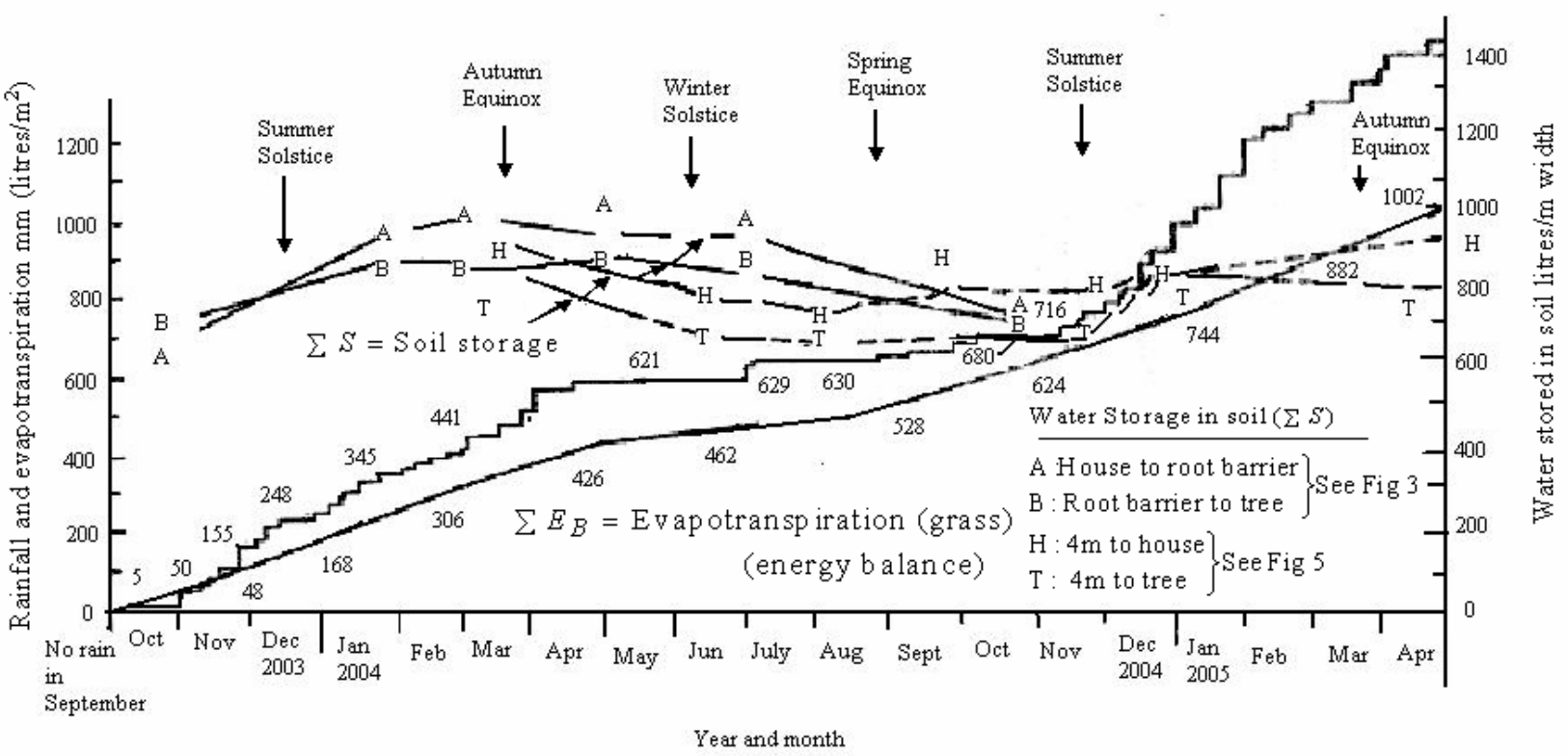

Figure 6.8 Water balance for the Clarens site showing soil water storage for root barrier-to-tree and tree-to-house measurements (Blight, 2006)

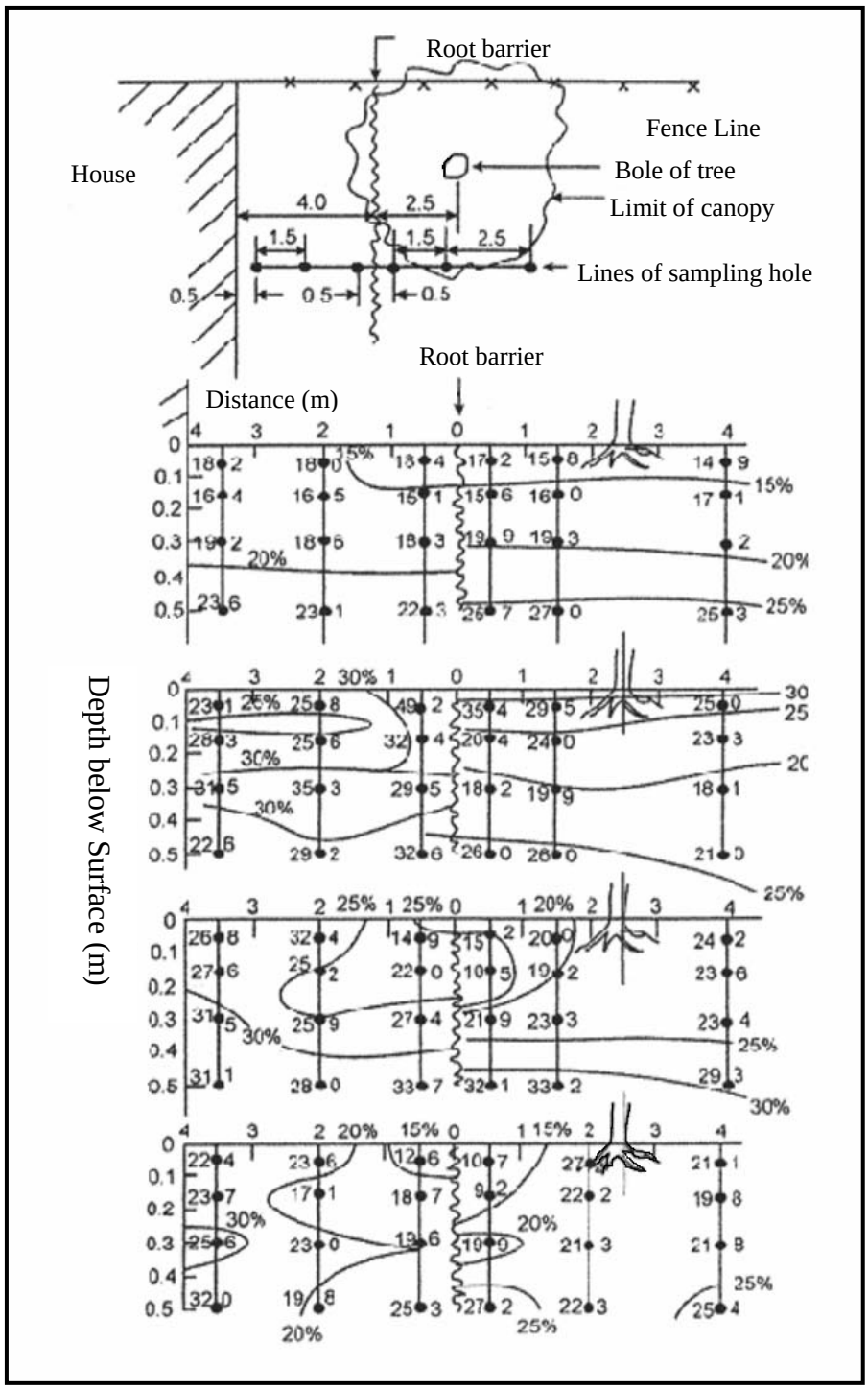

Figure 6.9 Effect of root barrier on soil water content during 2003/2004 year (Blight, 2006)

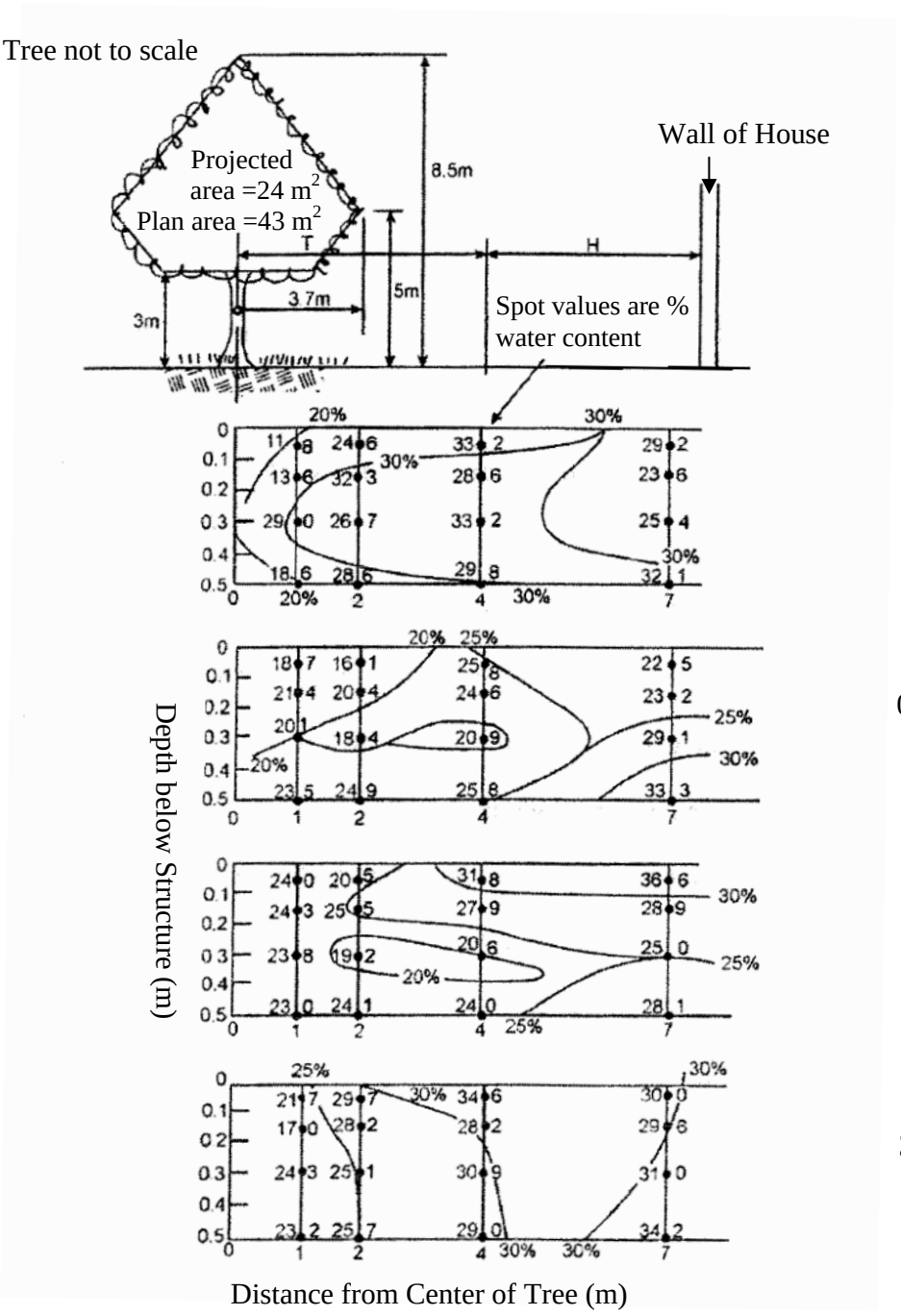

Figure 6.10 Contours of soil water content between tree and house during 2004/2005 year (Blight, 2006)

6.3 Cracking Spacing and Depth

The effect of the crack in relieving stress at the ground surface bears on the problem of crack spacing, and the rate of energy dissipation at the advancing crack tip is relevant to the problem of crack depth. The approach for exact prediction of crack spacing and crack depth is still an open question.

Desiccation cracking grows in a direction normal to the component of maximum tensile stress. As soil drying proceeds and matric suction increases, the dominant cracks tend to grow in both depth and horizontal length. The stress concentration in the vicinity of a crack tip results in crack propagation to a depth which is controlled by the intrinsic soil properties and the stress field such as the soil self-weight. The horizontal length is confined by the intersection with other cracks at angles closely approaching 90°, because the direction of the maximum tensile stress in the soil at the tip of a propagating crack adjacent to an existing open crack must be parallel to the plane of the crack due to the fact that the perpendicular tensile stress has been relieved by the cracking and thus the direction of propagation of the approaching crack is progressively turned towards the existing crack until they finally intersect perpendicularly. As matric suction tends to increase further, the blocks between existing cracks appear to break into smaller pieces. The secondary cracks which cause the block breakup propagate from about the middle of the longer sides of existing blocks of uncracked soil. They start at the ground surface and propagate downwards and sideways into previous uncracked soils. Initially, the tensile stresses are highest at the middle of the longest side of an existing block of soil formed by earlier cracking. The stresses are increased throughout the block by increasing

suctions. The restraint necessary for crack propagation is provided by underlying soil which is subjected to lower suctions and smaller suction-induced strains. The minimum self-weight stresses (zero value) and maximum suctions occur at the upper surface of the block, i.e., the ground surface. As desiccation proceeds, a block can be further subdivided by repeated occurrences of the same process. The subdivision stops when the decreasing size of the block in plan and the depth of cracking overcome the restraining stresses at the base of the block and matrix suctions reach equilibrium with the atmosphere.

At the first stage of soil drying, cracks appear as microcracks in the form of voids. Under tensile loading at the crack tips, macroscopic cracks are produced by the growth of these micro cracks. According to the fracture mechanics approach to crack propagation, there exist three basic modes of crack surface displacement as shown in Figure 6.11, the superposition of which is sufficient to describe the most general case of crack-tip displacement and stress fields. Mode I is an opening mode where the crack surfaces move directly apart, resulting in a tension crack. The movement is caused by tensile forces normal to the face of the crack and may occur under plane stress and plain strain conditions. Mode II is characterized by displacement in which the crack surfaces slide over each other in the direction perpendicular to the leading edge of the crack, producing a shear crack. In mode III, the crack surfaces slide over each other in the direction parallel to the leading edge. The result is a tearing or torsional crack. A crack in the core of clays subjected to a combination of normal and shear stresses, i.e., the superposition of mode I and II (Vallejo, 1989).

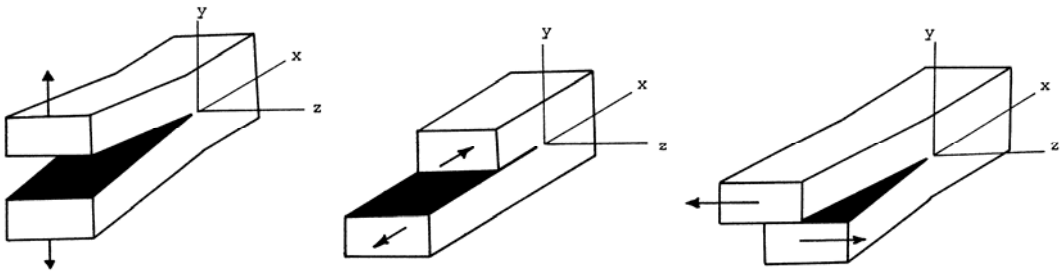

(a) (b) (c)

Figure 6.11 Basic modes of crack surface displacement: (a) tension mode; (b) shear mode; (c) torsion mode (Vallejo, 1989)

Lachenbruch (1961) used the modified Griffith theory of fracture by Irwin (1948) and Orowan (1950) in which the surface energy considered by Griffith is replaced by the energy of plastic deformation near the advancing crack tip and concluded that in naturally occurring tension-crack systems that evolve rapidly, the crack depth should be of the same order of magnitude of the crack spacing. The deeper cracks are more widely spaced because they relieve tension over greater horizontal distances than their shallow neighbors. Also since the reduction in tensile stress at the tips of shorter cracks is greater than that at the tips of deeper cracks, the growth of smaller and shallower cracks is retarded and eventually suppressed by the growth of adjacent larger and deeper cracks. The deep and widely spaced shrinkage cracks might represent seasonal desiccating crack effects and shallow, closely spaced cracks might result from the relief of surficial tension developed by rapid desiccation after a rain. Profound cracks with spacings more than 10ft can occur in the field.

Cracks propagating vertically and horizontally in soils can be stopped by weak interfaces (Lawn and Wilshaw, 1975), which happens, for instance, at the interface

between fine and coarse layers typical of varved clays or mine tailings. Ahead of the tip of a crack propagating vertically downwards, there is a zone with a vertical tensile stress component that is sufficient to cause tensile failure of any weak, horizontal interface lying ahead of the crack. The resulting transverse (horizontal) crack stops the propagation of the initial vertical crack by reducing the horizontal tensile stress at the top crack surface. Since the stresses perpendicular to the new horizontal crack are usually compressive, this crack rarely propagates any further.

Knight (1971) in Australia observed in the field that the crack depth in clay soils approximately equals the cracking spacing. Konrad and Ayad (1997) also stated that the maximum cracking depth d_c equals to cracking spacing s. The assumption of crack depth limited by cracking spacing leads to a staggered pattern of cracking as shown in Figure 6.12, which is the basis of the analysis of the effect of clay soil cracking in the latter parts in this chapter.

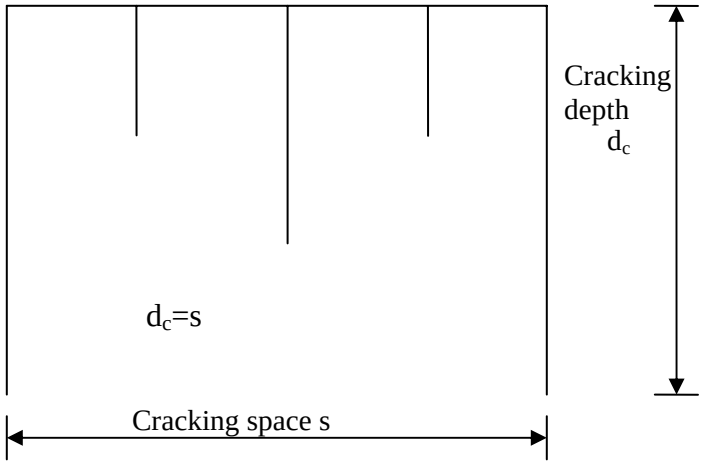

Figure 6.12 Analysis model for the effect of desiccation on diffusivity

6.4. Effect of Desiccation on Soil Diffusivity

As mentioned in previous chapters (chapter II, III and IV), the moisture diffusivity described in terms of diffusion coefficient α is a significant material parameter to control the moisture diffusion rate. Moisture travels much more easily in cracked soils between pods and clods than in intact soils. Field investigations report that the field diffusion coefficient is greater than the laboratory diffusion coefficient measurement for intact soil by the order of 10 to 100 times.

6.4.1 Diffusion Coefficient by Field Evidence

The actual field diffusion coefficient can be estimated from the decay of seasonal variations of surface suction with depth when the suction measurements made over time at various depths are provided. The one-dimensional analytical solution for the diffusion equation in Equation 6.2 gives one approach to back-calculate the diffusion coefficient α in actual field sites. McKeen and Johnson (1990) obtained values of α from field

measurements of suction decay which varied from 3.2-13m^2/yr (or (1.015~4.16)$\times 10^{-4}$ cm^2/s).

$$u(y,t) = u_e + u_0 \exp(-\sqrt{\pi y^2 n/\alpha}) \cos(2\pi nt - \sqrt{\pi y^2 n/\alpha}) \quad \text{(Equation 6.2)}$$

where, u_e is the equilibrium suction at the bottom of moisture active zone depth. U_0 is the amplitude of suction variations at the surface; y is the depth with respect to the ground surface; n is the number of cycles of suction variations during a year (cycles/year).

An alternative approach to estimate the diffusion coefficient α is to monitor the suction changes within the soil mass in response to the boundary suction conditions, such as a wetting boundary due to irrigation or rainfall, or a drying boundary due to the elimination of a source of surface moisture and evaportranspiration due to vegetation. Mitchell (1979) gave the following governing equation (Equation. 6.3) for both the wetting and drying scenarios:

$$u(y,t) = u_e + (u_e - u_s) erfc(y/2\sqrt{\alpha t}) \quad \text{(Equation 6.3)}$$

where u_s is a constantly maintained suction on the soil surface, which can be either greater or less than the equilibrium suction u_e in terms of the existence of boundary conditions (drying or wetting process). Mitchell (1979) used this approach to back-calculate the diffusion coefficient α at two separate sites with one site having a wetted surface boundary and the other associated with a drying boundary. Using Equation 6.2, a diffusion coefficient equaling 0.33m^2/yr (or 1.05×10^{-4} cm^2/s) was back-calculated from these two sites. McKeen and Johnson (1990) also adopted this method to interpret water

content measurements over time at a site with a flooded surface boundary and obtained the field estimations which fall within the range of α values from suction decay measurements from Equation 6.2.

Mitchell (1979) also proposed the time lag approach to back estimate the field diffusivity. The approach utilized Equation 6.2 and considered the time lag that will happen between when a peak of suction occurs at the ground surface and when it occurs at depth. The derived equation (Equation. 6.4) to measure time lag t_{lag} at depth y relating to the diffusion coefficient α is:

$$\alpha = y^2 /(t_{lag}{}^2 4\pi m) \qquad \text{(Equation 6.4)}$$

From data at a site where peaks of soil deformation measured at a depth of 1.2m were observed to lag the peaks of deformation at the ground surface by 3 months (Figure 6.13), an estimation of $\alpha = 1.9\text{m}^2/\text{yr}$ or $(6.025\times10^{-4}\ \text{cm}^2/\text{s})$ was obtained assuming the suction variation frequency n=1 cycle/yr.

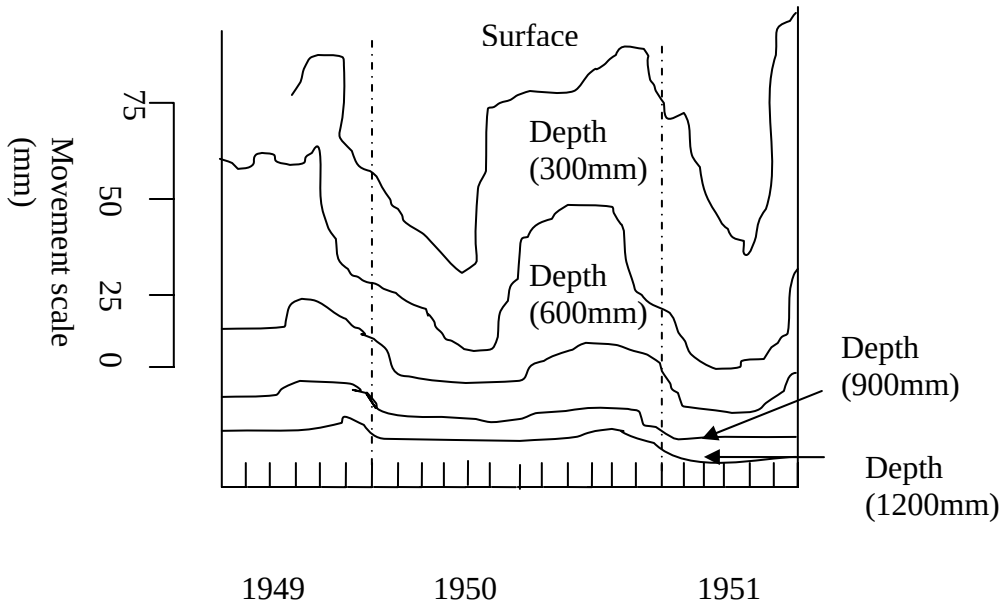

Figure 6.13 Observed seasonal soil movements of an expansive soil in open field in Adelaide, South Australia (Mitchell, 1979)

The laboratory diffusion coefficient measurements described in previous chapter provide a range of 10^{-5}~10^{-7}cm^2/s, which is less than that of the field estimation by a factor of 10 to 100 times. A likely source of the extreme magnitudes and variance of field diffusion coefficient estimations with respect to laboratory measurements is desiccation cracking within the soil mass. The crack fabrics in the clay soils which are generated by vegetation (roots, grasses or bushes) and surface drying provides lesser lateral restraint relative to intact soil and allows the soil to expand and contract large amounts both vertically and horizontally.

A series of numerical analyses have been conducted to study the effect of desiccation on field diffusivity by comparing the moisture active zone depth under different cracking depth cases with the value for intact soils. The following part in the

chapter will give a detailed description of this numerical study and the results in terms of the ratio of field diffusion coefficient estimations over the diffusion coefficients for intact soils.

6.4.2 Estimation of Diffusivity in terms of Seasonal Moisture Active Zone Depth z_c

Mitchell (1979) provided a one-dimensional solution for a periodic surface suction that varies in a sinusoidal manner in response to climatic cycle (Equation. 6.5):

$$u(y,t) = u_e - u_0 \exp\{-[(\frac{n\pi}{\alpha})^{0.5}]y\}\cos\{2n\pi t - [(\frac{n\pi}{\alpha})^{0.5}]y\} \qquad \text{(Equation 6.5)}$$

The climatic surface suction variation at the ground surface is expressed as $u(0,t)=u_a+u_0\cos(2\pi nt)$, where u_a is the average surface suction value, u_0 is the surface suction variation. Same as before, n is the climatic frequency (cycles/year).

The envelopes of the suction profile may be determined by first taking the derivative of Equation. 6.5 with respect to time, which leads to Equation 6.6 (McKeen and Johnson, 1990):

$$t = \frac{\sqrt{\frac{n\pi}{\alpha}}}{2n\pi} y \qquad \text{(Equation 6.6)}$$

and the equation of suction envelopes (Equation. 6.7, dry and wet envelopes) can be obtained by substituting Equation 6.5 back in Equation 6.4:

$$u(y) = u_e \pm u_0 \exp[-(\frac{n\pi}{\alpha})^{0.5} y] \qquad \text{(Equation 6.7)}$$

The difference between the maximum and minimum envelopes for a given depth, i.e., the maximum change in suction, $\Delta U_{\max}$ is:

$$\Delta U_{\max} = 2U_0 \exp[-(\frac{n\pi}{\alpha})^{0.5}]y \qquad \text{(Equation 6.8)}$$

Thus, the depth of seasonal moisture active zone can be calculated as follows:

$$z = \frac{\ln(\frac{2U_0}{\Delta U_{max}})}{\sqrt{\frac{n\pi}{\alpha}}} \qquad \text{(Equation 6.9)}$$

From the transformation of Equation 6.8, the diffusion coefficient can also be expressed as a function of moisture active zone depth and the maximum allowable suction change ΔU_{max}:

$$\alpha = \frac{n\pi z^2}{\ln(\frac{2U_0}{\Delta U_{max}})} \qquad \text{(Equation 6.10)}$$

McKeen and Johnson (1990) suggest the adoption of climatic frequency n equaling 0.5 for the design case.

6.4.3 Moisture Active Zone Depth from Field Observation

The depth of seasonal moisture active zone is related to the climate (Thornthwaite Moisture Index) and clay soil properties. When a marked separation occurred between wet and dry seasons, a large seasonal variation in soil moisture content occurred, a large moisture active zone depth is expected, whereas in areas which were either predominantly dry or predominantly wet for most part of the year, the changes in soil moisture content is not so marked (Mitchell, 1979).

Moisture active zone depth can be inferred from the suction measurements with the filter paper method or psychrometers in the field. Mitchell (1979) presented several field suction profiles measured in the area of Adelaide, South Australia (Mediterranean Climate) (Figure 6.14) with the depth of moisture active zone close to 1.5m-2.5m (5ft-8.5ft).

Lytton (1995) provided several profiles of field suction measurements as in Figures 6.15-6.16 and estimated the depths of moisture active zone where total suction reaches equilibrium suction level or there is an inferred presence of a water table. In Figure 6.15, the equilibrium suction level is reached at a depth of 4.2m (13.8 ft). In Figure 6.16, the depth of moisture active zone can be estimated from the inferred presence of water table at 5.2m (17.1 ft).

Depth of moisture active zone can also be inferred from the deepest recorded root fiber or inferred presence of cementation of the soil. Roots can affect the soil approximately 0.6m beyond the deepest root fiber. In Figure 6.17, from a suction profile in a root zone, the depth of moisture active zone is indicated around 4.8m (15.7 ft).

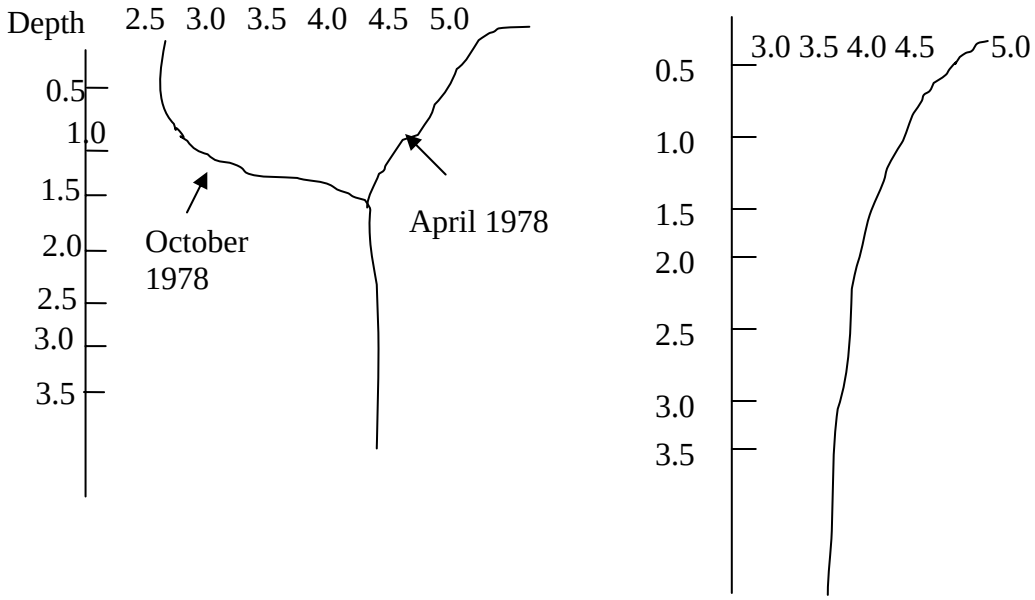

Figure 6.14 Measured seasonal suction in open paddock and under well ventilated floor (Mitchell, 1979)

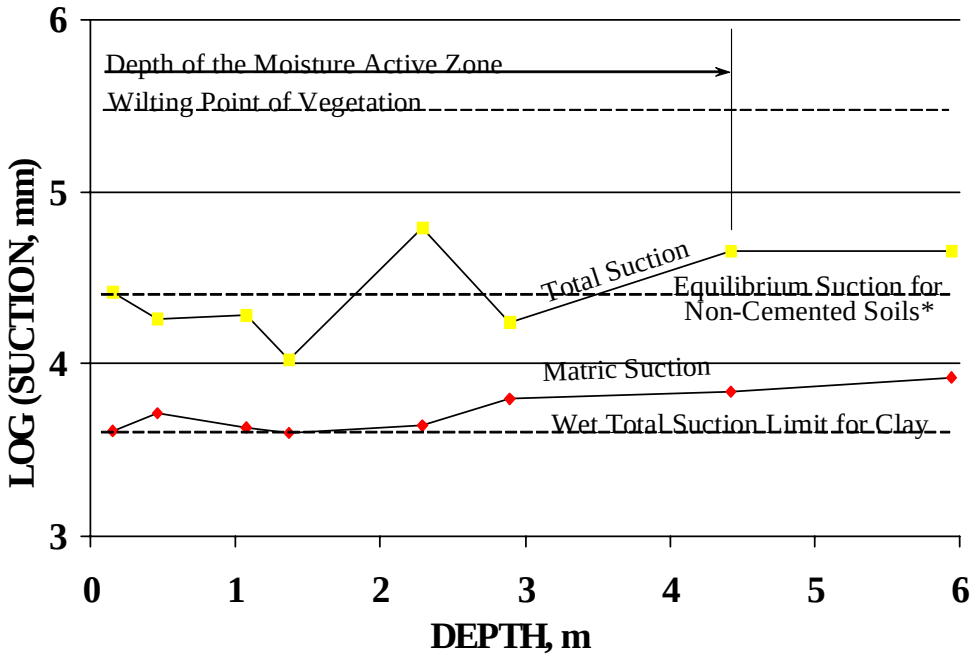

* From Epirical Relation of Thornthwaite Moisture Index with equilibrium suction (Russam and Coleman, 1961)

Figure 6.15 Suction profile with depth illustrating the point where suction becomes constant with depth. (Lytton, 1995)

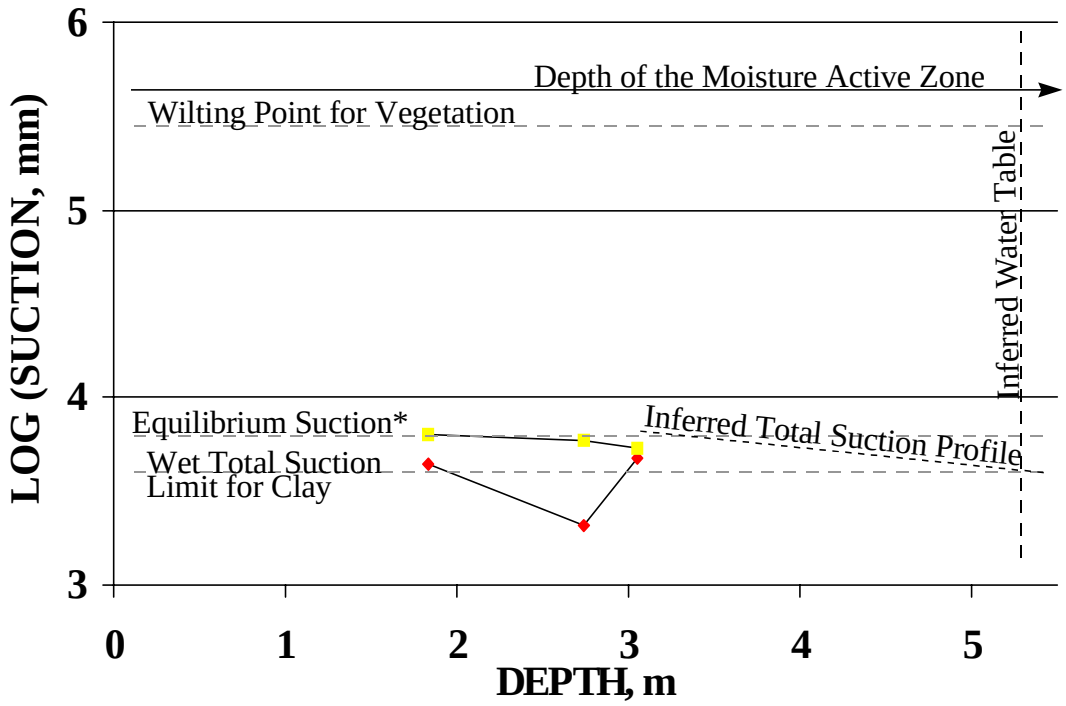

* From Empirical Thornthwaite Moisture Index Relation with equilibrium suction (Russam and Coleman, 1961)

Figure 6.16 Suction profile with depth illustrating the inferred presence of a water table (Lytton, 1995)

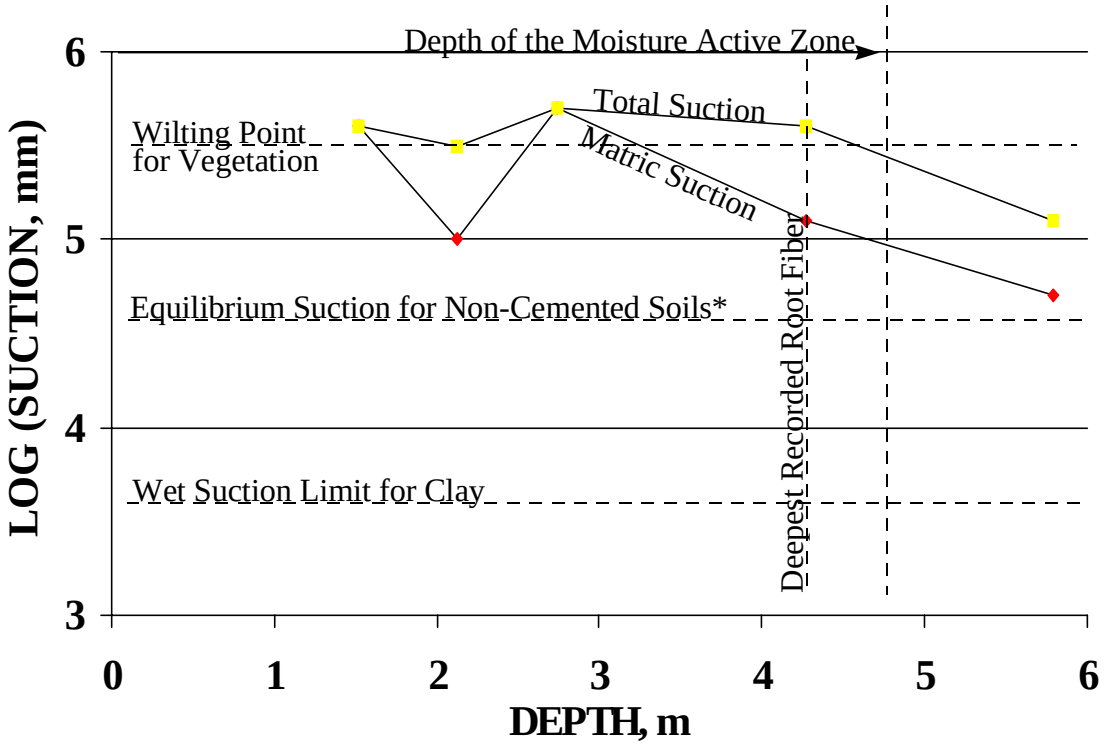

* From Empirical Relation of Thornthwaite Moisture Index with equilibrium suction (Russam and Coleman, 1961)

Figure 6.17 Suction profile in a tree root zone in summer (Lytton, 1995)

6.4.4 Numerical Modeling for Effects of Desiccation Cracking

For this study, a number of numerical simulations are conducted for the effect of desiccation cracking on soil diffusivity. From Equation 6.9, the ratio of field diffusivity verse that of intact soil $\alpha / \alpha_0 = (y_{ma} / y_{ma0})^2$, where y_{ma} is the moisture active zone depth in the field and y_{ma0} is the theoretical moisture active zone according to Equation 6.8 for the case of intact soil. Since the rate of moisture diffusion along cracks is much more rapid than in uncracked soil, the adopted two-dimensional numerical model assumes that suction on the surface of the cracks tracks suction at the free surface. Thus, a climatic

surface suction variation at the ground surface $u(0.t) = u_e + u_0 \cos(2\pi nt)$ also occurs throughout the depth of each crack. For the analysis, the moisture active zone depth y_{ma} is defined as the depth at which the thickness of the suction envelope at depth is less than 10% than its width at the ground surface, i.e., $\Delta u_{\max} = 0.1u_0$.

Since moisture transmission can be described with a linear diffusion equation, the analysis results of the diffusivity ratio α / α_0 in terms of the percentage of sampling locations are presented for different normalized crack depths (d_c / y_{ma0}). Four cases of crack depths (2ft, 4ft, 8ft and 16ft) are considered in the analyses. The geometries for numerical modeling are depicted in Figure 6.18.

For this analysis, an 8-node quadratic element with the size of 0.05 ft and aspect ratio 1:1 is adopted. The commercial computer program ABAQUS is employed and the heat transfer analysis type is selected to simulate the moisture diffusion problem.

As emphasized in previous chapters, for the moisture diffusion analysis (or transient heat transfer analysis) with second-order elements, in order to avoid spurious oscillations due to small time increments, there is a relationship between minimum usable time increment and the element size as indicated (Equation. 6.11):

$$\Delta t > \frac{1}{6\alpha} \Delta l^2 \qquad \text{(Equation 6.11)}$$

Where, Δt is the time step increment (time step); α is the moisture diffusion coefficient and Δl is the element dimension (the length of a side of element).

Repeating the exercise for a series of maximum (primary) crack depths of 1ft, 2ft, 4ft, 8ft and 16ft leads to Figure 6.19 which indicates the relationship between α / α_0 ratio and the percentage of sampling locations within the crack patterns in Figure 6.18 for different crack depths.

For the analysis, the adopted diffusion coefficient α equals 5×10^{-5} cm^2/s, which falls in the range of diffusion coefficient for intact soils. The plot shows two aspects of desiccation cracking on field diffusivity: first, it increases the magnitude of diffusion coefficient, sometimes to a factor of more than 100 times for deep crack systems; second, it creates the spatial variability in this material parameter, which is particularly marked for the case of large crack depths. For sampling locations closer to cracks, the change of moisture diffusion coefficient is more significant.

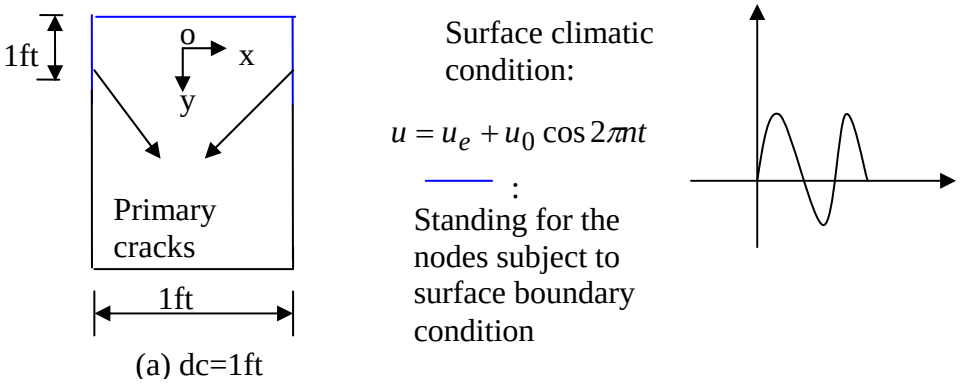

(a) dc=1ft

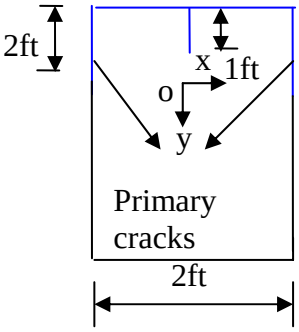

(a) dc=2ft

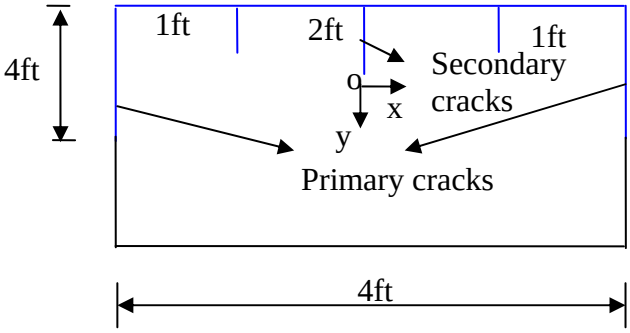

(b) dc=4ft

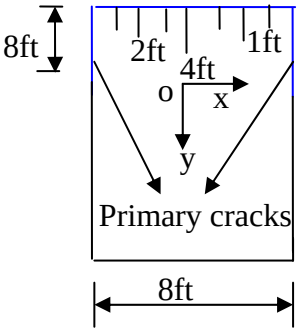

(c) dc=8ft

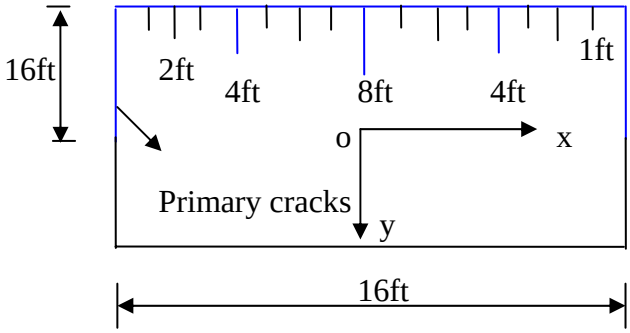

(d) dc=16ft

Figure 6.18 Geometries for different crack depths in the analysis

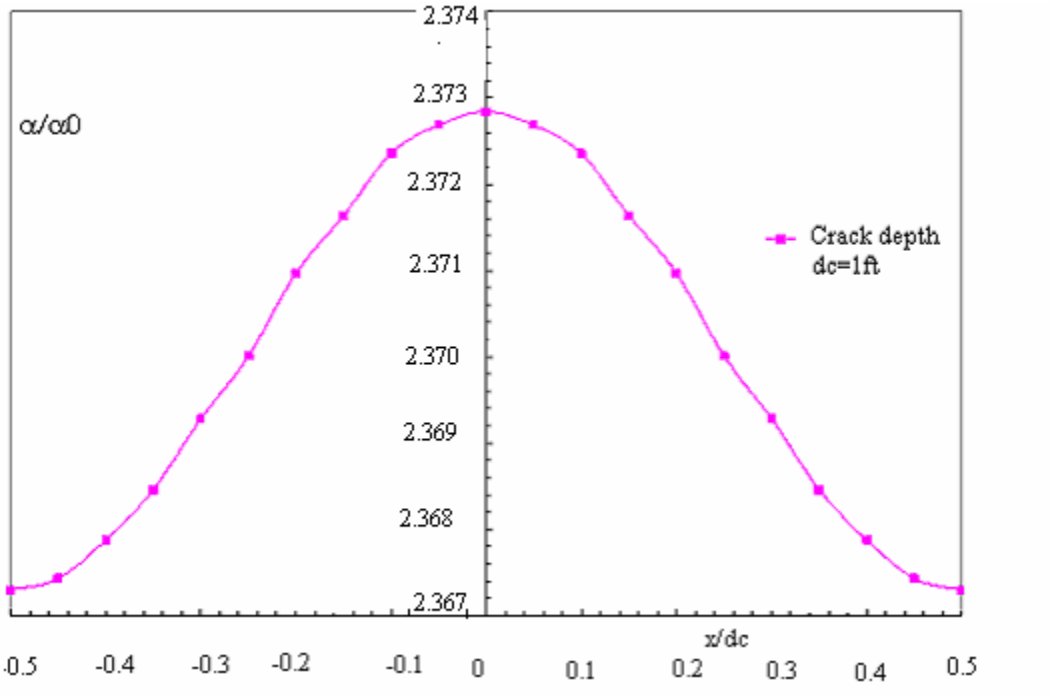

(a)

Figure 6.19 Crack depths (x/dc) vs. field to lab diffusivity ratio

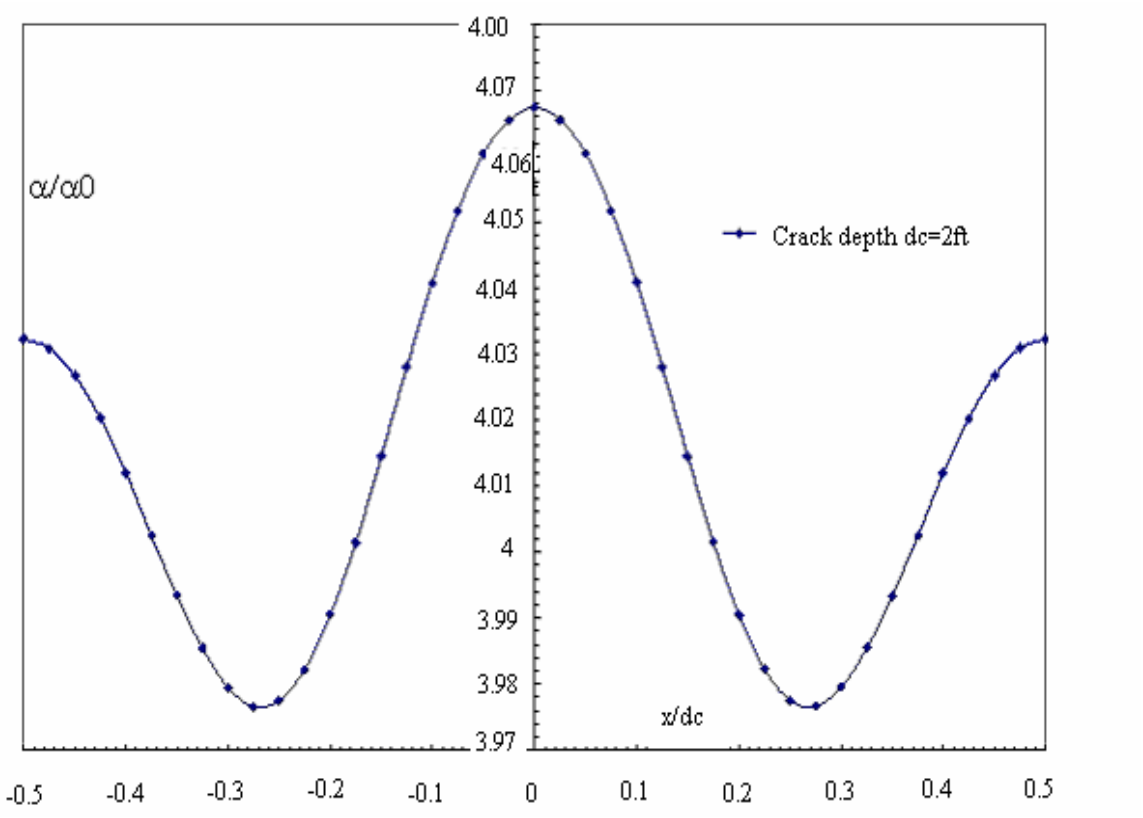

(b)

Figure 6.19 (Continued)

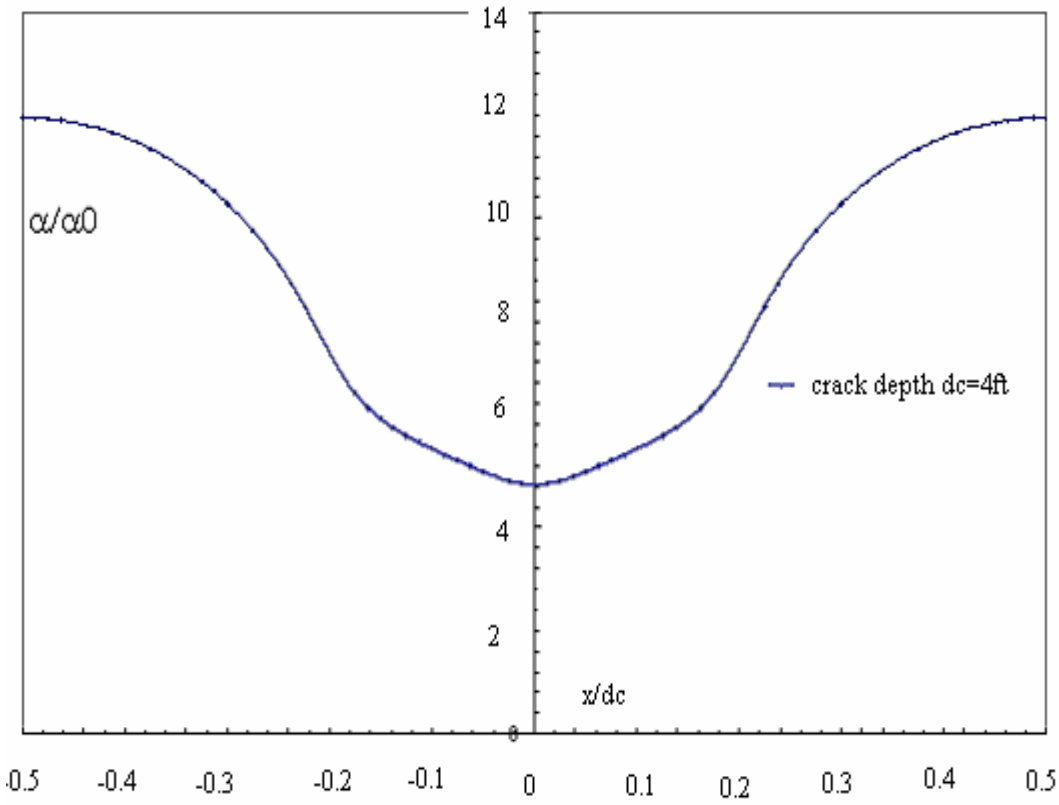

(c)

Figure 6.19 (Continued)

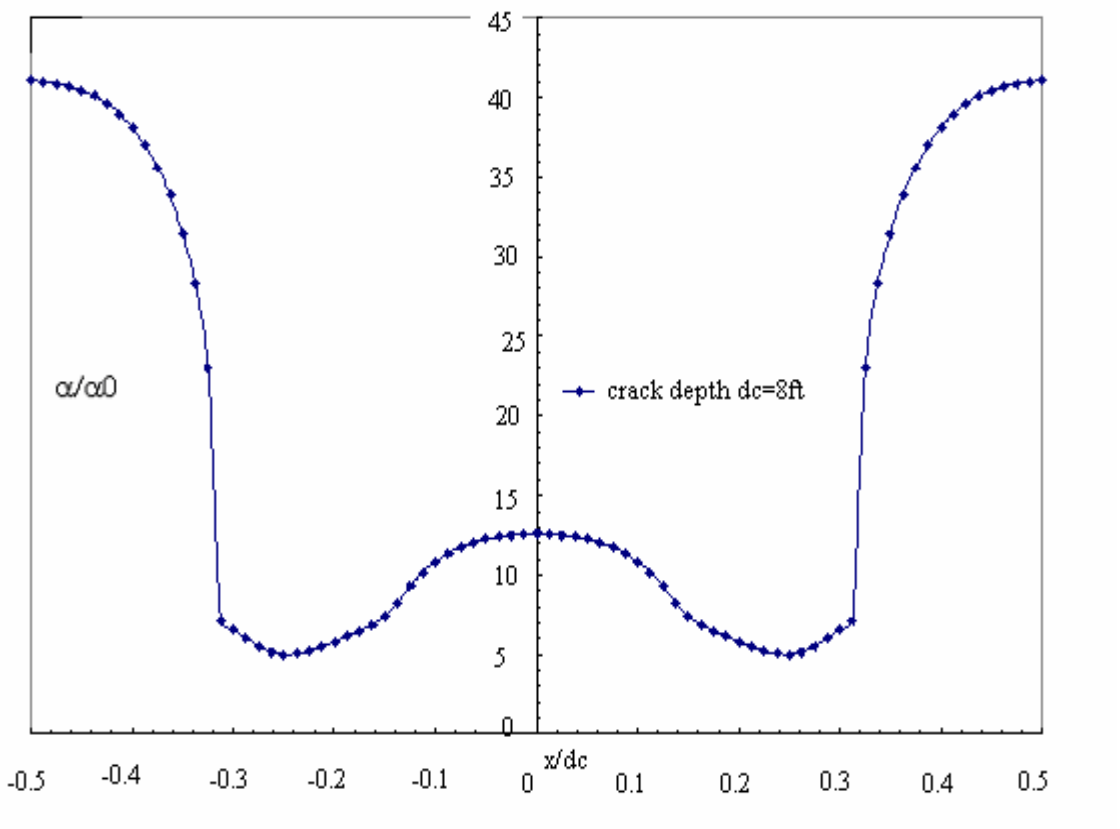

(d)

Figure 6.19 (Continued)

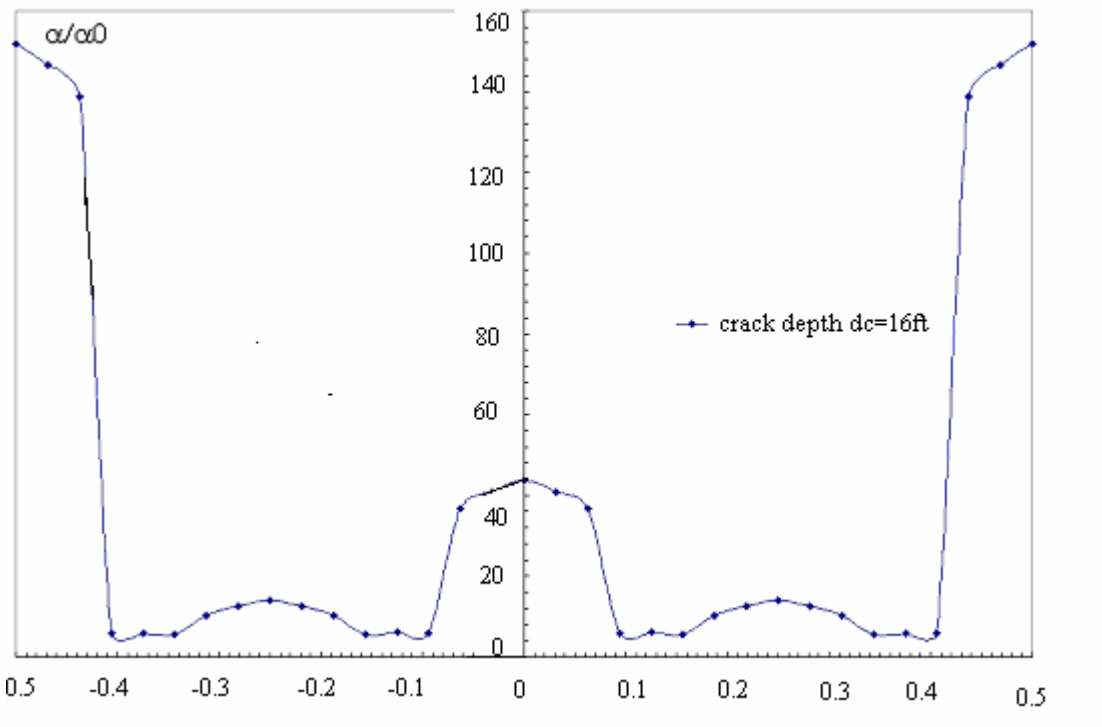

(e)

Figure 6.19 (Continued)

Uniform element size is employed through all the depth of the finite element mesh. For the case of crack depth 2ft, the width of the finite element mesh is 2ft and depth is 30ft. The nodes at the surface boundary and the nodes associated with cracks are subjected to the climatic cyclic surface variation throughout the analysis period, which is set to ten years. Likewise, the finite element mesh for the case of 4 ft, 8ft or 16ft crack depth is 4 ft, 8ft or 16ft $\times$30 ft. The number of nodes and elements utilized in the analyses for different crack depths are shown in Table 6.2.

Table 6.2. Number of Nodes and Elements for the Analyses

Crack depth (ft)	1ft	2ft	4ft	8ft	16ft
Number of nodes	37241	73281	145361	289521	577841
Number of elements	12000	24000	48000	96000	192000

For each crack depth, in terms of the ratio of field diffusion coefficient versus the laboratory measurement for intact soils, the mean, standard deviation and different percentiles (10^{th}, 20^{th}, 30^{th}, 40^{th}, 50^{th}, 60^{th}, 70^{th}, 80^{th}, 90^{th} and 100^{th}) are calculated and presented in Table 6.3 and Figure 6.20.

The semi-interquartile range is a measure of dispersion or spread. It is computed as one half the difference between the 75^{th} percentile (often called (Q3)) and 25^{th} percentile (often called (Q1)). Hence, the formula for the semi-interquartile range is (Q3-Q1)/2.0, where the 75^{th} percentile cuts off the upper 25% of the distribution and 25^{th} percentile cuts off the bottom 25% of the distribution.

Table 6.3. Mean, Standard Deviation and Percentiles in Terms of Field to Lab Diffusion Coefficient Ratio

Crack depth (ft)	1	2	4	8	16
Mean diffusivity ratio	2.3702	4.0149	8.6108	18.9905	36.6815
Standard deviation	0.0020	0.0286	2.6813	13.9904	49.0344
0^{th} percentile	2.3673	3.9766	4.8326	5.0004	7.2338
10^{th} percentile	2.3676	3.9795	5.0821	5.5338	7.5549
20^{th} percentile	2.3679	3.9855	5.5270	6.1514	7.7141
30^{th} percentile	2.3685	3.9933	6.1072	7.1922	7.8741
40^{th} percentile	2.3693	4.0024	7.3854	10.1751	9.2423
50^{th} percentile	2.3700	4.0145	9.1131	12.0385	14.3600
60^{th} percentile	2.3710	4.0268	10.2915	12.5732	16.6711
70^{th} percentile	2.3717	4.0309	11.2191	31.4785	32.9391
80^{th} percentile	2.3724	4.0409	11.6657	38.0976	47.4337
90^{th} percentile	2.3728	4.0604	11.9027	40.4447	142.4004
100^{th} percentile	2.3732	4.0673	11.9553	41.1331	164.5333

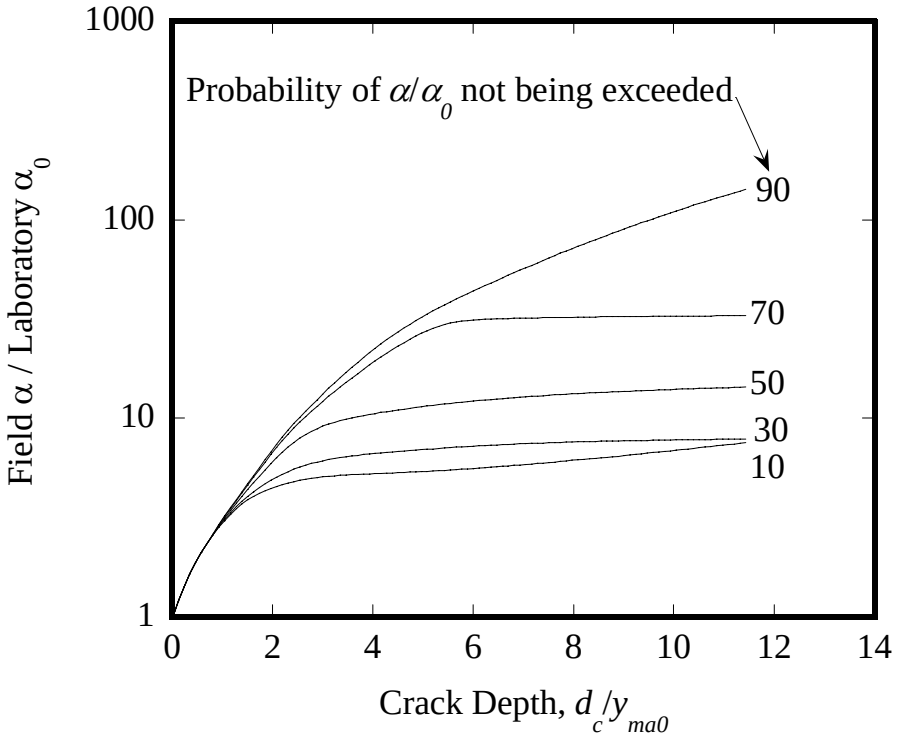

Figure 6.20 Cumulative probability density function of field to laboratory diffusion coefficient ratio versus the ratio of crack depth d_c to intact soil moisture active zone depth, y_{max} (Aubeny and Long, 2006)

Since half the scores in a distribution lie between Q3 and Q1, the semi-interquartile range is half the distance needed t o cover half the scores. In a symmetric distribution, an interval stretching from one semi-interquartile above the median will contain one half of the scores. However, for a skewed distribution, this is not the case.

Since the semi-interquartile range is little affected by extreme scores, it is a good measure of spread for skewed distributions. However, it is more subject to sampling fluctuation in normal distributions than is the standard deviation.

In Figures 6.21 and 6.22, the plots of mean, (mean+ standard deviation), (mean-standard deviation), (mean + semi-interquartile range) and (mean-semi-interquartile range) in terms of the ratio of (field diffusivity α) over (laboratory diffusivity α_0) are given in natural or logarithmic scale in terms of the field to laboratory diffusion coefficient ratio.

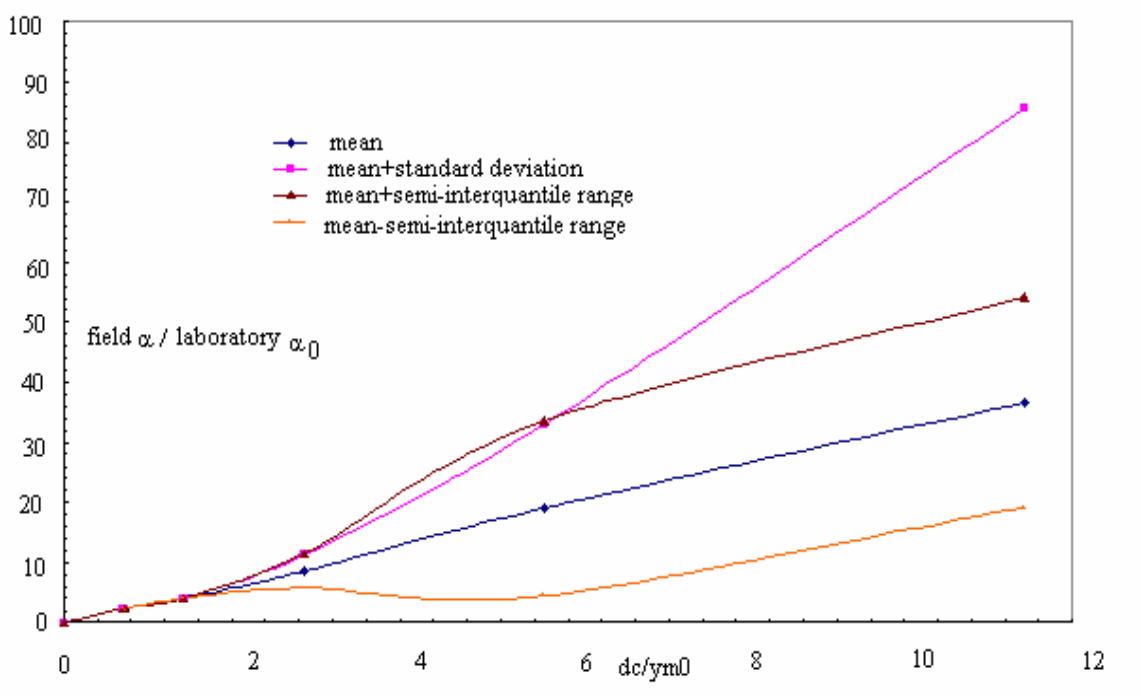

Figure 6.21 Normalized crack depth versus field to laboratory diffusion coefficient ratio (natural scale)

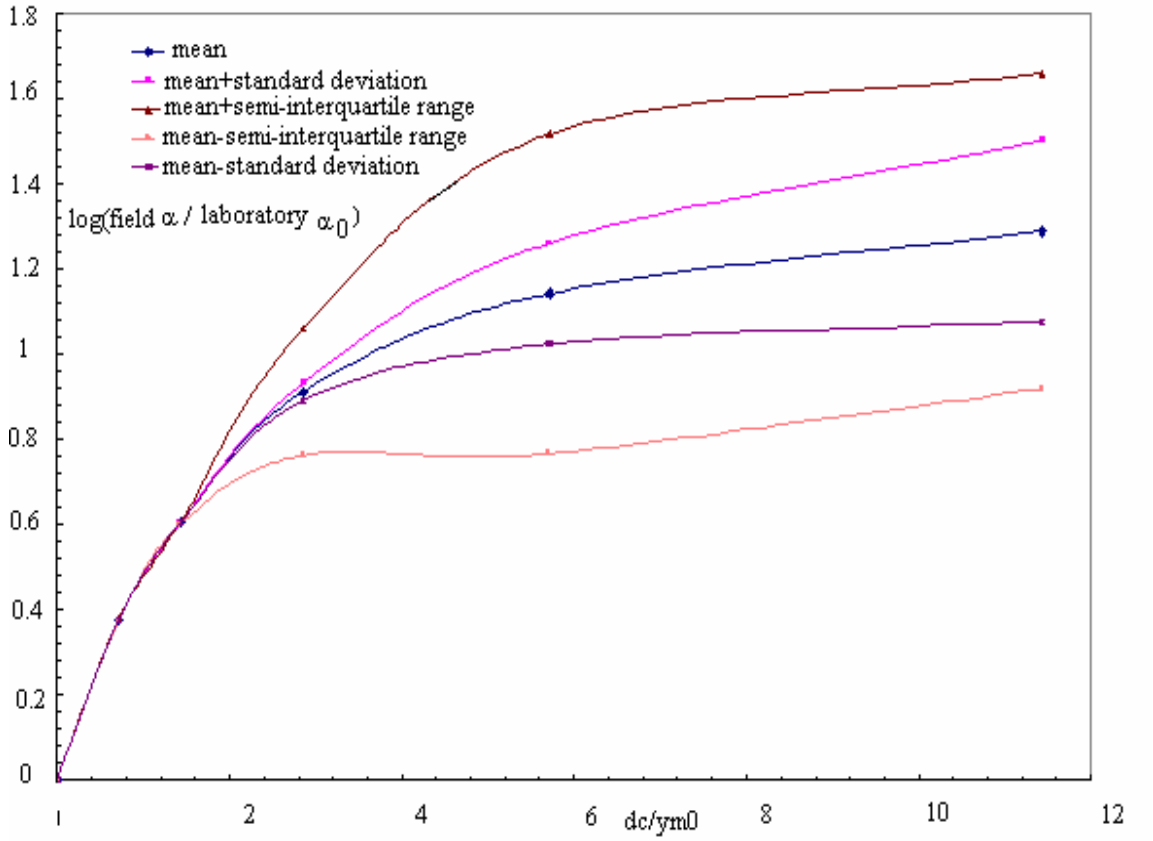

Figure 6.22 Normalized crack depth versus field to laboratory diffusion coefficient ratio in logarithmic scale

The cumulative probability plot is also presented in Figure 6.23. This plot gives the probable diffusion coefficient ratio associated with a given reliability level. The horizontal axis is the ratio of field to the laboratory diffusion coefficient and the vertical axis is the cumulative probability. For instance, in the case of a crack depth of 4ft, the ratio of field diffusion coefficient to that of intact soils is around 40 with a reliability of 80 percent.

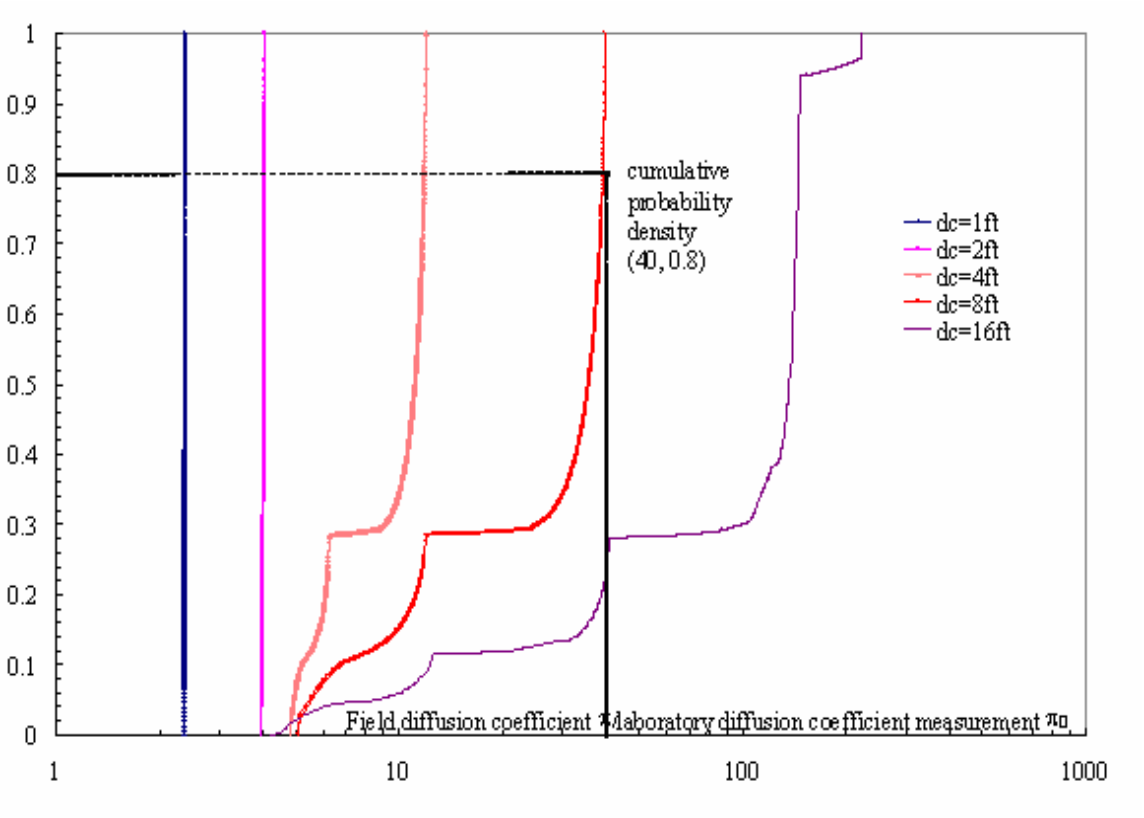

Figure 6.23 Reliability versus diffusion coefficient

(b) Effect of Element Size

As plotted in Figure 6.24, an exercise of different element size (1ft and 0.1ft) is also performed to study the effect of element size on the accuracy of the results. As the mesh becomes finer, the resulting diffusion coefficient ratio becomes slightly smaller and the shape of the curve is smoother.

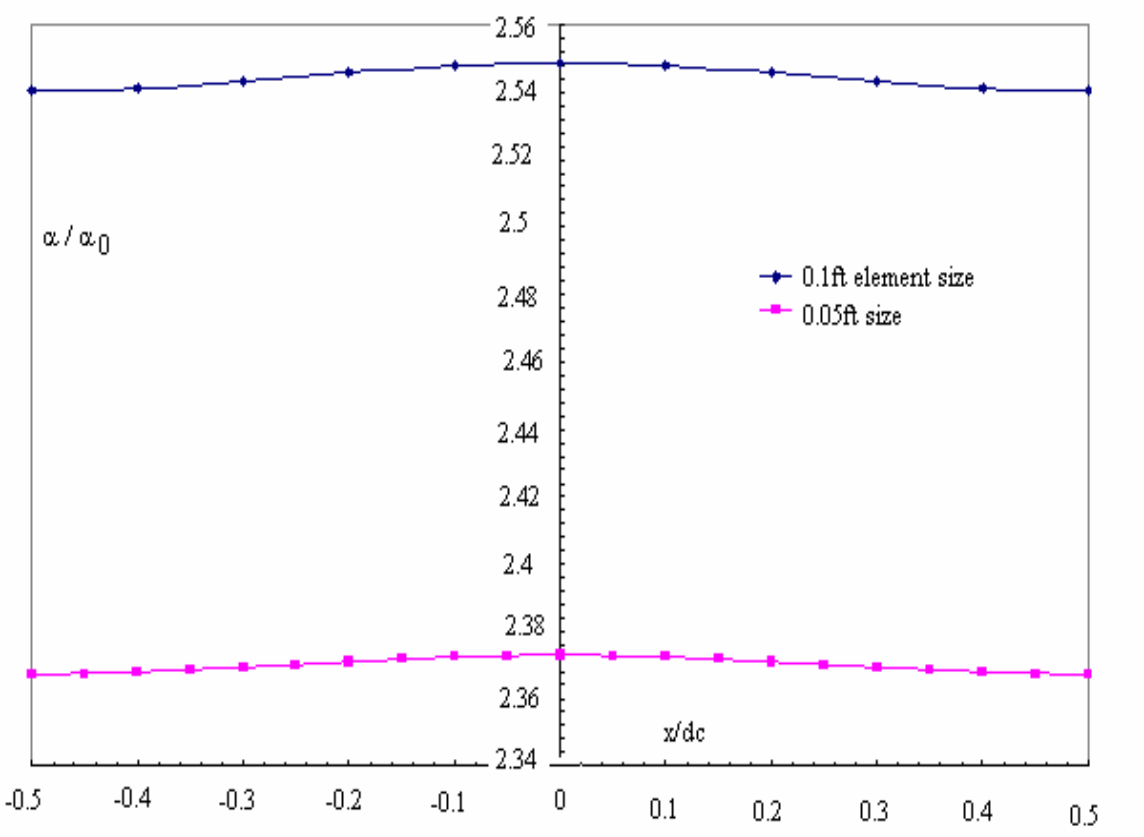

(a)

Figure 6.24 Effect of the mesh size on accuracy: (a) crack depth=1ft; (b) crack depth=2ft; (c) crack depth =4ft; (d) crack depth=8ft; (e) crack depth=16ft

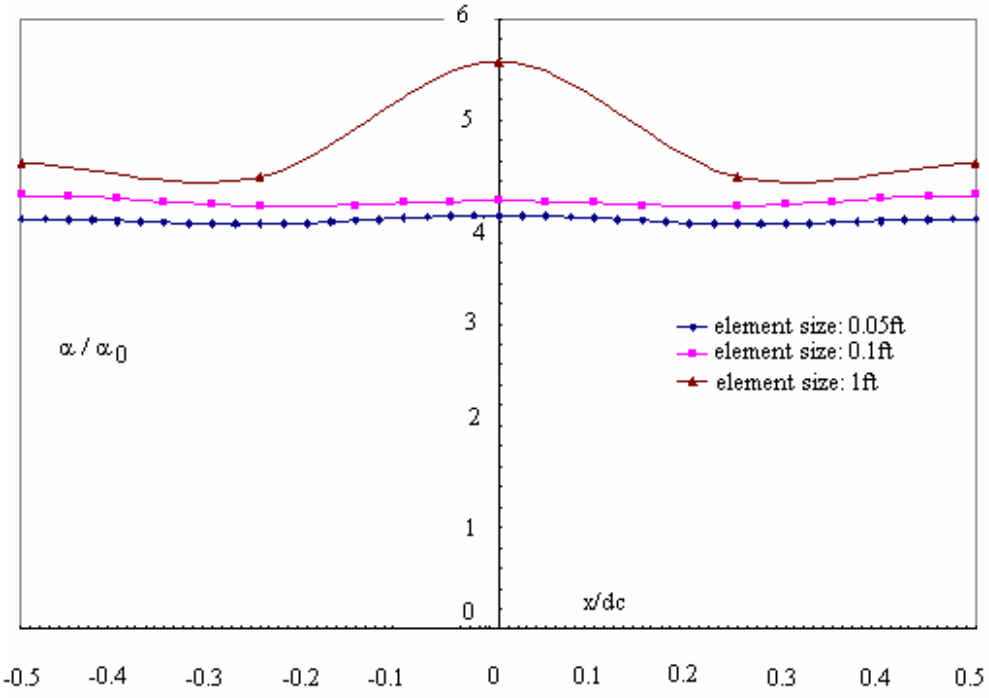

(b)

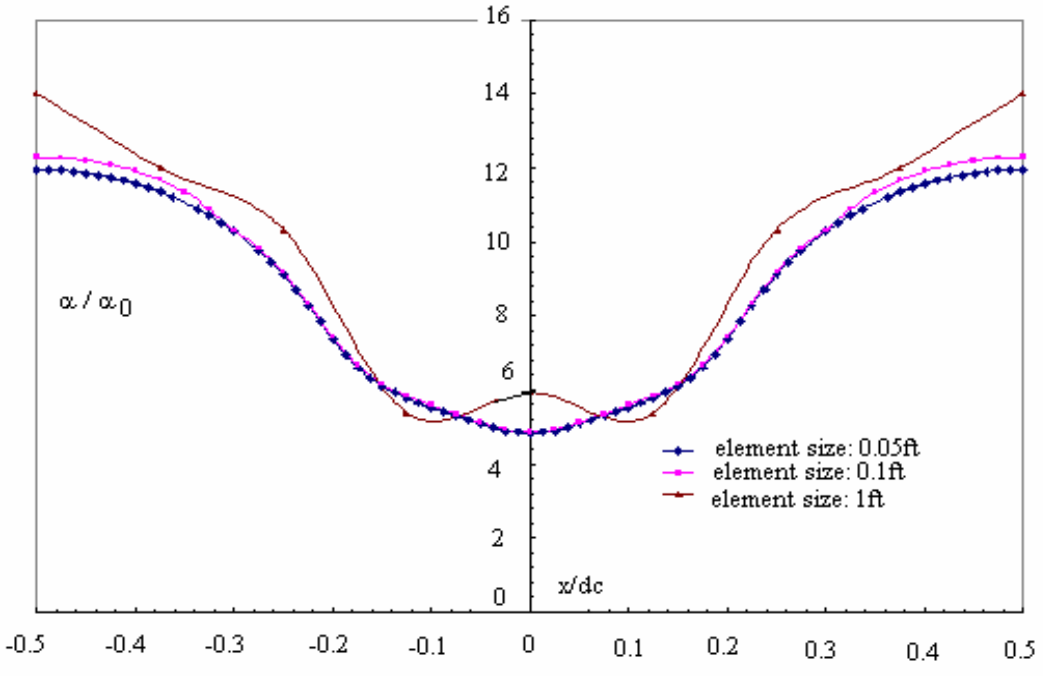

(c)

Figure 6.24 (Continued)

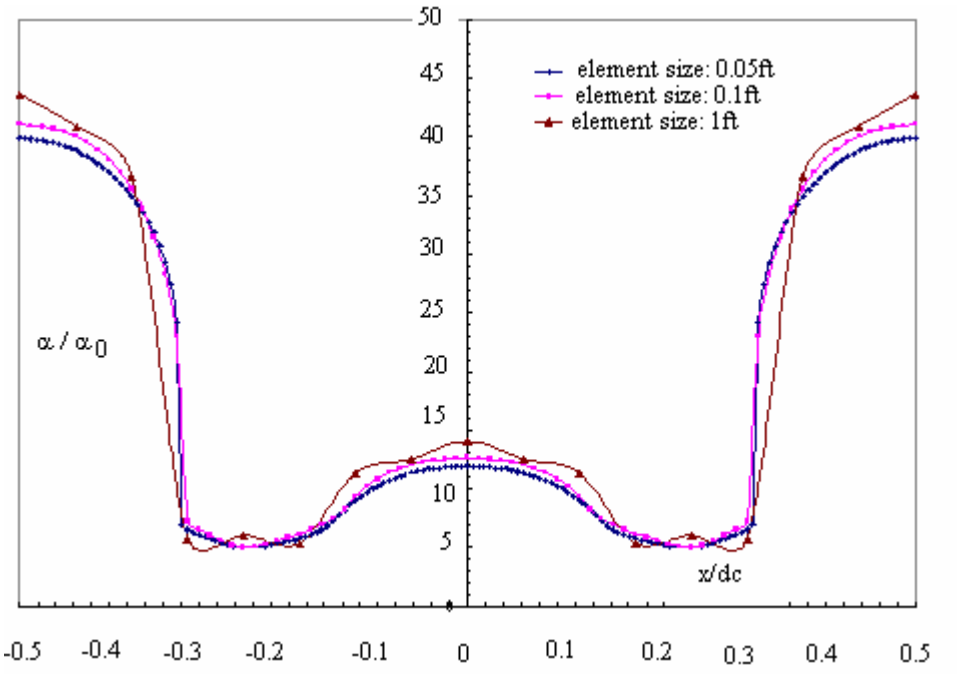

(d)

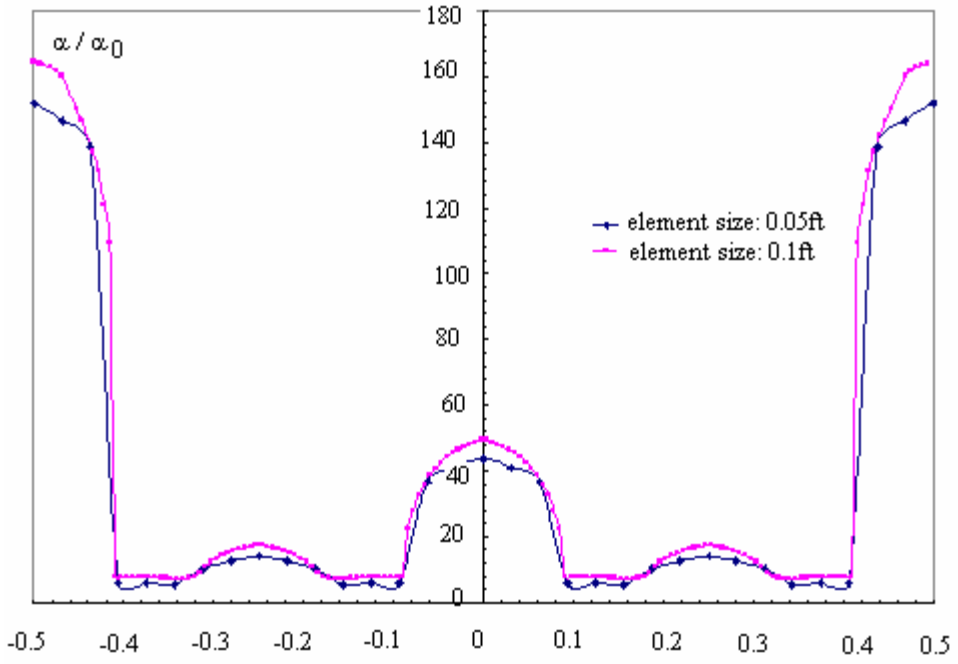

(e)

Figure 6.24 (Continued)

6.5. Needed Research

The study of cracking has received considerable attention in the literature of geotechnical engineering, soil science and agriculture. However, many treatment and research are behavioral and qualitative. The mechanism of clay soils drying and cracking remains unclear and a rational framework of analyzing desiccation under shrinkage and the propagation of cracks with the tensile stress release for the study of three-dimensional crack effects is highly demanded.

In the future study, the approach of fracture mechanics should be brought for the analysis of crack initiation, crack propagation, stress concentration in the vicinity of crack tip and the tensile stress release. Effect of vegetation on soil suction profile distribution like wet and dry envelopes needs more detailed consideration. Also more thorough field observations need be made to establish the crack pattern (cracking space, crack depths and angles of intersection).

CHAPTER VII

SUMMARY AND CONCLUSIONS

7.1 Conclusions

In this dissertation, the investigations on engineering properties of expansive soils have been conducted. An analytical study has been undertaken for the development and modification of a windows-based two-dimensional finite element program FLODEF that performs a sequentially coupled flow-displacement analysis for the prediction of moisture transmission and the induced volume change in civil infrastructures. The theoretical formulations of moisture flow and stress-deformation components of the model have been introduced in detail. Model material parameters, such as the coefficient of moisture diffusion α, which is an important parameter in governing the moisture flow and determining the depth of moisture active zone for design of foundation structures, and suction volumetric change index γ_h, have been presented and discussed.

The capabilities of the model are illustrated through the case studies of shear strength envelope forecast for retaining walls, embankments and slopes together with the parametric studies of transient flow-deformation prediction in highway project sites to evaluate the effectiveness of vertical moisture barriers, horizontal barriers, soil replacement or improvement, and paved median in reducing swell-shrink deformations beneath the surface of pavement structure. The degree and rate of strength degradation as well as the extent of moisture changes have been addressed.

Desiccation cracking plays an important role on the engineering properties of expansive soils especially the hydraulic conductivity and soil moisture diffusivity. A series of numerical simulations have been executed to study the field moisture diffusivities using a conceptual model of moisture diffusion in a fractured soil mass and rough correlation between field and the laboratory values of moisture diffusion coefficients have been presented for different cracking depths. The numerical analysis adopts an assumption that the maximum cracking depth equals to cracking space.

7.2 Recommendations

Experimental and analytical studies of soil shrinkage and the ensuing desiccation cracks are of utmost importance in the understanding of expansive soil engineering behavior since cracking entails degradation of many soil properties. Cracks are possibly the main cause of the significant difference between field moisture diffusivity and the laboratory measurement for intact soils (around two orders of magnitude) as demonstrated in Chapter VI. They are also a possible precursor for inception of softening and stability loss of embankments and slopes as discussed in Chapter IV. The mechanism of cracking formulation and propagation has not been completely understood. Further research and effort is highly desired to establish a rational analytical framework for the three-dimensional desiccation cracking analysis and present reasonable field observances of cracking patterns and network.

The transient flow-deformation numerical analysis utilizes a nonlinear elastic deformation model, which provides accurate prediction for the scenario of elastic behavior and combinations of soil stress state below the critical state. It is recommended

that an incorporation of plastic yielding into the model to address plastic effects which are likely restricted to very shallow soil zones where the variations in suction are most extreme.

Given the fact that vegetation has considerable effect on moisture distribution and crack onset, there is a strong need to develop a thorough methodology to predict the rate of vegetation water uptake, distribution of root density and the potential evapo-transpiration.

The extent and type of soil volumetric change depends on the soil type, fabric and structure defined as the arrangement of particles and voids, which involves particle size and shape, particles orientation and position, pore size distribution and particle cementation, etc. (Collins and McGown 1974; Gens et al. 1995; Gonzalez and Colmenares 2006; Ferber et al. 2006). Special devices and methods such as electron microscopy, porosimetry, X-ray diffraction etc., can be used to describe the soil microstructure. It is recommended for the future research to obtain a general model to establish the link between microstructure and macrostructure behavior for a better understanding of fundamental mechanism regarding volume change.

REFERENCES

ABAQUS Version 6.1 User's Manual (2000). Hibbett, Karlson and Sorensen, Inc, Pawtucket, R.I.

Abramento, M., and Carvalho, C.S. (1989). "Geotechnical parameters for the study of slopes instabilisation at Serra do Mar-Brazilian Southeast." *Proc. of the 12th International Conference on Soil Mechanics and Foundation Engineering*, Rio de Janeiro, 3, 1599-1602.

Agriculture and natural resources (2005). *Soil water reservoir*. University of California, Davis, CA. http://ucce.ucdavis.edu/files/filelibrary/2019/2945.pdf.

Ahuja, L. R. (1973). "A numerical and similarity analysis of infiltration into crusted soils." *Water Resour. Res*., 9, 987-994.

Ahuja, L. R. (1974). "Unsaturated hydraulic conductivity from cumulative inflow data." *Proc. Soil Sci. Soc. of Am*., 36, 695-699.

Aitchison, G. D., and Richards, B. G. (1965). "A broad scale study of moisture conditions in pavement subgrades throughout Australia. 2: Techniques adopted for the measurement of moisture variables." *Moisture equilibria and moisture changes in soil beneath covered areas.* Butterworths, London. 537-566.

Ali, N. and Rees, S.W.(2006). "Simulating water uptake by tree roots: an initial assessment." Geotechnical Special Publication No. 147. *Proceedings of the Fourth International Conference on Unsaturated Soils*. April 2-6, 2006. Carefree, AZ. 1, 2244-2255.

Alonso, E.E., Gens, A., and Josa A. (1990). "A constitutive model for partially saturated soils." *Geotechnique* 40(3), 405-430.

ASTM (2005a). "D4829 Standard Test Method for Expansion Index of Soil," *Annual Book of ASTM Standards*, vol.04.08, Soil and Rock(I),ASTM, Philadelphia, 157-162.

ASTM (2005b). "D5298-94 Standard Test Method for the Measurement of Soil Potential (Suction) Using Filter Paper," *Annual Book of ASTM Standards*, vol.04.09, Soil and Rock (II): D4943-latest, ASTM, Philadelphia, 157-162.

Aubeny, C. P. and Long, X. (2006). "Moisture diffusion in shallow clay masses." *J. of Geotech. and Geoenviron. Eng.* Submitted.

Aubeny, C.P. and Lytton, R.L. (2003). "Long-term strength of compacted high-PI clays." *Research Report 2100-1,* Texas Transportation Institute, Texas A&M University.

Bagge, G. (1985). "Tension cracks in saturated clay cuttings." *Proc. 11th International Conference on Soil Mechanics and Foundations Engineering,* San Francisco, 2, 393-395.

Bao, C., Gong, B., and Zhan, L. (1998). "Properties of unsaturated soils and slope stability of expansive soils." *Keynote lecture, Proc. of the 2nd International Conference on Unsaturated Soils (UNSAT 98).* Beijing, China, 1, 71-98.

Biddle, P. G. (1983). "Patterns of soil drying and moisture deficit in the vicinity of trees on clay soils." *Geotechnique*, 33(2), 107-126.

Biddle, P. G. (1998). *Tree root damage to buildings*., Vol. 1-2, Willowmead Publishing Ltd, Wantage, UK.

Bishop, A.W., and Blight, G.E. (1963), "Some aspects of effective stress in saturated and partially saturated soils." *Geotechnique*, 13, 177-197.

Blight, G. E. (2005). "Desiccation of a clay by grass, bushes and trees." *Geotech. Geolog. Eng.*, 23, 697-720.

Blight, G. E. (2006). "Interaction between trees and buildings on shrinkable soils- a detailed field study." Geotechnical Special Publication No. 147. *Proceedings of the Fourth International Conference on Unsaturated Soils*. April 2-6, 2006. Carefree, AZ. 2, 281-292

Bredenkamp, S., Scullion, T., Ragsdale, J., and Sebesta, S. (1998). "Vertical moisture barrier evaluation at IH 45 near Palmer, Texas." *Project summary report 3930-S.* Vertical moisture barriers, field monitoring and future directions. Texas Transportation Institute. The Texas A&M University System.

Bronswijk, J. J. B. (1991). "Drying, cracking and subsidence of a clay soil in a lysimeter." *Soil Sci.*, 152, 92-99.

Brooks, R.H., and Corey, A. T. (1966). "Hydraulic properties of porous media." *Hydrology Paper No.3*. Colorado State University, Fort Collins, CO.

British Building Research Establishment (1985). "The influence of trees on house foundations in clay soils." *Digest 298.* Building Research Establishment, Watford, U.K.

Bulut, R. (2001). “Finite element method analysis of slabs on elastic half space expansive soil foundations, Ph.D dissertation, Texas A&M Univ., College Station.

Bulut, R., Lytton, R., and Wray, W. K. (2001). “Soil suction measurements by filter paper.” *Proc. of Geo-Institute Shallow Foundation and Soil Properties Committee Sessions at the ASCE 2001 Civil Engineering Conference, Geotechnical Special Publication 115*,Houston, 1,243-258.

Cameron, D.A. (2001). “The extent of soil desiccation near trees in a semi-arid environment.” *Geotech. Geolog. Eng.*, 19, 357-370.

Campbell, J. D. (1973). “Pore pressure and volume changes in unsaturated soils,” PhD dissertation, Univ. of Illinois at Urbana-Champaign.

Christensen, H. R. (1943). “Permeability-capillary potential curves for three prairie soils.” *Paper J-1167 Project 504 of Iowa Agricultural Experiment Station*, 381-390.

Collins, K., and McGown, A.(1974). “The form and function of microfabric features in a variety of natural soils.” *Geotechnique*, 24(2): 223-254.

Cooling, L. F., and Golder, H. Q. (1942). “The analysis of the failure of an earth dam during construction.” *J. Institute of Civil Eng.*, 19, 38-55.

Covar, A. P., and Lytton, R.L. (2001). “Estimating soil swelling behaviour using soil classification properties, Expansive clay soils and vegetative influence on shallow foundations.” *Proc. of Geo-Institute Shallow Foundation and Soil Properties Committee Sessions at the ASCE 2001 Civil Engineering Conference, Geotechnical Special Publication 115*, Houston,1,44-63.

Cutler, D.F., and Richardson, I.B.K. (1989). *Tree roots and buildings*, Longman Scientific and Technical, Singapore.

Dane, J. H., and Klute, A. (1977). “Salt effects on hydraulic properties of a swelling soil.” *Soil Sci. Soc. Am. J.*, 41, 1043-1049.

Davidson, J. M., Stone, L.R., Nielsen, D.R., and Larue, M.E. (1969). “ Field measurement and use of soil-water properties.” *Water Resour. Res.*, 5, 1312-1321.

De Bruijn, C. M. A. (1965). “Some observations on soil moisture conditions beneath and adjacent to tarred roads and other surface treatments in South Africa.” In

Moisture equilibria and moisture changes in soils beneath covered areas (ed. G. D. Aitchison), pp. 135-142. Butterworths, London.

Duarte, A.P.L. and, de Campos, T.M.P. (2006). "Thermal properties for unsaturated soils." *Proceedings of the Fourth International Conference on Unsaturated Soils. Geotechnical Special Publication No. 147*. April 2-6, 2006. Carefree, AZ. 2, 1707-1717.

Feddest, R.A., Kabat, P., Van Bakel, P.J.T., Brownswijk, J.J.B,. and Halbertsma, J. (1988). "Modelling soil-water dynamics in the unsaturated zone-state of the art." *Journal of Hydrology*, Vol.100, 69-111.

Ferber ,V., Auriol ,J.C., Magnan , J.P., Cui,Y.J., Delaure, E., and Gerente, C.(2006). "A microstructure model for the volume changes of unsaturated clayey soils due to wetting." *Proceedings of the Fourth International Conference on Unsaturated Soils, Geotechnical Special Publication No. 147.* April 2-6, 2006, Carefree, AZ. 1, 861-872.

Fredlund D.G., and Morgenstern, N.R. (1977). "Stress state variables for unsaturated soils." *J. Geotech. Eng.*, 103, 447–466.

Fredlund D.G., Morgenstern N.R., and Widger R.A. (1978), "The shear strength of unsaturated soil." *Can. Geotech. J*., 15, 313–321.

Fredlund, D.G., and Rahardjo, H. (1993a). "An overview of unsaturated soil behaviour," *Unsaturated Soils, Geotechnical Special Publication No. 39* (ed. S.L. Houston and W.K. Wray), New York: ASCE, 1-31.

Fredlund, D.G., and Rahardjo, H. (1993b). *Soil mechanics for unsaturated soils*. John Wiley and Sons, Inc, New York.

Gan, J.K.M.,and Fredlund, D.G. (1988). "Multistage direct shear testing of unsaturated soils." *Geotechnical Testing Journal*, 11(2), 132-138.

Gardner, R. (1937). "A method of measuring the capillary tension of soil moisture over a wide moisture range." *Soil Sci*., 43. 277-283.

Gardner, W.R. 1958. "Some steady state solutions of the unsaturated moisture flow equation with application to evaporation from a water-table." *Soil Sci.*, 85, 228-232.

Gardner, W.R. (1961). "Soil suction and water movement." *Pore pressure and suction in soils*, Butterworths, London,137-140.

Garven, E.A. and Vanapalli, S.K. (2006). "Evaluation of empirical procedures for predicting the shear strength of unsaturated soils." *Proceedings of the Fourth International Conference on Unsaturated Soils, Geotechnical Special Publication No. 147,* April 2-6, 2006. Carefree, AZ. 2, 2570-2581.

Gay, D.A.(1994). "Development of a predictive model for pavement roughness on expansive clay." Ph.D dissertation. Texas A&M University.

Gens, E.E, Alonso, J. Suriol and A. Lloret (1995). "Effect of structure on the volumetric behaviour of a compacted soil." *First International Conference on Unsaturated Soils-UNSAT'95,* September, 1995. Paris. 1, 83-89.

Gillham, R. W., Klute, A., and Heermann, D. F. (1976). "Hydraulic properties of a porous medium: measurement and empirical representation." *Soil Sci. Soc. Am. J.*, 40, 203-207.

Gonzalez, N. A., and Colemenares, J.E.(2006). "Influence of matric suction on the volume change behavior of a compacted clayey soil." *Proc. of the Fourth International Conference on Unsaturated Soils, Special Publication No. 147.* April 2-6, 2006. Carefree, AZ, 2, 825-836.

Graham, J., and Shields, D.H. (1985). "Influence of geology and geological processes on the geotechnical properties of a plastic clay." *Eng. Geol. (Amsterdam),*22, 109-126.

Haines, W. B. (1923). "The volume change associated with variations in water content in soils." *J. Agr. Sci.* 13: 296-316.

Head, K.H. (1986). *Manual of soil laboratory testing*. John Wiley and Sons, Inc., New York.

Hilf, J.W. (1956). "An investigation of pore-water pressure in compacted cohesive soils." *Tech. Memo. No. 654,* U.S. Dept. of the Interior, Bureau of Reclamation, Design and Construction Div., Denver, CO.

Hillel, D. (1982). *Introduction to soil physics*. Academic Press, New York.

Holtz, R. D., and Kovacs, W. D. (1981). *An introduction to geotechnical engineering.* Prentice-Hall, Englewood Cliffs, NJ.

Hoyos, L.R.,Takkabutr, P. and Puppala, A.J. (2006). "A modified Pressure Plate Device for SWCC Testing Under Anisotropic Stress States." *Proceedings of the Fourth*

International Conference on Unsaturated Soils, Geotechnical Special Publication No. 147, April 2-6, 2006. Carefree, AZ, 2, 1753-1763.

Indraratna, B., Fatahi, B. and Khabbaz, H. (2006). "Numerical prediction of vadose zone behaviour influenced by vegetation." *Proc. of the Fourth International Conference on Unsaturated Soils, Geotechnical Special Publication No. 147.* April 2-6, 2006. Carefree, AZ, 2, 2256-2267.

Indrawan, I. G. B., Rahardjo, H. and Leong, E. C. (2006). "Study of infiltration characteristics in the field." *Proc. of the Fourth International Conference on Unsaturated Soils, Geotechnical Special Publication No. 147.* April 2-6, 2006. Carefree, AZ, 2, 179-190.

Irwin, G.R. (1948). *Fracturing of metals*, American Society of Metals, Cleveland, OH.

Jaksa, M.B. (1998). "The influence of trees on expansive soils." Available: http://training.ce.washington.edu/WSDOT/Modules/04_design_parameters/shink-swell_soils.htm. Accessed 1/5/05.

Jayatilaka, R., and Lytton, R. L. (1997). "Prediction of expansive clay roughness in pavements with vertical moisture barriers." *Research Report 187-28F*. Texas Transportation Institute, The Texas A&M University System.

Kayyal, M. K., and Wright, S. G. (1991). "Investigation of long-term strength properties of Paris and Beaumont clays in earth embankments." *Research Report no. 1195-2F*. Center for Transportation Research, University of Texas at Austin, Austin, Texas.

Keen, B. A. (1931). *The physical properties of soil*. Longmans: London.

Khalili, N., and Khabbaz, M. H. (1998). "Unique relationship for χ , for the determination of the shear strength of unsaturated soils." *Geotechnique*, 48(5), 681-687.

Khalili, N., Geiser, F., and Blight, G.E. (2004). Effective stress in unsaturated soils: review with new evidence. *Internat. J. Geomech*. 4(2), 115-126.

Knight, M. J. (1971). "Structural analysis of selected duplex soils." Ph.D. dissertation, University of Melbourne, Australia.

Konrad, J.-M., and Ayad, R.(1997). "Desiccation of a sensitive clay: field experimental observations." *Can. Geotech. J.*, 34, 929-943.

Krahn, J., and Fredlund, D.G. (1972). “On total, matric and osmotic suction.” *Soil Sci.*, 114(5), 339-348.

Lachenbruch, .A.H.(1961). “Depth and spacing of tension cracks.” *J. Geophys. Res.*, 66(12), 4273-4292.

Laliberte, G. E., Corey, A. T., and Brooks, R.H. (1966). “Properties of unsaturated porous media.” *Hydrology Paper No. 17*, Colorado State University, Fort Collins, CO.

Lamborn, M. J. (1986). “A micromechanical approach to modeling partly saturated soils.” M.S. Thesis, Texas A&M University.

Lang, A.R.G. (1967). “Osmotic coefficients and water potentials of sodium chloride solutions from 0 to 40°C.” *Aust. J. Chem.*, 20, 2017-2023.

Lawn, B. R. and Wilshaw, T. R. (1974). *Fracture of brittle solids*. Cambridge University Press, Cambridge.

Lawton, B., and Klingenberg, G. (1996). *Transient temperatures in engineering and science*. Oxford University Press, Oxford.

Lee, I.K., and Ingles, O.C. (1968). “Strength and deformation of soil and rocks.” In *Soil mechanics*, Butterworths, Sydney,1-57.

Lee, I.-M., Sung, S.-G., and Cho, G.-C. (2005). “Effect of stress state on the unsaturated shear strength of a weathered granite.” *Can. Geotech. J.*, 42, 624-631.

Leong, E.C. and Rahardjo, H. (1997). “Review of soil-water characteristic curve equations.“ *J. Geotech. Geoenvir. Eng.*, 123(12), 1118-1126.

Leong, E.-C., He, L., and Rahardjo, H. (2002). “Factors affecting the filter paper method for total and matric suction measurements.” *Geotech. Test. J.*, 25 (3), 322-333.

Lloret, A, and Alonso, E.E. (1980). “Consolidation of unsaturated soils including swelling and collapse behaviour.” *Geotechnique*, 30(4), 449-477.

Long, X., Aubeny, C. P. and Lytton, R. L. (2006). “Two-dimensional shrink-swell model for pavement surface movement prediction.” *Proc. of the Fourth International Conference on Unsaturated Soils, Geotechnical Special Publication No. 147*. April 2-6, 2006. Carefree, AZ, 2, 2150-2161.

Lu, Z. (1992). “The relationship of shear strength to swelling pressure for unsaturated soils.” *Chinese J. of Geotech. Eng.*, 143, 1-8. (in Chinese)

Lytton, R.L. (1994). "Prediction of movement in expansive clay." *Proc. Settlement '94, Geotechnical Special Publication 40.* College Station,16-18 June 1994. Edited by A.T. Yeung and G.Y.Feaalio. American Society of Civil Engineers, 1827-1845.

Lytton (1995). Foundations on expansive soils. Class notes, CVEN 646, Texas A&M University.

Lytton, R. (1997). "Engineering structures in expansive soils." Keynote address, *Proc. 3rd International Symposium on Unsaturated Soils*, Rio de Janeiro, Brazil,1, 3-15.

Lytton, R.L. (2002). Foundations on expansive soils. Class Notes. Texas A&M University.

McCormack, D.E., and Wilding, L.P. (1979). "Soil properties influencing strength of Canfield and Geeburg Soils." *Soil Sci. Soc. Amer. J.*, 43 (1), 167-173.

Mckeen, R.G. (1992). "A model for predicting expansive soil behavior." *Proc. 7th International Conference on Expansive Soils*, Dallas, 1, 1-6.

Mckeen, R.G., and Johnson, L. D. (1990). "Climate-controlled soil design parameters for mat foundations." *J. Geotech. Eng.*, 116(7), 1073-1094.

Miao, L., Liu, S., and Lai, Y. (2002). "Research of soil-water characteristics and shear strength features of Nanyang expansive soils." *Eng. Geol*., 65(4), 261-267.

Miller, D.J. and Nelson, J.D. "Osmotic Suction in Unsaturated Soil Mechanics." *Proceedings of the Fourth International Conference on Unsaturated Soils, Geotechnical Special Publication No. 147*. April 2-6, 2006. Carefree, AZ, 2, 1382-1393.

Mitchell, P. W. (1979). "The structural analysis of footings on expansive soil." *Kenneth W.G. Smith and Associates Research Report No. 1*, pp. 1-159, Newton, South Australia.

Morris, P.H., Graham, J., and Williams, D. J. (1992). "Cracking in drying soils." *Can. Geotech. J.*, 29, 263-277.

Naiser, D. D., JR. (1997). "Procedures to predict vertical differential soil movement for expansive soils." M.S. Thesis. Texas A&M Univ., College Station, Tex.

Ng, C. W.W., and Pang, Y.W. (2000). "Influence of stress state on soil-water characteristics and slope stability." *J. Geotech. and Geoenviron. Eng.,* 126(2),157-166.

Nunn, A. P., Holden, J. C., Ma, M., and Dimos, A. (1992). "Restoration of tree-affected building foundations." *7th International Conference on Expansive Soils*, Dallas, TX, 1, 143-148.

Oberg, A., and Sallfours, G. (1997). "Determination of shear strength parameters of unsaturated silts and sands based on the water retention curve." *Geotech. Testing J*., 20, 40-48.

Oliveria, O.M., and Fernando, F.A.M. (2006). "Study of equilibrium time in the pressure plate." *Proceedings of the Fourth International Conference on Unsaturated Soils, Geotechnical Special Publication No. 147*. April 2-6, 2006. Carefree, AZ, 2, 1864-1874.

Orowan, E. (1950). "Fundamentals of brittle behavior in metals." *MIT Symposium on Fatigue and Fracture of Metals*, John Wiley and Sons, New York, 139-154.

Parry, L. N. (1992). "Desiccation, some examples measured in London Clay." *Proc. 7th International Conference on Expansive Soils*, Dallas, TX, 1, 404-408.

Perera, Y.Y., Zapata, C.E., Houston, S.L., and Houston, W.N. (2004). "Moisture equilibria beneath highway pavements." *Transportation Research Board 83rd Annual Meeting-Session 410*, Washington DC, January 11-15, 12-29.

Perpich, W. M., Lukas, R. G., and Baker, C. N., Jr. (1965). "Desiccation of soil by trees related to foundation settlement." *Can. Geotech. J*., 2(1), 23-39.

Philip, J. R. (1986). "Linearized unsteady multidimensional infiltration." *Water Resour. Res*., 22,1717-1727.

Picornell, M. (1985). "The development of design criteria to select the depths of a vertical moisture barrier." Ph.D. dissertation. Texas A&M University, College Station.

Post-Tensioning Institute (PTI) (2005). *Design of post-tensioned slabs-on-ground*. 3rd Ed. Phoenix, Arizona.

Prasad, R. (1988). "A linear root water uptake model." *J. Hydrol.*, 99, 297-306.

Rahardjo, H. and Leong, E.C.(2006) "Suction measurements." *Proceedings of the Fourth International Conference on Unsaturated Soils. Geotechnical Special Publication No. 147*. April 2-6, 2006. Carefree, AZ, 1, 81-104.

Rassam, D. W., and Williams, D. J. (1999). "A relationship describing the shear strength of unsaturated soils." *Can. Geotech. J*., 36, 363-368.

Rassam, D. W., and Cook, F. J. (2002). "Predicting the shear strength envelope of unsaturated soils." *Geotech. Testing J*., 28, 215-220.

Richards, B.G., Peter, P., and Emerson, W.W. (1983). "The effects of vegetation on the swelling and shrinkage of soils in Australia." *Geotechnique,* 33(2), 127-139.

Richards, L. A. (1931). "Capillary conduction of liquids through porous medium." *Phys*., 1, 318-333.

Ritjema, P. E. (1965). "An analysis of actual evapotranspiration." *Agric. Res. Rep. 659* Wageningen, The Netherlands.

Rode, A. A.(1969). "Moisture properties of soils and movement of soil water." In *Theory of soil moisture,* Vol. 1. Translated from Russian. Israel Program for Scientific Translations Jerusalem.

Russam, K., and Coleman, J. D. (1961). "The effect of climatic factors on subgrade moisture conditions." *Geotechnique*, 11, 22-28.

Russam, K., and Dagg, M. (1965). "The effect of verge slope and cover on soil moisture distribution under a road in Kenya." In *Moisture equilibria and moisture changes in soils beneath covered areas* (ed. G.D.Aitchison), pp.100-121. Butterworths, London.

Russell, J. S. (1977). "Evaluation of residual nutrients in soils." *Aust.J. Agric. Res*. 28: 461-475.

Schick, P. (2004). "Scherfestigkeit Durch Kapillaritat in unzementierten ungesattigten bindigen Boden (Capillary strength of uncemented and unsaturated cohesive soils in direct shear)." *Bautechnik*, 81(1), 31-37.

Shen, Z. (1996). "The problems in the present studies on mechanics for unsaturated soils." *Proc. of the Symposium on Geotechnical Aspects of Regional Soils, Nanjing*. (in Chinese) ,379-392.

Snethen, D. R., Johnson, L. D., and Patrick, D. M. (1977). "An evaluation of expedient methodology for identification of potentially expansive soils." *Report No. FHWA-RD-77*. Office of Research and Development, Federal Highway Administration, US Department of Transportation, Washington, DC.

Stark, T., and Duncan, J. M. (1991). "Mechanisms of strength loss in stiff clays." *J. Geotech. Eng*., 117(11), 139-154.

Stirk, G. B. (1954). “Some aspects of soil shrinkage and the effect of cracking upon air entry into the soil.” *Aust. J. Soil Res.*, 5:279–290.

Tekinsoy, M.A., Kayadelen, C.,.Keskin, M.S., and Soylemez, M.. (2004). “An equation for predicting shear strength envelope with respect to matric suction.” *Computers and Geotechnics,* 31, 589-593.

Terzaghi, K. (1943). *Theoretical soil mechanics*. John Wiley &Sons Inc., New York.

Thakur, A. (2005). “Determination of diffusion coefficient through laboratory tests and analytically validating it using empirical relations for unsaturated soils.” M.S. thesis, Texas A&M Univ., College Station.

Thielen, A., and Springman, S. M. (2006). “Monitoring field experiment in an unsaturated sandy soil slope in Switzerland.” *Proc. of the Fourth International Conference on Unsaturated Soils. Geotechnical Special Publication No. 147.* April 2-6, 2006. Carefree, AZ, 2, 191-202

Thornthwaite, C.W. (1948). An approach toward a rational classification of climate. *Geographical Review*, 38, 55-94.

Thornthwaite, C.W., and Mather, J.R. (1955). *The water balance*. Laboratory of Climatology, Centerton NJ.

Thu, T.M., Rahardjo, H. and Leong, E.C.(2006). “Effects of hysteresis on shear strength envelopes from constant water content and consolidated drained triaxial tests.” *Proceedings of the Fourth International Conference on Unsaturated Soils. Geotechnical Special Publication No. 147.* April 2-6, 2006. Carefree, AZ, 1, 1212-1222.

Vallejo, L.E.(1989). “Mechanics of crack propagation in stiff clays.” *Geotechnical aspects of still and hard clays, Geotechnical Special Publication # 2,* American Society of Civil Engineers, Reston,VA, 14-27.

Vanapalli S.K., Fredlund, D.G., Pufahl, D.E., and Clifton, A.W. (1996). “Model for the prediction of shear strength with respect to soil suction.” *Can. Geotech. J.* 33, 379-92.

Vermeer, P.A., and Verruijt, A. (1981). “An accuracy condition for consolidation by finite elements.” *International Journal for Numerical and Analytical Methods in Geomechanics,* 5(11),1-14.

VOLFLO 1.5 (2005). Geostructural Took Kit, Inc, Austin, TX.

Watkins, A. and Hughes S.(2006). "Landslides, slope failure, and other mass wasting processes." *Environmental Geology-Geol 406/506*. Department of Geosciences. Idaho State University, Pocatello ID. http:/wapi.isu.edu/envgeo/ EG4_mass_wasting/EG_module_4.htm.

Weeks, L. V., and Richards, S. J. (1967). "Soil-water properties computed from transient flow data." *Proc., Soil Sci. Soc. Am.*, 31, 721-725.

Wheeler, S., and Karube, D. (1996). "Constitutive modeling." *Proc. of the 1st Int. Conf. on Unsaturated Soils, UNSAT 95*, Balkema, Rotterdam, The Netherlands, 3, 1323-1356.

Wheeler, S. J., Sharma, R. S. and Buisson, M. S. R. (2003). "Coupling of hydraulic hysteresis and stress-strain behavior in unsaturated soils." *Geotechnique*, 53(1), 41-54.

Wilding , L. P., and Tessier, D. (1988). "Genesis of vertisols: shrink-swell phenomena." In Vertisols: their distribution, properties, classification and management. (Eds LP Wilding, R Puentes. Technical monograph No.18. (Soil Management Support Service). Texas A&M University, College Station, TX.) pp 55-81

Wind, G. P. (1955). "Field experiment concerning capillary rise of moisture in heavy clay soil." *Netherlands J. Agric. Sci*., 3, 60-69.

Xu, Y. F. (1997). "Mechanical properties of unsaturated expansive soils and its application in engineering." Ph.D. dissertation, HoHai University, Nanjing. (in Chinese)

Xu, Y. F., and Sun, D. A. (2001). "Determination of unsaturated shear strength using a fractal model." *Fractals*, 91, 51-60.

Xu. Y. F. (2004). "Fractal approach to unsaturated shear strength." *J. Geotech. Geoenviron. Eng*., 130(3, 264-273.

Yang, H. E., and Zheng, J. (2006). "The new engineering treatment techniques of expansive soils subgrade for Guangxi Nanning-Youyi Guan expressway." *Proc. of the Fourth International Conference on Unsaturated Soils. Geotechnical Special Publication No. 147*. April 2-6, 2006. Carefree, AZ, 2, 439-450.

Yu, H. S. (1998). "CASM: a unified state parameter model for clay and sand." *International Journal for Numerical and Analytical Methods in Geomechanics*, 22(8), 621-653.

Yu, P.,and Chen, Y. (1965). “Pore water state and pore air state in unsaturated soils and relationship with its mechanics properties.” *Chinese Journal of Hydraulic Engineering*, 1, 16-23. (in Chinese).

Zachmann, D. W., Ducthateau, P. C., and Klute, A. (1981). “The calibration of the Richards flow equation for a draining column by parameter identification.” *J. Soil Sci. Soc. Am.*, 45, 1012-1015.

Zienkiewicz, O. C., and Taylor, R. L. (1989*). The finite element method - basic formulation and linear problems.* 4th ed. McGraw-Hill, New York.

VITA

Xiaoyan Long is a citizen of P.R. China; her permanent mailing address is:

No.2 Elementary School

Yiyang County, Jiangxi Province

P.R. China, 334400

Xiaoyan Long was born on July 2, 1974 in Shangrao, Jiangxi Province, P. R. China. She received her B.E. degree in civil engineering from Changsha Railway University (Changsha, P. R. China) in July 1994. After that, she worked for three years at the Bridge Design and Research Institute, Railway Ministry (Wuhan, P. R. China). She graduated with her M.S. degree in civil engineering from Tongji University (Shanghai, P. R. China) in February 2000. After working six months for a real estate company in Shanghai, P. R. China, she came to the United States and studied at the University of Toledo starting in August 2000. In August 2001, she started research towards this doctoral dissertation at Texas A&M University, and received her Ph.D. degree in civil engineering in August 2006.